Thermal Barrier Coating Life Prediction Model Development

Phase II – Final Report

S. M. Meier, D. M. Nissley and K. D. Sheffler

UNITED TECHNOLOGIES CORPORATION
Pratt & Whitney
Materials Engineering

July 1991

NASA

National Aeronautics and
Space Administration

N93-12589
Unclas
G3/27 0126977

(NASA-CR-189111) THERMAL BARRIER
COATING LIFE PREDICTION MODEL
DEVELOPMENT, PHASE 2 Final Report
(PWA) 198 p

NASA Contractor Report <u>189111</u>

Thermal Barrier Coating Life Prediction Model Development

Phase II – Final Report

S. M. Meier, D. M. Nissley and K. D. Sheffler

UNITED TECHNOLOGIES CORPORATION
Pratt & Whitney
Materials Engineering

July 1991

FOREWORD

TABLE OF CONTENTS

LIST OF ILLUSTRATIONS

LIST OF ILLUSTRATIONS

LIST OF ILLUSTRATIONS

LIST OF ILLUSTRATIONS (Continued)

LIST OF ILLUSTRATIONS (Continued)

LIST OF ILLUSTRATIONS (Continued)

LIST OF ILLUSTRATIONS (Continued)

LIST OF TABLES

1.0 SUMMARY

The objective of this program was to develop life prediction methodology for Thermal Barrier Coatings (TBC) used in gas turbine components. These coatings consist of a thin (nominal 0.254 mm (0.010")) layer of insulative ceramic (typically zirconia-based) applied over a highly oxidation resistant metallic "bond coat" of 0.127 mm (0.005") nominal thickness. The program was conducted in two phases. Phase I, completed in 1989 (NASA CR-182230) (Ref. 1), developed a model for a plasma deposited TBC system. In Phase II the Phase I model was adapted to a more recently developed and much more durable electron beam-physical deposited (EB-PVD) ceramic.

The EB-PVD ceramic TBC studied in Phase II differed from the Phase I plasma deposited ceramic in two significant ways. The plasma deposited ceramic structure is essentially isotropic and contains a high level of porosity and microcracking, both of which are thought to increase the ceramic cyclic thermal strain tolerance. The EB-PVD ceramic structure on the other hand, is highly columnar with the columns aligned perpendicular to the metal-ceramic interface. It is believed that the columnar EB-PVD structure provides a much higher level of "strain tolerance". A second major difference is the topology of the metal-ceramic interface, which is very rough (5 to 10 microns or 200 to 400 micro inches) in the plasma deposited system as opposed to being essentially planar in the EB-PVD system.

Phase I studies showed that plasma deposited TBC failure occurs as a result of cracking in the ceramic parallel and adjacent to, but not coincident with the very rough metal-ceramic interface. Phenomological evidence indicates that cyclic life is strongly influenced both by the severity of cyclic strain in the ceramic phase and by the amount of bond coat oxide which results from cyclic thermal exposure in the gas turbine engine. While no direct evidence of oxide induced ceramic crack initiation was found, the phenomological evidence for the strong influence of oxidizing (and only oxidizing) thermal exposure was overwhelming. The interactive life model developed in Phase I was designed to account for both the oxidative and mechanical forms of TBC degradation.

Observations of EB-PVD TBC failure indicated that ceramic spallation predominantly occurs as a result of cracking at the interface between the metal bond coat and the oxide scale. This oxide scale, predominantly composed of alumina, grows during prolonged thermal exposure.

Specific activities involved in development of the EB-PVD life prediction model included measurement of EB-PVD ceramic physical and mechanical properties and adherence strength, measurement of TGO growth kinetics, generation of quantitative cyclic thermal spallation life data, and development of a spallation life prediction model. The results for EB-PVD TBC are presented and compared with selected results obtained for plasma deposited TBC.

Thermal expansion and thermal conductivity were measured to support heat transfer and thermal stress analyses required for life prediction modeling. The thermal expansion results showed no significant difference between the expansion properties of the plasma and EB-PVD deposited ceramic. The thermal conductivity results, on the other hand, indicated that the EB-PVD structure has about twice the conductivity of plasma sprayed coating.

EB-PVD zirconia mechanical property data was obtained and modeled for use in analysis of EB-PVD ceramic cyclic stress and strain. Compression tests showed that the EB-PVD ceramic exhibits higher strength than the plasma sprayed ceramic. Tensile tests showed that the EB-PVD ceramic does have some apparent in-plane tensile strength, although it's only about 6.9 MPa (1 ksi) or less.

Interfacial strength tests were conducted on virgin EB-PVD coatings and on coatings which were thermally exposed. Attempts to test as-received ceramic all resulted in failure of the epoxy adhesive, indicating an out-of-plane strength greater than 41.4 MPa (6000 psi). Strengths of the exposed specimens were all below this level, with essentially no dependence of strength on thermal exposure.

Based on the demonstrated influence of oxidation on the plasma deposited TBC spallation life in Phase I and on the EB-PVD failure location, a bond coat oxidation model was developed as part of the EB-PVD life modeling effort. The oxidation model for the EB-PVD TBC system correlated the TGO growth rate within about 20% of measured values.

Past experience with plasma sprayed TBC indicated that inelastic deformation of the ceramic was a critical life parameter. However, nonlinear analysis of the EB-PVD ceramic behavior during burner rig specimen thermal cycling indicated that the EB-PVD ceramic remained elastic. For that reason and because spallation failure of the EB-PVD TBC system is caused by cracking at the thermally grown oxide (TGO)/metallic bond coat interface, life modeling efforts have used TGO elastic strains instead of EB-PVD ceramic strains.

Several cyclic damage models for the TGO were evaluated by applying them to the life data. Each damage model was taken to be a power law relation, consistent with elementary fatigue models and with the damage model developed for plasma sprayed TBC. The fatigue model formulation contains both mechanical cyclic and TGO oxidation damage terms which are integrated over the cycle. Calculated lives of the baseline data set were within a factor of ± 2 of the actual lives. The model was successfully exercised by predicting the lives of three verification tests within the $\pm 2x$ life scatter band.

2

2.0 INTRODUCTION

Thermal barrier coatings (TBC's) offer a number of benefits, including up to 149C (300F) metal temperature reduction, significant fuel savings, and improved durability (ref. 2,3). Plasma deposited TBC's have been used for over twenty years to extend the durability of combustors and augmentors as well as stationary turbine components. As turbine inlet temperatures continued to increase, an improved electron beam-physical vapor deposited (EB-PVD) coating was developed for application on both stationary and rotating turbine components.

Until recently, TBC's have been used to extend the life of existing or derivative component designs. Achievement of maximum TBC benefit potential, however, requires incorporation of the TBC thermal insulation as an integral element of initial component design. This in turn requires development of a TBC design system and supporting TBC life prediction methodology.

The purpose of this program was to provide TBC life prediction methodology for subsequent incorporation into coated component design systems. Specific objectives were to create the analytical methodology required to predict thermal barrier coating life in the operating environment of the gas turbine engine, as well as to generate quantitative life data and to better understand the mechanism(s) of coating degradation and failure.

This program was conducted in two phases. The first phase was conducted with a plasma deposited thermal barrier coating system, designated PWA 264, which currently is bill-of-material on various stationary turbine components in several commercial engines. Results of this first phase indicated that plasma deposited TBC ceramic spallation results from progressive, near-interfacial cracking of the ceramic. Phenomenological evidence indicated that interfacial oxidation accelerates this process. Mechanical behavior of the ceramic was found to be unusual for ceramics, exhibiting highly inelastic stress-strain behavior, creep, and fatigue. A life prediction model was developed which incorporated cyclic inelastic strain and interfacial oxidation as the primary degradation modes. This model was shown to correlate cyclic thermal spallation life results within a factor of ± 3 over a broad range of relative mechanical and oxidative exposure severities.

The second phase of this program adapted the plasma deposited TBC life model to a more recently developed electron beam-physical vapor deposited ceramic coating, designated PWA 266. The columnar EB-PVD ceramic structure provides up to ten times the cyclic thermal coating durability of the plasma deposited coating. The Phase II program objectives were accomplished in four tasks, numbered V through VIII. Task V involved evaluation of EB-PVD ceramic mechanical behavior and physical properties, while in Task VI, oxidation at the metal-ceramic interface was measured and modeled. Quantitative life data was generated and modeled over a broad range of relative oxidizing and mechanical severities in Phase VII, and in Phase VIII substantiation tests were conducted to verify the model.

3.0 PHASE II – ELECTRON BEAM–PHYSICAL VAPOR DEPOSITED THERMAL BARRIER COATING LIFE PREDICTION MODEL DEVELOPMENT

3.1 Coating System Description

Two generations of thermal barrier coatings have been developed for the gas turbine engine environment. The first, PWA 264, incorporates 7 weight % yttria stabilized zirconia, air plasma-sprayed over an oxidation resistant, low-pressure plasma-sprayed NiCoCrAlY bond coat (Figure 1). The second incorporates the 7 weight % yttria stabilized zirconia composition applied by electron beam-physical vapor deposition (EB-PVD), also over a vacuum processed bond coat. The EB-PVD coating is produced by condensation of ceramic vapor onto the component (Ref. 4). The vapor is produced by electron beam melting and evaporation of the ceramic in a crucible placed under the workpiece. Coating is performed in a vacuum chamber to permit generation of the electron beam and vaporized species, as well as to avoid contaminating the molten material in the crucible and the vapor phase or the condensate (coating).

The microstructure of EB-PVD ceramic is fundamentally different from that of plasma ceramic. As shown in Figure 2, the EB-PVD ceramic grows in columnar form when processed under the appropriate conditions. Ideally, individual ceramic columns are poorly bonded to adjacent columns, but are tightly bonded to the underlying substrate (Figure 3). This extremely fine columnar structure is highly tolerant of thermal strains induced by differential expansion of the underlying substrate (Ref. 3). The influence of ceramic structure on cyclic thermal spallation life is shown in Figure 4 (Refs. 5,6,7). Whereas relatively dense ceramic fails very quickly (Refs. 8,9), the porous, microcracked plasma-deposited and columnar EB-PVD ceramic structures provide progressively increasing coating durability.
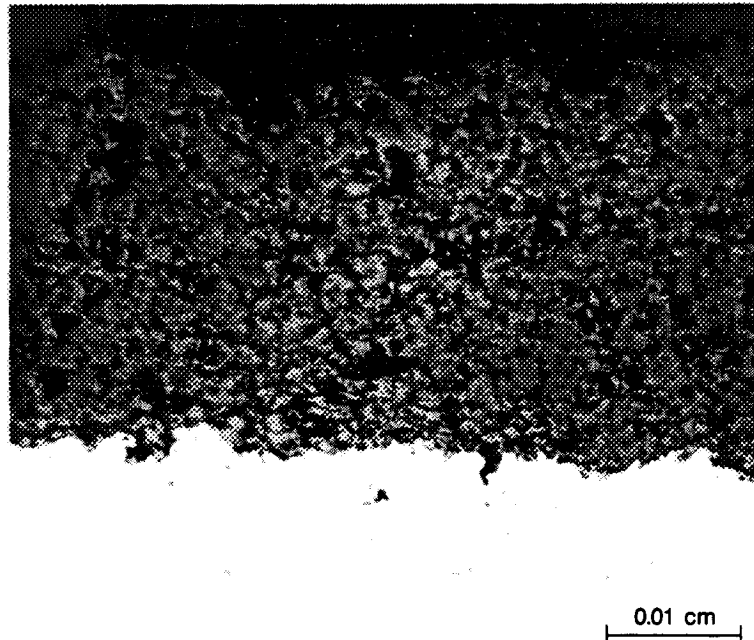
0.01 cm

Figure 1.– The Microstructure of Air Plasma-Deposited 7 Weight Percent Yttria Stabilized Zirconia.

4
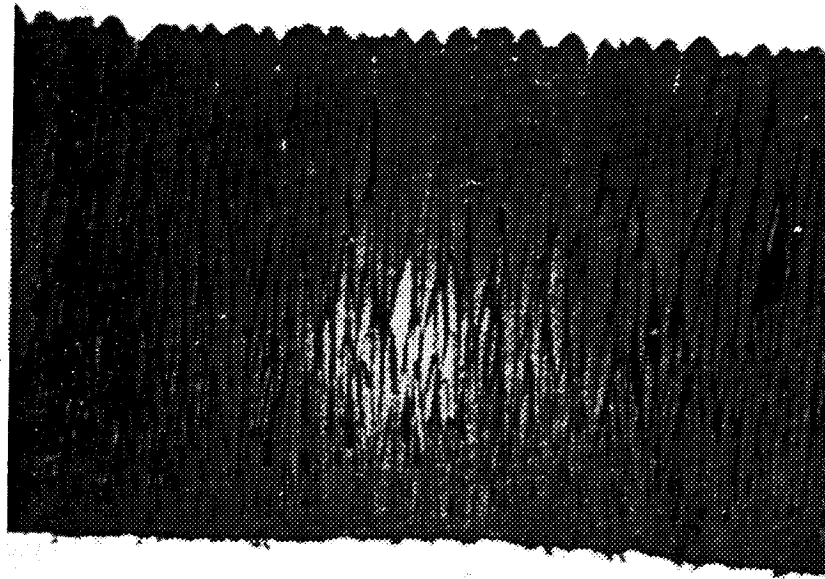
0.01 cm

Figure 2.– The Microstructure of an Electron Beam– Physical Vapor Deposited
(EB-PVD) Ceramic Coating, Showing the Highly Columnar
Microstructure Produced by the EB-PVD Process.

Segmented
ceramic

Metal

Segments separate, no tensile
stress developed in ceramic coating
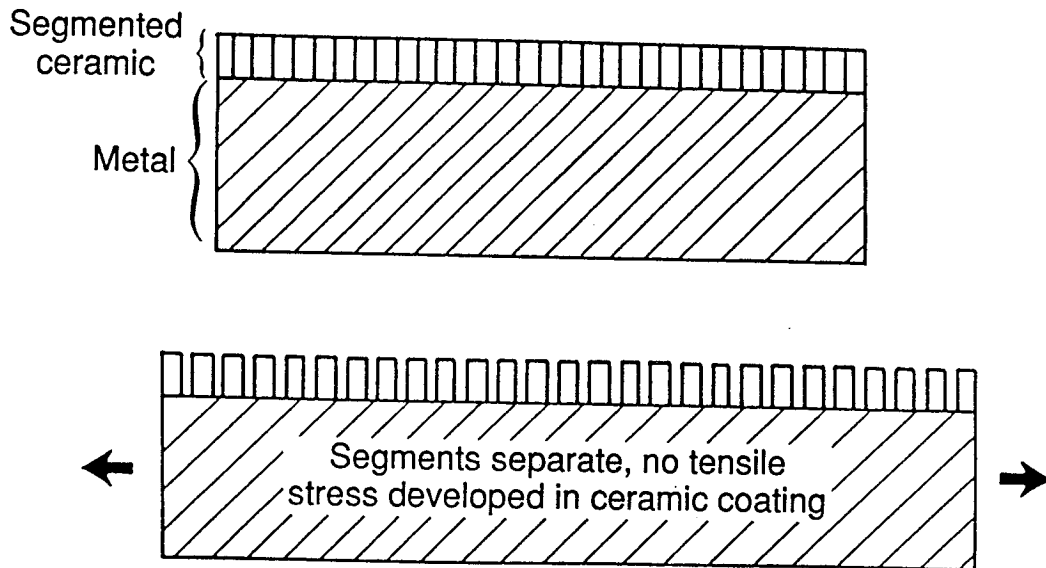
Figure 3.– Schematic of the Idealized EB-PVD Strain Tolerant Ceramic Coating
System.

5
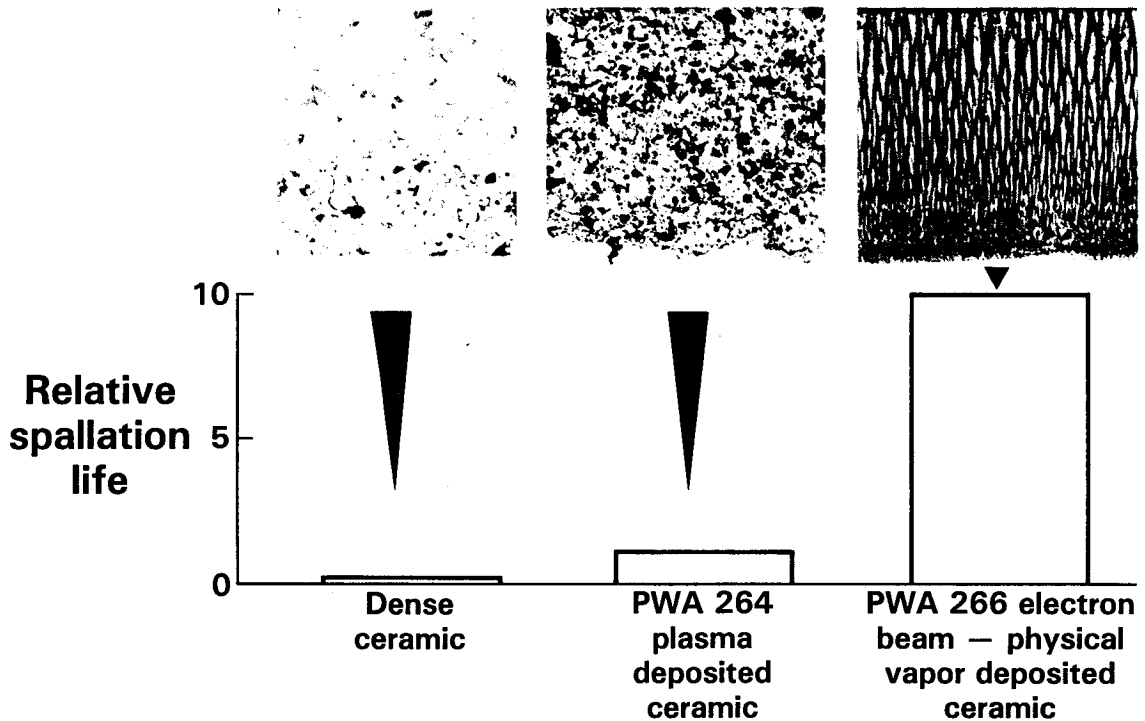
Figure 4. Ceramic Microstructure Modification Provides Increases in Life.

The two layer EB-PVD thermal barrier coating system investigated in this program is designated PWA 266. The inner low pressure chamber sprayed NiCoCrAlY metallic bond coat is 0.1270 ±0.0254 mm (0.005 ±0.001 in) thick. The raw material from which this bond coat is produced is designated as PWA 1386 with a nominal composition as listed in Table I. The ceramic outer layer has a nominal composition of 7 weight % partially stabilized zirconia, and is deposited by the EB-PVD process to a thickness of 0.1270 to 0.3810 ±0.0508 mm (0.010 to 0.015 ±0.002 in). The substrate alloy, designated PWA 1480, is a single crystal nickel base superalloy of nominal composition also listed in Table I.

TABLE I
COMPOSITION OF PROGRAM MATERIALS
(Weight Percent)

	Ni	Co	Cr	Al	Ta	W	Ti	Y	Hf	Si
PWA 1480	Remainder	5.5	10.0	5.0	12.0	4.0	1.5	—	—	—
PWA 1386	Remainder	22.0	17.0	12.5	—	—	—	0.6	0.25	0.4

Prior to conducting tests in Phase II, all raw materials were characterized to ensure acceptability. The chemical (x-ray fluorescence) and particle size (microtrac) analyses of the coating materials are presented in Table II. Both are well within the Pratt & Whitney specification requirements.

TABLE II
METALLIC AND CERAMIC POWDER ANALYSES

Material	Chemical Analysis	Particle Size Analysis (Volume %)	(Mesh/Microns)
NiCoCrAlY	22.59 w% Co	0.0	+270
	17.08 w% Cr	0.2	-270+325
	12.46 w% Al	12.0	-325+400
	0.48 w% Y	32.9	-400+500
	0.33 w% Si	55.9	-500
	0.28 w% Hf	80.0	-37 microns
	Bal. -Ni	3.0	-5 microns
w% Y203	7.67 w% Y203	0	+4
	0.08 w% SiO2	94.4	+16
	0.05 w% Fe2O3	5.6	-16
	0.26 w% TiO2		
	0.37 w% Al2O3		
	0.16 w% CaO2		
	0.01 w% MgO		
	<1.50 w% HfO2		
	238 ppm U		
	185 ppm Th		
	Bal. ZrO2		

3.2 Task V – Material Property Determination

The objective of this task was to obtain physical property data required for subsequent analysis and life modeling. The data was obtained through thermal conductivity/expansion tests and out-of-plane strength evaluations.

3.2.1 Task VA – Physical Property Tests

The objective of this subtask was to obtain thermal conductivity and expansion data required for heat transfer and thermal stress analyses.

3.2.1.1 Ceramic Thermal Expansion

Thermal expansion tests were performed at Holometrix Inc. of Cambridge, Massachusetts. Thermal expansion was measured both parallel and perpendicular to the EB-PVD ceramic columns on both virgin (as-deposited) ceramic and on ceramic that had been thermally exposed for 50 hours at 1149C (2100F) to simulate the effects of sintering or phase changes that might occur in an engine environment. The test matrix for thermal expansion is presented in Table III. A vitreous silica dilatometer was used for the testing. The samples were heated and cooled at a rate of approximately 1.7 C/min (3.06 F/min) in the silica holder within the furnace. During heating and cooling, the temperature was measured by a chromel-alumel thermocouple and the length of the sample was continually monitored with a linear variable differential transformer (LVDT). The thermal expansion of the sample holder was determined by comparing it to an NBS standard material and calibration of the LVDT involved measuring a known displacement of the transformer core with a micrometer.

7

TABLE III
THERMAL EXPANSION TEST MATRIX

Direction of Measurement	Number of Samples	Pre-Exposure Conditions	Test Temperature (C)	(F)
Perpendicular to columns	4	None		
Perpendicular to columns	2	50 hrs @ 1149C (2100F) in Air	538 >1094	1000 >2000
Parallel to columns	2	None		
Parallel to columns	2	50 hrs @ 1149C (2100F) in Argon	538 >1094	1000 >2000
Total Number of Samples: 10				

In order to measure thermal expansion perpendicular to the columnar ceramic structure, the EB-PVD ceramic was deposited on sacrificial 0.635 cm x 5.08 cm (0.25" x 2.0") PWA 286 panels (Figure 5). Boiling HCl was used to remove the ceramic deposit from the metal and polishing eliminated rough edges which could hinder dilatometer performance. Samples shorter than 4 cm (1.57") were measured by inserting a quartz extension to make up the difference in distance between the holder and the push rod of the dilatometer. Table IV presents the mean coefficient of thermal expansion (CTE) results at temperatures between 300 and 900C (572 and 1652F).

TABLE IV
THERMAL EXPANSION PERPENDICULAR TO THE CERAMIC COLUMNAR STRUCTURE

Sample	Exposure	Length (cm)	Mean CTE (ppm/C) @			
			300C	500C	700C	900C
1	Virgin (none)	2.164	10.1	10.4	10.6	10.7
2	Virgin (none)	1.716	9.9	10.2	10.6	10.8
3	Virgin (none)	1.945	9.9	10.3	10.5	10.7
4	Virgin (none)	4.862	10.2	10.4	10.6	10.7
Average	Virgin (none)		10.0	10.3	10.6	10.7
5	Argon (50 hrs 1149C)	1.678	9.9	10.5	11.0	11.3
6	Argon (50 hrs 1149C)	4.880	10.2	10.5	10.9	11.1
Average	Argon (50 hrs 1149C)		10.0	10.5	10.9	11.1

The error of these data is less than 5%. It is improved for samples 4 cm (1.57") or greater due to the elimination of the quartz extensions. Within the range of experimental error, the results show that the EB-PVD ceramic thermal expansion is insensitive to thermal exposure.

Continuous recording of the perpendicular sample lengths showed no heating/ cooling hysteresis (Figure 6), indicating the absence of ceramic phase transformation in the temperature range of measurement.

8

EB-PVD CERAMIC

MCRALY SUBSTRATE
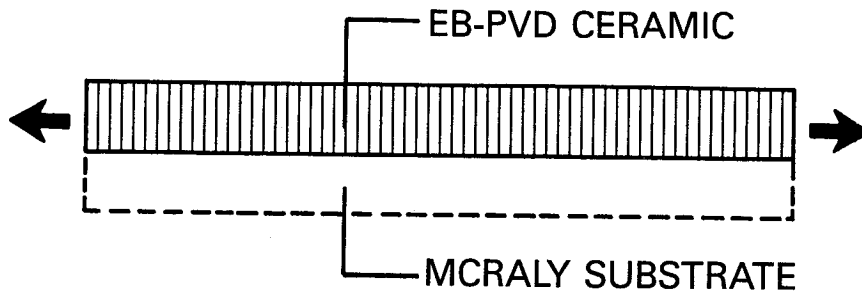
Figure 5.- Thermal Expansion Test Specimen Geometry for Measurement
Perpendicular to the Columnar Ceramic Structure. The EB-PVD ceramic
was deposited on sacrificial PWA 286 panels.

Multiply Y-scale by 100   Multiply X-scale by 1000

Change in length, microns

Temperature, °C   Sample:7Y
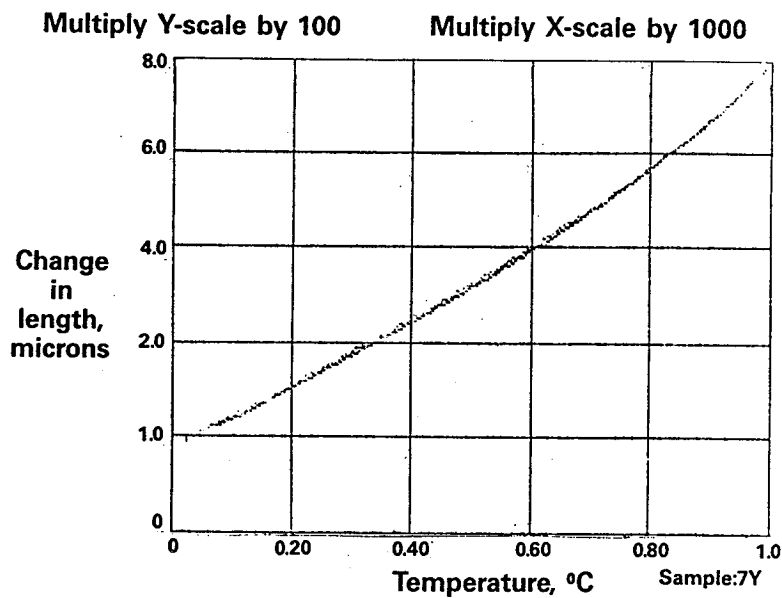
Figure 6.- Continuous Thermal Expansion Recording of Perpendicular Sample 1X.

PWA 1480

PWA 266
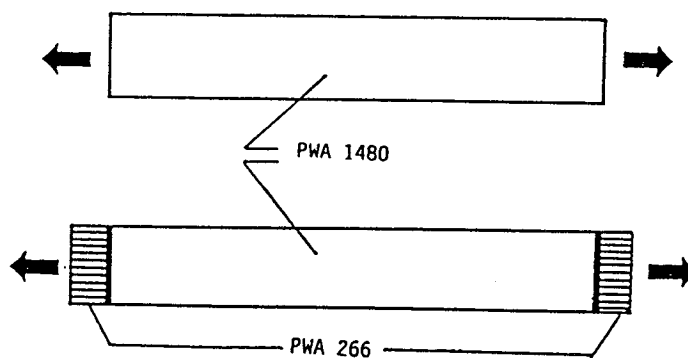
Figure 7.- Thermal Expansion Test Specimen Geometry for Measurement Parallel
to the Columnar Ceramic Structure. A comparative technique of
coated and uncoated substrates was used.

TABLE V
DIMENSIONAL MEASUREMENTS FOR PARALLEL THERMAL EXPANSION SAMPLES

Sample	Exposure	$L_{(tot)}$ (cm)	$L_{(bond)}$ (cm)	$L_{(cer)}$ (cm)	$L_{(sub)}$ (cm)
1Y	None	5.081	--	--	5.081
4Y	Argon (50 hrs @ 1149C)	5.085	--	--	5.085
2Y	None	5.097	0.015	--	5.082
6Y	None	5.097	0.015	--	5.082
8Y	Argon (50 hrs @ 1149C)	5.097	0.018	--	5.079
10Y	Argon (50 hrs @ 1149C)	5.096	0.013	--	5.083
3Y	None	5.466	0.018	0.378	5.070
7Y	None	5.484	0.020	0.386	5.078
5Y	Argon (50 hrs @ 1149C)	5.467	0.018	0.378	5.071
9Y	Argon (50 hrs @ 1149C)	5.479	0.015	0.394	5.070

TABLE VI
MEAN CTE FOR COMPOSITE STRUCTURES
USED IN PARALLEL THERMAL EXPANSION TESTS

Sample	Exposure	Mean CTE (tot) (ppm/C) @ 300C	500C	700C	900C
1Y	None	12.03	12.67	13.34	14.38
4Y	Argon (50 hrs @ 1149C)	12.20	12.78	13.23	14.22
2Y	None	12.10	12.69	13.17	14.12
6Y	None	12.16	12.74	13.23	14.18
8Y	Argon (50 hrs @ 1149C)	11.97	12.64	13.22	14.21
10Y	Argon (50 hrs @ 1149C)	12.19	12.70	13.28	14.21
3Y	None	11.93	12.43	13.05	13.98
7Y	None	11.83	12.44	13.02	13.94
5Y	Argon (50 hrs @ 1149C)	11.90	12.46	13.02	13.97
9Y	Argon (50 hrs @ 1149C)	11.78	12.40	13.02	13.99

The change in length of the composite samples is given by the following equation:

$$\Delta L_{(tot)} = \left\{ \alpha_{(sub)} L_{(sub)} + \alpha_{(cer)} L_{(cer)} + \alpha_{(bond)} L_{(bond)} \right\} \Delta T = \alpha_{tot} L_{tot} \Delta T \qquad \text{Equation 1}$$

where $\alpha_{(sub)}$, $\alpha_{(cer)}$, and $\alpha_{(bond)}$ = Thermal expansion of the substrate, ceramic, and bond coat, respectively, (ppm/C)

$L_{(sub)}$, $L_{(cer)}$, and $L_{(bond)}$ = Length of the substrate, ceramic, and bond coat, respectively (cm)

ΔL = Change in length (cm)

ΔT = Change in temperature (C)

The following three equations were used to determine the thermal expansion of each component in the thermal barrier coating system.

$$\alpha_{(sub)} = \alpha_{(tot)}$$

Equation 2

$$\alpha_{(bond)} = \left\{ \alpha_{(tot)} L_{(tot)} - \alpha_{(sub)} L_{(sub)} \right\} / L_{(bond)}$$

Equation 3

$$\alpha_{(cer)} = \left\{ \alpha_{(tot)} L_{(tot)} - \alpha_{(sub)} L_{(sub)} - \alpha_{(bond)} L_{(bond)} \right\} / L_{(bond)}$$

Equation 4

The CTE of the substrate was determined through Equation 2. Equation 3 was used to determine the CTE of the bond coat; data from samples 2Y and 6Y were used in Equation 3 to determine the CTE of the as-received bond coat, and data from samples 8Y and 10Y were used in Equation 3 to determine the CTE of thermally exposed bond coat. Subsequently, Equation 4 was employed to obtain the CTE for ceramic coated samples 3Y, 7Y, 5Y, and 9Y, representing as-received and thermally exposed samples. The resulting thermal expansion of the ceramic coating parallel to columnar structure (perpendicular to the plane of the coating) is listed in Table VII. Again, phase stability is evident due to the absence of a heating/cooling hysteresis in the thermal expansion curve (see Figure 8).

TABLE VII
THERMAL EXPANSION PARALLEL TO THE CERAMIC COLUMNAR STRUCTURE

Sample	Exposure	300C	Mean CTE (ppm/C) @ 500C	700C	900C
3Y	None	8.9	8.5	10.8	12.3
7Y	None	7.4	8.6	10.6	12.2
Average	None	8.2	8.6	10.7	12.2
5Y	Argon (50 hrs @ 1149C)	9.1	9.6	10.1	11.2
9Y	Argon (50 hrs @ 1149C)	7.7	8.9	10.0	11.1
Average	Argon (50 hrs @ 1149C)	8.4	9.2	10.0	11.2

For thermal expansion measurement of the coating perpendicular to the EB-PVD columns, the measurement did not involve the calibration of the dilatometer since the expansion of the composite sample was compared to that of the substrate. The accuracy of the coefficient of thermal expansion in this direction is less than that of the perpendicular measurements since the thickness of the coating is much smaller (0.384 cm or 0.151" average). The reproducibility of the total coefficient of thermal expansion is less than 1%, especially at higher temperatures. Two standard substrate/bond coat samples agreed to within 0.5% or better from 300 to 900C (572 to 1652F) (see Table V). Since the total sample length is 13 times longer than the EB-PVD ceramic coating, the expected reproducibility of the coefficient of thermal expansion in the parallel direction is approximately 10%. Hence, the difference between thermally pre-exposed and as-received samples in the parallel direction is not thought to be significant since it is within the estimated accuracy of the measurements.

Multiply Y-scale by 100   Multiply X-scale by 1000
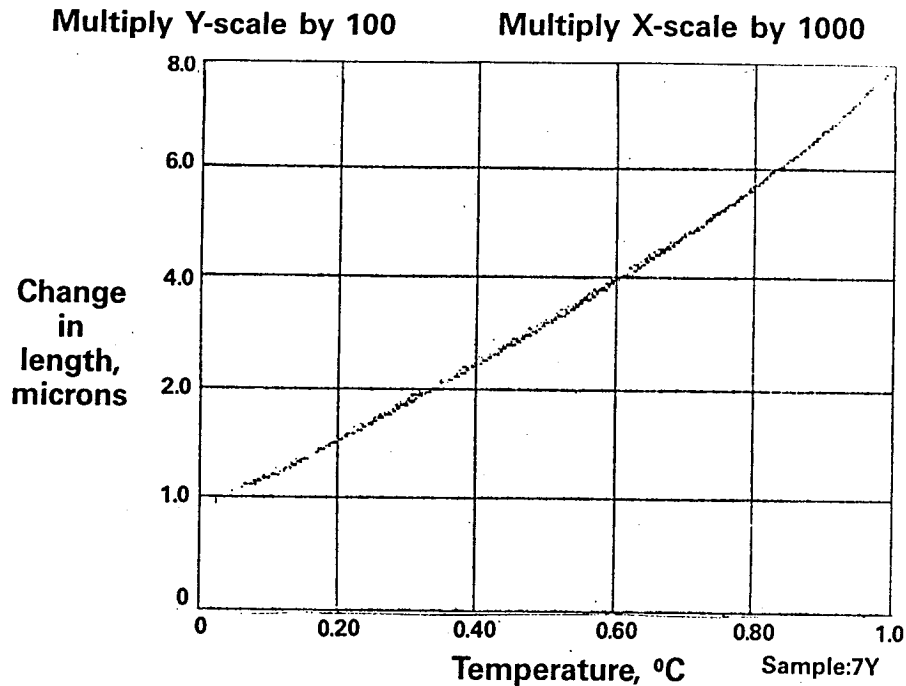
Figure 8.– Continuous Thermal Expansion Recording of Parallel Sample 7Y.

The in-plane and out-of-plane thermal expansion measurements were measured with a fused quartz dilatometer up to temperatures of 900C (1652F). Since modeling required readings up to 1094C (2100F), an additional measurement was performed using an alumina dilatometer up to 1200C (2192F) to note any inflections which would prevent extrapolation of the previous results. The change in lengthof the sample (in the direction perpendicular to the ceramic columns) is illustrated in Figure 9. Table VIII contains the mean CTE calculated from the alumina dilatometer results as well as from the quartz dilatometer results of this particular sample. The CTE exhibited a slight decrease at 1100C (2012F). Although measurements taken by the quartz dilatometer are more accurate than the alumina dilatometer, the difference between the two measurements are approximately 10% which is within the accuracy of the alumina dilatometer.

TABLE VIII
THERMAL EXPANSION OF THE EB–PVD CERAMIC MEASURED ON DIFFERENT SYSTEMS

Temperature (C)	Mean CTE (ppm/C) Alumina	Quartz
300	10.5	10.2
500	11.0	10.4
700	11.4	10.6
900	11.5	10.7
1000	11.6	––
1100	11.5	––
1200	11.3	––

MULT. Y-SCALE BY 100   MULT. X-SCALE BY 1000
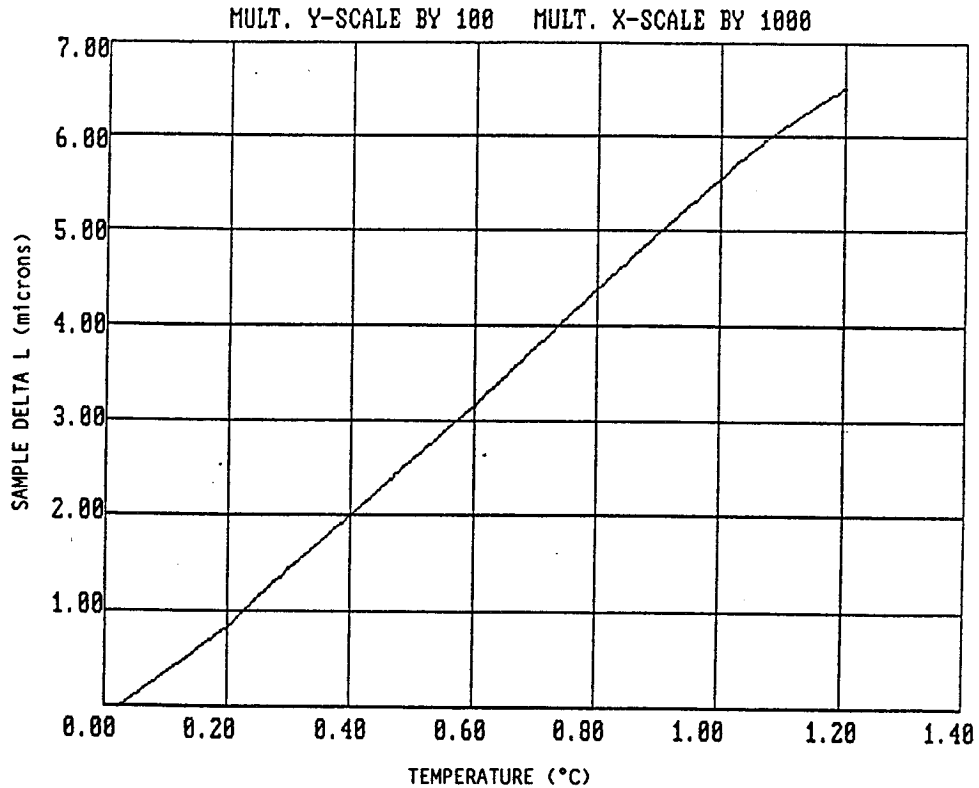
Figure 9.- Continuous Thermal Expansion Recording on an Alumina Dilatometer of a Perpendicular Sample

Thermal expansion results both parallel and perpendicular are shown in Figure 10. Included for reference are results obtained on plasma deposited ceramic in Phase I of this contract (Ref. 1). Within the range of experimental error (Table IX), these results show no significant difference between the expansion properties of the plasma and EB-PVD ceramic. The plasma deposited ceramic was reported in Phase I as having a phase composition of 55-60 v% f.c.c. zirconia and 45-50v% tetragonal zirconia. The EB-PVD ceramic is basically 100v% f.c.c. zirconia (see Section 3.3.2.1). Tetragonal zirconia could account for a slightly lower coefficient of thermal expansion since the monoclinic zirconia CTE = 6 ppm/C, the tetragonal zirconia CTE = 9 ppm/C, and cubic zirconia CTE = 10 ppm/C.

TABLE IX
THERMAL EXPANSION MEASUREMENTS OF EB-PVD CERAMIC
COMPARED TO PHASE I PLASMA SPRAYED CERAMIC

Temperature (C)	Plasma Sprayed Mean CTE (ppm/C)	EB-PVD Perpendicular to columns, % difference vs plasma	EB-PVD Parallel to columns, % difference vs plasma
300	9.82	+2%	-17%
500	9.64	+7%	-13%
700	9.88	+7%	+8%
900	10.19	+5%	+5%
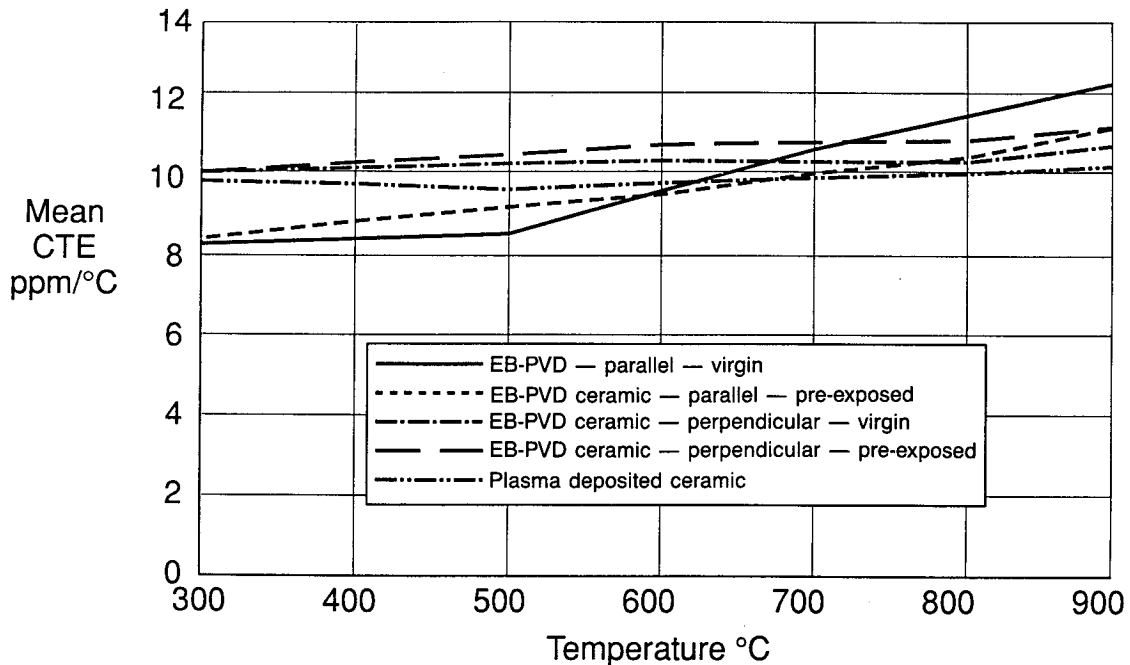
Figure 10.- Thermal Expansion of Seven Percent Yttria Stabilized Zirconia Coatings.

3.2.1.2 Ceramic Thermal Conductivity

Thermal conductivity tests were performed at Holometrix Inc. of Cambridge, Massachusetts, under subcontract. The tests were performed on virgin ceramic and also on ceramic that was thermally exposed at 1149C (2100F) for 50 hours in argon. Measurements were recorded in the direction of interest, along the length of the ceramic columns. Table X shows the thermal conductivity test plan matrix.

TABLE X
THERMAL CONDUCTIVITY TEST PLAN MATRIX

Number of Specimens	Temperature Thermal Pre-Exposure	(C)	(F)
3	None	538	1000
		871	1600
		$\geq$1094	$\geq$2000
2	50 hrs at 1149C (2100F) in argon	538	1000
		871	1600
		$\geq$1094	$\geq$2000

The steady state comparative method, ASTM E1225-87, was the thermal conductivity measurement technique used. A thermal heat flow circuit was used in this test since it is the analog to an electrical circuit with resistances in series. Inconel 718 was chosen as the reference material since its thermal conductivity is similar to that of the sample. These reference standards have the same cross-sectional dimensions as the sample (2.54 cm or 1" diameter) and are placed above and below the sample (Figure 11).

14
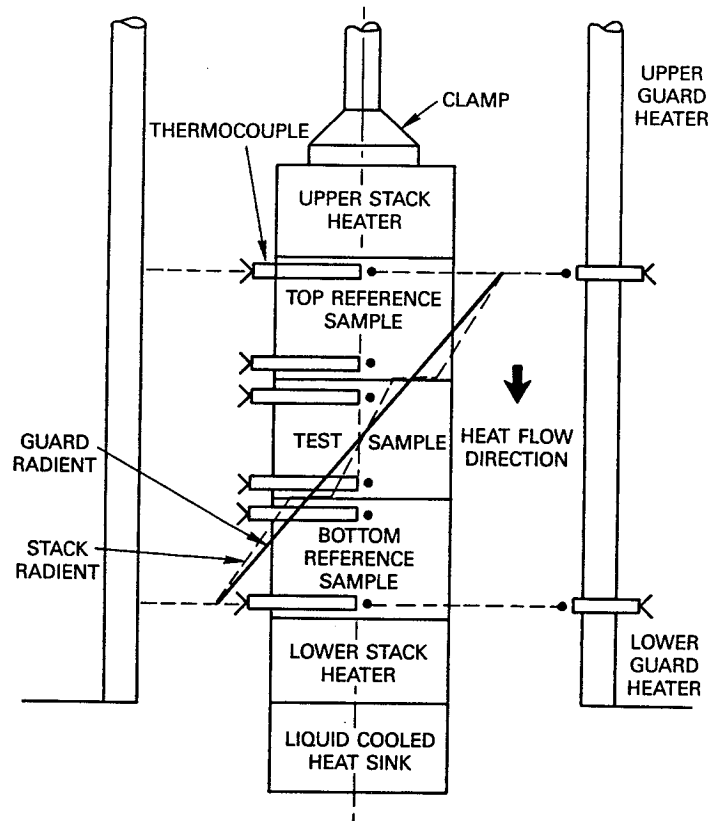
Figure 11.- Schematic Diagram of the Steady State Comparative Method, ASTM
E1225-87, for Thermal Conductivity Measurements.

Essentially, the EB-PVD ceramic and bond coat are deposited on both the top and
the bottom of the PWA 1480 substrate. Since the thermal conductivity knowledge
base of PWA 1480 is good, the substrate was used as a secondary heat meter as
well as the Inconel references. An upper heater, a lower heater, and a heat
sink are also incorporated into the stack as represented in Figure 11 in order
to complete the heat flow circuit.

In order to provide intimate contact between the sample coating and the refer-
ence material, the stack is clamped with a load applied to it and the coating
is polished with a 30 grit material. A guard tube is placed around the stack to
produce a linear flow of heat down the stack and to reduce the amount of radial
heat flow. The space remaining between the guard tube and the sample stack was
filled with insulating grains or powder.

This comparative method is essentially a steady state measurement of thermal
conductivity. Upon reaching equilibrium, the heat flux down the stack is
determined from the reference material. The heat into the sample is as follows:

$$Q_{(in)} = \lambda_{(top)}(dT/dx)_{(top)}$$

Equation 5

and the heat out of the sample is given by

$$Q_{(out)} = \lambda_{(bottom)}(dT/dx)_{(bottom)}$$

Equation 6

15

where λ = thermal conductivity
       dT/dx   = temperature gradient

       top refers to upper reference
       bottom refers to lower reference

$Q_{(in)}$ and $Q_{(out)}$ would be equal if the heat was confined solely to flow down the stack. If these two are in reasonable agreement, the average heat flow is calculated from

$$Q = \left(Q_{(in)} + Q_{(out)}\right)/2$$

                       Equation 7

The thermal conductivity of the sample is then calculated from

$$\lambda_{(sample)} = Q/(dT/dx)_{(sample)}$$

                       Equation 8

Temperature gradients along the stack are measured with type K (chromel/alumel) thermocouples placed in holes or grooves within the references and the sample. Three holes are placed within the substrate (see Figure 12) to extrapolate the temperature profile to the interface between the ceramic coating and the PWA 1480. Since the coating is in intimate contact with the substrate, interface resistance is minimal. One of the uncertainties in this measurement is the temperature of the thermocouple within the ceramic. This thermocouple is cemented into a 0.0381 cm (0.015") deep groove along the diameter of the free surface of the coating with the junction line at the centerline of the cylinder (Figure 12). As the heat flows across the microscopic points of intimate contact, the isotherms at the interface between the Inconel 718 and the coating are distorted. To provide a qualitative assessment of the number of points of intimate contact, surface roughness measurements of an EB-PVD ceramic thermal conductivity sample (polished down to 80 grit) was measured (Table XI). For comparison purposes, a plasma sprayed ceramic thermal conductivity sample of the same geometry (also polished) and a PWA 1480/PWA 266 burner rig bar were measured. The roughness measurements of the thermal conductivity specimens were post-test measurements; therefore, the results could be influenced slightly by residual material from testing (note the difference between the EB-PVD burner rig and thermal conductivity specimens). The groove introduces an uncertainty of approximately half of its depth, which is in this case, 10% of the thickness of the coating.
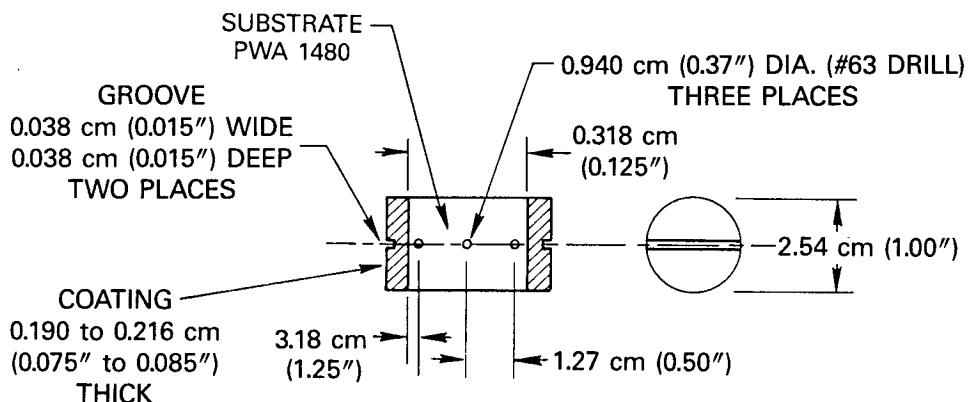
Figure 12.- PWA 266 Thermal Conductivity Sample Configuration.

TABLE XI

EB-PVD AND PLASMA SPRAYED CERAMIC SURFACE ROUGHNESS MEASUREMENTS

Specimen	Surface Roughness (microinch AA)
EB-PVD thermal conductivity specimen	114.5
EB-PVD erosion bar	106.8
Plasma Sprayed thermal conductivity specimen	20.2

Although the heat flux could be measured along the stack due to knowledge of the thermal conductivity of the reference samples, it was noted that the heat flux decreased as heat flowed down the stack. Techniques were incorporated to produce a more uniform flow of heat; the most effective of these being the introduction of isothermal plates extending from the stack out close to the guard at the height of the surface of the top heat meter and the bottom surface of the bottom heat meter. Although this technique improved uniform flow, a 10 to 20% variation still occurred along the stack.

In order to determine the thickness of the ceramic coating on the top and bottom of the sample substrate, the thickness of the sample was measured before and after ceramic deposition. This provides only the total thickness of the two coatings. Due to variations in the conductivity calculated from the average value of the coating thickness, it was obvious that the top and bottom coating layers were not equal in thickness. Therefore, the conductivity of the top and bottom layers were averaged and assigned to the average temperature of the two coatings. This is considered a valid procedure since there was only a 30 to 40C (54 to 72F) difference in temperature and the thermal conductivity varied very slowly with temperature.

The results of the thermal conductivity measurements are listed in Table XII. The high temperature data falls within a range of 1.80 to 2.05 W/mK, and over this temperature range, the conductivity decreases slightly. No significant difference in thermal conductivity values was observed between the thermally pre-exposed samples (4 and 5 exposed for 20 hours in argon at 1149C or 2100F) compared to the as-received samples (1, 2, and 3).

Thermal conductivity of the EB-PVD ceramic was compared to the plasma sprayed ceramic. In Phase I of the contract, the thermal conductivity was measured using a bulk sample. Since a composite sample was required for EB-PVD ceramic in Phase II to hold the ceramic in place, a composite plasma sprayed ceramic sample was tested for comparison purposes. The compilation of these measurements is listed in Table XIII. Figure 13 graphically compares the thermal conductivity measurements of these two ceramic TBC's. The EB-PVD ceramic has approximately 2.9 times the thermal conductivity of the plasma sprayed ceramic recorded in Phase I on a bulk sample and approximately 2 times the thermal conductivity of the plasma sprayed ceramic in the similar composite form. From these results it appears as though the composite sample may lead to slightly higher results.

TABLE XII
THERMAL CONDUCTIVITY OF 7YSZ EB-PVD CERAMIC COATING
AS MEASURED BY THE STEADY STATE COMPARATIVE METHOD ASTM E1225-87

Sample	Thickness (cm)	Thickness (in)	Temperature (C)	Temperature (F)	Thermal Conductivity (W/mK)	Thermal Conductivity Btu in/hr ft sq F)
1 As-received			110	230	1.69	11.97
	0.221	0.087	300	572	1.79	12.69
			538	1000	1.84	13.05
			545	1013	2.06	14.61
2 As-received			544	1011	2.04	14.46
	0.190	0.075	545	1013	2.04	14.46
			876	1609	1.98	14.04
			1018	1864	1.92	13.61
3 As-received			538	1000	1.97	13.97
	0.221	0.087	867	1593	1.78	12.62
4 Pre-exposed (*)			550	1022	1.98	14.04
	0.196	0.077	553	1027	2.00	14.18
			858	1576	1.84	13.05
			861	1582	1.90	13.47
			880	1616	1.96	13.90
			990	1814	1.79	12.69
5 Pre-exposed (*)			536	997	1.90	13.47
	0.190	0.075	863	1585	1.84	13.05
			1015	1859	1.82	12.90

(*) Thermally pre-exposed for 20 hours at 1149C (2100F) in argon

In order to verify the thermal conductivity of the EB-PVD ceramic as well as to obtain values at higher temperatures, the laser flash diffusivity method was used. This work was performed under subcontract at the Thermophysical Properties Research Laboratory at Purdue University. The specific heat of the EB-PVD ceramic was measured using a differential scanning calorimeter using sapphire as a reference material. The standard and sample, were subjected to the same heat flux and the differential power required to heat the sample at the same rate was recorded by a digital data acquisition system. The specific heat of the sample is computed from knowing the mass of the standard, the differential power, and the known specific heat of the sapphire standard. Essentially, this technique involves subjecting the front face of a small disc-shaped sample to a short laser burst and recording the resulting rear face rise in temperature. The highly developed apparatus at the Thermophysical Properties Research Laboratory consists of a Korad K2 laser, a high vacuum system including a bell jar with windows for viewing the sample, a tantalum tube heater surrounding a sample holding assembly, a spring-loaded thermocouple or an I.R. detector, appropriate biasing circuits, amplifiers, A-D converters, crystal clocks and a minicomputer based digital data acquisition system capable of accurately taking data in the 40 micro-second and longer time domain. The specific heat and the thermal diffusivity were then used to calculate the thermal conductivity of the EB-PVD ceramic. The results are listed in Table XIII. The EB-PVD thermal conductivity values

TABLE XIII
THERMAL CONDUCTIVITY OF EB-PVD AND PLASMA SPRAYED CERAMIC

| Temperature (C) | Comparative Method | | | Laser Flash EB-PVD (W/mK) |
	Bulk Plasma* (W/mK)	Composite Plasma (W/mK)	Composite EB-PVD (W/mk)	
23	--	--	--	1.79
100	--	--	--	1.81
110	--	--	.69	--
200	--	--	--	1.78
300	--	--	--	1.82
330	--	--	1.79	--
400	--	--	--	1.76
500	--	--	--	1.80
516	--	0.92	--	--
538	0.64	--	1.91	--
544	--	--	2.04	--
545	--	--	2.05	--
556	--	0.95	--	--
600	--	--	--	1.84
700	--	--	--	1.89
800	--	--	--	1.94
867	--	--	1.78	--
871	0.68	--	--	--
872	--	--	2.06	--
876	--	--	1.98	--
878	--	1.00	--	--
900	--	--	--	--
1000	--	--	--	1.99
1018	--	--	1.92	2.06
1100	0.66	--	--	--
1200	--	--	--	1.90
1400	--	--	--	1.83
1600	--	--	--	1.87
1800	--	--	--	1.93
1982	--	--	--	1.98

*The bulk plasma thermal conductivity results were reported in Ref. 1.

measured by the steady-state comparative method and the laser flash technique are in excellent agreement. Therefore, the difference between the bulk and the composite plasma sprayed ceramic thermal conductivity results as measured by the steady-state comparative method could be related to microstructural differences in the ceramic (i.e. porosity).

As shown in Figure 13, there is a significant difference between the conductivities of the two structures. This is attributed to the anisotropy of the EB-PVD ceramic as compared to the isotropic plasma structure (Figure 4). Nevertheless, very significant metal temperature reduction (Ref. 10) and durability benefits have been shown in engine testing of EB-PVD ceramic coated airfoils.

3.2.2 Task VB - Out-of-Plane Tensile Strength Evaluations

The effect of thermal pre-exposure on the EB-PVD ceramic coating adherence and failure was studied. These room temperature "pull tests" were used to obtain the interfacial strength values as well as to observe failure sites.
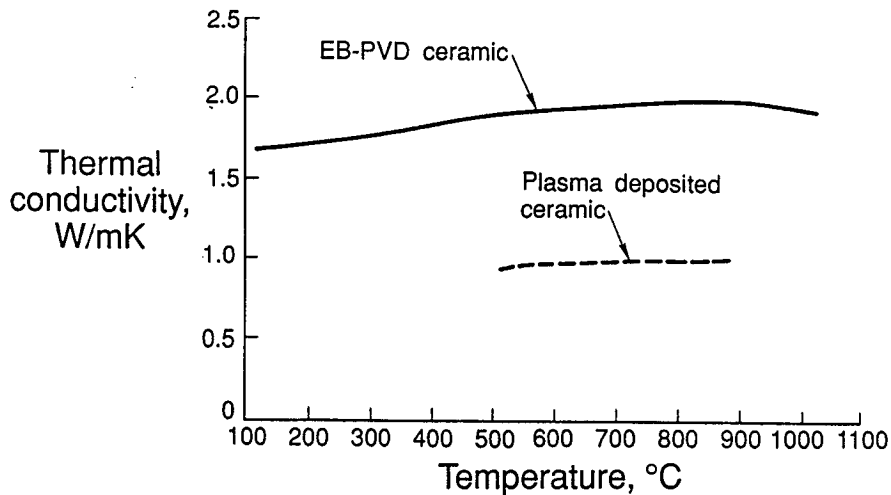
Figure 13.- Thermal Conductivity of Seven Percent Yttria Stabilized Zirconia
Coatings. Note the significant difference between the
conductivities of the two structures.

3.2.2.1 Out-Of-Plane Strength Tests

Spallation of EB-PVD ceramic TBC occurs by cracking at the thermally grown
oxide (TGO) layer (predominantly alumina)-metallic bond coat interface (Figure
14). This TGO grows between the metal and the EB-PVD ceramic layers during
prolonged thermal exposure. The results of the out-of-plane strength tests
helped to understand the cyclic failure mechanism(s).

Out-of-plane strength tests were designed to utilize a conventional tensile
machine. Flexible cable pull fixtures (Figure 15) were incorporated for
improved alignment. Samples consisted of two simple rod specimens. One piece
was a 0.635 cm (0.25") diameter rod machined from PWA 1480 and coated with
standard PWA 266 coating (see Figure 16). This PWA 266 coated piece was then
pre-exposed. The other piece was an aluminum pull pin of the same dimensions.
The aluminum pin was bonded to the ceramic surface using an organic adhesive
in a specially designed pull test bonding fixture (Figure 17). Tape was wrapped
around the PWA 1480/PWA 266 specimen to mask the edges and the sides of the
ceramic coating from the adhesive during bonding of the two pieces.

A total of 42 PWA 266 coated samples were out-of-plane strength tested. These
tests were conducted on as-deposited EB-PVD coatings and on coatings which were
thermally exposed for times and temperatures ranging from 20 to 500 hours and
from 1038 to 1149C (1900 to 2100F). The results are summarized in Table XIV.

Since the initial tests (samples 3, 4, and 6) illustrated that the as-coated
EB-PVD ceramic coating out-of-plane strength was stronger than the adhesives
available, the test matrix was adjusted to include thermal pre-exposures to
weaken the coating system. Specimen 5, thermally pre-exposed at 1038C (1900F)
for 20 hours, indicated that the adhesive strength was approaching the out-of-
plane strength of the coating. This specimen failed at 40.75 MPa (5910 psi)
with 60% cohesive failure within the adhesive, 10% of the adhesive attached to
the aluminum, and 30% of the adhesive attached to the ceramic (Figure 18).
Failure had initiated along the edge of the specimen. Further testing employed
more deleterious thermal pre-exposures.

20
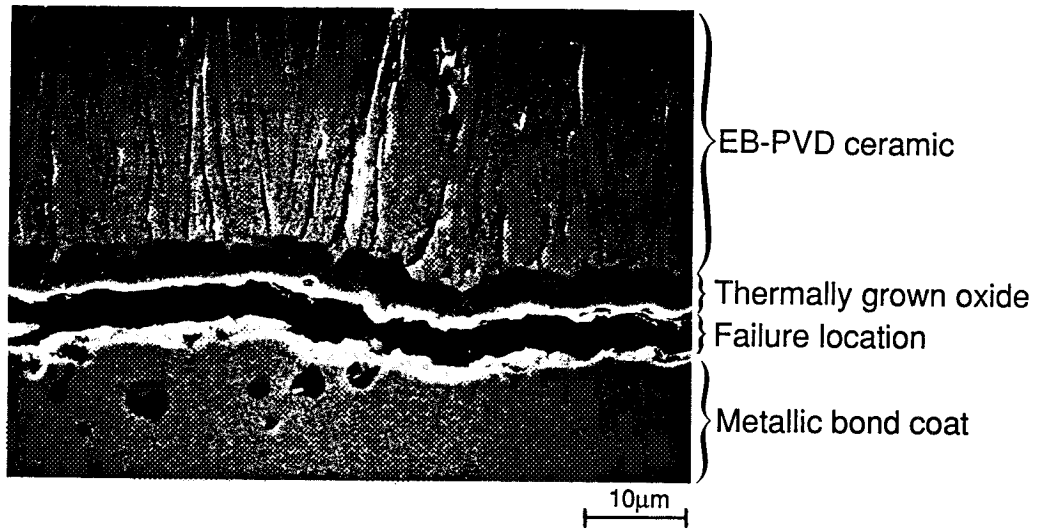
Figure 14.– Ceramic Spallation Failure Observed on Laboratory and Engine Test Components. Note separation at TGO–metal interface.
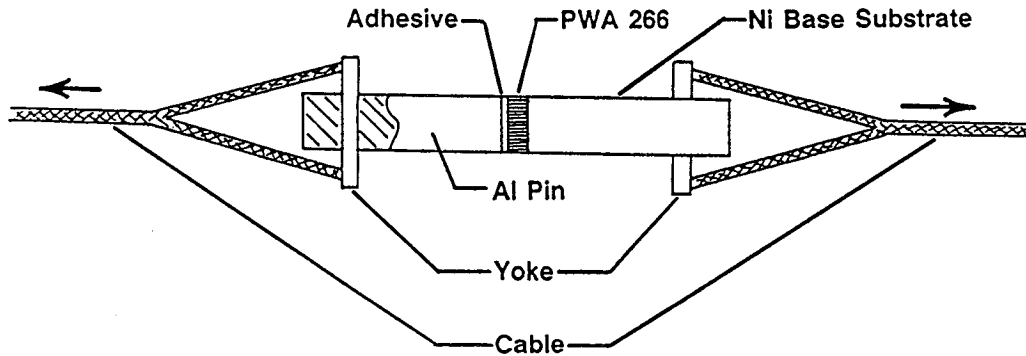
Figure 15.– Flexible Cable Pull Fixtures Improve Alignment of Out–of–Plane Strength Test Modified Tensile Machine Apparatus.
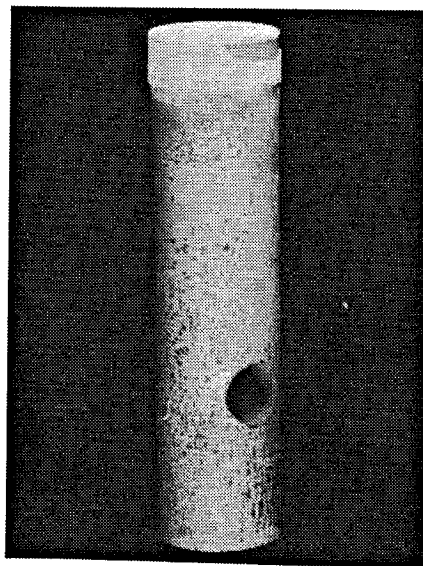
Figure 16.– PWA 1480/266 Processed Pull Test Pin for Out–of Plane Strength Tests.

WEIGHT

PWA 1480 PIN

CERAMIC COATING

ADHESIVE

HEAT CURE

ADHESIVE LAYER

ALUMINUM PIN
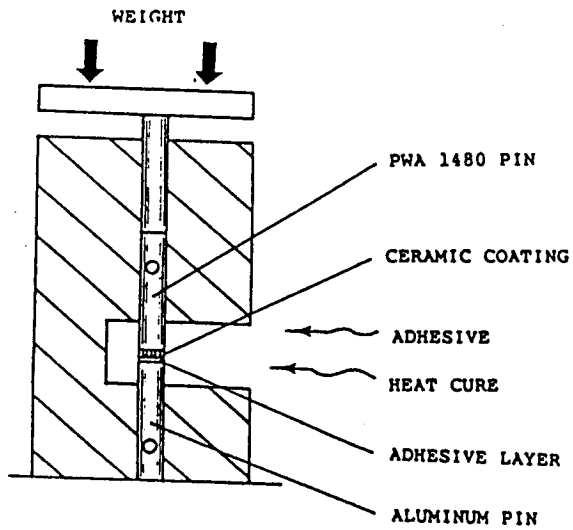
Figure 17a.- Pull Test Bonding
Fixture Schematic.
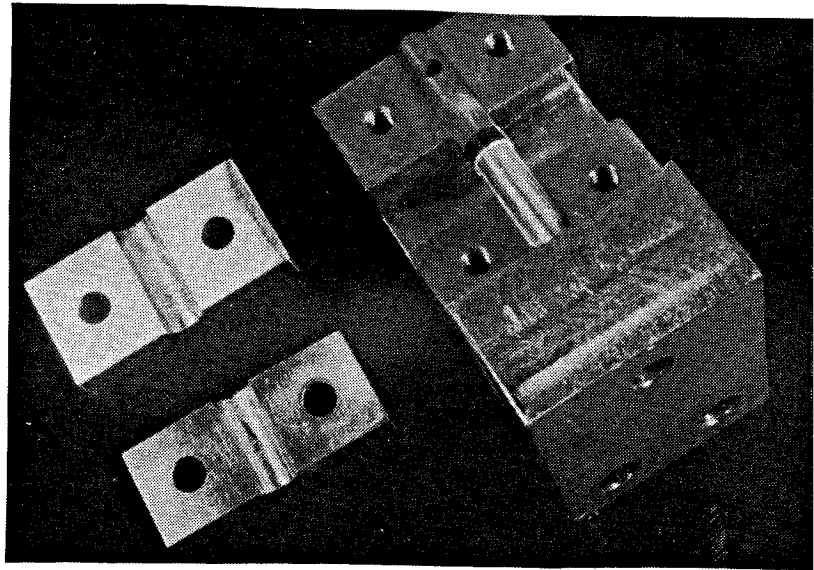
Figure 17b.- Pull Test Bonding Fixture Prepared
for Bonding.

Ceramic Edge Failure
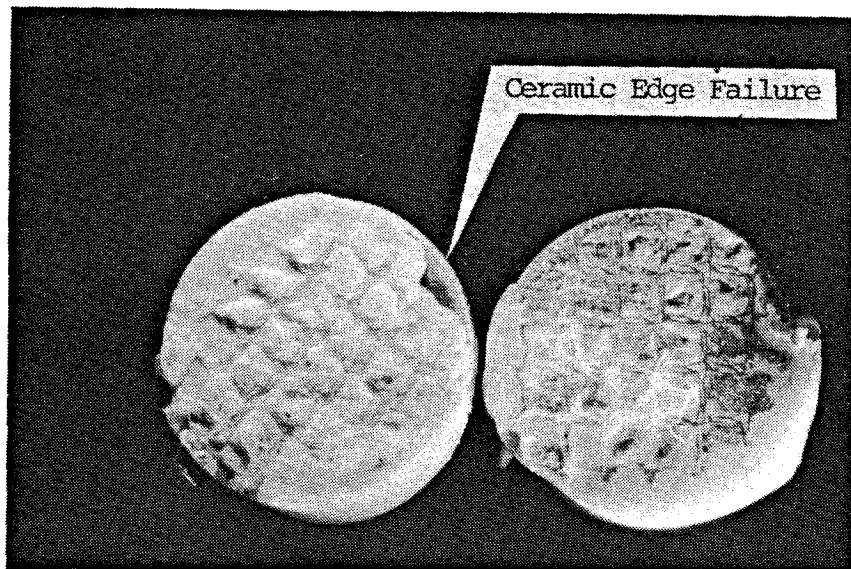
Figure 18.- Ceramic Edge Failure of 1038C(1900F)/20 Hours Thermally
Pre-exposed Pull Test Specimen Number 5.

TABLE XIV
PWA 266 EB-PVD TBC OUT-OF-PLANE STRENGTH TEST RESULTS

Spec. Number	Ceramic Thickness (mm)	(in)	Pre-Exposure Temperature (C)	(F)	Time (hrs)	Adhesive	Load (N)	(lbs)	Strength (MPa)	(psi)
3		0.0093	No pre-exposure			AF163		302	Adhesive fail	
4		0.0107	No pre-exposure			AF163		109	Adhesive fail	
5	0.254	0.0100	1038	1900	20*	EA9628	1290	290	Adhesive & bond	
6	0.246	0.0097	No pre-exposure			EA9628	1348	303	Adhesive & bond	
7	0.236	0.0093	Furnace failed							
8	0.254	0.0100	Furnace failed							
9	0.244	0.0096	Furnace failed							
10	0.254	0.0100	Furnace failed							
11	0.249	0.0098	1149	2100	50	EA9628	956	215	30.20	4380
12	0.233	0.0092	1149	2100	50	EA9628	1312	295	41.44	6011
13	0.221	0.0087	1149	2100	100	EA9628	814	183	25.75	3735
14	0.254	0.0100	1149	2100	50	EA9628	1148	258	36.30	5265
15	0.241	0.0095	1149	2100	50	EA9628	1290	290	40.74	5909
16	0.224	0.0088	1149	2100	100	EA9628	1090	245	34.42	4992
17	0.213	0.0084	1149	2100	100	EA9628	1014	228	32.03	4646
19	0.262	0.0103	1149	2100	100	EA9628	1085	244	34.28	4972
20	0.241	0.0095	1149	2100	200#	EA9628	1179	265	37.23	5400
21	0.254	0.0100	1149	2100	200#	EA9628	1023	230	32.34	4690
22	0.236	0.0093	1149	2100	200#	EA9628	712	160	22.48	3260
23	0.246	0.0097	1149	2100	200#	EA9628	845	190	26.68	3870
24	0.264	0.0104	1149	2100	100#	EA9628	1112	250	35.16	5100
25	0.264	0.0104	1149	2100	100#	EA9628	409	92	12.69	1840
26	0.254	0.0100	1149	2100	100#	EA9628	921	207	29.10	4220
27	0.264	0.0104	1149	2100	100#	EA9628	730	164	23.03	3340
28	0.234	0.0092	1149	2100	50#	EA9628	Handling failure			
29	0.279	0.0110	1149	2100	50#	EA9628	814	183	25.72	3730
30	0.259	0.0102	1149	2100	50#	EA9628	676	152	21.37	3100
31	0.269	0.0106	1149	2100	50#	EA9628	912	205	28.82	4180
32	0.262	0.0103	1038	1900	500	EA9628	712	160	22.48	3260
33	0.264	0.0104	1038	1900	500	EA9628	867	195	27.37	3970
34	0.269	0.0106	1038	1900	500	EA9628	1076	242	33.99	4930
35	0.259	0.0102	1038	1900	500	EA9628	1290	290	40.75	5910
36	0.251	0.0099	1149	2100	20#	EA9628	1045	235	33.02	4790
37	0.269	0.0106	1149	2100	20#	EA9628	934	210	29.51	4280
38	0.277	0.0109	1149	2100	20#	EA9628	1036	233	32.75	4750
39	0.259	0.0102	1149	2100	20#	EA9628	721	162	22.75	3300
40	0.254	0.0100	1149	2100	1hr cyc	EA9628	Coating failed @18 cyc			
41	0.274	0.0108	1149	2100	1hr cyc	EA9628	Coating failed @18 cyc			
42	0.302	0.0119	1149	2100	1hr cyc	EA9628	Coating failed @18 cyc			
43	0.264	0.0104	1149	2100	1hr cyc	EA9628	Coating failed @18 cyc			
44	0.262	0.0103	1149	2100	10hr cyc	EA9628	Coating failed @2 cyc			
45	0.262	0.0103	1149	2100	10hr cyc	EA9628	Coating failed @2 cyc			

(*) - No slow cool
(#) - Furnace failure at 760C (1400F) during slow cool cycle

Considerable care was required to retain ceramic and oxide layers on thermally exposed specimens during cool-down after removal from the furnace. Whereas the EB-PVD ceramic has exceptional resistance to cyclic thermal spallation, its tolerance to static exposure is limited for the specimen geometry used in this test. The sensitivity to static exposure seemed to be related to the interface stresses which arise at the specimen free edges. Spallation during cool-down from furnace exposure could be prevented by very slow cooling. Specimens 11 through 39 incorporated a slow cool cycle (56C/24 hours or 100F/24 hours) to avoid spallation associated with rapid cooling of samples exposed at high temperatures. Furnace failures plagued the testing during the static thermal pre-exposure (samples 7-10) so that the time at temperature was not known. Furnace failures also affected the slow cool of samples 20-31 and 36-39. These particular samples were slowly cooled to 760C (1400F) whereupon a furnace failure caused a quench to room temperature. It appears as though this rapid cool from 760C (1400F) produced a larger scatter in the data compared to comparative tests with the correct slow cool cycle. The fact that thermal exposure reduces the adherence strength substantiates the theory that oxidation of the coating ultimately reduces PWA 266 coating life.

Cyclic thermal pre-exposure tests were conducted to test the effect of thermal cycles on the out-of-plane strength of PWA 266. A 1 hour/20 cycle pre-exposure at 1149C (2100F) was attempted; however, the specimens (samples 40-43) failed upon completion of 18 cycles. To correlate with the 1149C (2100F) furnace test, a 10-hour cyclic furnace pre-exposure was also selected (samples 44 and 45). These samples, however, failed upon 2 cycles in contrast to the furnace specimens exposed to the same conditions which did not fail until the completion of 9 cycles (see Section 3.3.1.4). This difference in coating life was attributed to the difference in specimen geometry. This specimen geometry effect prevented a thorough cyclic out-of-plane strength investigation.

Out-of-plane test specimen failure occurred at the thermally grown oxide-metallic bond coat interface, which accurately simulated the failure mode seen in engine and rig testing (Figures 19a-e and 20a-e). X-ray maps of the nickel pull test pin from samples 13 and 14 indicate the presence of bond coat at the failure site (Figure 21 and 22, respectively). The x-ray maps of the respective aluminum pull test pins indicate thermally grown oxide is present (Figures 23 and 24, respectively). The aluminum pin from the 50-hour pre-exposure, however, exhibited more exposed zirconia than the sample that had additional thermal exposure. The zirconia present is thought to be the EB-PVD ceramic coating showing through the thermally grown oxide layer.

Typical surface failure topographies of these pull tests were compared to typical failure topographies obtained from burner rig testing and furnace testing. A hot time trend was noted with the surface features. In general, the fracture surface was more planar with increased hot time and oxide thickness (Figures 25-35). The exception to this observation was the 2.54 cm (1") burner rig HSTC2-04 strain cycles specimen (Figure 26, see Section 3.4.2.2 for additional details) which failed by two mechanisms in localized regions, one hot failure and one room temperature failure. It is possible that the ceramic chips were taken from the room temperature failure location for analysis and thus would not correlate with the other specimens. The FTSB-28 furnace specimen (Figure 35, see Section 3.3.1.3 for additional details), which was exposed to elevated temperatures for an order of magnitude longer, also did not correlate

with the increased time/ smoother surface observations. Test conditions and corresponding SEM photographs of the thermally grown oxide surface are listed in Table XV. Generally, based on the failure surface data, a progressive oxide or time-dependent process is appropriate for failure modeling. However, there was essentially no dependence of strength on exposure time, once there has been some reasonable amount of oxidation exposure, i.e. >20 hours (Figure 36). This suggests that the fracture at the thermally grown oxide-metallic bond coat interface is due to the presence of edge induced stress intensity.

TABLE XV
EB-PVD CERAMIC COATING SYSTEM FRACTURE SURFACES COMPARISON

Sample	Test Type	Temperature (C)	(F)	Cycles	Hot Hours	Section	Figure
HSTC2-30	Strain	1177	2150	1474	12	3.4.2.2	25
HSTC2-04	Strain	1177	2150	1728	14	3.4.2.2	26
HSTC2-28	Strain	1121	2050	2422	20	3.4.2.2	27
HSTC2-09	Strain	1177	2150	2658	22	3.4.2.2	28
HSTC2-06	Oxide	1107	2025	1258	52	3.4.2.2	29
HSTC2-02A	Oxide	1107	2025	3307	94	3.4.2.2	30
Pin # 16	Oxide	1149	2100	1	100	3.2.2.1	31
HSTC2-16	Mixed Mode	1079	1975	2839	364	3.4.2.2	32
HSTC2-02	Oxide	1107	2025	4109	527	3.4.2.2	33
HSTC2-21	Oxide	1107	2025	1575	570	3.4.2.2	34
FTSB-28	Oxide	1149	2100	1	1800	3.3.1.3	35

KEY: HSTC2-# = One-Inch Burner Rig Specimen (Section 3.4.2.2)
      Pin # = Out-of-Plane Strength Test Specimen (Section 3.2.2.1)
      FTSB-# = Furnace Specimen
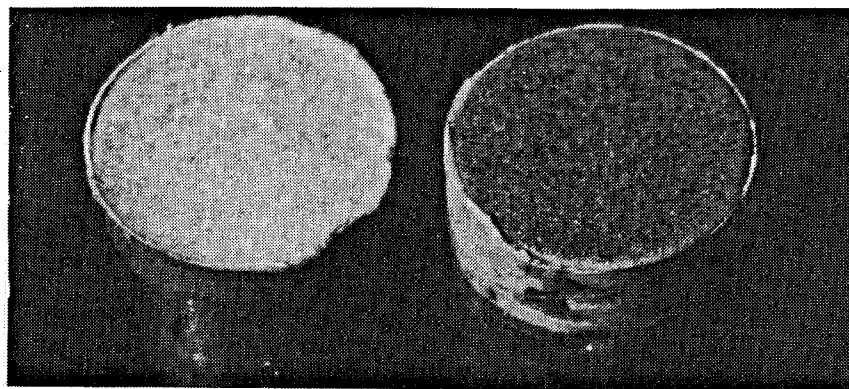
a. Al pin   (6x)   Ni pin   (6x)
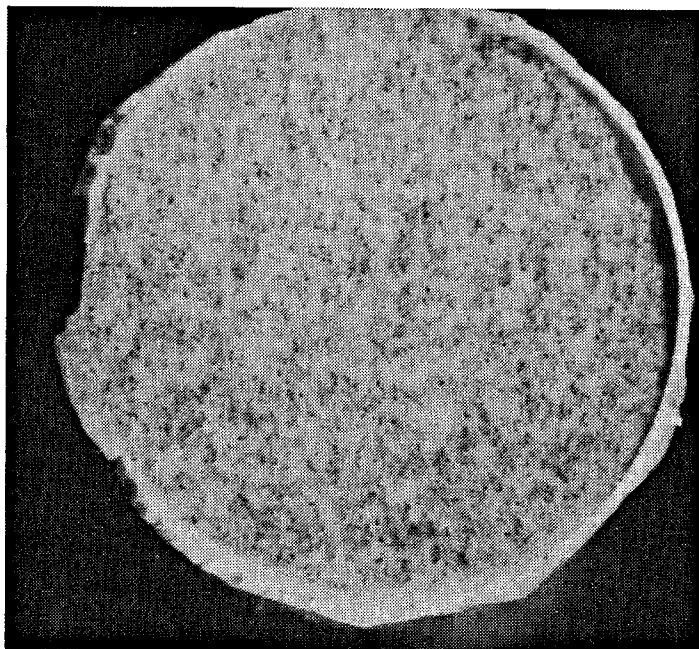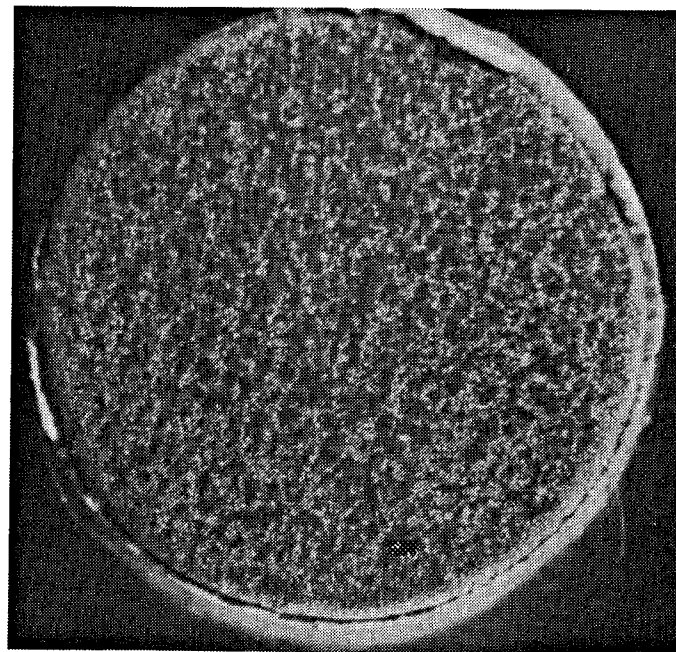
b. Al pin. (12x)   c. Ni pin. (12x)

Figure 19.- Sample 14 PWA 1480/266, Heat Treated for 50 StaticHours at 1149C
           (2100F) in Air, Failed at 36.30 MPa (5265 psi)in the Out-of-Plane
           Strength Test Between the Thermally Grown Oxide and the Metallic
           Bond Coat.

Figure 19.- Continued

d. Al pin showing adherent thermally grown oxide. (30x)

e. Ni pin showing adherent metallic bond coat. (30x)

27
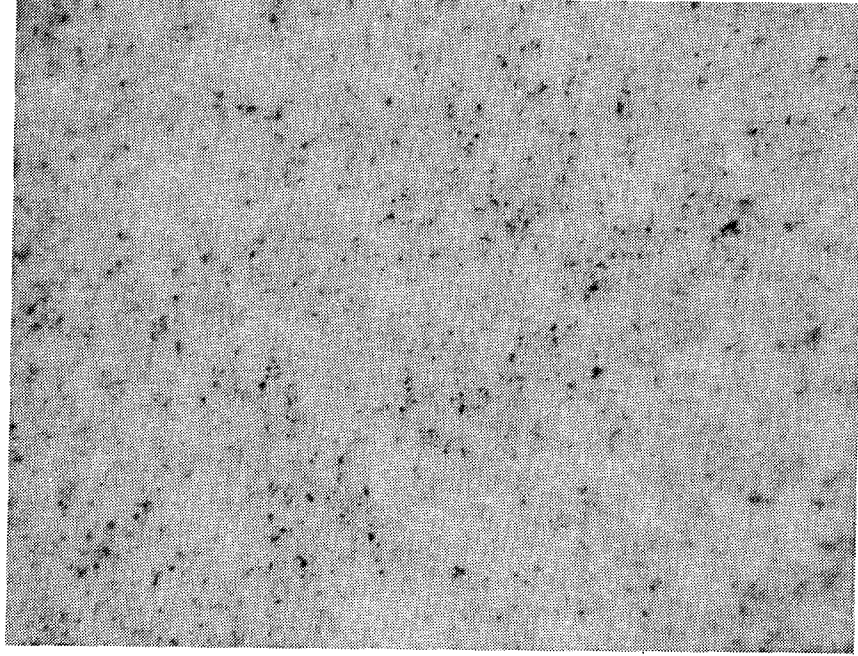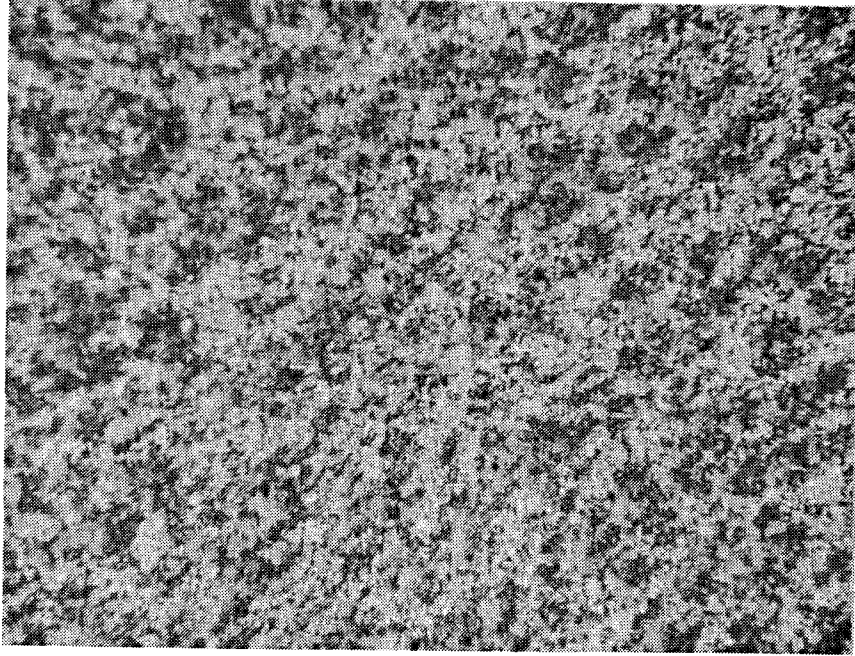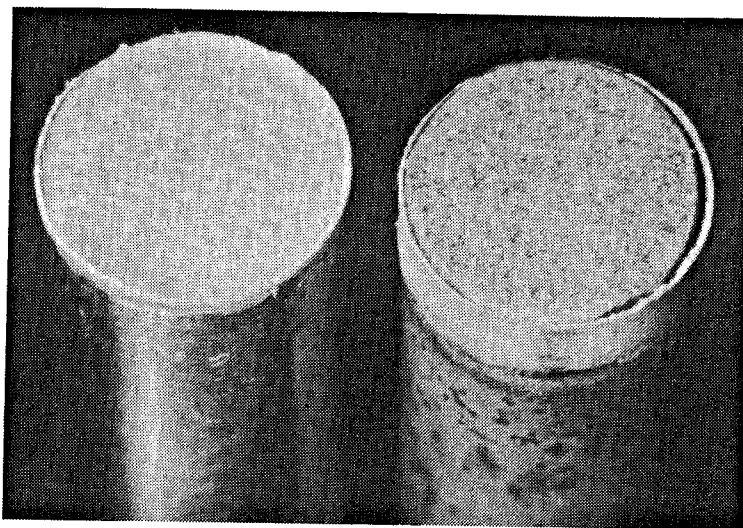
a. Al pin   (6x)   Ni pin   (6x)
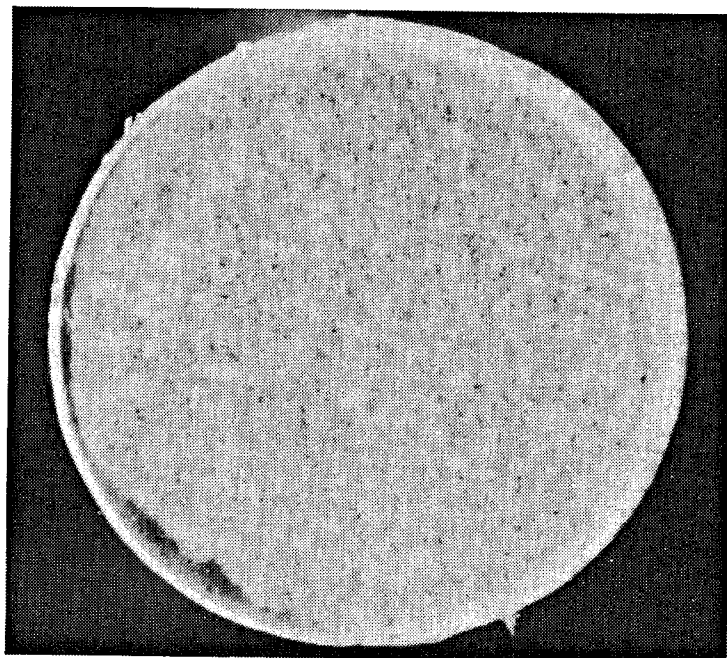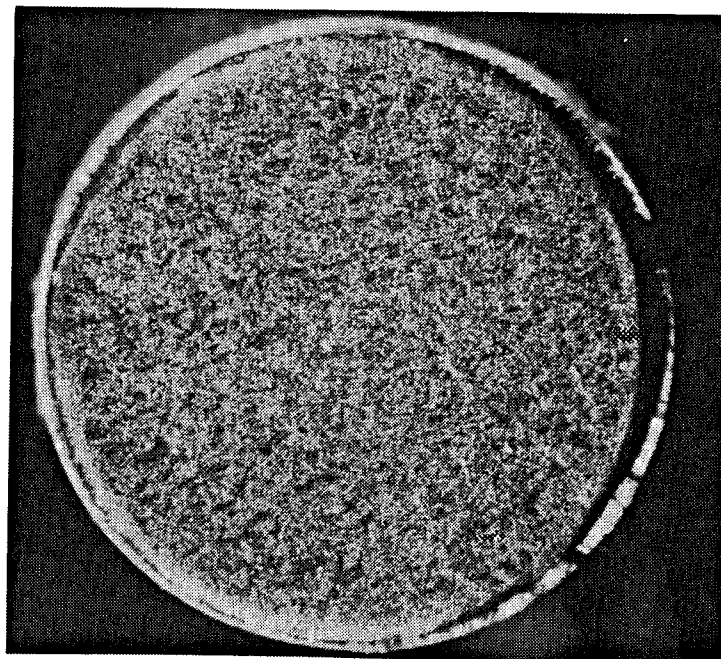
b. Al pin (12x)   c. Ni pin (12x)

Figure 20.- Sample 13 PWA 1480/266, Heat Treated for 100 Static Hours at 1149C
(2100F) in Air, Failed at 25.75 MPa (3735 psi) in the Out-of-Plane
Strength Test Between the Thermally Grown Oxide and the Metallic
Bond Coat.

28

(a) (100x)

(b) Al Map (100x)

(c) Ni Map (100x)

(d) Cr Map (100x)

Figure 21.- X-ray Maps of Post-Test PWA 266 Coated PWA 1480 Pull Test Pin Number 13 Pre-exposed for 50 Hours at 1149C (2100F) in Air.
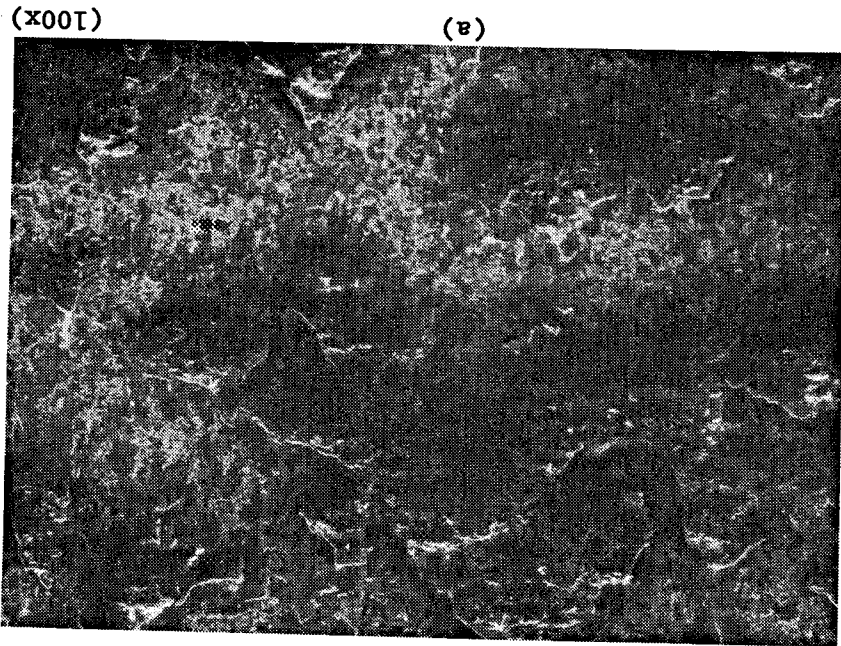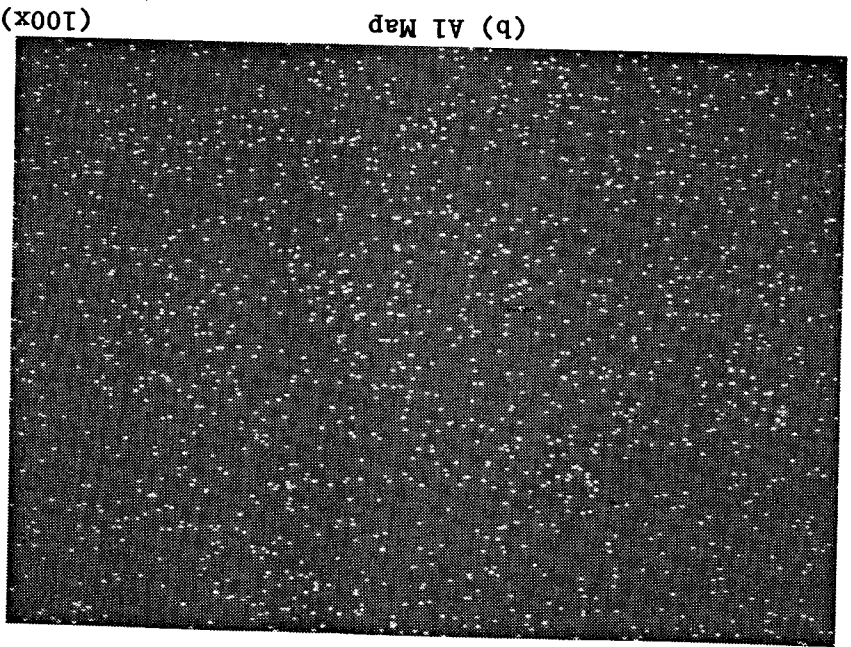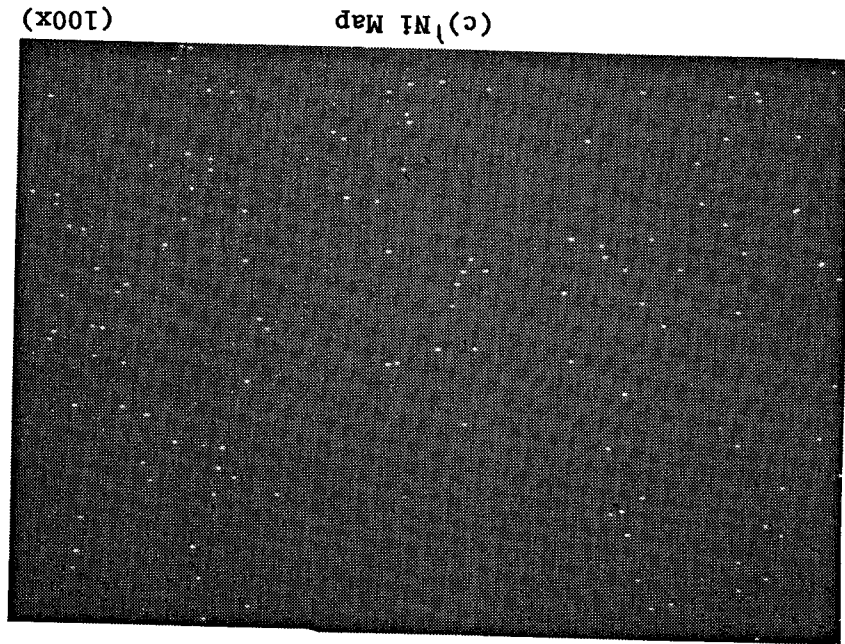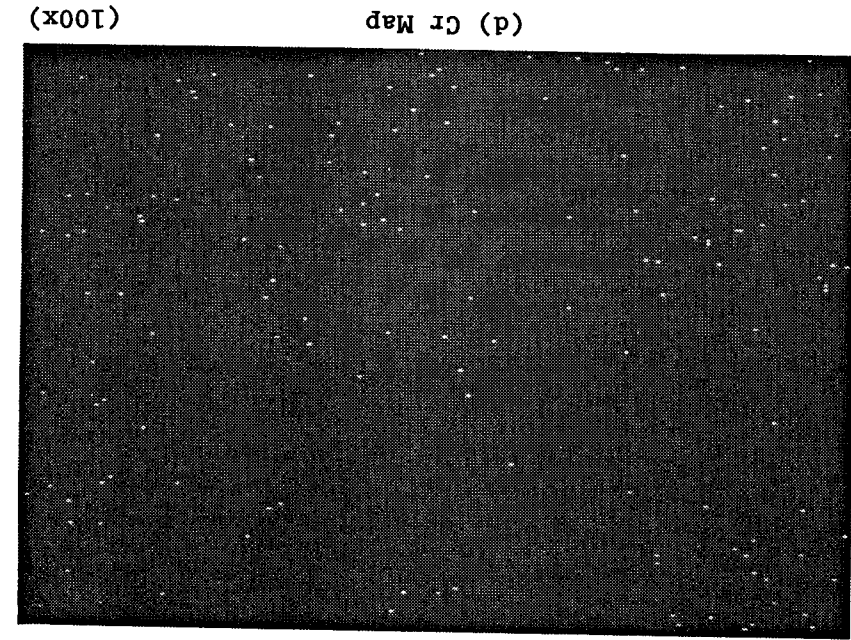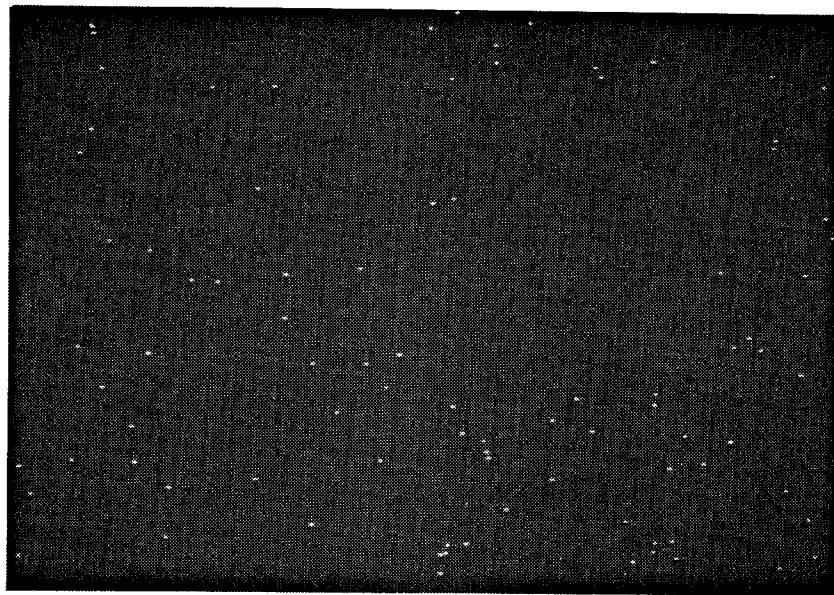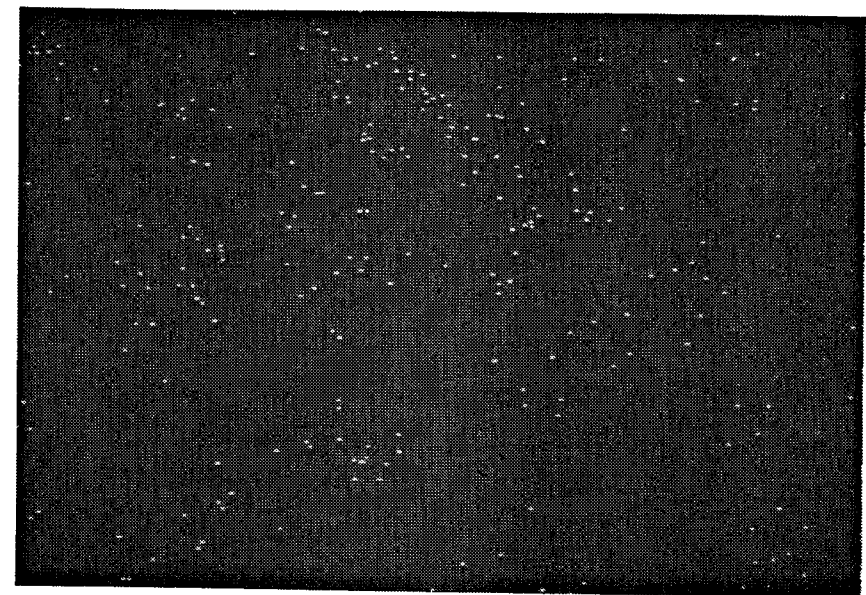
(e) Co Map   (100x)   (f) Zr Map   (100x)

Figure 21.- Continued
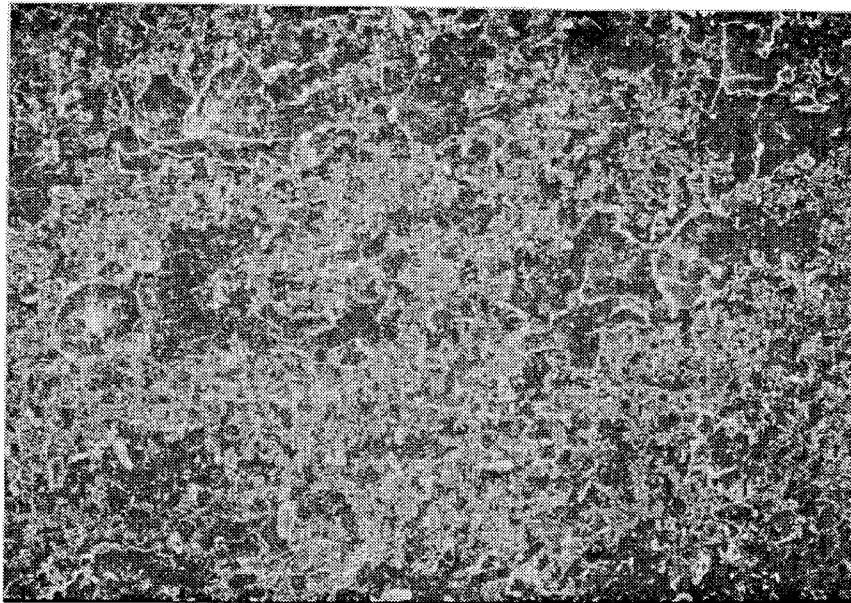
(a)   (100x)
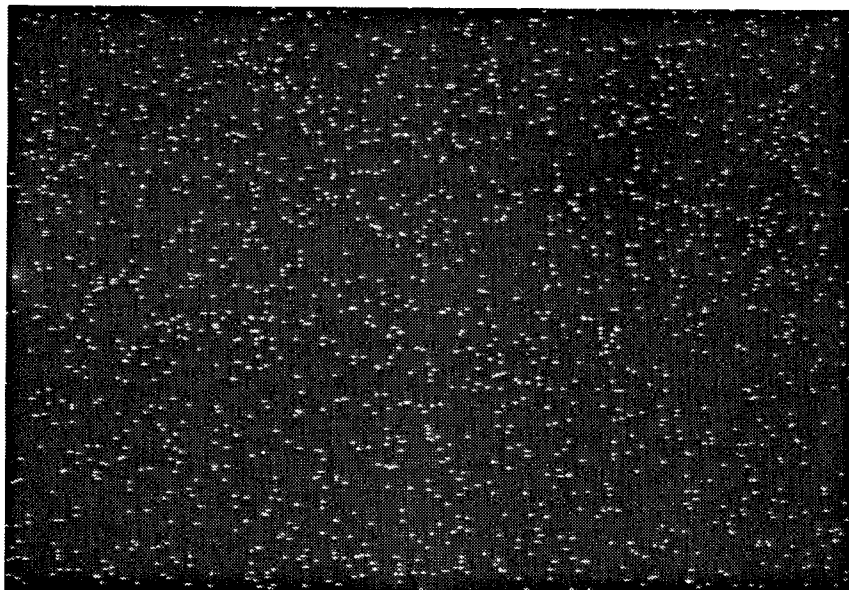
(b) Al Map   (100x)
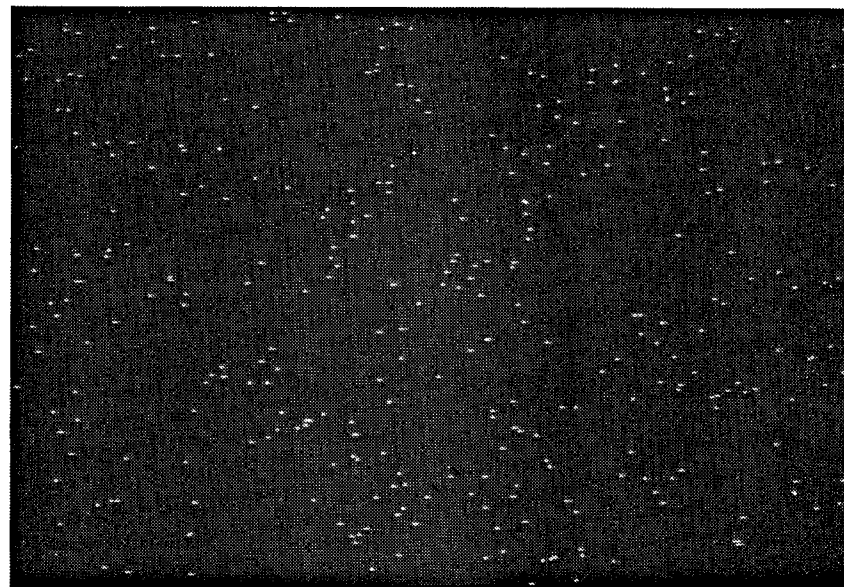
(c) Ni Map   (100x)

Figure 22.- X-ray Maps of Post-Test PWA 266 Coated PWA 1480 Pull Test Pin
Number 14 Pre-exposed for 50 Hours at 1149C (2100F) in Air.
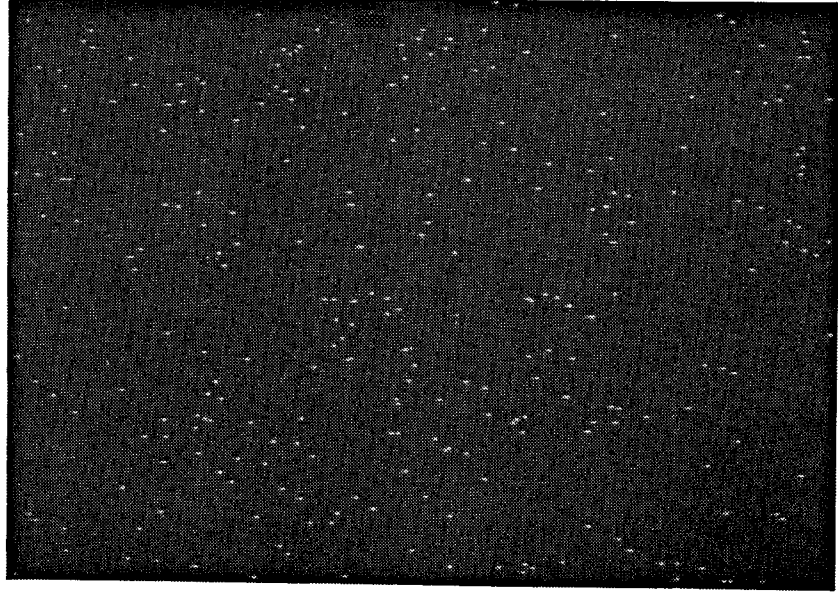
(d) Cr Map (100x)
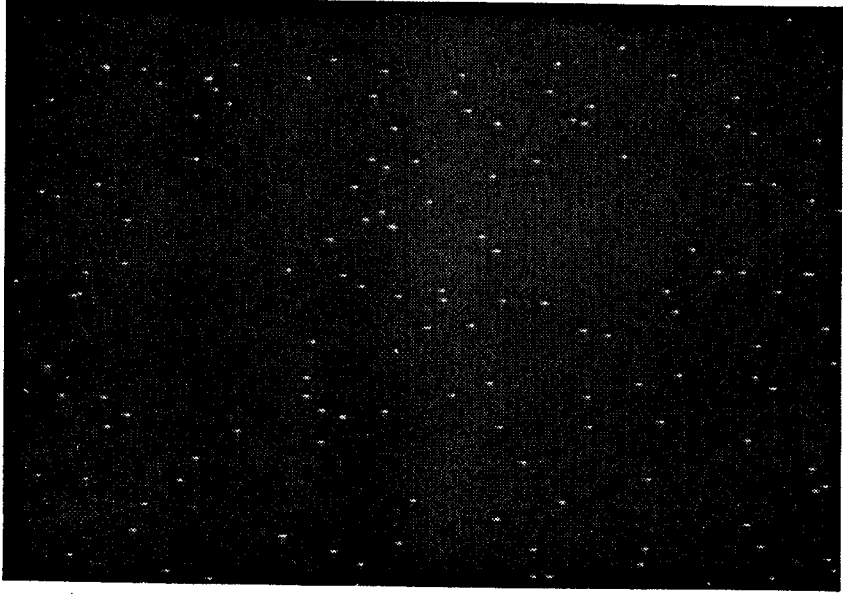
(e) Co Map (100x)

Figure 22.- Continued
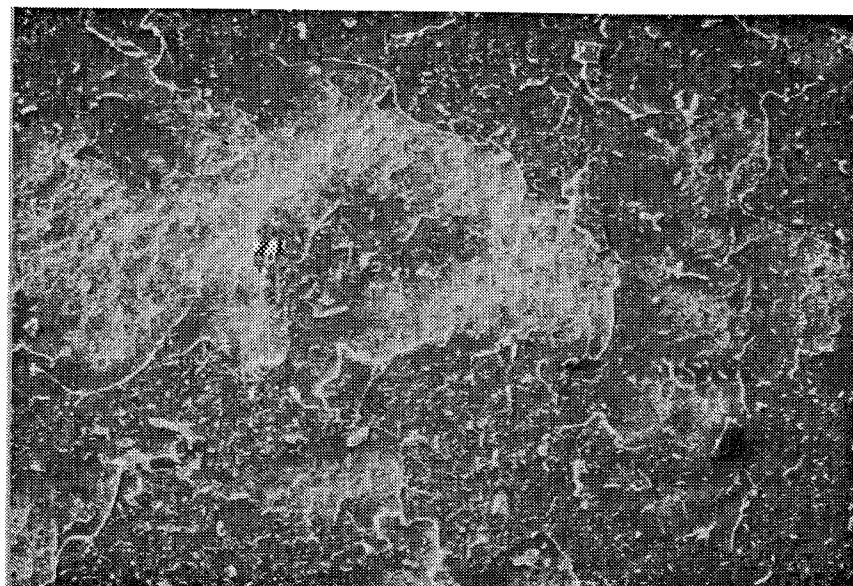
(a)   (100x)
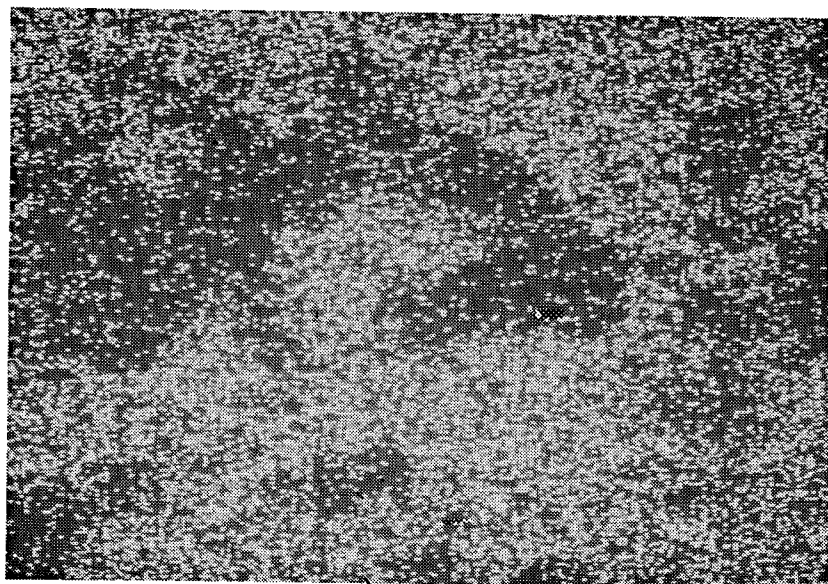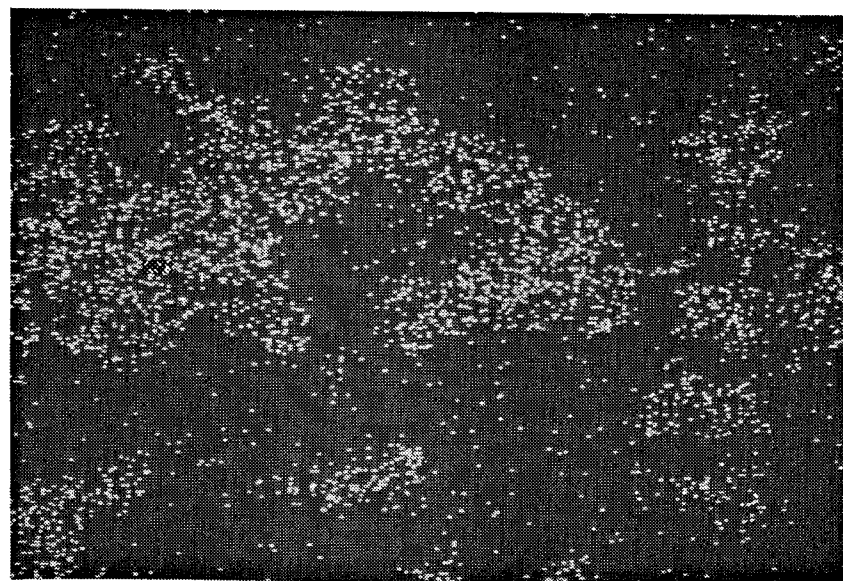
(b) Al Map   (100x)   (c) Zr Map   (100x)

Figure 23.- X-ray Maps of Post-Test Aluminum Pull Test Pin Number 13
Pre-exposed for 50 Hours at 1149C (2100F) in Air.

Figure 24.– X-ray Maps of Post-Test Aluminum Pull Test Pin Number 14
Pre-exposed for 100 Hours at 1149C (2100F) in Air.

(c) Zr Map   (100x)

(b) Al Map   (100x)

(a)   (100x)

35
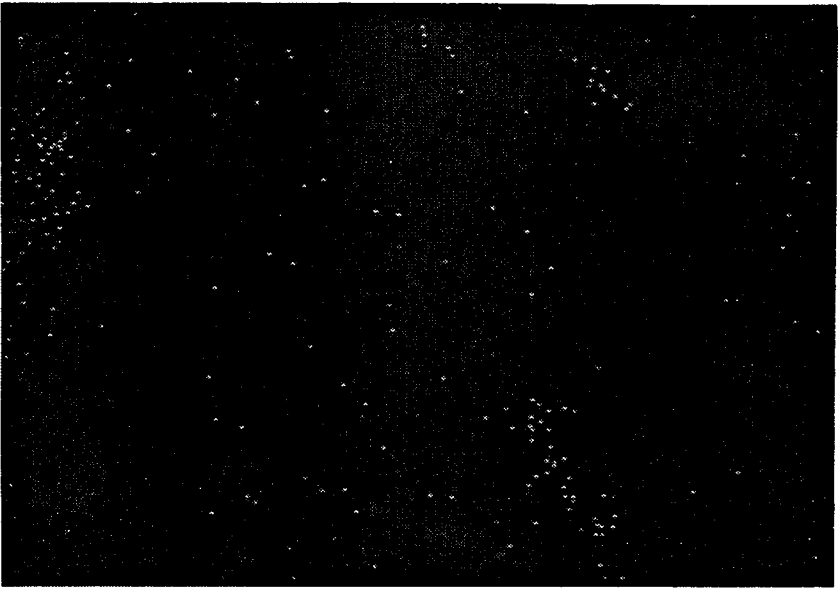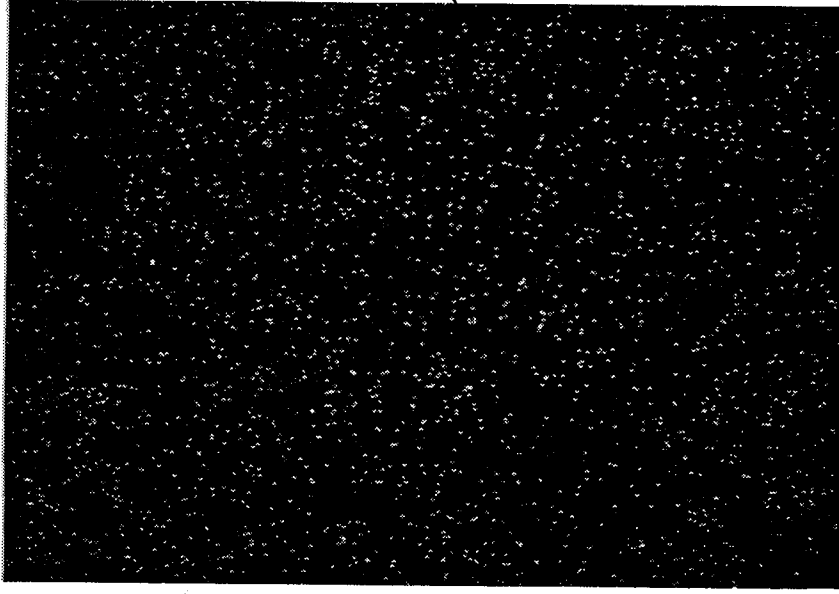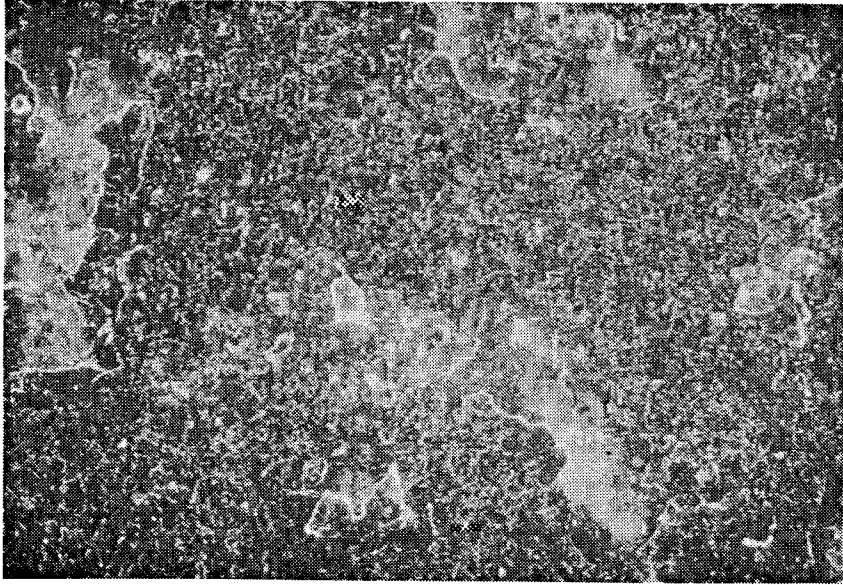
Figure 25.- SEM Photomicrograph of the Thermally Grown Oxide Surface of a Ceramic Chip from Failed Specimen HSTC2-30, Strain Emphasis 0.254 cm (One-Inch) Burner Rig Test at 1177C (2150F) for 1474 Cycles and 12 Hot Hours. (100x)

Figure 26.- SEM Photomicrograph of the Thermally Grown Oxide Surface of aCeramic Chip from Failed Specimen HSTC2-04, Strain Emphasis 0.254 cm (One-Inch) Burner Rig Test at 1177C (2150F) for 1728 Cycles and 14 Hot Hours. (100x)

36

Figure 27.- SEM Photomicrograph of the Thermally Grown Oxide Surface of a
Ceramic Chip from Failed Specimen HSTC2-28, Strain Emphasis
0.254 cm (One-Inch) Burner Rig Test at 1121C (2050F) for 2422
Cycles and 20 Hot Hours. (100x)

Figure 28.- SEM Photomicrograph of the Thermally Grown Oxide Surface of a
Ceramic Chip from Failed Specimen HSTC2-09, Strain Emphasis 0.254
cm (One-Inch) Burner Rig Test at 1121C (2050F) for 2658 Cycles and
22 Hot Hours. (100x)

37

Figure 29.- SEM Photomicrograph of the Thermally Grown Oxide Surface of a Ceramic Chip from Failed Specimen HSTC2-06, Oxide Emphasis 0.254 cm (One-Inch) Burner Rig Test at 1107C (2025F) for 1258 Cycles and 52 Hot Hours. (100x)

Figure 30.- SEM Photomicrograph of the Thermally Grown Oxide Surface of a Ceramic Chip from Failed Specimen HSTC2-02A, Oxide Emphasis 0.254 cm (One-Inch) Burner Rig Test at 1107C (2025F) for 3307 Cycles and 94 Hot Hours. (100x)

38

Figure 31.– SEM Photomicrograph of the Thermally Grown Oxide Surface of a Ceramic Chip from Failed Pull Test Specimen # 16, Thermally Pre-Exposed at 1149C (2100F) for 1 Cycle and 100 Hour Hours. (100x)

Figure 32.– SEM Photomicrograph of the Thermally Grown Oxide Surface of a Ceramic Chip from Failed Specimen HSTC2-16, Mixed Mode Emphasis 0.254 cm (One-Inch) Burner Rig Test at 1079C (1975F) for 2839 Cycles and 364 Hot Hours. (100x)

39

Figure 33.- SEM Photomicrograph of the Thermally Grown Oxide Surface of a
Ceramic Chip from Failed Specimen HSTC2-02, Oxide Emphasis 0.254
cm (One-Inch) Burner Rig Test at 1107C (2025F) for 4109 Cycles and
527 Hot Hours. (100x)
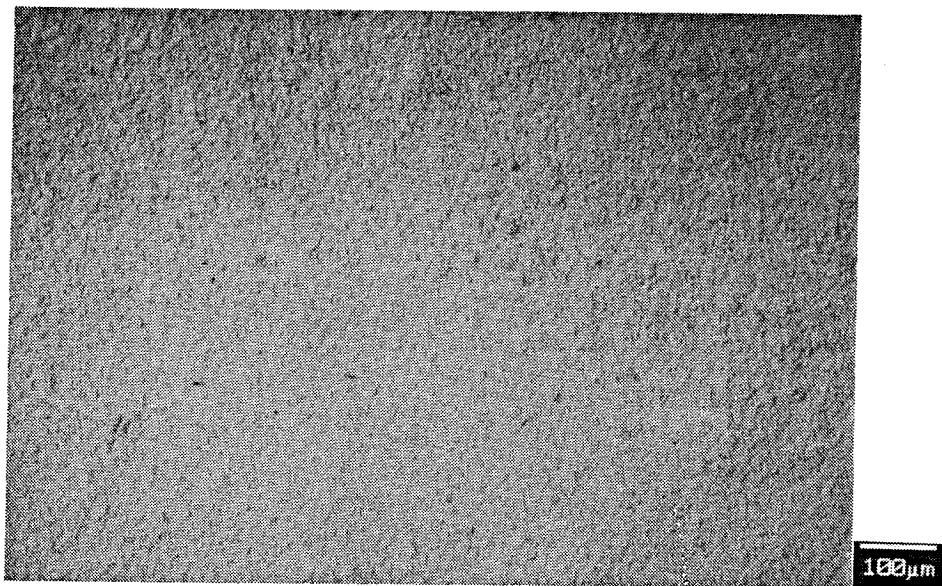
Figure 34.- SEM Photomicrograph of the Thermally Grown Oxide Surface of a
Ceramic Chip from Failed Specimen HSTC2-21, Oxide Emphasis 0.254
cm (One-Inch) Burner Rig Test at 1107C (2025F) for 1575 Cycles and
570 Hot Hours. (100x)

40

Figure 35.- SEM Photomicrograph of the Thermally Grown Oxide Surface of a
Ceramic Chip from Failed Specimen FTSB-28, Furnace Test at 1149C
(2100F) for 1 Cycle and 1800 Hot Hours. (100x)
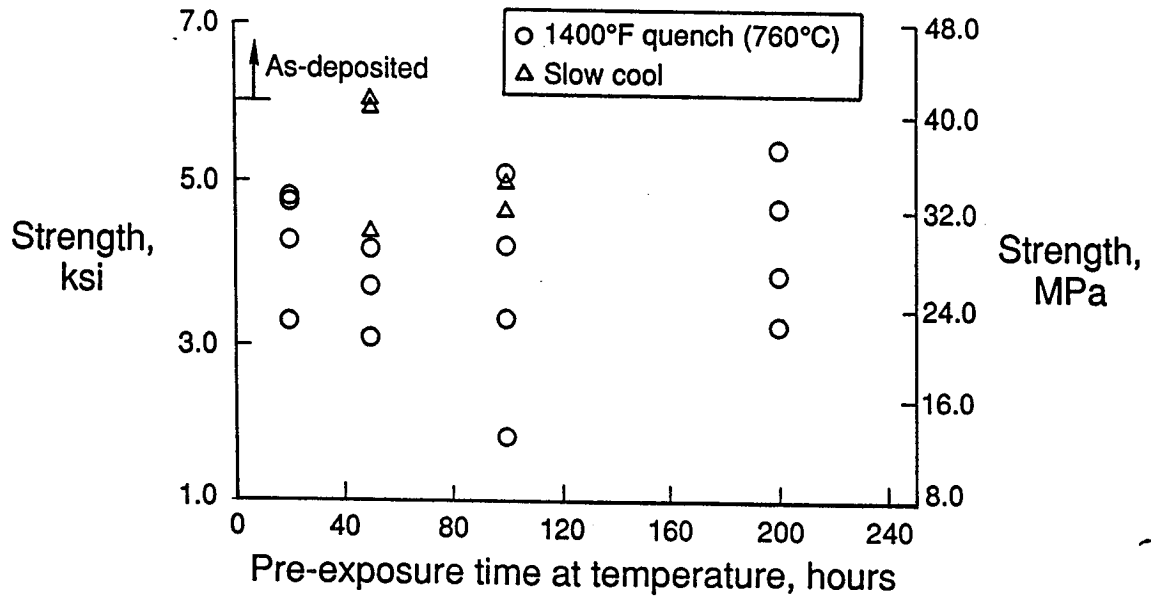
Figure 36.- Adherence Strength of EB-PVD Ceramic as a Function of Exposure
Time at 1149C (2100F).

41

3.3 TASK VI - EMPIRICAL OXIDATION MODEL

The effects of bond coat oxidation were evaluated and an oxidation model was developed based on measurements of the MCrAlY oxide scale developed during thermal exposure. The oxide scale data was grown by static and cyclic thermal conditions.

3.3.1. Task VIA - Quantification of Oxidation Kinetics

Experiments were conducted to develop an empirical oxidation model. These experiments, consisting of burner rig, cyclic furnace, and static furnace tests provided information concerning the effects and rate of oxidation of the metallic bond coat on ceramic spallation life (Table XVI). The burner rig tests addressed the effects of thermal pre-exposure in oxidizing and non-oxidizing environments. The cyclic and static furnace tests aided in defining the oxide growth rate as a function of temperature. The static furnace tests challenged the Phase I PWA 264 model assumption that the oxide grows as a function of the previous oxide thickness. The fractional exposure test specimens provided information on progressive damage.

TABLE XVI
OXIDATION EVALUATION EXPERIMENTS

Test Type	Cycle Length	Temperature 1038C 1900F	1094C 2000F	1149C 2100F	No. of Specimen	Specimen Condition
Burner Rig	6 min.	--	--	x	12	Thermal Pre-exposure in Air & Argon
Cyclic Furnace	10 hrs	x	x	x	12	Fractional Exposures
Static Furnace	Various	x	x	x	12	Various Exposures with a Slow Cool
Static Furnace	100 hrs	x------->x			1	Consecutive fractional exposure @ each temperature: slow cool
Static Furnace	100 hr	x------->x------->x			1	Consecutive fractional exposure @ each temperature: slow cool

3.3.1.1. Preliminary Oxidation Comparison Test

Based on the demonstrated influence of oxidation on the plasma deposited TBC spallation life in Phase I (Ref. 1) and on the EB-PVD failure location (Figure 14), a bond coat oxidation model was developed as part of the EB-PVD life modeling effort. Oxide thickness data for the EB-PVD oxidation model were obtained from both furnace and burner rig tested specimens.

In order to compare the oxidation performance in the two test vehicles, PWA 266 coated 1.27 cm (1/2") diameter burner rig bars (Figure 37) were tested in the burner rig (Appendix A) and their corresponding tip sections were tested in the furnace. The test conditions consisted of a 60/15 minute cycle (60 minutes at temperature and 15 minutes forced air cool) at 1135C (2075F) in air. Samples were tested to failure and to 25, 50, and 75 % fractional exposures of the coating failure life. Burner rig samples were rotated to minimize circumferential thermal gradients. Destructive oxide thickness measurements were obtained using scanning electron microscopy of metallographic sections. The resulting oxide thickness measurements of this comparative furnace and burner rig test are listed in Table XVII and graphically represented in Figure 38.

Within experimental error of oxide thickness measurements, the furnace and the burner rigs showed no significant difference. For all subsequent tests, the two tests were considered to have comparable results.

TABLE XVII
OXIDE THICKNESS MEASUREMENTS OF THE COMPARATIVE
BURNER RIG AND FURNACE TEST

Test	Fractional Exposure (%)	Time (hrs)	Oxide Thickness μm	(microinches)	Delta μm	Oxide Thickness (microinches)
Pre-test	0	0	1.74	68.50	0	0
Furnace	10	14	5.16	203.15	3.42	134.65
Furnace	25	40	7.23	284.65	5.49	216.14
Furnace	25	36	7.04	277.17	5.30	208.66
B.Rig	25	36	5.53	217.72	3.79	149.21
B.Rig	25	36	7.04	277.17	5.30	208.66
Furnace	50	72	7.57	298.03	5.83	229.53
B.Rig	50	72	6.78	266.93	5.04	198.43
Furnace	75	108	7.61	299.61	5.87	231.10
B.Rig	75	108	7.09	279.13	5.35	210.63
Furnace	100	144	9.95	391.73	8.21	323.23
Furnace	100	144	9.82	386.61	8.08	318.11
B.Rig	100	96	7.03	276.77	5.29	208.27
B.Rig	100	79	11.03	434.25	9.29	365.75
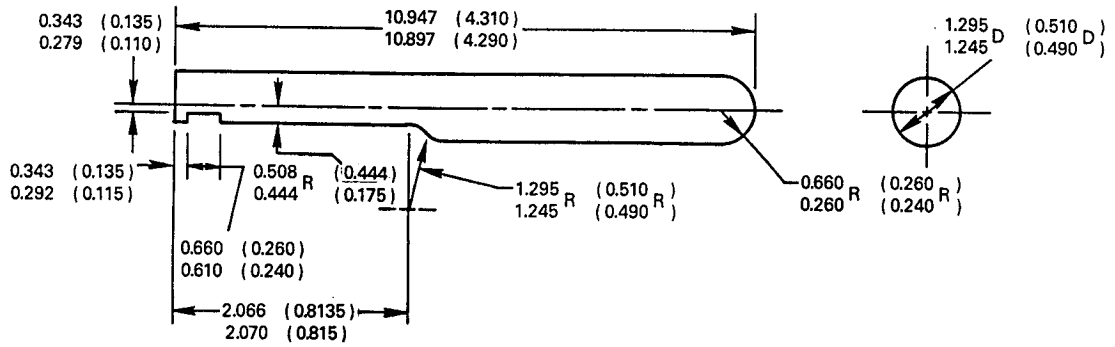
Figure 37.- 1.27 cm (0.5") Burner Rig Specimen Geometry in cm (inches) for the Oxidation Kinetics Study.
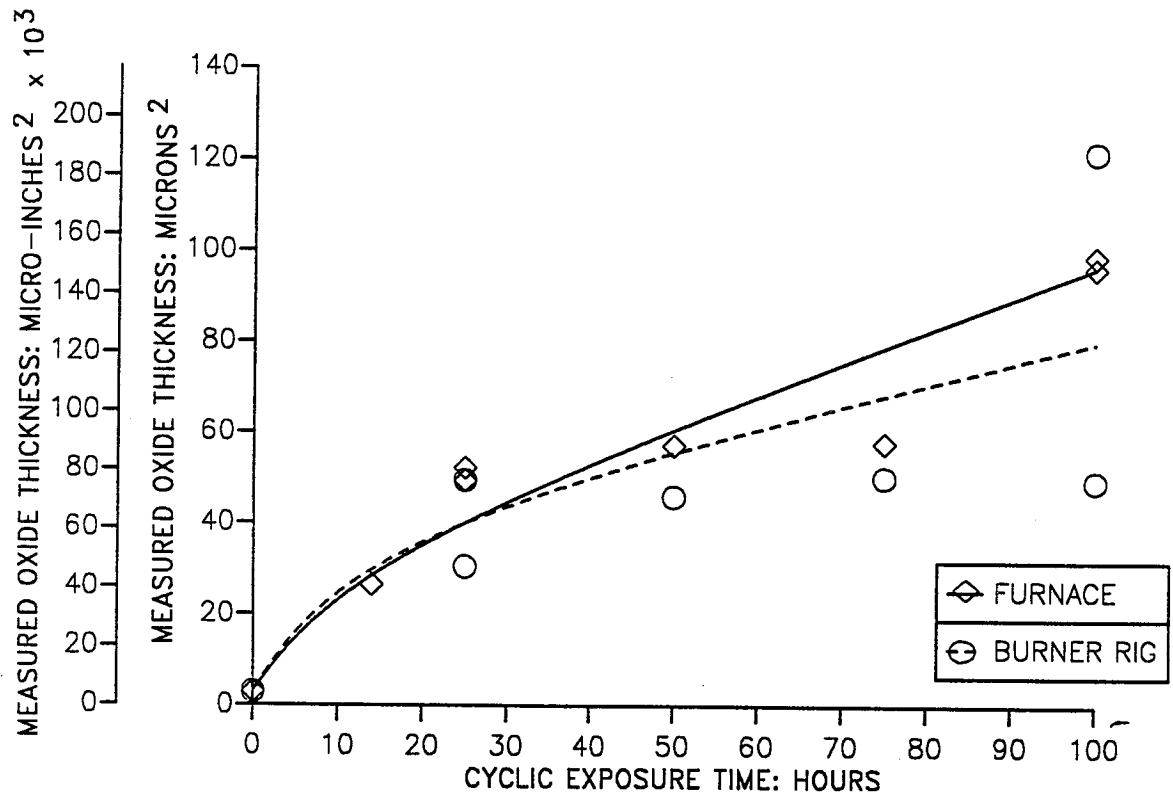
Figure 38.- Oxide Thickness Measurements Vs Time for the Comparative Burner Rig and Furnace Test.

44

3.3.1.2 Burner Rig Testing

The specimen used for the cyclic burner rig testing in this subtask is illustrated in Figure 37. The specimen was thermal barrier coated on all surfaces except for the grip end. A 1.27cm (0.5") tip section was cut prior to burner rig testing for pre-test metallographic examination.

The burner rig experiment was designed to test the effects of the ceramic and the thermally grown oxide, both critical components in respect to life, by varying the pre-exposure conditions. The resulting thermally grown oxide thickness measurements were used for oxidation model development.

After pre-exposure, the 1.27 cm (0.5") burner rig specimens were tested in a 1135C (2075F), 4/2 burner rig cycle (4 minutes at temperature followed by a 2 minute forced air cool). Specimens were removed from test upon spallation of the ceramic coating (Figure 39). Destructive oxide thickness measurements were obtained from pre-test burner rig sample tip sections and from post-test samples using scanning electron microscopy of metallographic sections. The resulting burner rig lives and corresponding sample oxide thicknesses are listed in Table XVIII. Oxide thicknesses on pre-test samples were measured because a thin oxide layer forms between the ceramic and the metallic bond coat during coating processing (Figure 40).

TABLE XVIII
THERMAL PRE-EXPOSURE BURNER RIG OXIDATION TEST

| | | Oxide Thickness | | | | | |
| Pre-Exposure | Test Time | Pre-Test | | Post-Test | | Delta | |
	(Hours)	(μm)	(μin)	(μm)	(μin)	(μm)	(μin)
As-received	896.9	1.69	66.54	6.98	274.80	5.29	208.27
As-received	1236.1	1.47	57.87	8.40	330.71	6.93	272.83
As-received	1544.5	1.25	49.21	6.40	251.97	5.15	202.76
As-received	1544.5	1.83	72.05	6.71	264.17	4.88	192.13
Average	1305.5	1.56	61.42	7.12	280.41	5.56	219.00
Air	793.1	3.74	147.24	7.48	294.49	3.74	147.24
Air	1018.4	4.30	169.29	7.47	294.09	3.17	124.80
Air	1163.0	4.11	161.81	6.59	259.45	2.48	97.64
Air	1544.5	3.75	147.64	7.33	288.58	3.58	140.94
Average	1129.8	3.98	156.50	7.22	284.15	3.24	127.66
Argon	1018.4	2.35	92.52	6.40	251.97	4.05	159.45
Argon	1107.2	1.52	59.84	8.15	320.87	6.63	261.02
Argon	1236.1	2.27	89.37	7.60	299.21	5.33	209.84
Argon	1832.2	1.83	72.05	8.30	326.77	6.47	254.72
Average	1298.8	1.99	78.44	7.61	299.70	5.62	221.26
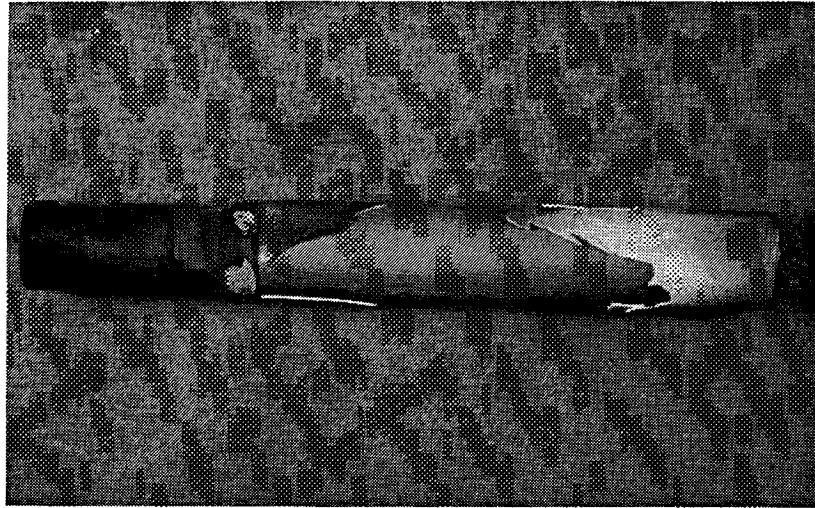
Figure 39.- Typical Failed 1.27 cm (0.5") Burner Rig Specimen. Sample HSTP2-32, no pre-exposure failed at 1545 hours in a 1135 C (2075 F)/6 Minute Cycle Burner Rig.

THERMALLY GROWN OXIDE (TGO)
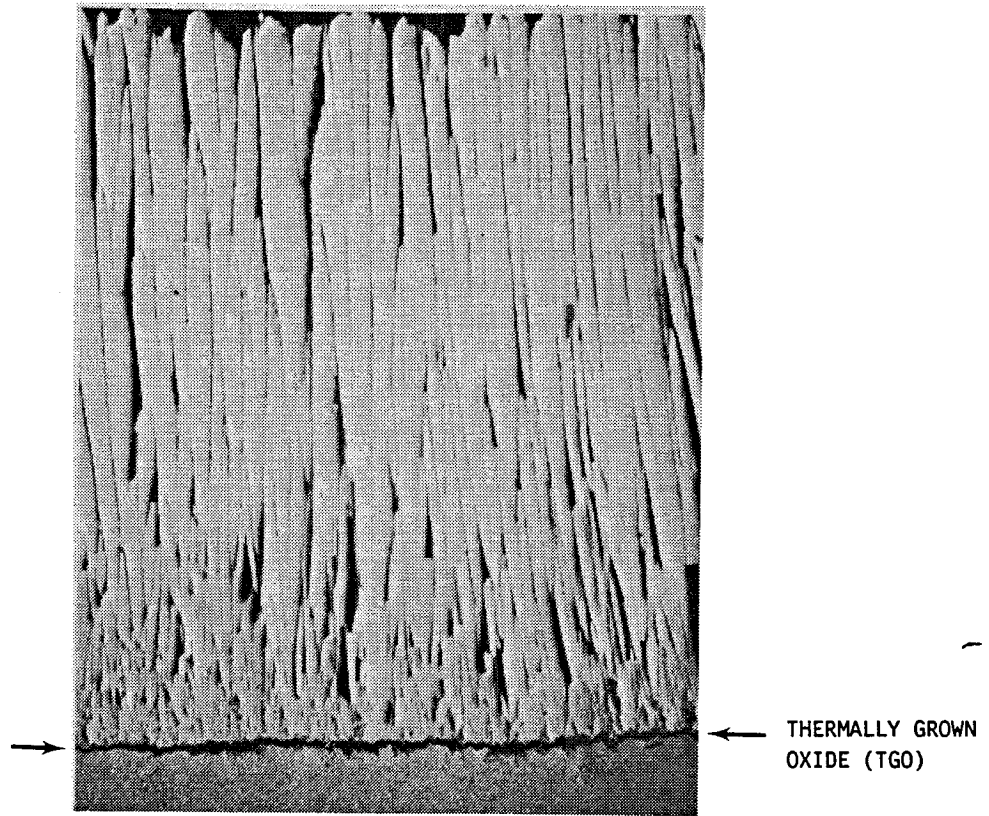
Figure 40.- Transverse View of the Virgin PWA 266 System (450x).

The 20-hour 1149C (2100F) thermal pre-exposure in air caused a slight reduction in burner rig cyclic oxidation life. Both oxidation of the bond coat and sintering of the ceramic columns could account for the life reduction. However, the 20-hour 1149C (2100F) argon pre-exposed burner rig cyclic oxidation lives were essentially identical to that of the as-received burner rig lives. These argon pre-exposed samples showed no oxidation of the bond coat during pre-exposure. Therefore, the sintering occurring within 20 pre-exposure hours did not affect the coating life. This observation indicated that oxidation is a primary thermal barrier coating degradation mechanism.

These results are in agreement with the results achieved in Phase I with the plasma deposited coating (Ref. 1). In an effort to assess the influence of thermal exposure on spallation life as well as to separate the thermal and the environmental effects in Phase I, plasma sprayed ceramic was pre-exposed in both an oxidizing and a non-oxidizing environments for approximately one-half the anticipated burner rig hot time. The isothermal pre-exposure in air caused a significant reduction of cyclic spallation life whereas the non-oxidizing pre-exposure did not reduce coating life. However, the total time at temperature to spallation of the air pre-exposed specimen is roughly comparable to the hot time to failure for the as-received plasma sprayed specimens. EB-PVD coated specimen lives were reduced with air pre-exposure. Isothermal air pre-exposure for the EB-PVD coating was, therefore, more damaging than it was for the plasma sprayed coating.

3.3.1.3 Static Furnace Tests

The specimen used for cyclic and static furnace testing is illustrated in Figure 41. The entire surface of the specimen, with the exception of the ends, was coated. The specimen was tapered to minimize the uncoated region.

Considerable care was required to retain ceramic and oxide layers on static furnace exposure specimens during cool-down after removal from the furnace. Whereas the EB-PVD ceramic has exceptional resistance to cyclic thermal spallation, its tolerance to static exposure is limited for the specimen geometries used in this program. Spallation occurred during cool-down from furnace exposures as short as 40 static isothermal hours. In contrast, this same coating system survived up to 90 hours at 10 hour cycles and up to 1000 cumulative hours of hot time in cyclic burner rig exposure at comparable temperatures. The sensitivity to static exposure seemed to be related to the interface stresses which arise at the specimen free edges. Previous work with the plasma ceramic system in Phase I indicated that it also would spall during cool-down from static furnace exposure, but only after exposure times of the same magnitude as those accumulated prior to failure in cyclic testing at the same temperature. In both cases (plasma and EB-PVD ceramic), spallation during cool-down from furnace exposure could be prevented by very slow cooling.

Static furnace tests for this subtask were cooled at 56C (100F) per 24 hours. Since coating spallation was prevented by slow cooling, various exposure times were employed. The resulting oxide thicknesses, obtained by destructive metallographic examination using scanning electron microscopy, are reported in Table XIX. The 1149C (2100F) test specimen incurred a more rapid cooling rate. This specimen catastrophically failed and had no ceramic remaining on the "bullet" specimen. The material spalled in small chips which were used to measure the thermally grown oxide adhering to the zirconia. This measurement was less than ideal since flakes of the oxide scale could fall off during handling, but it did provide a lower limit of thickness.

47

COATED SURFACE

L

d

D DIA

d
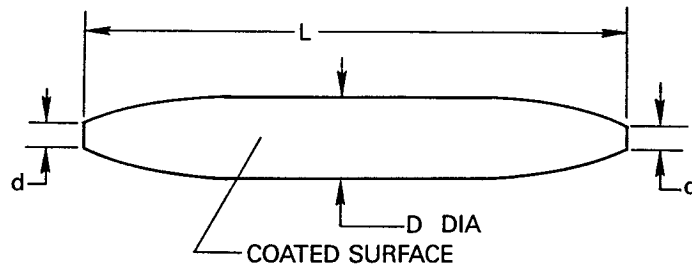
Figure 41.– Furnace Specimen With Tapered Ends to Minimize the Uncoated
Region and the Edge of the Ceramic Layer.

TABLE XIX
ISOTHERMAL STATIC FURNACE TESTS

| Temperature | | Test Time | Oxide Thickness | | | | | |
| | | | Pre-Test | | Post-Test | | Delta | |
(C)	(F)	(hrs)	(μm)	(μin)	(μm)	(μin)	(μm)	(μin)
1038	1900	100	1.68	66.14	3.08	121.26	1.40	55.12
1038	1900	350	1.74	68.50	4.39	172.83	2.65	104.33
1038	1900	1800	1.71	67.32	6.55	257.87	4.84	190.55
1094	2000	50	1.56	61.42	4.25	167.32	2.69	105.91
1094	2000	100	1.64	64.57	3.54	139.37	1.90	74.80
1094	2000	1800	1.84	72.44	11.20	440.94	9.36	368.50
1149	2100	50	1.55	61.02	4.59	180.71	3.04	119.69
1149	2100	100	1.54	60.63	5.09	200.39	3.55	139.76
1149	2100	1800	1.54	60.63	12.60	496.06	11.06	435.43

The static progressive exposure tests challenged the oxidation model assumption
that the oxide growth rate is proportional to existing oxide thickness. Table
XX shows the resulting oxide lives for the two tests. One test involved heating
the furnace specimen for 100 hours at 1038C (1900F) followed by increasing the
temperature to 1094C (2000F) for an additional 100 hours and finally a slow
cooling to room temperature. The second test involved heating the furnace
specimen for 100 hours at 1038C (1900F) followed by increasing the temperature
to 1094C (2000F) for another 100 hours, followed by another increase in
temperature to 1149C (2100F) for an additional 100 hours, and finally a slow
cool to room temperature.

TABLE XX
STATIC PROGRESSIVE EXPOSURE TESTS

| Temperature | | Oxide Thickness | | | | | |
| | | Pre-Test | | Post-Test | | Delta | |
(C)	(F)	(μm)	(μin)	(μm)	(μin)	(μm)	(μin)
1038 to 1094C (1900 to 2000F)		1.45	57.09	3.64	143.31	2.19	86.22
1038 to 1094 to 1149C (1900 to 2000 to 2100F)		1.57	61.81	7.21	283.86	5.64	222.05

48

Three important observations were noted. First, the fractures which occurred in the furnace tests occurred at the thermally grown oxide-bond coat interface, consistent with engine experience. Second, these failures were eliminated by a slow cool to room temperature. Third, the fracture surfaces appear to be the most planar in appearance (see Section 3.2.2.1).

The fact that spallation failure of the ceramic coating did not occur during isothermal exposure but instead during cool-down is in agreement with Phase I results and is actually a well known phenomena. The nominal stress across the coating during cool-down are much lower than that of the out-of-plane strength test results (Section 3.2.2.1). Thus the furnace failures were attributed to the coating edge stresses at the specimen ends. The free edge coating stress field demands that the in-plane thermal mismatch stress reduce to zero at the edge of the ceramic. The transition of the in-plane stress to zero causes strong tensile out-of-plane stress along the coating interface. By employing a slow cooling cycle, the edge stress tends to be relieved.

It is hypothesized that the static furnace as well as the cyclic furnace (Section 3.3.1.4) failures are caused by edge stresses which overload the oxide at the free edge of the ceramic. Only these stresses are large enough to overcome the strength of the thermally grown oxide. In light of these results, a failure mechanism based upon fatigue and time or oxide thickness influences was favored over a direct tensile failure (Section 3.4.1.2) of the EB-PVD ceramic coating.

3.3.1.4 Cyclic Furnace Tests

In order to provide information concerning the rate of accumulation of coating oxidation damage and the effect of temperature and cycle length, a fractional exposure test was conducted. In this test, specimens were cycled to 25%, 50%, and 75% fractions of the cyclic failure life. A specimen was first tested to failure (Figure 42) and then life fractions of the other specimens in the group were adjusted accordingly. The furnace cycle employed was 10 hours at temperature and 2 hours forced air cooling. The oxide thickness results are listed in Table XXI. Figures 43 and 44 illustrate an as-received sample and a failed (100% life), 1149C (2100F)/10 hour cycle furnace specimen. The failure (crack indicated by brackets in Figure 44) occurred at the thermally grown oxide-metallic bond coat interface.

In the absence of a slow cool cycle, the results indicated that shorter cycles increase the life of the EB-PVD coating. In addition, the data indicated that exposure temperature influences spallation life. A comparison of coating life at 1149C (2100F) and 1038C (1900F) indicated approximately 95% reduction in life for a 111C (200F) increase in exposure temperature.

49
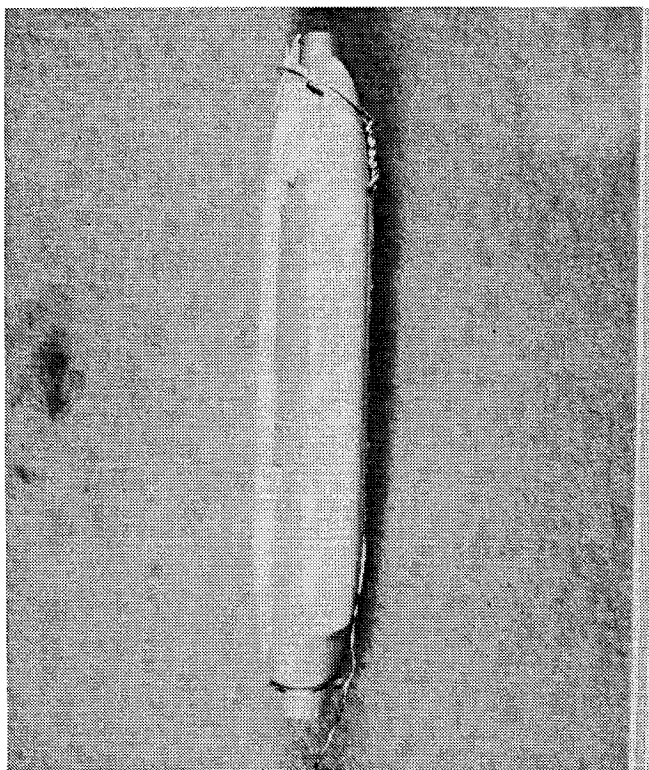
Figure 42.– Failed (90 Hours/9 Cycles) "Bullet" Shaped 1149C (2100F)/10 Hour
Cycle Furnace Specimen. (1x)

TABLE XXI
10 HOUR CYCLIC FURNACE TESTS

Temperature		Test Time	Exposure	Pre-Test		Post-Test		Delta	
(C)	(F)	(hrs)	(%)	(μm)	(μin)	(μm)	(μin)	(μm)	(μin)
1038	1900	440	22	1.69	66.54	3.54	139.37	1.85	72.83
1038	1900	510	25	1.90	74.80	4.72	185.83	2.82	111.02
1038	1900	1020	50	1.52	59.84	6.99	275.20	5.47	215.35
1038	1900	1530	75	1.64	64.57	6.16	242.52	4.52	177.95
1038	1900	2020	100	1.69	66.54	7.95	312.99	6.26	246.46
1094	2000	20	25	1.81	71.26	3.49	137.40	1.68	66.14
1094	2000	40	50	1.68	66.14	3.10	122.05	1.42	55.91
1094	2000	40	75	1.88	74.02	3.56	140.16	1.68	66.14
1094	2000	80	100	1.79	70.47	3.83	150.79	2.04	80.31
1149	2100	20	25	1.99	78.35	3.17	124.80	1.18	46.46
1149	2100	50	50	1.99	78.35	3.79	149.21	1.80	70.87
1149	2100	75	70	1.99	78.35	3.67	144.49	1.68	66.14
1149	2100	100	90	1.99	78.35	4.32	170.08	2.33	91.73
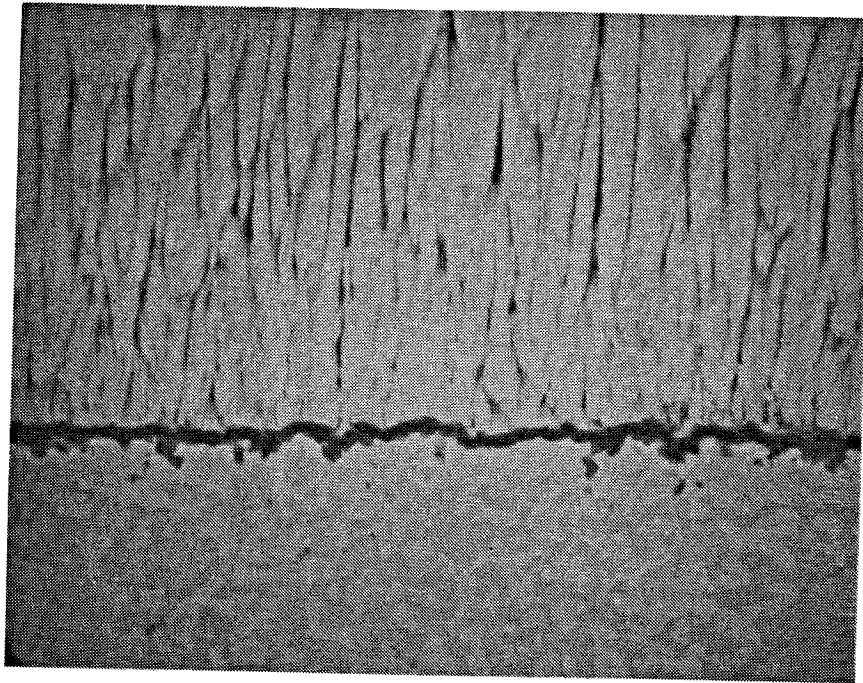
Figure 43.– Transverse View of an As-Received "Bullet" Shaped Furnace
Specimen. (1500x)
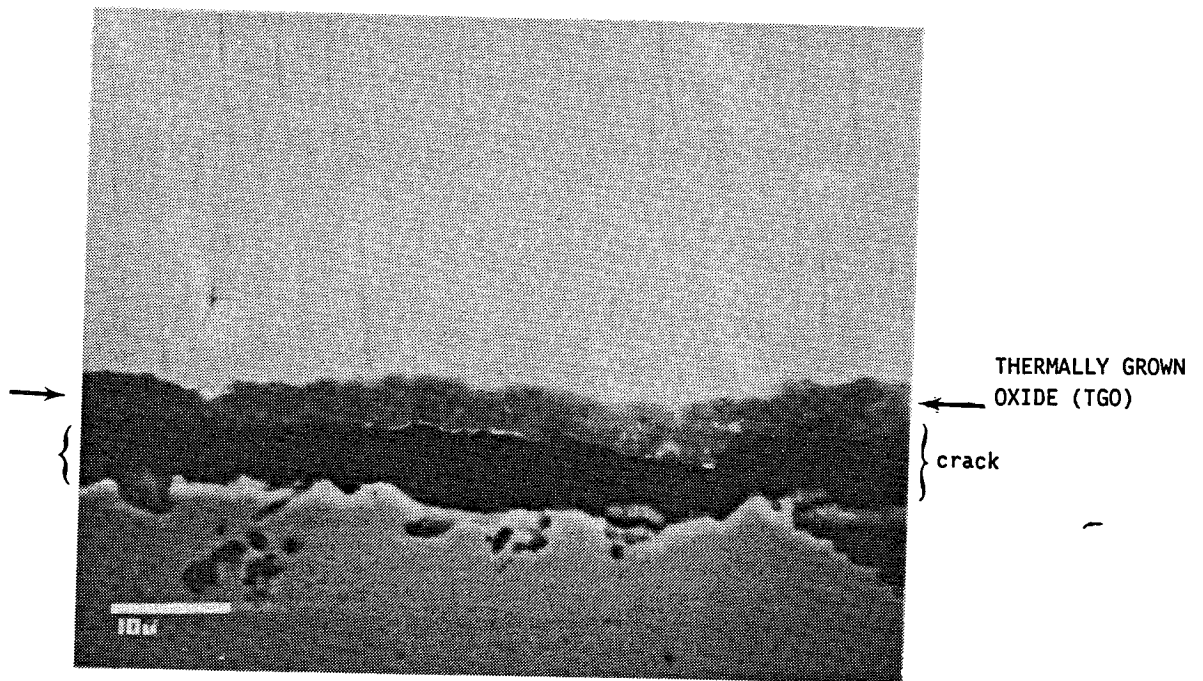
Figure 44.– Transverse View of a Failed (90 Hours/9 Cycles) "Bullet" Shaped
1149C (2100F)/10 Hour Cycle Furnace Specimen. (1500x)

3.3.1.5 Bond Coat Oxidation Model

A bond coat oxidation model was developed using measured oxide thickness data obtained from cyclic burner rig (Section 3.3.1.4) and static and cyclic furnace experiments (Section 3.3.1.2 and 3.3.1.3). The conventional oxidation model was described as follows:

$$\delta = A\left[C_{exp}(-\Delta H/RT)t\right]^n$$

Equation 9

where:

δ = Oxide thickness
ΔH = Apparent activation energy
R = Gas constant
T = Temperature
t = time
and A, C, and n are correlation constants.

It is interesting to note that the best fit of the experimental data produces a growth exponent smaller than the normally assumed parabolic growth constant of one-half. The significance of this observation is not clear at the present time.

To facilitate material and correlation constant determination, a nonlinear regression analysis technique was employed using a simplified form of the above equation:

$$\delta = \left\{\exp\left[Q\left(\frac{1}{To}-\frac{1}{T}\right)\right]t\right\}^n$$

Equation 10

where: $Q = \Delta H/R$
and $to = Q/\ln (A\ exp(1/n)C)$

The following oxide thickness model was obtained:

$$\delta_{(\mu m)} = \left\{\exp\left[Q\left(\frac{1}{To}-\frac{1}{T}\right)\right]t\right\}^n$$

Equation 11

where:

δ = oxide thickness (micrometers)
Q = $\Delta H/R$ = 27777.4
ΔH = apparent activation energy
R = Universal gas constant
T_o = temperature constant = 2423.7K
n = 0.332
T = temperature (K)
t = time (sec)

Cyclic transients and the static furnace slow cool cycle (56C/day or 100F/day) used to prevent ceramic spallation were included in the oxide thickness calculations.

The model is shown in Figure 45. All data is calculated within about 20% which is considered excellent. The observed absence of data segregation of cyclic burner rig specimen data for the various pre-exposures (Section 3.3.1.2) indicates that for the range of pre-exposures tested, the bond coat oxidation rate depends only on the current oxide thickness and thermal exposure, consistent with the proposed model.

52

$$\delta = \left\{\exp[Q(1/T_0 - 1/T)]t\right\}^n$$
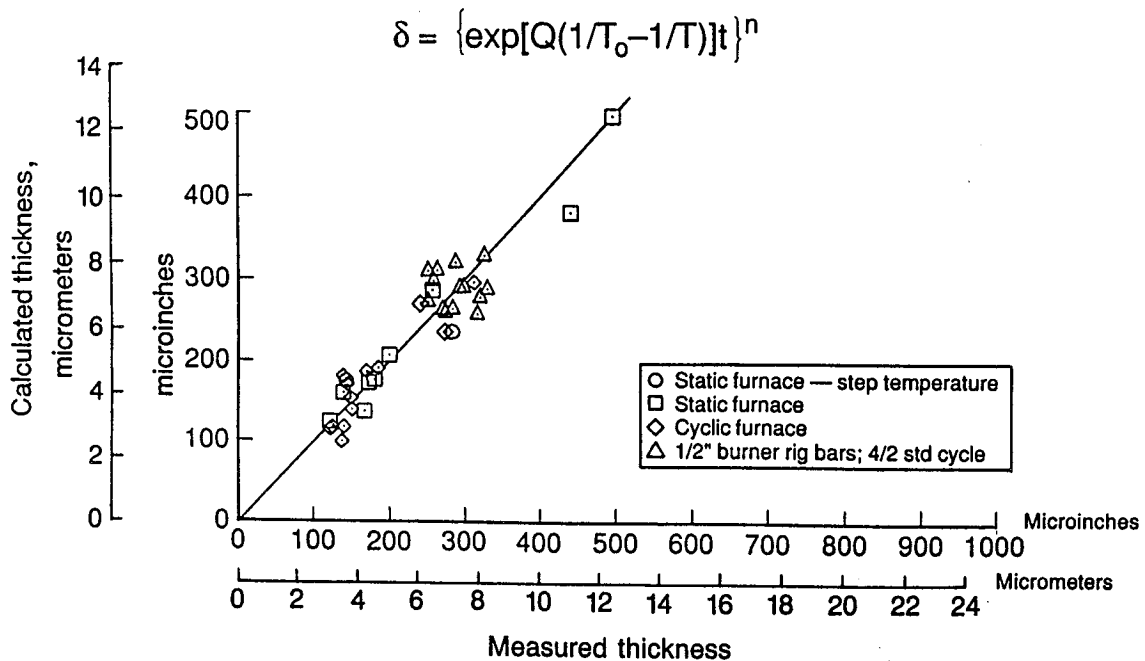
Figure 45.- Calculated Vs. Measured Thermally Grown Oxide Thickness.

3.3.2 Task VIB – Structural/Chemical Analyses

The bond coat oxide was fully characterized to further understand TBC failure at the thermally grown oxide-metal interface. Oxide growth rates and thicknesses were determined through metallographic examination of the test pieces at various fractional exposure conditions and reported in the previous section. Structural and chemical investigations were conducted on the oxide. In addition, the EB-PVD zirconia ceramic and the metallic bond coat were analyzed.

3.3.2.1 EB-PVD Zirconia Ceramic Analyses

As shown in Figure 40, the EB-PVD ceramic grows in columnar form when processed under the appropriate conditions. Individual ceramic columns are poorly bonded to adjacent columns, but are tightly bonded to the underlying substrate. This extremely fine columnar structure is highly tolerant of strains induced by expansion of the underlying substrate.

The tips of two 1.27 cm (0.5") burner rig bars were removed and the virgin EB-PVD ceramic was x-rayed while attached to the substrate. The samples exhibited a very strong $\langle 100 \rangle$ texture perpendicular to the substrate. A summary of the phases present and the corresponding lattice parameters is listed in Table XXII. Quantitative volume percent estimates were impossible since some reflections such as $\langle 111 \rangle$ and $\langle 220 \rangle$ for the f.c.c. zirconia were completely absent; hence a qualitative summary is presented.

TABLE XXII

X-RAY PHASE ANALYSIS OF VIRGIN EB-PVD CERAMIC

Sample	Major Phase & Lattice Parameter (Å)	Minor Phase & Lattice Parameter (Å)
1	f.c.c. zirconia $a_0 = 5.1176$	tetragonal zirconia $a_0 = 5.110$ & $c_0 = 5.178$
2	f.c.c. zirconia $a_0 = 5.1212$	tetragonal zirconia $a_0 = 5.122$ & $c_0 = 5.170$

Numerous tests in Phase II were conducted on thermally exposed EB-PVD ceramic in addition to virgin (as-received) ceramic in order to simulate the effects of sintering or phase changes that might occur in an engine environment. For example, the parallel thermal expansion measurements (Section 3.2.1.1) were thermally exposed for 50 hours at 1149C (2100F). Since specimens designed for this measurement required the presence of a substrate, an inert atmosphere (argon) was employed during the heat treatment in order to eliminate oxidation which is a critical factor in the adherence of the ceramic. X-ray phase analysis (Table XXIII) confirmed that the inert atmosphere at these exposure conditions did not affect the phases present; hence, heat treated specimens in an inert atmosphere as well as in air can be compared without being concerned for phase differences.

TABLE XXIII

EB-PVD CERAMIC PHASE ANALYSIS COMPARISON
AFTER HEAT TREATMENT IN AIR VS ARGON

Heat Treat Condition	Phase Analysis
50 hrs/1149C(2100F)/air	Single phase, f.c.c. zirconia structure ($a_0 = 5.0860$ Å) Very strong <100> & weaker <111> texture
50 hrs/1149C(2100F)/argon	$\geq$99v% f.c.c. zirconia structure ($a_0 = 5.1075$ Å) With very strong <100> texture $\leq$1 v% monoclinic zirconia structure

In addition, burner rig design data generation and furnace oxidation post-test samples did not show a zirconia phase transition. X-ray results of selected samples showed that the ID surfaces of spalled EB-PVD ceramic chips are f.c.c. zirconia (Table XXIV). The absence of a phase transition due to thermal exposure implies that the effect of aging was insignificant under the exposure conditions (time and temperature) utilized.

54

TABLE XXIV

X-RAY DIFFRACTION OF SPALLED CERAMIC CHIPS

	Strain	Oxide	Oxidation (Furnace)	Oxidation Furnace	Mixed Mode
Test ID	TASK VIIA Test # 11	TASK VIIA Test # 3	TASK VIA Cyclic Test	TASK VIIA Static Furnace	TASK VIIA Test #13
Section	3.4.2.2	3.4.2.2	3.3.1.4	3.3.1.3	3.4.2.2
Test Conditions	1177C(2150F)/6min burner rig	1107C(2025F)/12min burner rig	1149C(2100F)/10 hr cyclic furnace	1149C(2100F) furnace	1079C(1975F)/6 min burner rig
Time to Failure	167 hours 1670 cycles	712 hours 4274 cycles	90 hours 9 cycles	1800 hours 1 cycle	1352 hours 9014 cycles
OD ZrO2 XRD	f.c.c. ZrO2 a_0 = 5.105 Å very strong <100>	f.c.c. ZrO2 a_0 = 5.099 Å very strong <100>	f.c.c. ZrO2 a_0 = 5.098 Å trace tetragonal very strong <100>	f.c.c. ZrO_2 a_0 = 5.092 Å trace tetragonal	91 v% f.c.c. ZrO_2 a_0 = 5.096 Å 8 v% tetragonal ZrO_2 a_0 = 5.105 A and c_0 = 5.156Å Trace monclinic ZrO_2 Extremely strong <100> texture

)

In order to determine any yttria concentrations or migration during the coating process or during thermal exposure, a microprobe trace of the yttria along the length of the EB-PVD ceramic columns was performed. The yttria distribution along a pre-test and a post-test (Section 3.4.2.2) are depicted in Figures 46 and 47, respectively. Figure 46a shows the microprobe trace of yttria across the trace location of a pre-test sample represented in Figure 46b. The nominal yttria value is 6.7 weight %, and deviations from this value, for example the decrease to 5 weight % yttria at a 35 micron distance into the trace location, is probably representative of crossing a porous region between columns. Figure 47a shows the microprobe trace of yttria across the trace location of a post-test sample represented in Figure 47b. The nominal yttria value of the post-test sample is 6.1 weight %. Deviations from the nominal 6.1 weight % yttria within Figure 47a are again most likely due to the probe transversing across two columns. The difference between the pre and post-test yttria content is within experimental error as well as within the range of the allowable Pratt & Whitney specification of the ceramic powder (6 to 8 weight % yttria). The relatively constant values of the yttria composition across the columns from ID to OD surfaces are in good agreement with x-ray diffraction results. X-ray diffraction results show ID (Section 3.3.2.3) and OD (this section) zirconia lattice parameters as equivalent values. If there had been a gradient in the yttria distribution, the lattice parameter would have decreased with an increase in yttria content.

In addition to investigating the effect of thermal exposure on the chemistry and phase analysis of the EB-PVD ceramic, the effect of thermal exposure on the EB-PVD structure was also studied. In essence, sintering of the EB-PVD ceramic columns for a variety of test types was investigated. The spalled ceramic chips studied were oxide emphasis test # 3 (712 hours to failure), strain emphasis test # 11 (167 hours to failure), mixed mode emphasis test # 13 (1352 hours to failure), and 1149C (2100F) static furnace in air for 1800 hours. A chart summarizing the history of each of these samples is included in Table XXV.

TABLE XXV
EB-PVD CERAMIC COLUMN SINTERING STUDY

Spec.# (Test#)	Test Type	Temp C (F)	Cycle (min)	Failure Time (hrs)	Cycles	Hot Time (hrs)	Figure Number
Trial Expansion	Thermal	RT	0	Virgin	0	0	48a-c
HSTC-04	Strain	1177 (2150)	6	167	1728	14	49a-b
HSTC2-19	Mixed Mode	1079 (1975)	6	1352	9014	331	50a-c
HSTC2-02	Oxide	1107 (2025)	12	712	4109	527	51a-c
FTSB-28	Static Furnace (air)	1149 (2100)	1	1800	1	1800	52a-d 53a-b
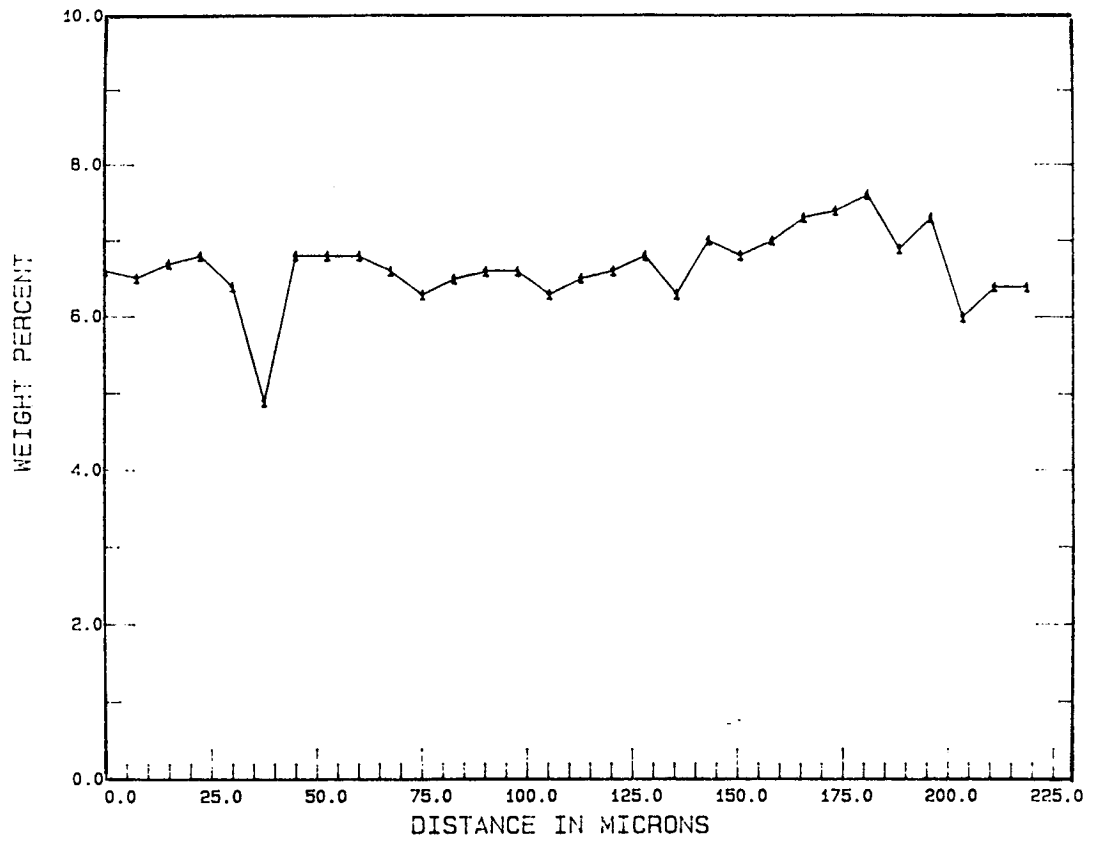
Figure 46a.- Microprobe Trace of Yttria Along the Ceramic Column of a Pre-Test 2.54 cm (1") Burner Rig Bar.
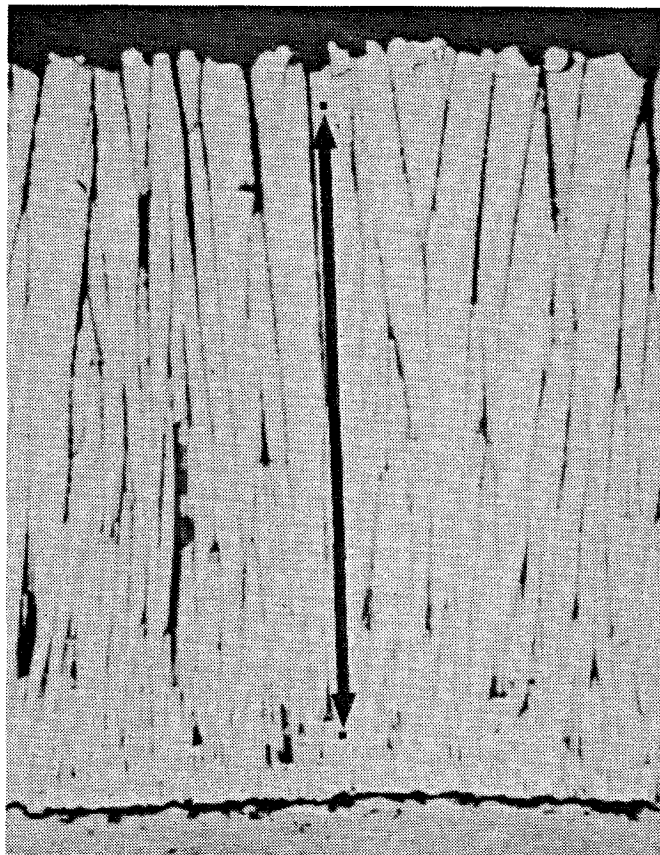
Figure 46b.- Scanning Electron Photomicrograph of the Microprobe Trace Location of Yttria Represented in Figure 46a. Mag: 444x

57
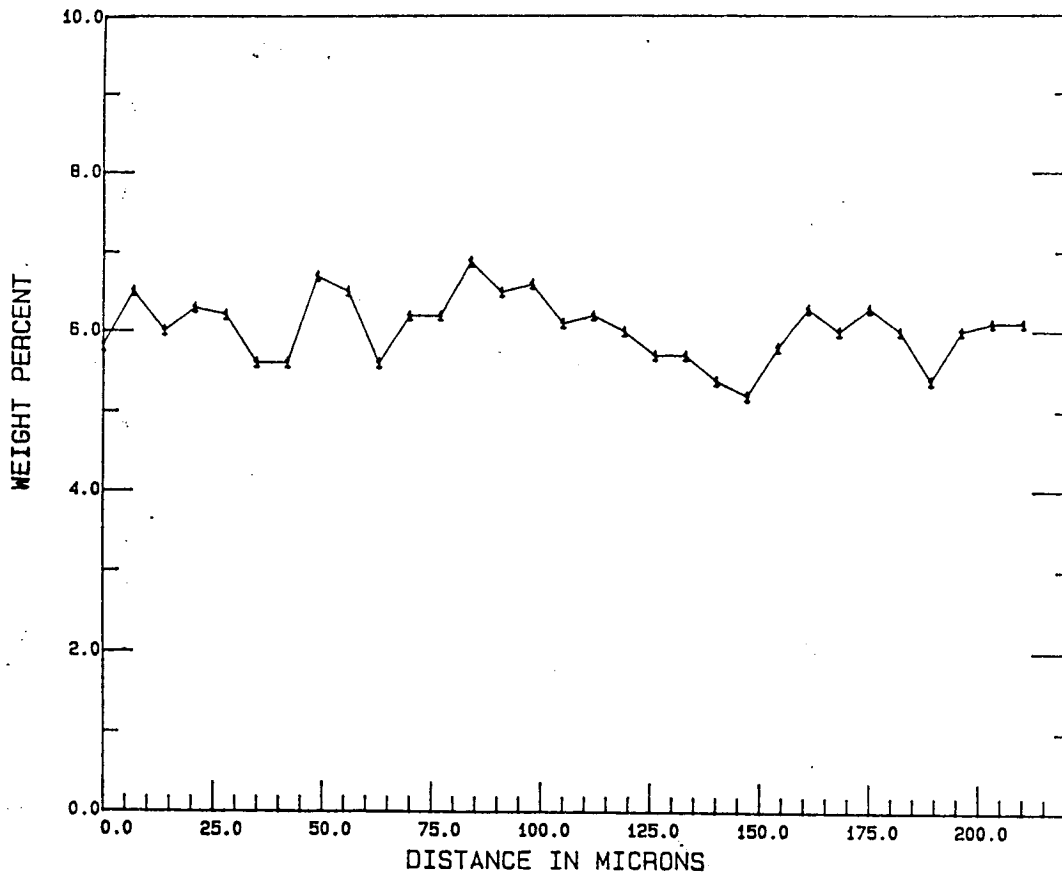
Figure 47a.– Microprobe Trace of Yttria Along the Ceramic Columnof a Post-Test
2.54 cm (1") Burner Rig Bar (Oxide Emphasis TASK VIIA test #3,
1107C (2025F)/12 Minute Cycle Which Failed at 712 Hours). Mag: 300x
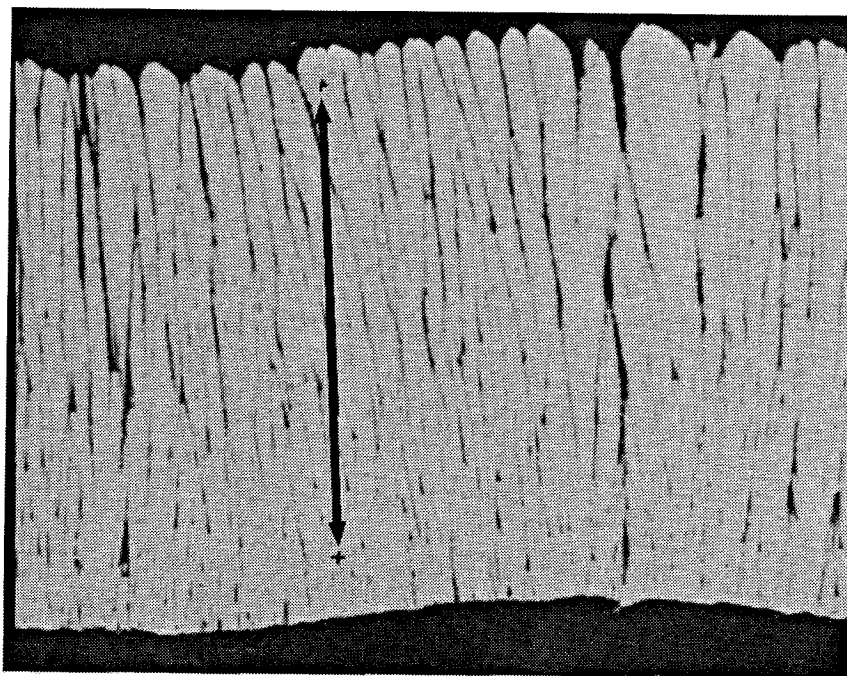
Figure 47b.– Scanning Electron Photomicrograph of the Microprobe Trace
Location of Yttria Represented in Figure 47a. Mag: 300x

Sintering between the EB-PVD ceramic columns within the thermal barrier coating is undesirable since sintering would destroy the desired strain tolerant structure. The driving force for sintering is the decrease in surface free energy. This lowering of the surface free energy is accompanied by a decrease in surface area by the elimination of solid-vapor interfaces. During sintering, material may be transferred into the neck area due to differences in surface curvature and consequently vapor pressure. The important factor in terms of strength is the bond area in relation to the columnar size. The rate at which this necked area between the columns forms is reported to vary as the two-third power of time with a decreasing rate curve. The sintering rate is also sensitive to temperature changes.

A thermal expansion trial specimen was used for sintering examination of an as-received ceramic chip. This specimen, as well as all other specimens in this study, was prepared by fracturing the ceramic chip in order to expose a fresh surface. Figure 48a-c shows a ceramic columnar area in increasing magnification. No sintering, or necking, is observed between the columns. The columnar features appear to be quite angular.

The strain emphasis ceramic chip also shows no apparent sintering between columns (Figure 49a-b). Perhaps this absence is caused by a relatively low hot time (167 hours), but more likely the high number of cycles imposed upon the coated burner rig bar either prevents necking or cyclically re-breaks incipient necks as a result of cyclic thermal displacement between adjacent columns. Hot time exposure is evident on this sample in the form of angular features transposing to a more rounded, smoother appearance (Figure 49b). This decrease in surface area is the result of a lowering of surface free energy by eliminating the solid-vapor interfaces.

The mixed mode emphasis ceramic coated burner rig bar was exposed at elevated temperatures for an extended time. The mixed mode emphasis specimen is illustrated in Figure 50a-c. Necking between ceramic columns was evident in localized areas of the fractured ceramic chip. The loss of angular features was also noted.

The oxide emphasis ceramic specimen experienced slightly higher temperatures than the mixed mode emphasis specimen but not higher than the strain emphasis specimen. The total test time for the oxide emphasis sample was not as high, but due to its longer cycle lengths at elevated temperatures, this specimen did experience more hot time. The combination of the hot time and the elevated temperature resulted in increased sintering between columns (Figure 51a-c).

The static furnace test specimen exhibits the most pronounced sintering effects in this study (Figure 52a-d, 53a-b). This ceramic was exposed to a very high temperature, and the necked regions were not broken due to the absence of thermal cycling. Figure 52d is an excellent example of the strength of the sintered bond since it displays the preferred mode of fracture within a ceramic column as opposed to intercolumnar fracture. The cutaway view obtained due to partial fracture of a column (Figure 53) also shows a well-sintered bond between columns.

In summary, exposure to elevated temperatures does promote sintering between the zirconia columns. The act of cycling a ceramic coated specimen does appear to minimize/prevent necking between ceramic columns.
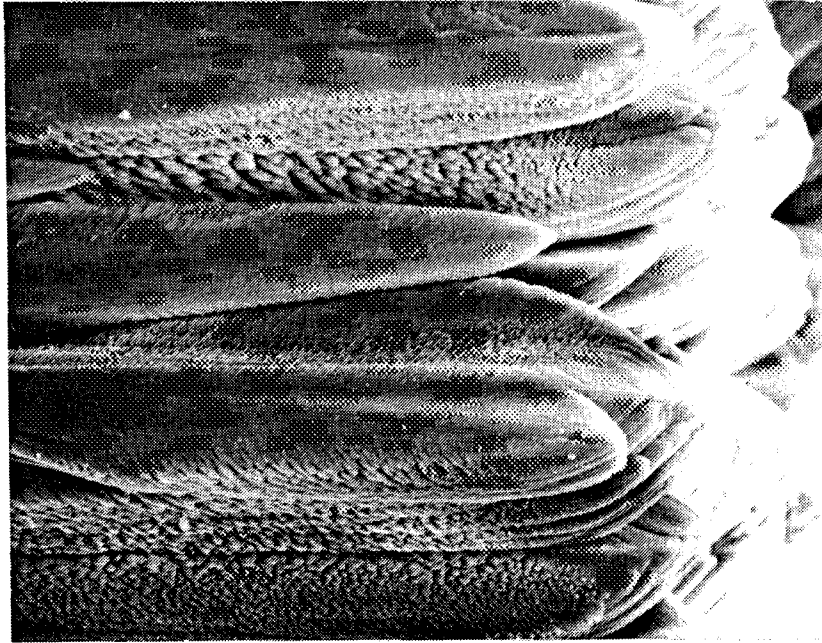
(A)   1000x

Figure 48.- Cross-Section of a Virgin PWA 266 EB-PVD
Ceramic Chip Used as a Thermal Expansion Trial Specimen.

(B)   3000x
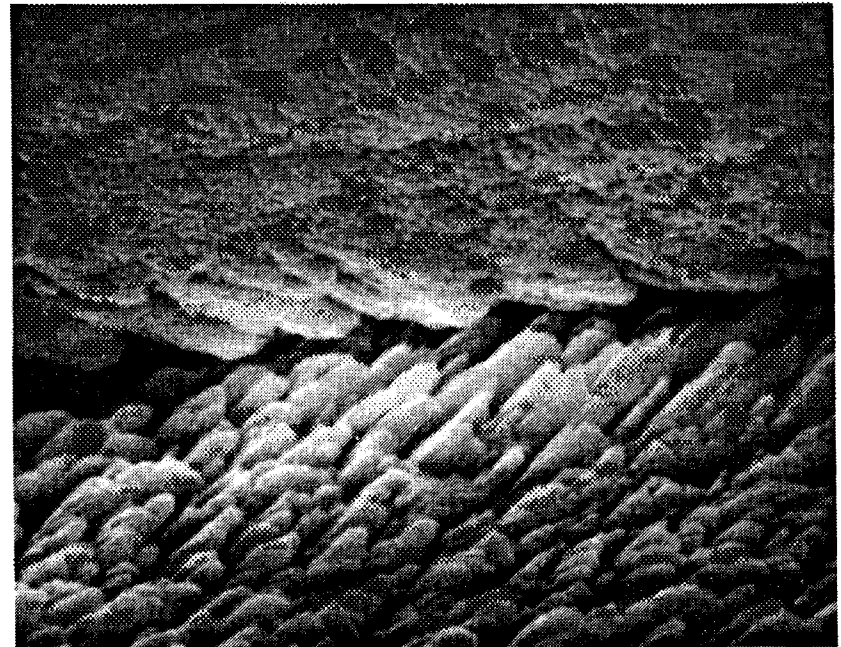
(C)   10,000x
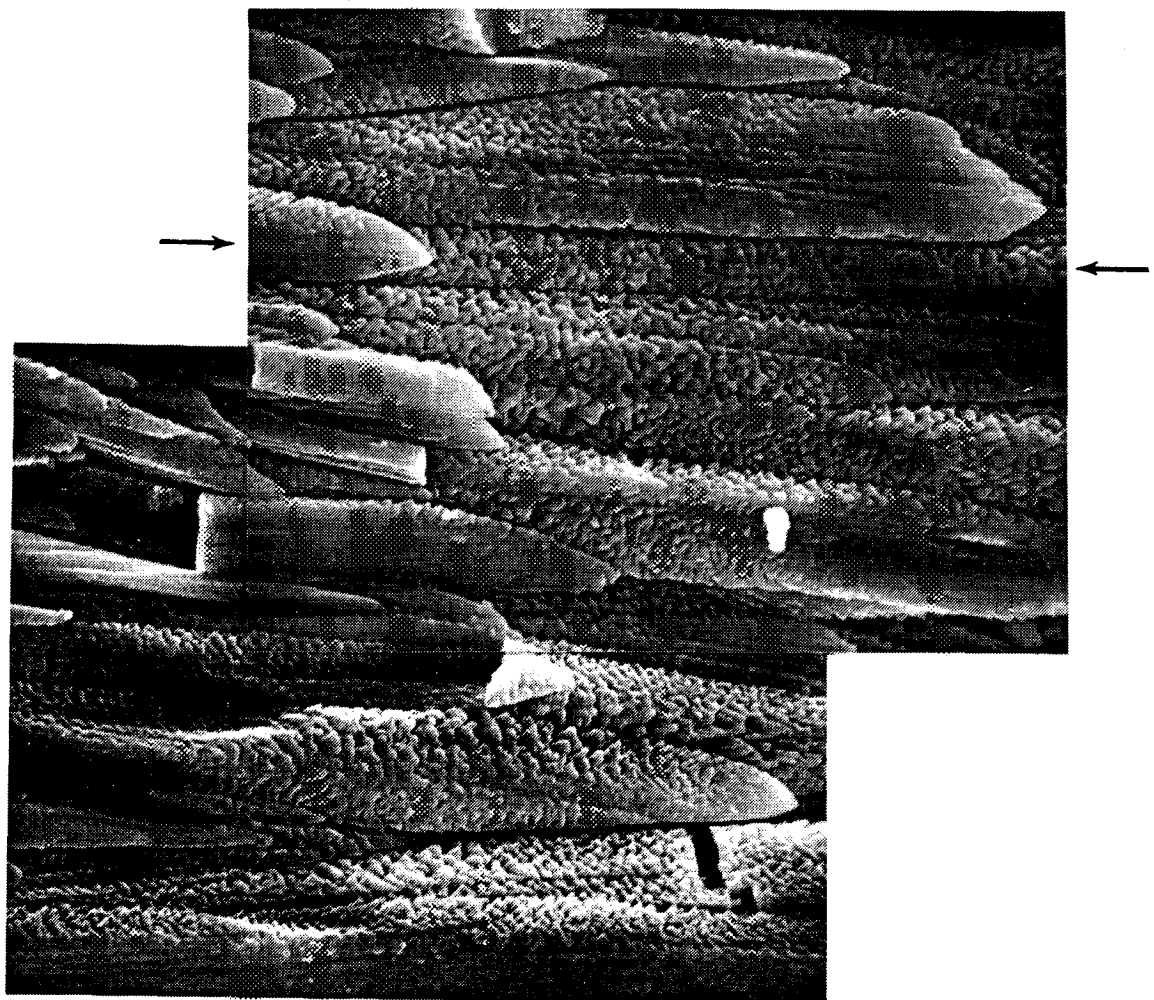
(A)   3000x
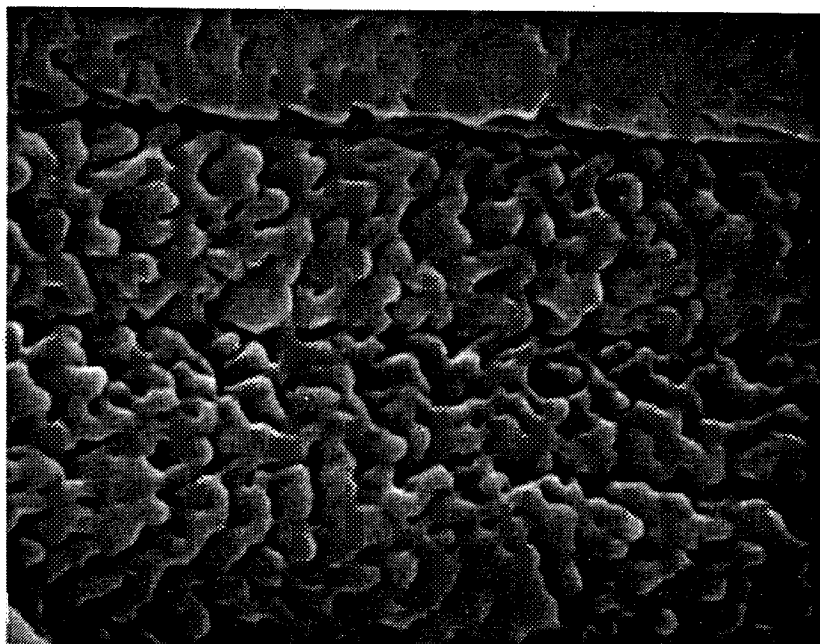
(B)   10,000x

Figure 49.- Cross-Section of a Strain Emphasis (Test #4, 1177C (2150F)/6
        Minute, 167 Total/14 Hot Hours, Specimen HSTC2-04) PWA 266 Ceramic
        Chip.

61
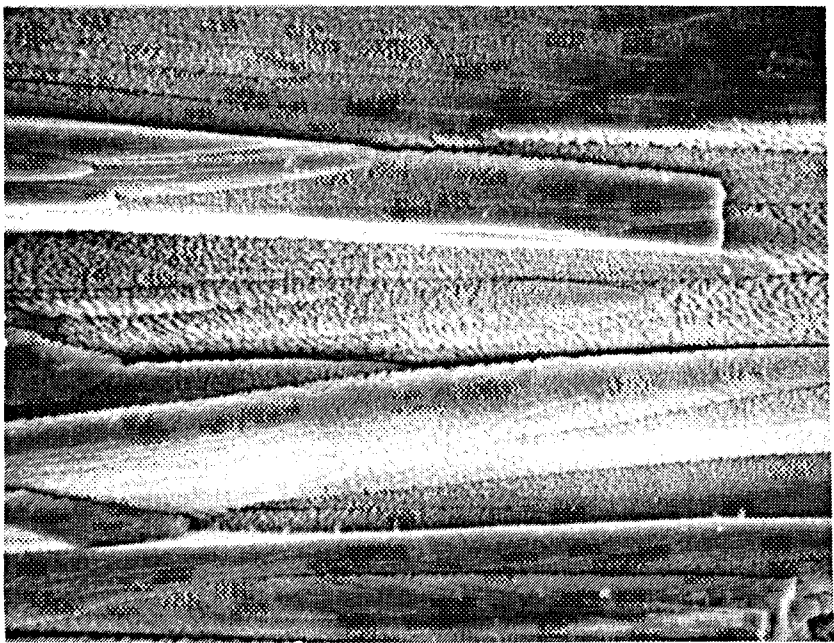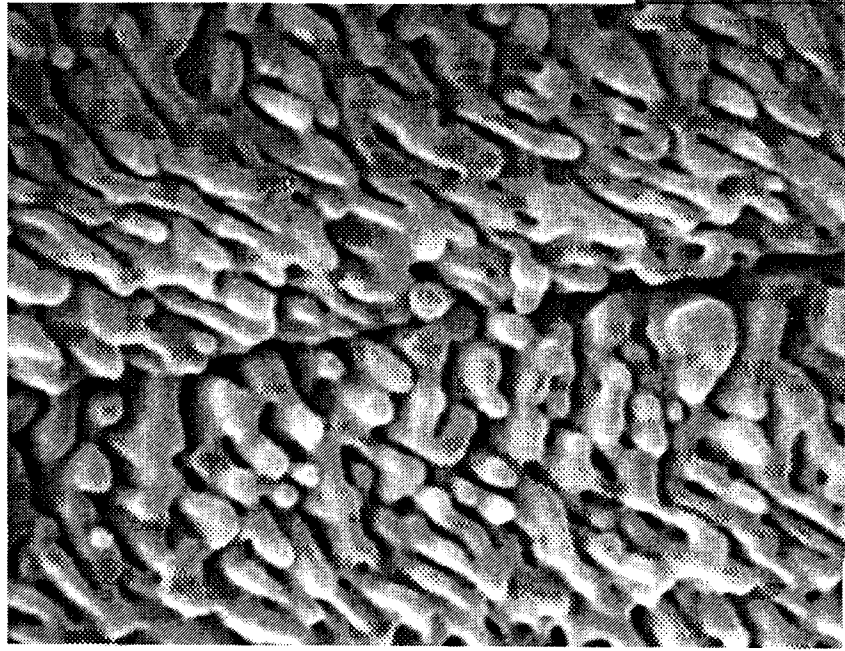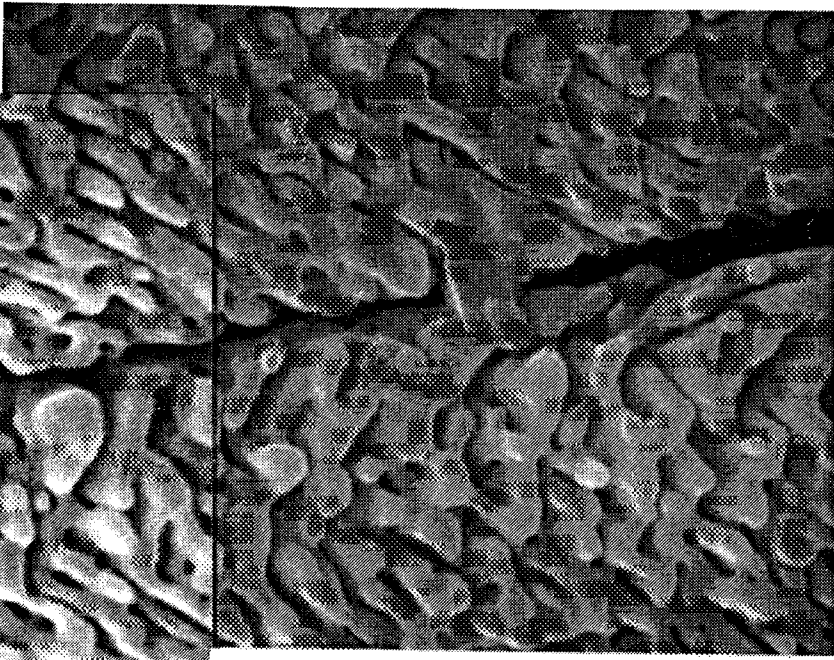
Figure 50.-
Cross-Section of a Mixed Mode Emphasis (Test #13, 1079C(1975F)/6
Minutes, 1353 Total/331 Net Hours. Specimen USTC3 10) DWA 266

(A) 1000x
(B) 3000x
(C) 10,000x
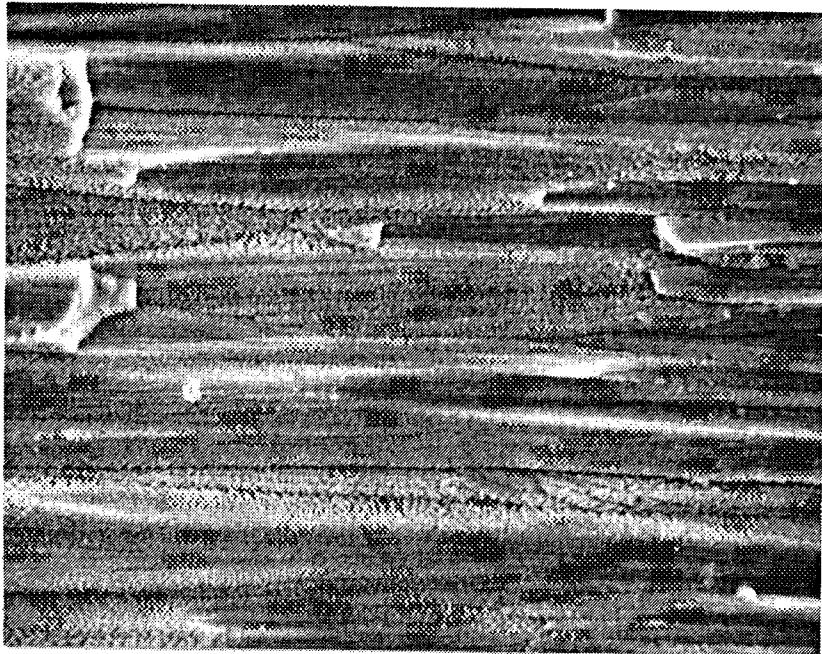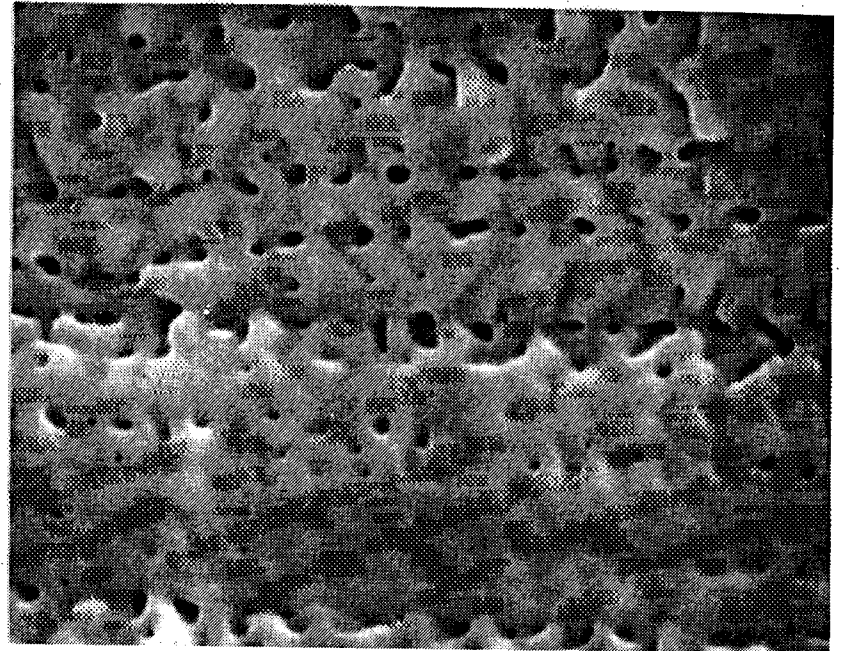
(A)   1000x

(C)   10,000x
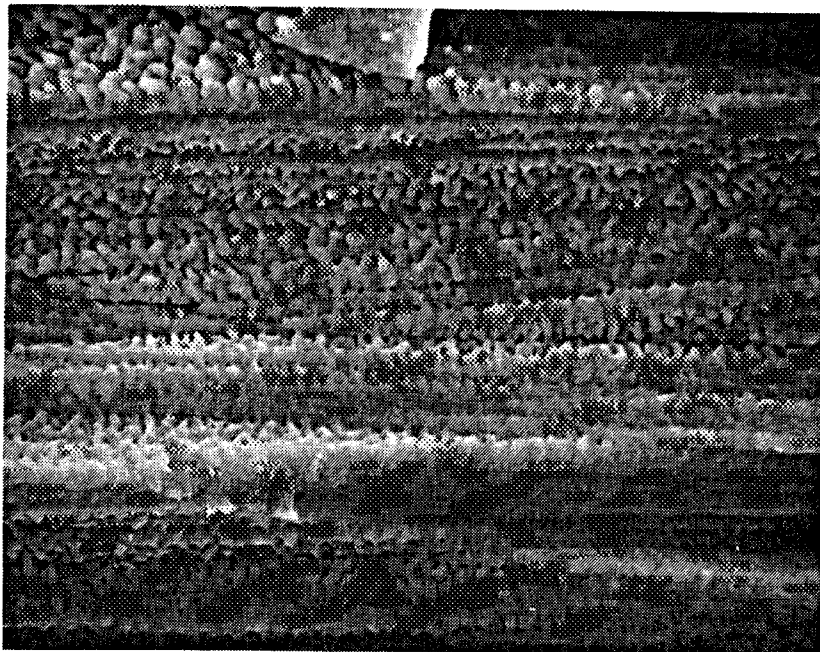
(B)   3000x

Figure 51.-
Cross-Section of an Oxide Emphasis
(Test #3, 1107C (2025F)/12 Minute, 712
Total/527 Hot Hours, Specimen HSTC2-02)
PWA 266 Ceramic Chip.

63
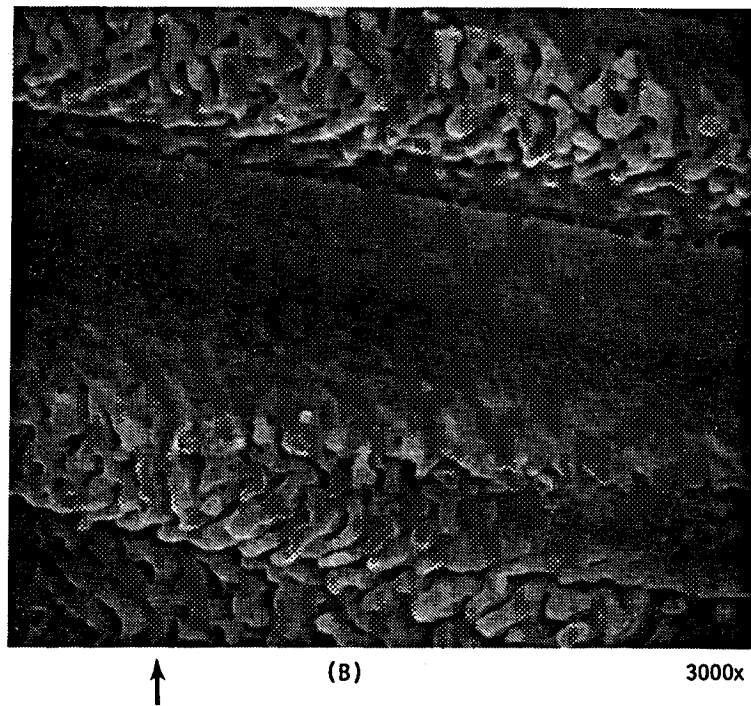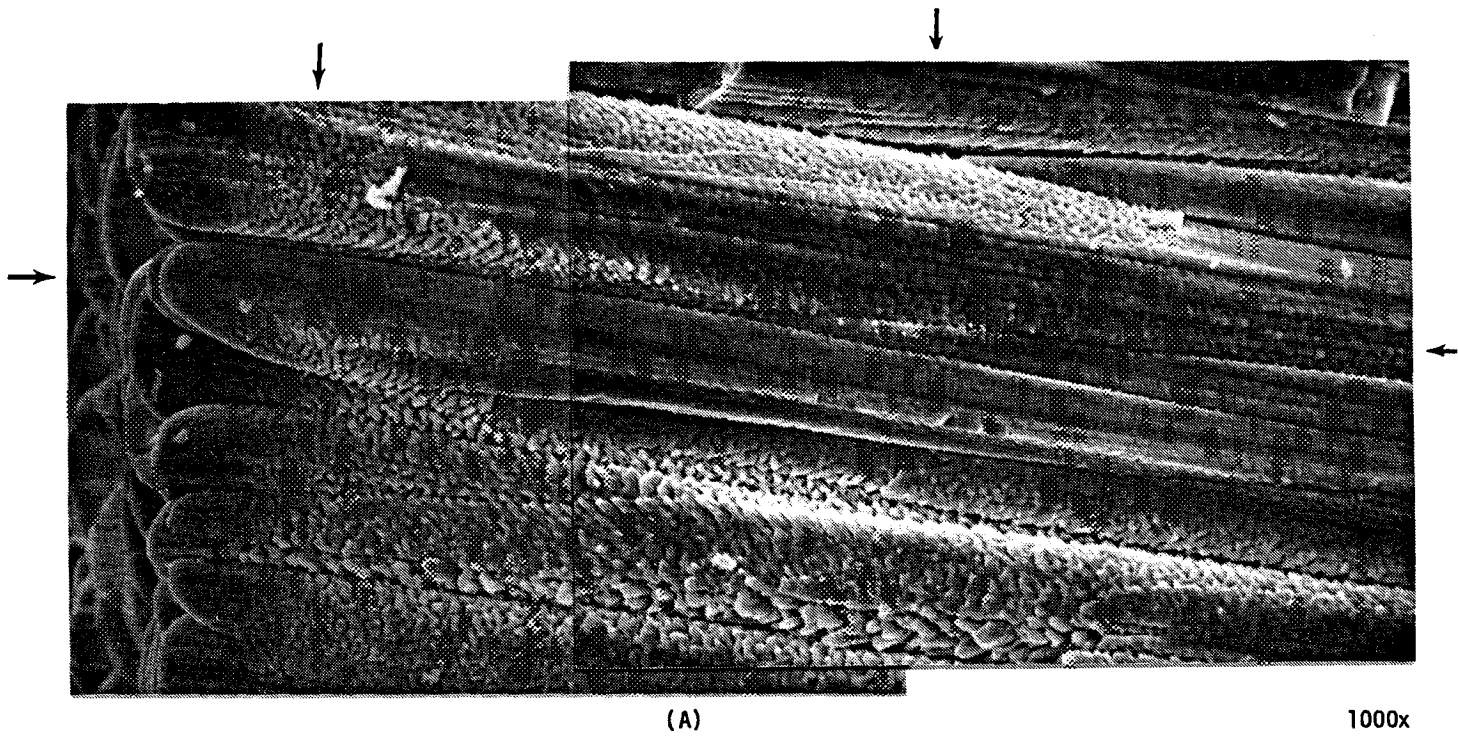
(A)   1000x

(B)   3000x

Figure 52.– Cross-Section of a Static Air Furnace Test (1149C (2100F)/1800
Hours, Specimen FTSB-28) PWA 266 Ceramic Chip.
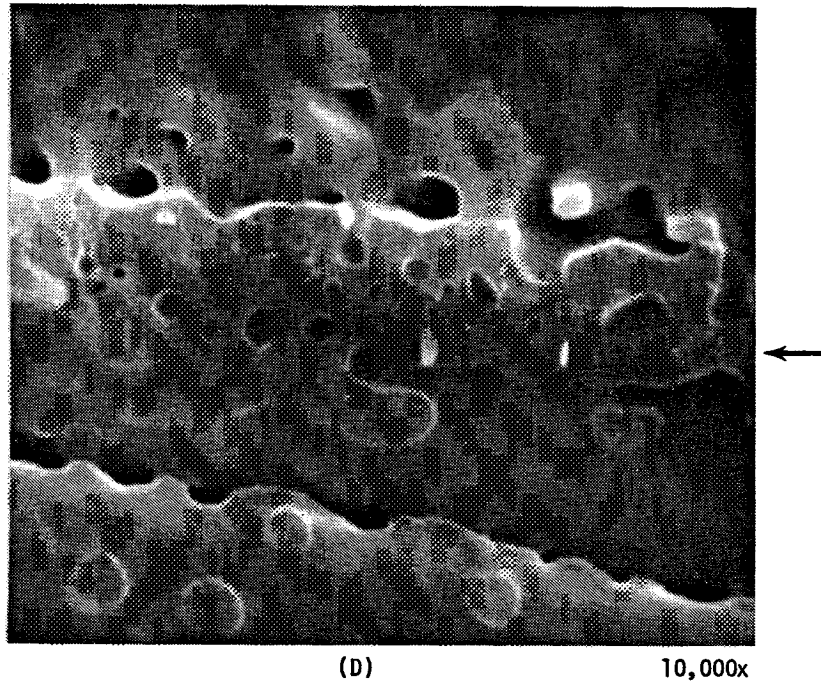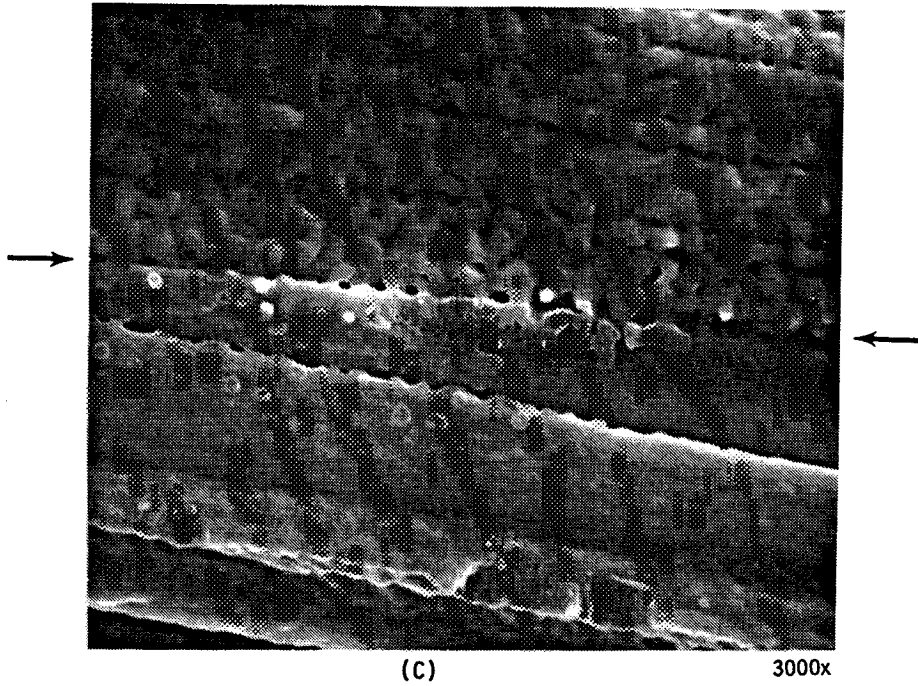
(C)   3000x

(D)   10,000x

Figure 52.-   Continued
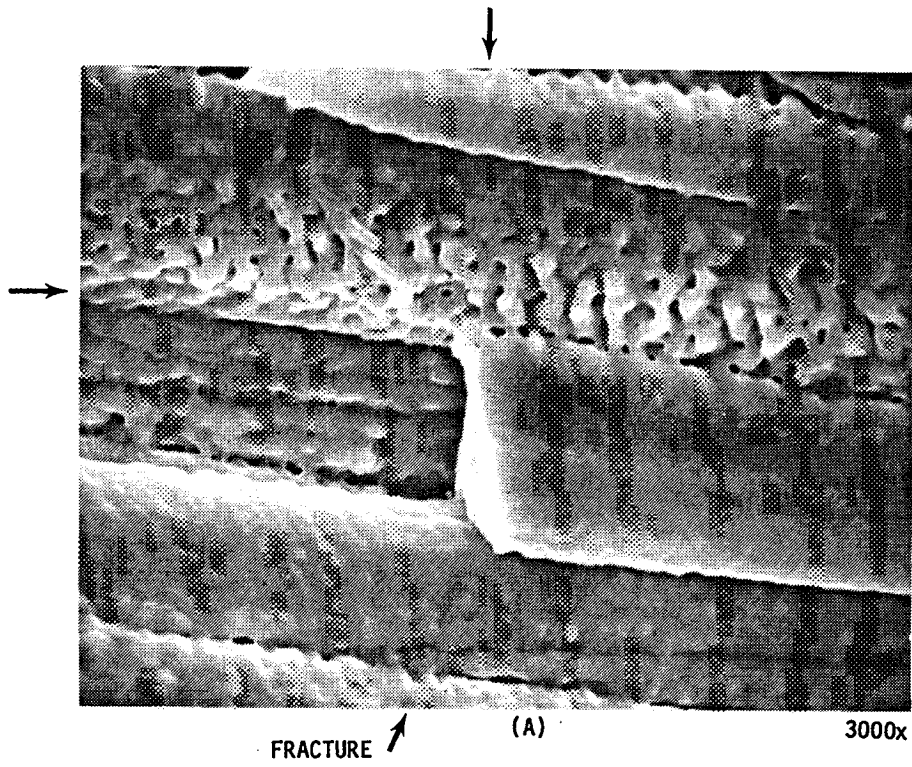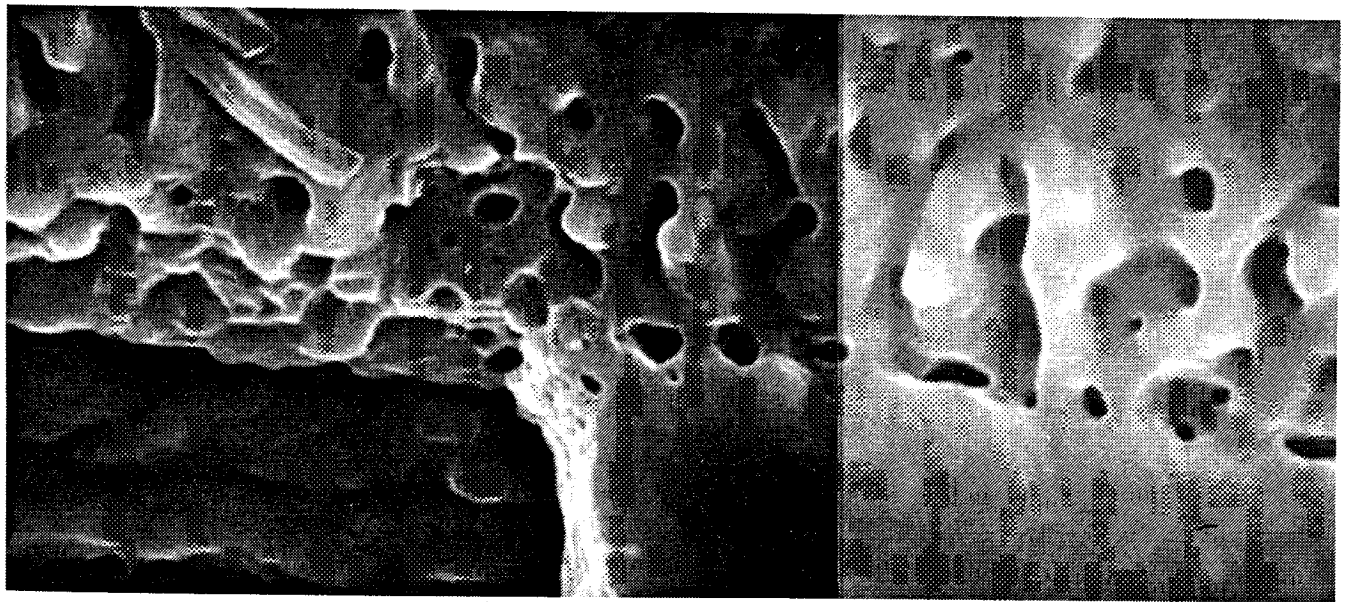
(A)   3000x
FRACTURE

(B)   10,000x
FRACTURE

Figure 53.– Cross-Section of a Static Air Furnace Test (1149C (2100F)/1800
Hours, Specimen FTSB-28) PWA 266 Ceramic Chip.

66

3.3.2.2 EB-PVD Thermal Barrier Coating Metallic Bond Observations

The metallic bond coat for the PWA 266 EB-PVD thermal barrier coating is formulated to provide oxidation resistance and to chemically "tie" the ceramic to the underlying superalloy structure. During thermal exposure, this bond coat oxidizes and forms an aluminum oxide layer between the ceramic and the bond coat. Since the failure location for this thermal barrier coating is located between the bond coat and this thermally grown oxide, a chemical analysis was performed on the bond coat to further understand it.

The structure of the bond coat for the pre-test and post-test (oxide emphasis Task VIIA test #3, 2.54 cm (1") burner rig bar was examined. Figures 54a and 54b are electron back scatter photomicrographs of the pre and post-test systems, respectively. In Figure 54a, fine beta (NiAl) and gamma solid solution phases are apparent. The beta phase is a hard, brittle, intermetallic phase. The bright spots represent active elements such as Hf which appear to reside predominantly at the beta gamma interface. With exposure time, a coarse bond coat structure forms (Figure 54b). The aluminum has a great affinity to combine with oxygen to form a thermally grown oxide. The beta particles are capable of providing aluminum to the surrounding gamma solid solution phase to form the aluminum oxide at the surface. It is obvious that the #3 test sample still had aluminum to provide growth of the oxide. It is also noted that as the structure gets coarser with hot time, clusters of particles form within the beta phase. At this point it is not known whether these particles are oxides, intermetallics, or clusters of Hf-rich regions. As the alumina grows along the EB-PVD ceramic/bond coat interface, the thermally grown oxide incorporates surface particles of the bond coat. The following paragraph describes the chemical distribution of the thermally grown oxide by x-ray maps of such surface particles as Hf, Y, and Cr.

3.3.2.3 EB-PVD TBC Thermally Grown Oxide

Spallation of the EB-PVD ceramic occurs by cracking at the thermally grown oxide (TGO) layer-metallic bond coat interface. This TGO grows between the metal and the EB-PVD ceramic layers during prolonged thermal exposure. The chemistry, microstructure, and surface topography of the failed TGO layer was analyzed. Techniques employed included x-ray diffraction (XRD), scanning electron microscopy (SEM) including KEVEX analysis for elements present, and transmission electron microscopy (TEM). Thermally grown oxide examination was performed to help determine fracture modes of the coating between various test conditions. Chips were retrieved from a variety of tests for examination: strain emphasis test, oxide emphasis, cyclic oxidation, static oxidation, and mixed mode emphasis. As summarized in Table XXVI and Figures 55 through 72, these chips exhibit a number of similarities and perhaps one or two significant differences.

The similarities include adherence of the aluminum oxide scale to the ID of the ceramic chip, pebbly, craze-cracked appearance, and similar x-ray results. The thermally grown oxide consists basically of alpha-hexagonal alumina.
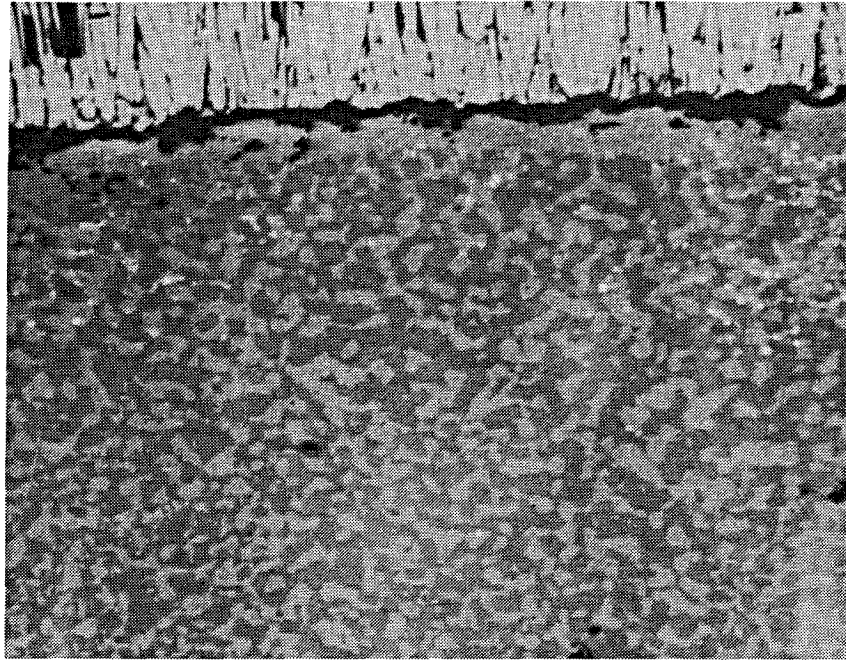
Figure 54a.– Electron Back Scatter Photomicrograph of a Pre-Test 2.54 cm (1")
Burner Rig Bar Emphasizing Bond Coat Structure. Mag: 600x

Figure 54b.– Electron Back Scatter Photomicrograph of a Post-Test 2.54 cm (1")
Burner Rig Bar Emphasizing Bond Coat Structure (Oxide Emphasis
TASK VIIA Test #3, 1107C (2025F)/12 Minute Cycle Which Failed at
712 Hours). Mag: 600x

68
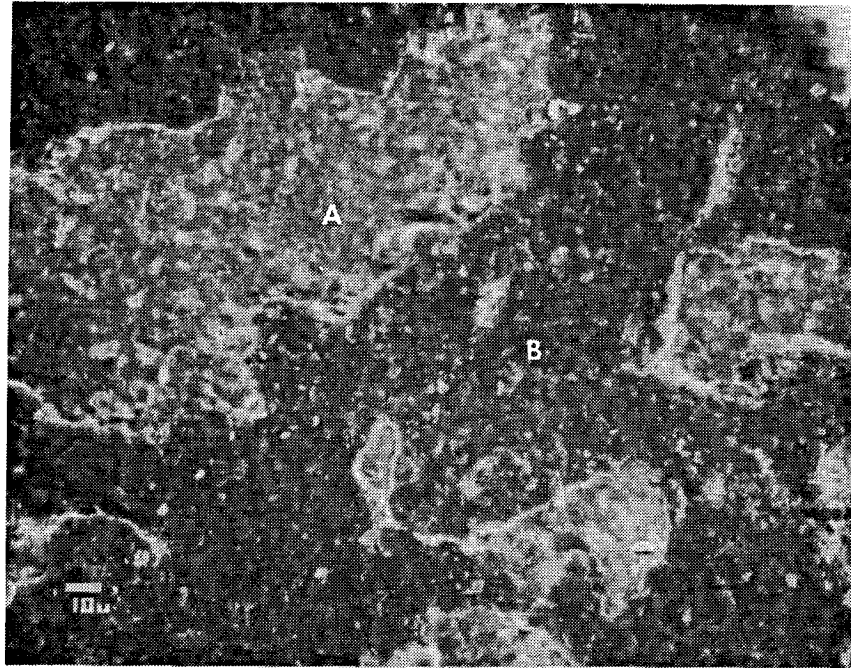
Figure 55a.- Photomicrograph of the ID of a Spalled Ceramic Chip From a Strain
Emphasis 1177C(2150F)/6 Minute Cycle Test (TASK VIIA Test #11/167
Hours to Failure). Mag: 500x
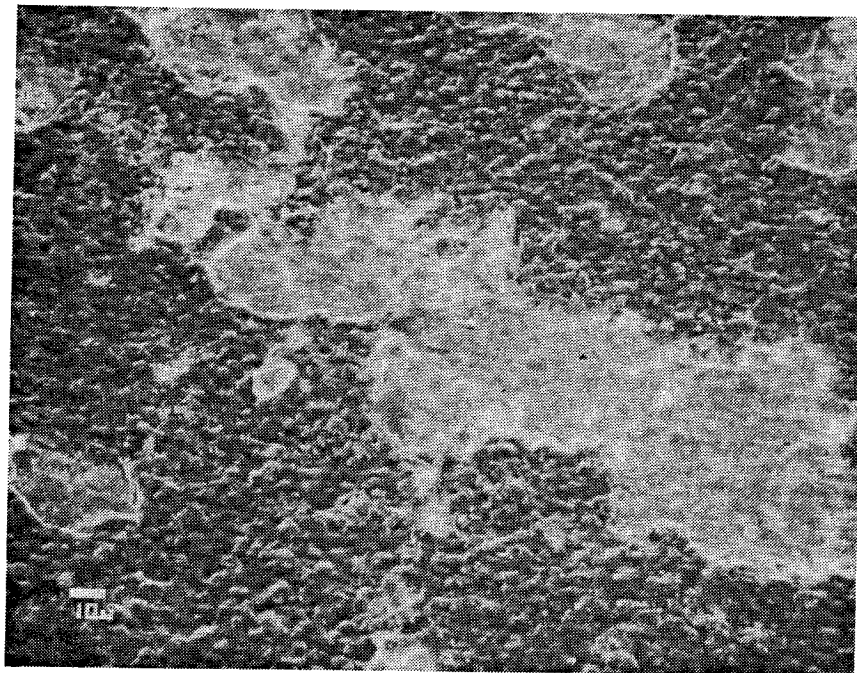
Figure 55b.- Photomicrograph Taken at an Angle of a Spalled Ceramic Chip From
a Strain Emphasis 1177C(2150F)/6 Minute Cycle Test (TASK VIIA
Test #11/167 Hours to Failure). Mag: 500x
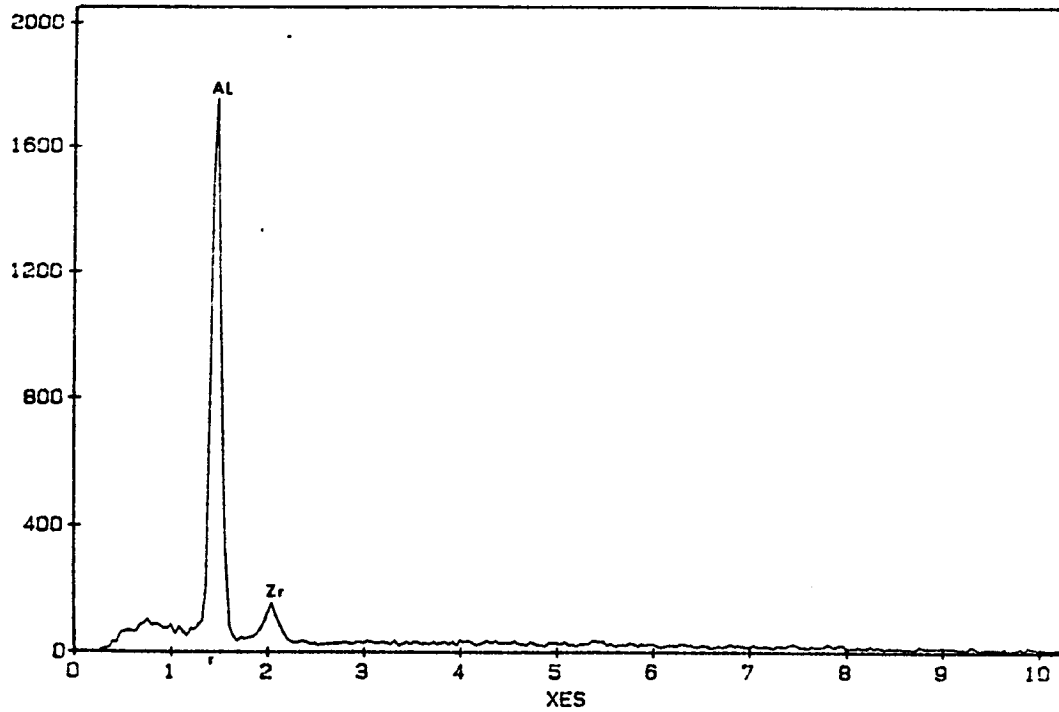
Figure 56a.- KEVEX Analysis of the Entire Field of View in Figure 55a, the ID
of a Spalled Ceramic Chip From a Strain Emphasis 1177C(2150F)/6
Minute Cycle Test (TASK VIIA Test #11/167 Hours to Failure).
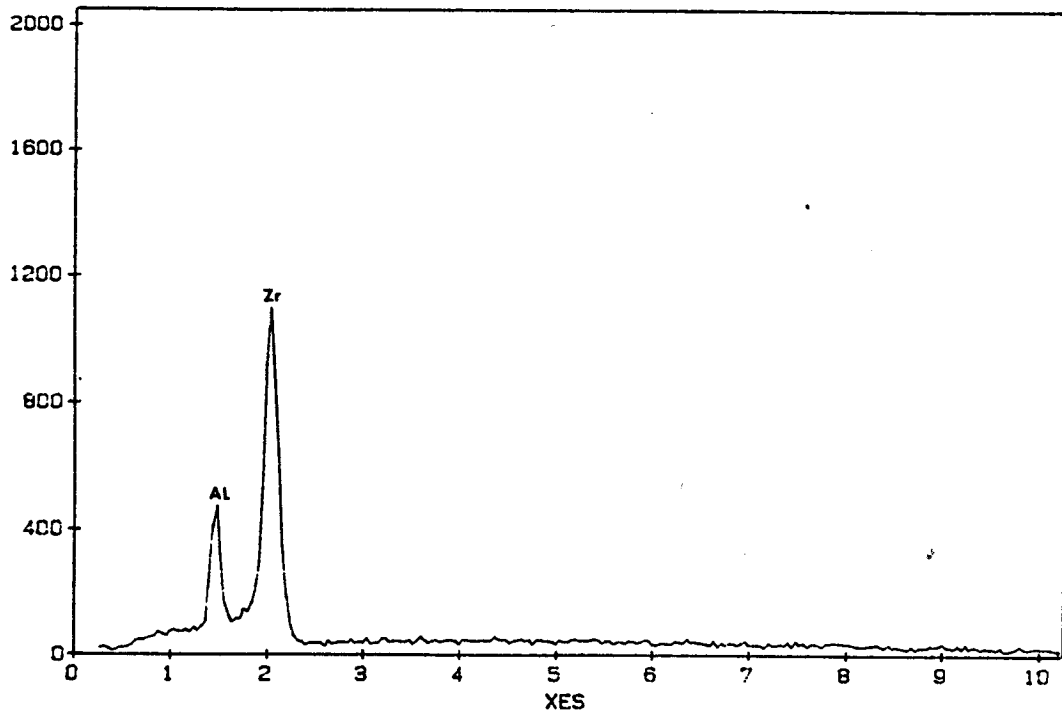
Figure 56b.- KEVEX Analysis of Location "A" in Figure 55a the ID of a Spalled
Ceramic Chip From a Strain Emphasis 1177C(2150F)/6 Minute Cycle
Test (TASK VIIA Test #11/167 Hours to Failure).
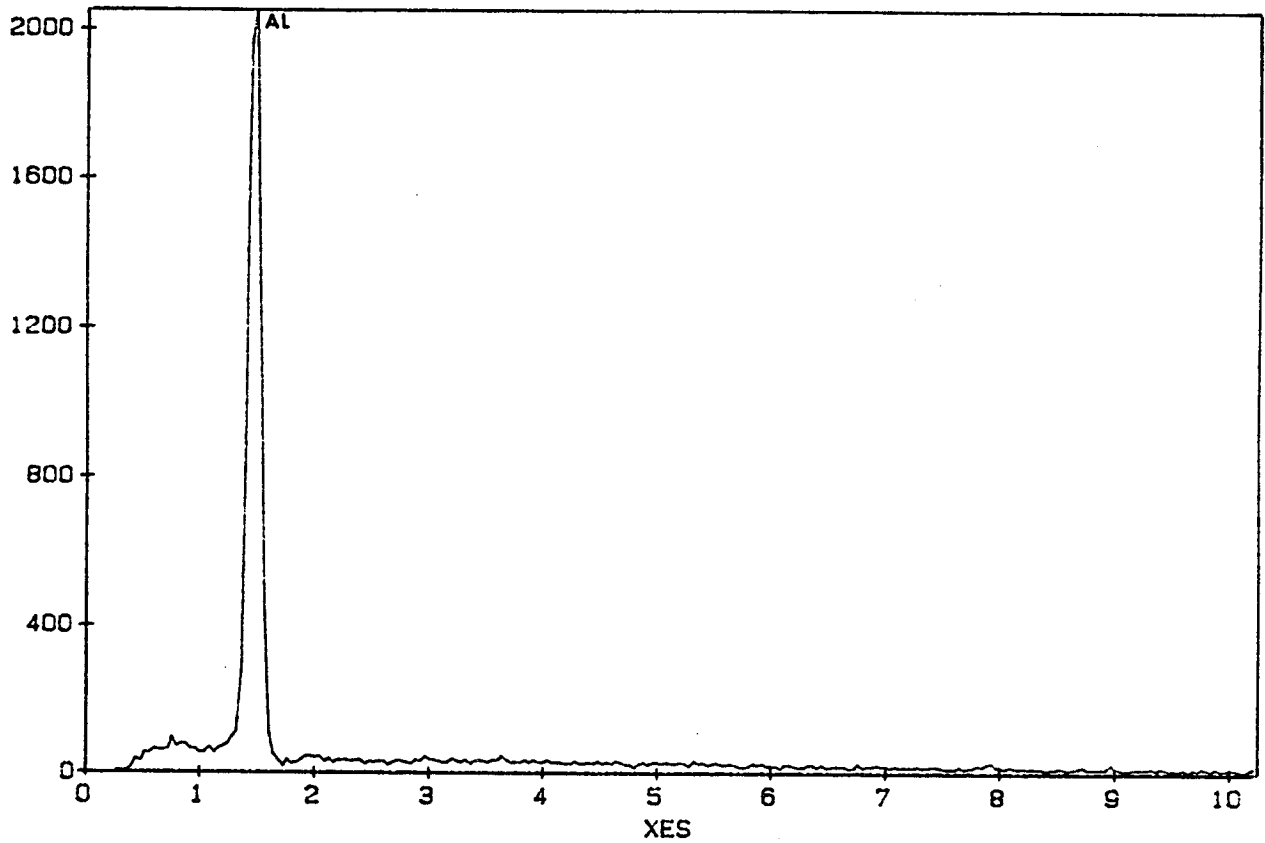
Figure 56c.- KEVEX Analysis of Location "B" in Figure 55a the ID of a Spalled
Ceramic Chip From a Strain Emphasis 1177C(2150F)/6 Minute Cycle
Test (TASK VIIA Test #11/167 Hours to Failure).
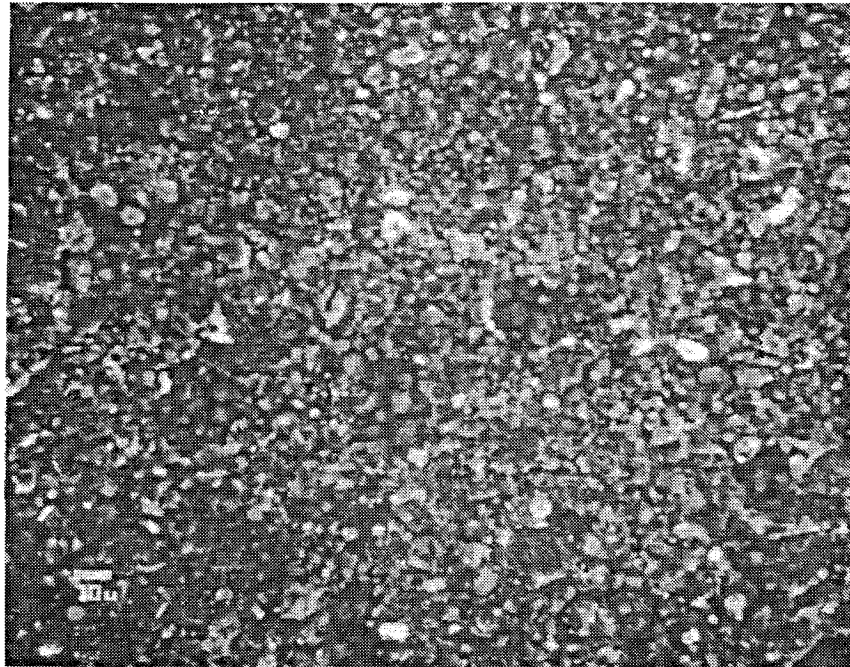
Figure 57a.- Photomicrograph of the ID of a Spalled Ceramic Chip From an Oxide
Emphasis 1107C(2025F)/6 Minute Cycle Test (TASK VIIA Test #1/243
Hours to Failure). Mag: 500x
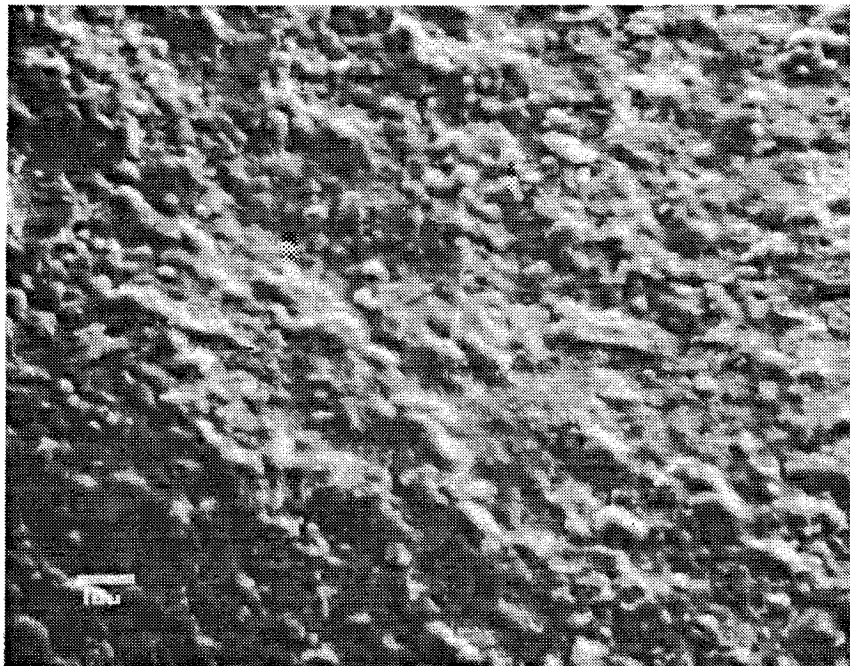
Figure 57b.- Photomicrograph Taken at an Angle of the ID of a Spalled Ceramic
Chip From an Oxide Emphasis 1107C (2025F)/6 Minute Cycle Test
(TASK VIIA Test # 1/ 243 Hours to Failure). Mag: 500x
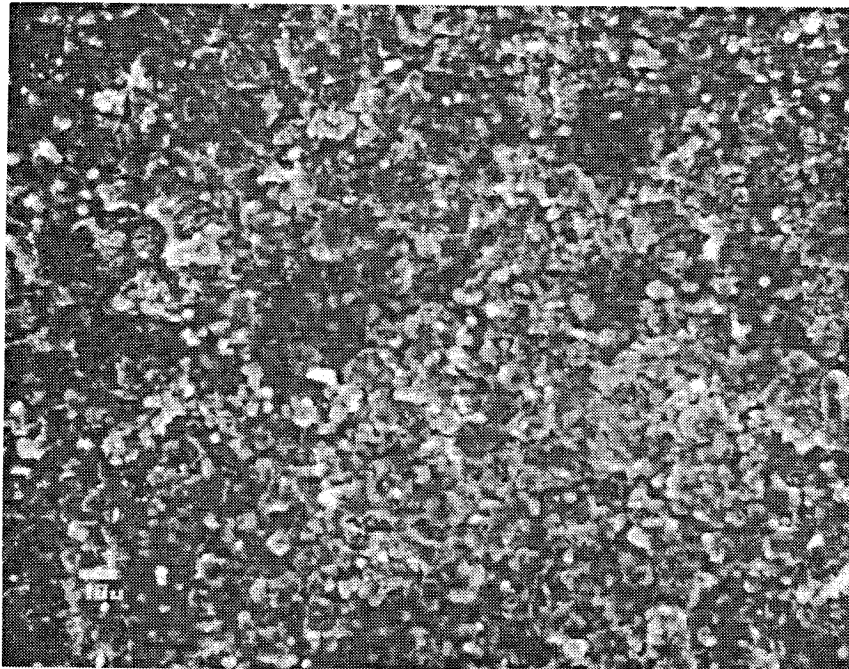
Figure 58a.- Photomicrograph of the ID of a Spalled Ceramic Chip From an Oxide Emphasis 1107C(2025F)/12 Minute Cycle Test (TASK VIIA Test #3/712 Hours to Failure). Mag: 500x
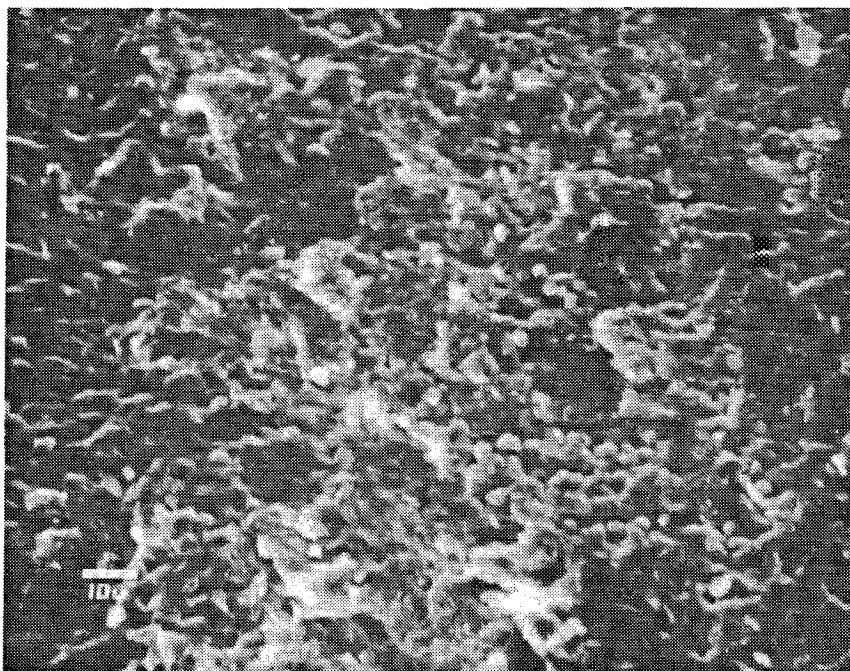
Figure 58b.- Photomicrograph Taken at an Angle of the ID of a Spalled Ceramic Chip From an Oxide Emphasis 1107C(2025F)/ 12 Minute Cycle Test (TASK VIIA Test #3/712 Hours to Failure). Mag: 500x
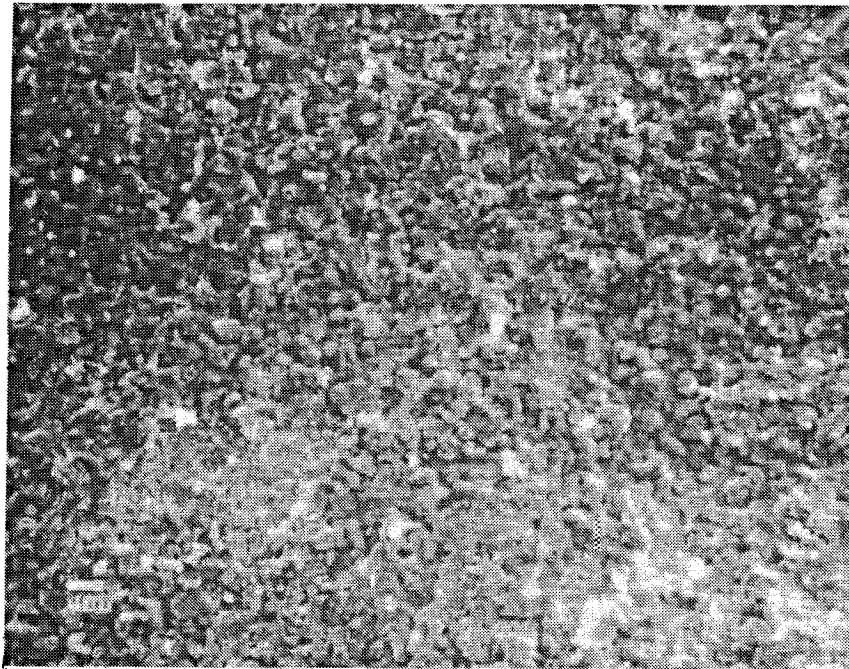
Figure 59a.- Photomicrograph of the ID of a Spalled Ceramic Chip From a 1149C
(2100F)/10 Hour Cyclic Furnace Test (TASK VIA Test/90 Hours to
Failure). Mag: 500x
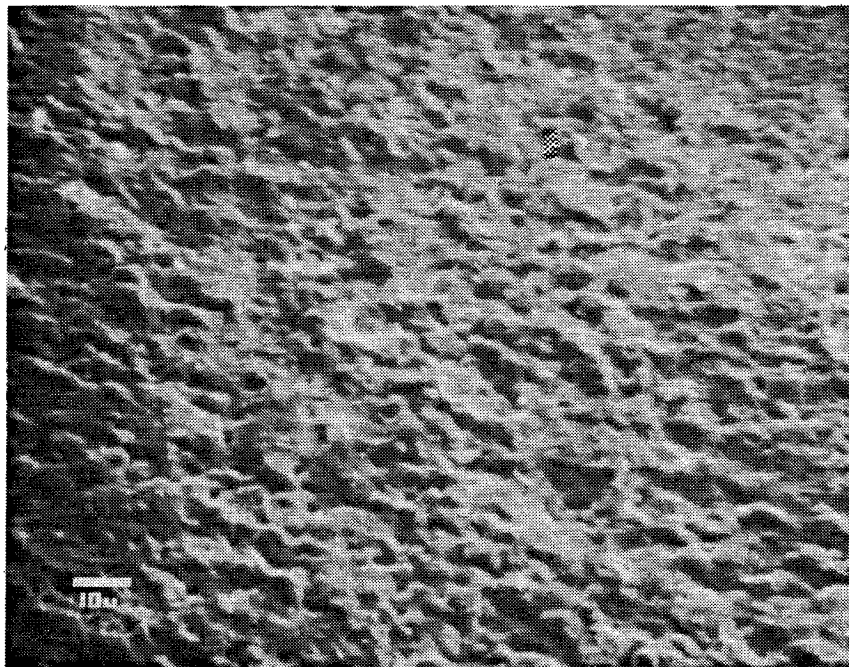
Figure 59b   Photomicrograph Taken at an Angle of a Spalled Ceramic Chip From
a 1149 (2100F)/10 Hour Cyclic Furnace Test (TASK VIA Test/90
Hours to Failure). Mag: 500x

74
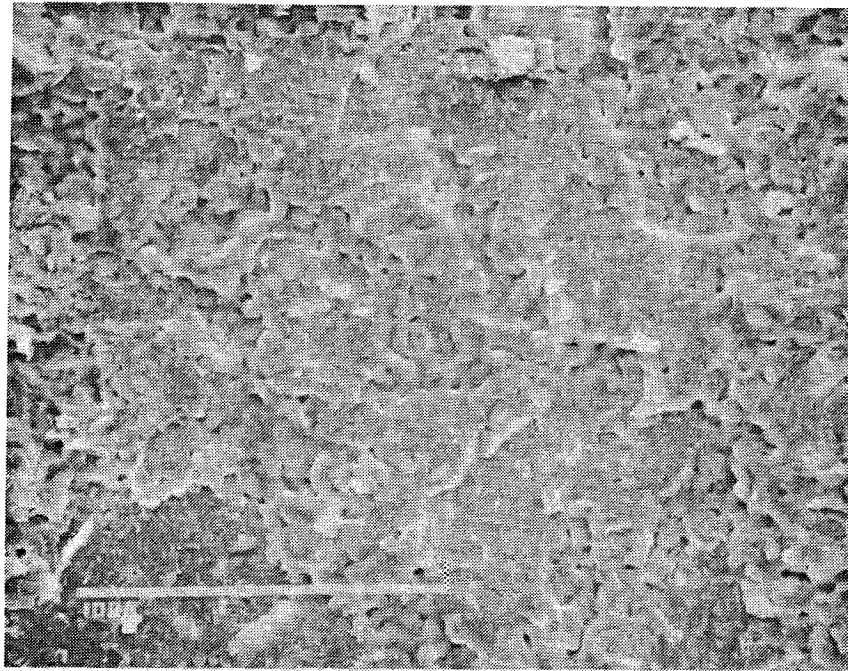
Figure 60a.- Photomicrograph of the ID of a Spalled Ceramic Chip From a
        1149C(2100F) Static Furnace Test at 1800 Hours (TASK VIA Test).
        Mag: 500x
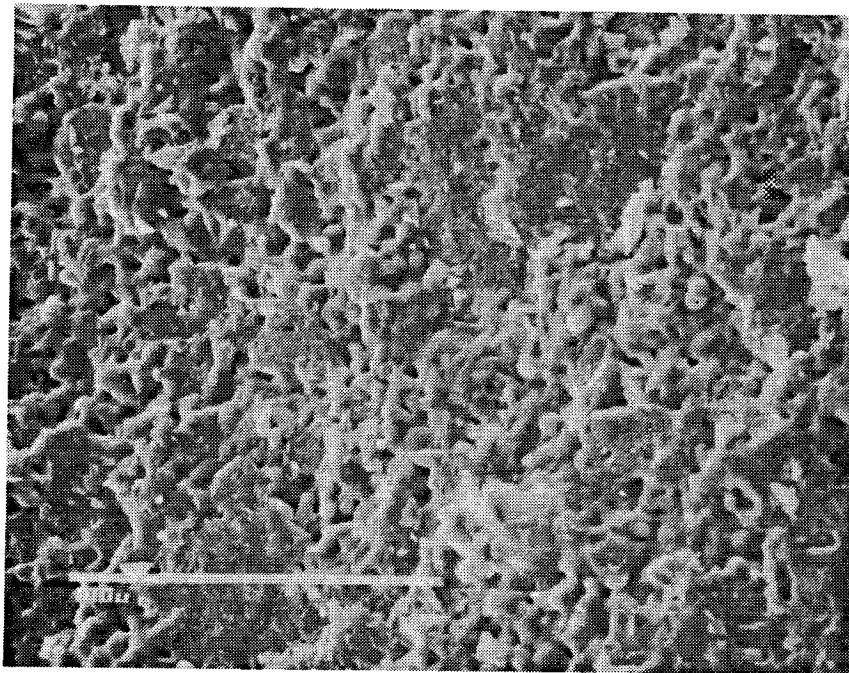
Figure 60b.- Photomicrograph Taken at an Angle of the ID of a Spalled Ceramic
        Chip From a 1149C(2100F) Static Furnace Test at 1800 Hours (TASK
        VIA Test). Mag: 500x

75
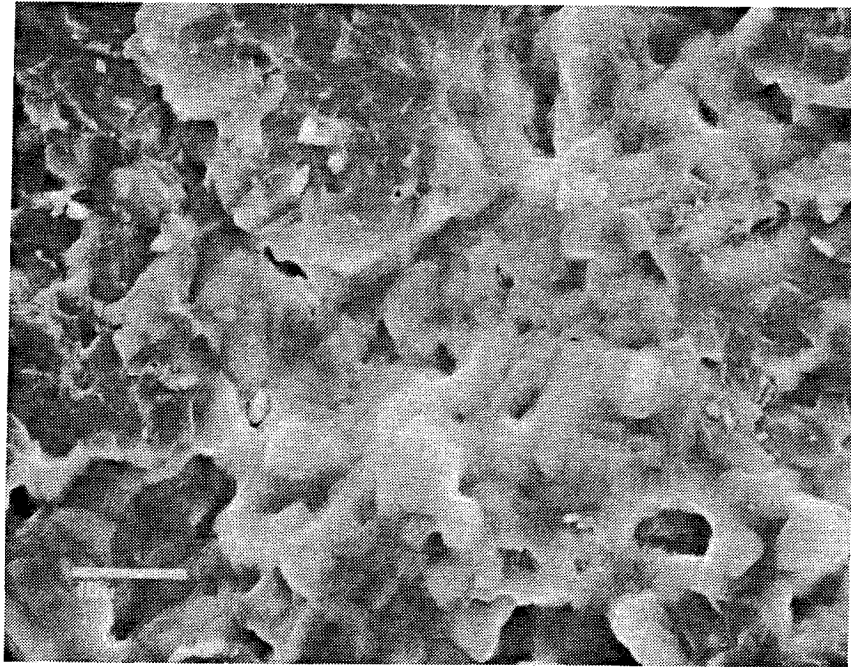
Figure 61a   Photomicrograph of the ID of a Spalled Ceramic Chip From a 1149C (2100F) Static Furnace Test at 1800 Hours (TASK VIA Test). Mag: 500x
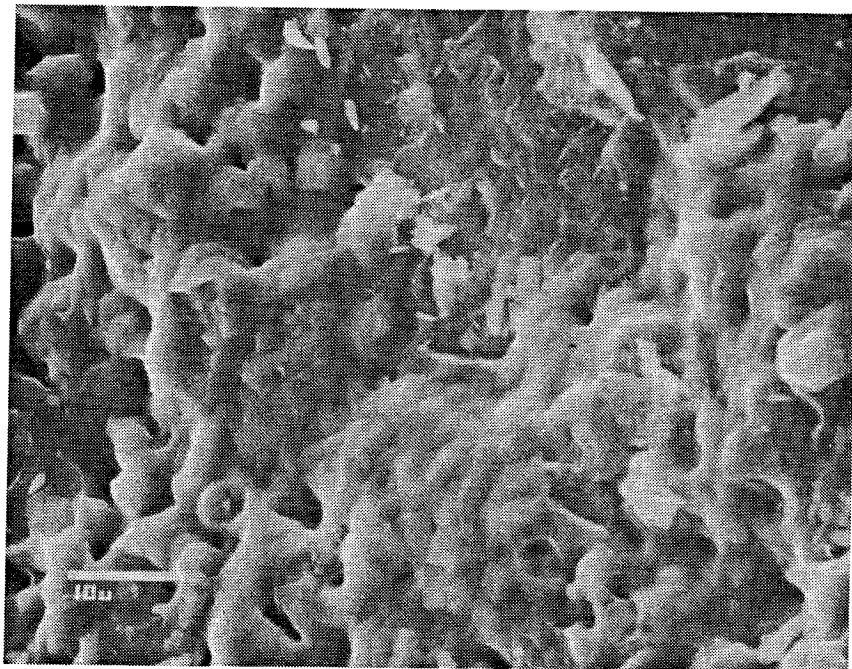
Figure 61b.-   Photomicrograph Taken at an Angle of the ID of a Spalled Ceramic Chip From a 1149C (2100F) Static Furnace Test at 1800 Hours (TASK VIA Test). Mag: 1500x

76
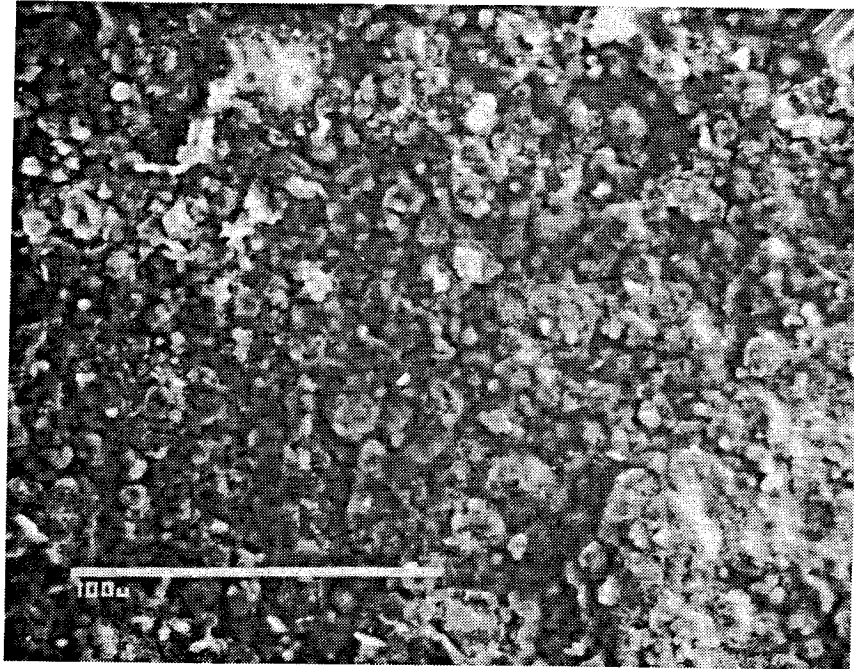
Figure 62a.- Photomicrograph of the ID of a Spalled Ceramic Chip From a Mixed
Mode Emphasis 1079C (1975F)/6 Minute Cycle Test (TASK VIIA Test
#13/1352 Hours to Failure). Mag: 500x
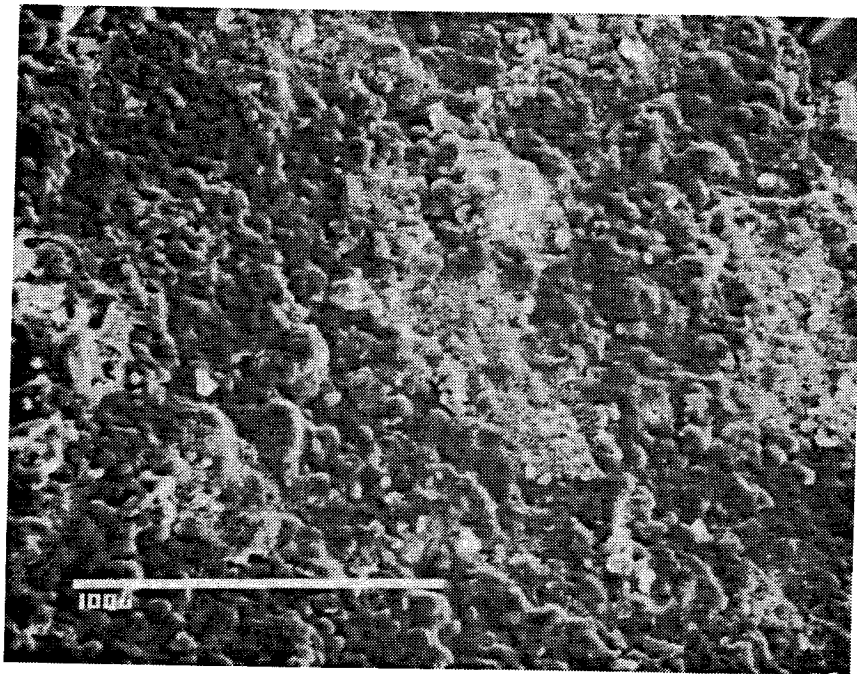
Figure 62b.- Photomicrograph Taken at an Angle of the ID of a Spalled Ceramic
Chip From a Mixed Mode Emphasis 1079C (1975F)/6 Minute Cycle Test
(TASK VIIA Test #13/1352 Hours to Failure). Mag: 500x

77
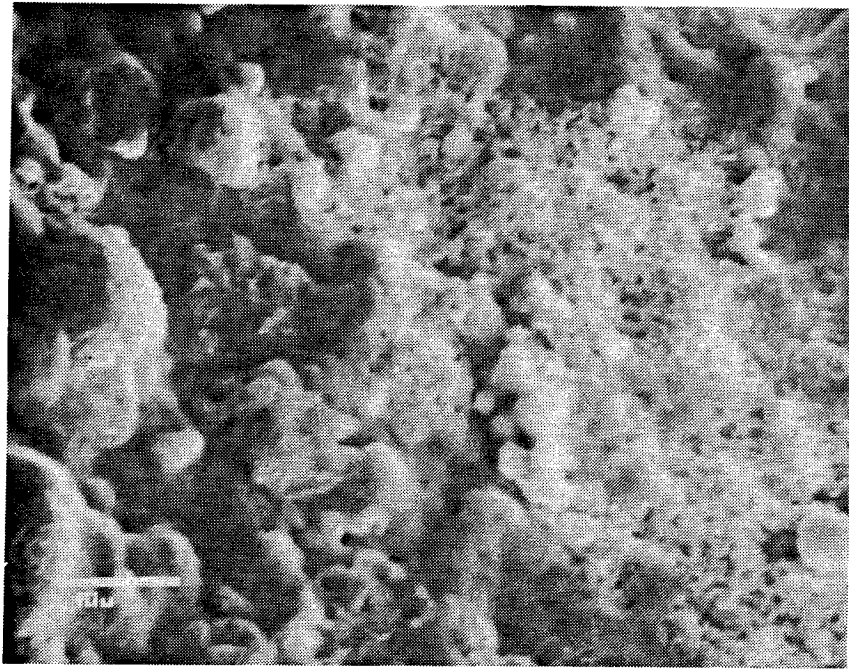
Figure 63.— Photomicrograph of a Unique, Porous, Localized Region on the ID of
a Spalled Ceramic Chip From a Mixed Mode Emphasis 1079C (1975F)/6
Minute Cycle Test (TASK VIIA Test #13/1352 Hours to Failure).
Mag: 500x

78
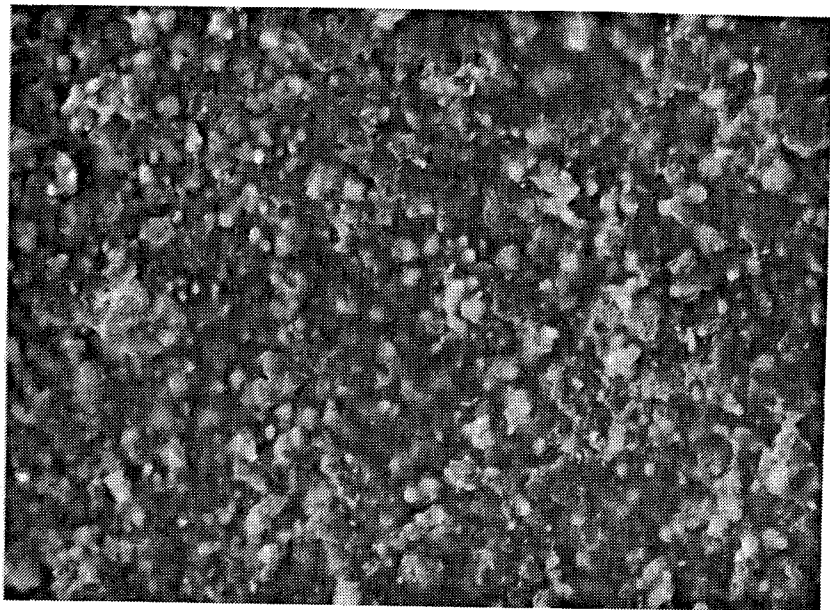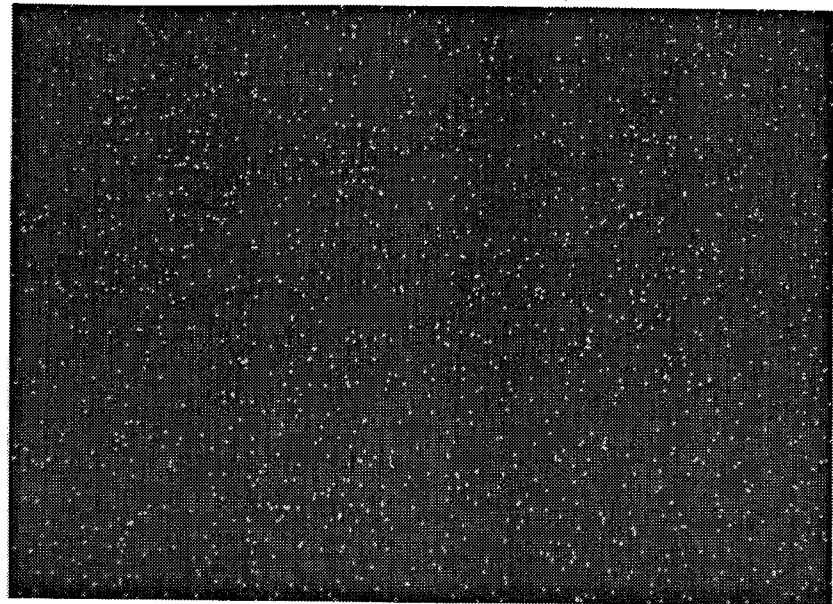
A SEI   1000x   B   Hf X-ray Map   1000x
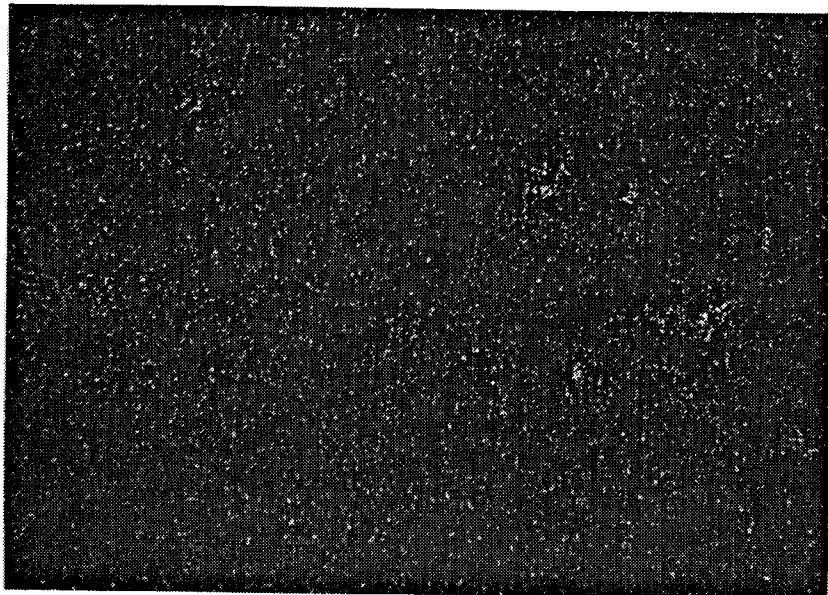
C   Ni X-ray Map   1000x   D   Cr X-ray Map   1000x

Figure 64.- The ID Surface of a Spalled Ceramic Chip From a Strain Emphasis
1177C(2150F)/6 Minute Burner Rig Test (167 Hours to Failure).

Figure 65.- The ID Surface of a Spalled Ceramic Chip From an Oxide Emphasis 1107C(2025F)/12 Minute Burner Rig Test (712 Hours to Failure).

A SEI	1000×
B Ti X-ray Map	1000×
C Ni X-ray Map	1000×
D Cr X-ray Map	1000×
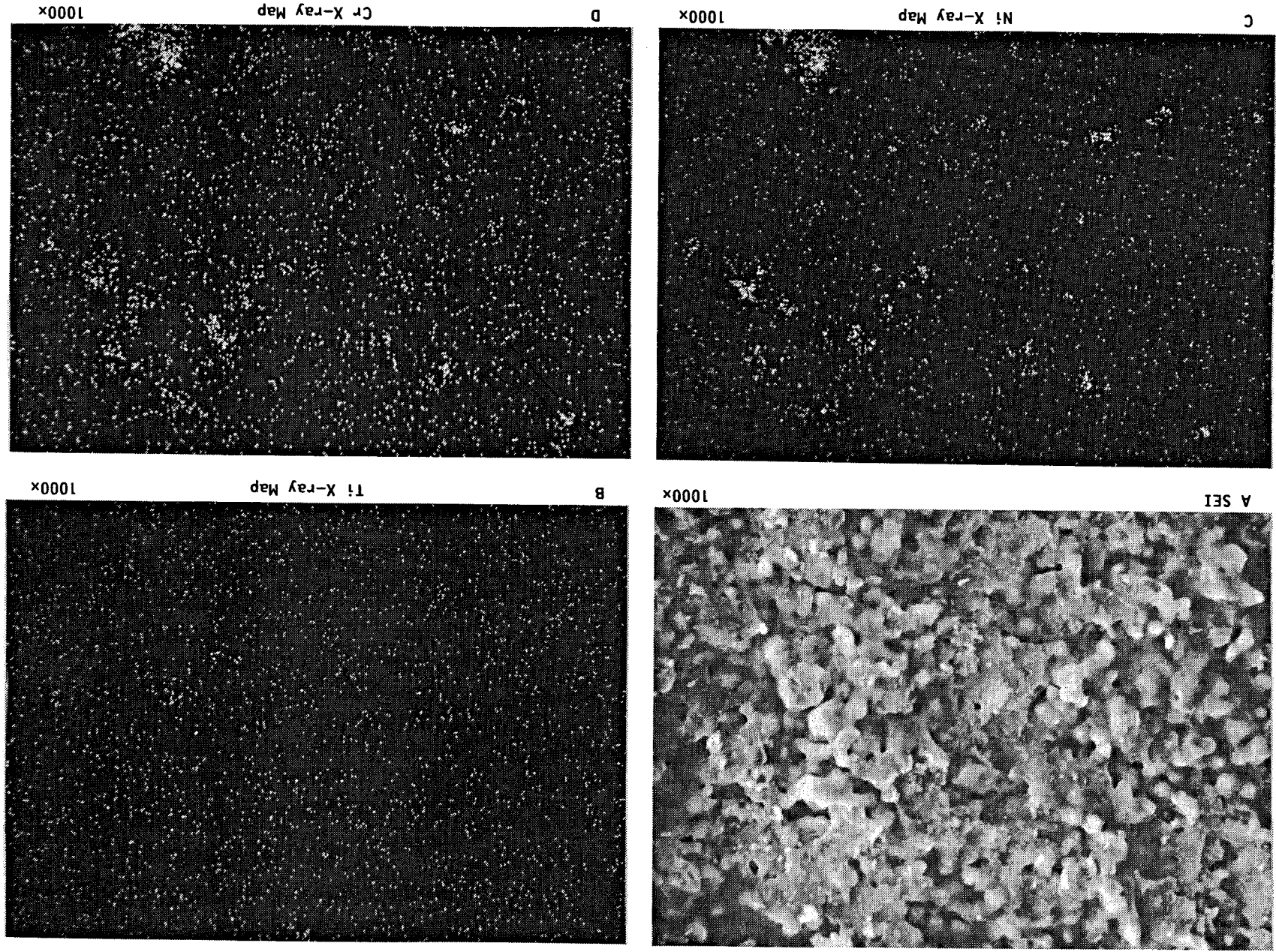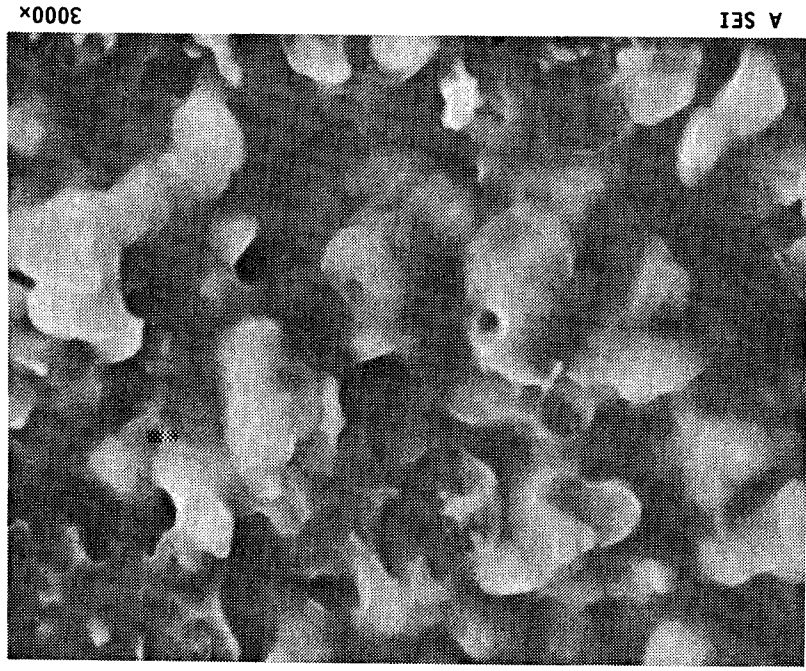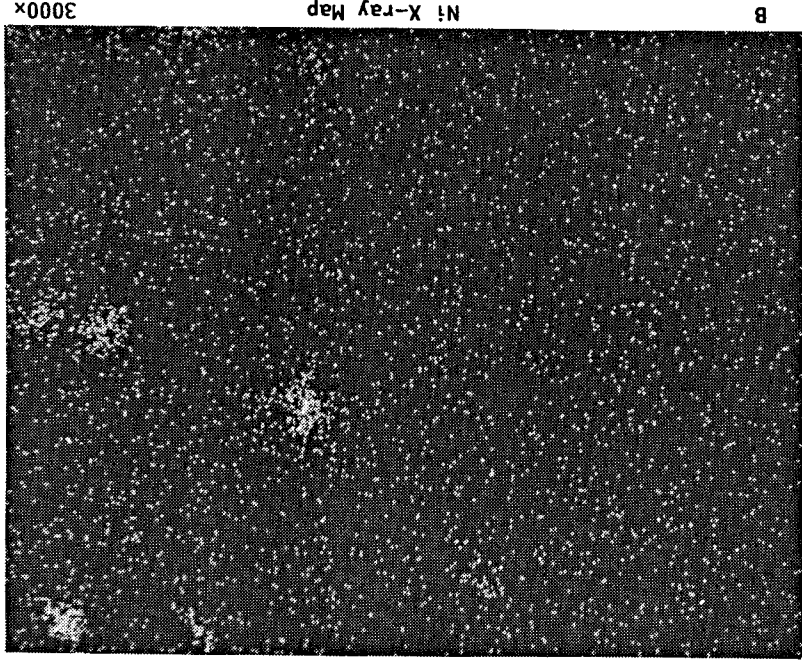
Figure 66.– The ID Surface of a Spalled Ceramic Chip From an Oxide Emphasis 1107C(2025F)/12 Minute Burner Rig Test in a Location Free of Fracture (712 Hours to Failure).

Figure 67.- The ID Surface of a Spalled Ceramic Chip From an Oxide Emphasis
1107C(2025F)/12 Minute Burner Rig Test in a Location of Fractured
TGO (712 Hours to Failure).
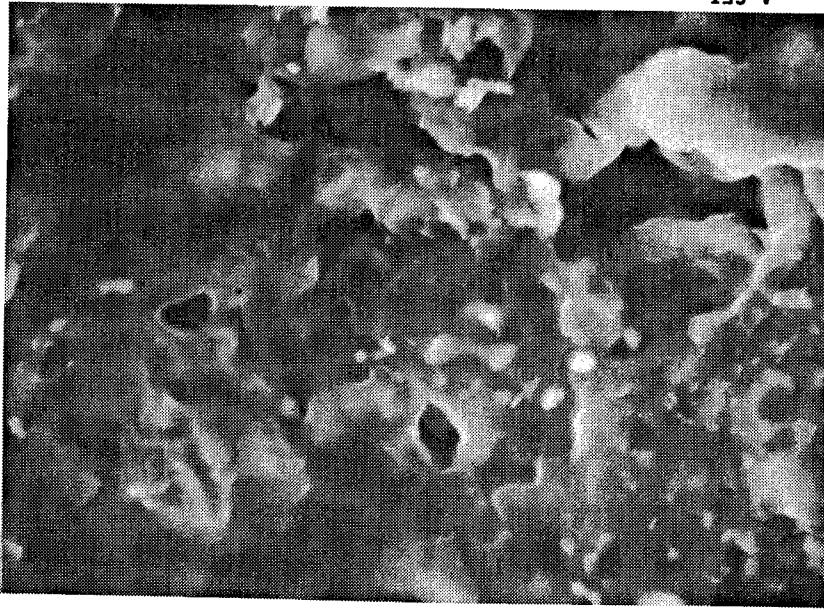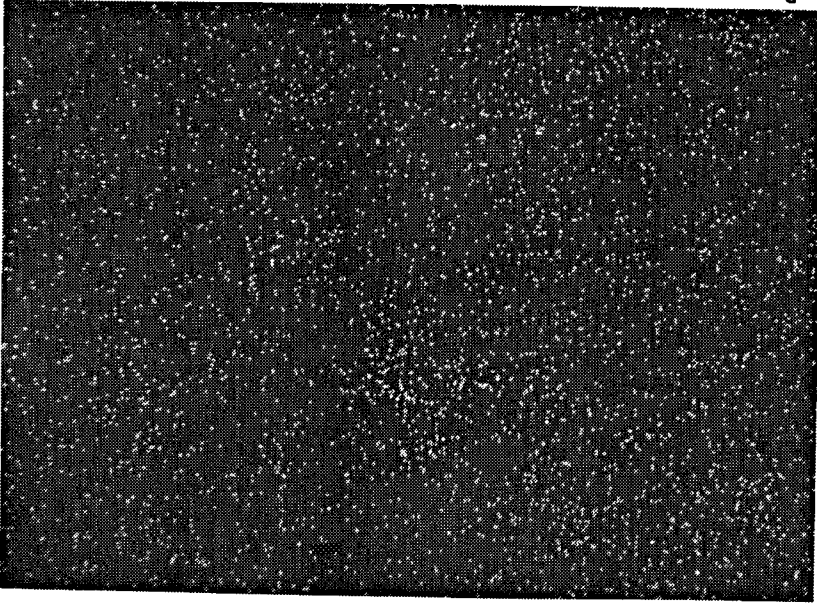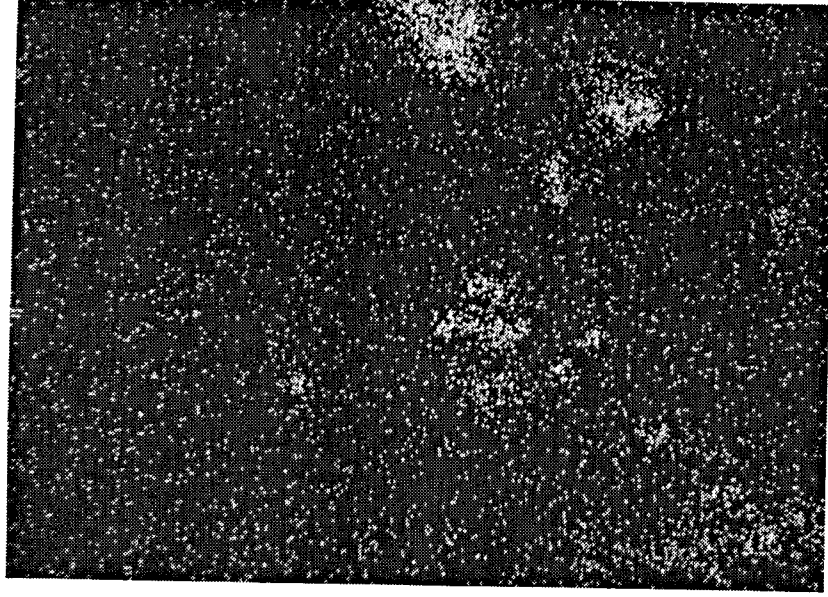
Figure 68.- The ID Surface of a Spalled Ceramic Chip From a 1149C(2100F)
Static Furnace Test (1800 Hours).

A SEI   300x

B   Ni X-ray Map   300x

D	Cr X-ray Map	1000×

C	Ni X-ray Map	1000×

B	Hf X-ray Map	1000×

A SEI		1000×
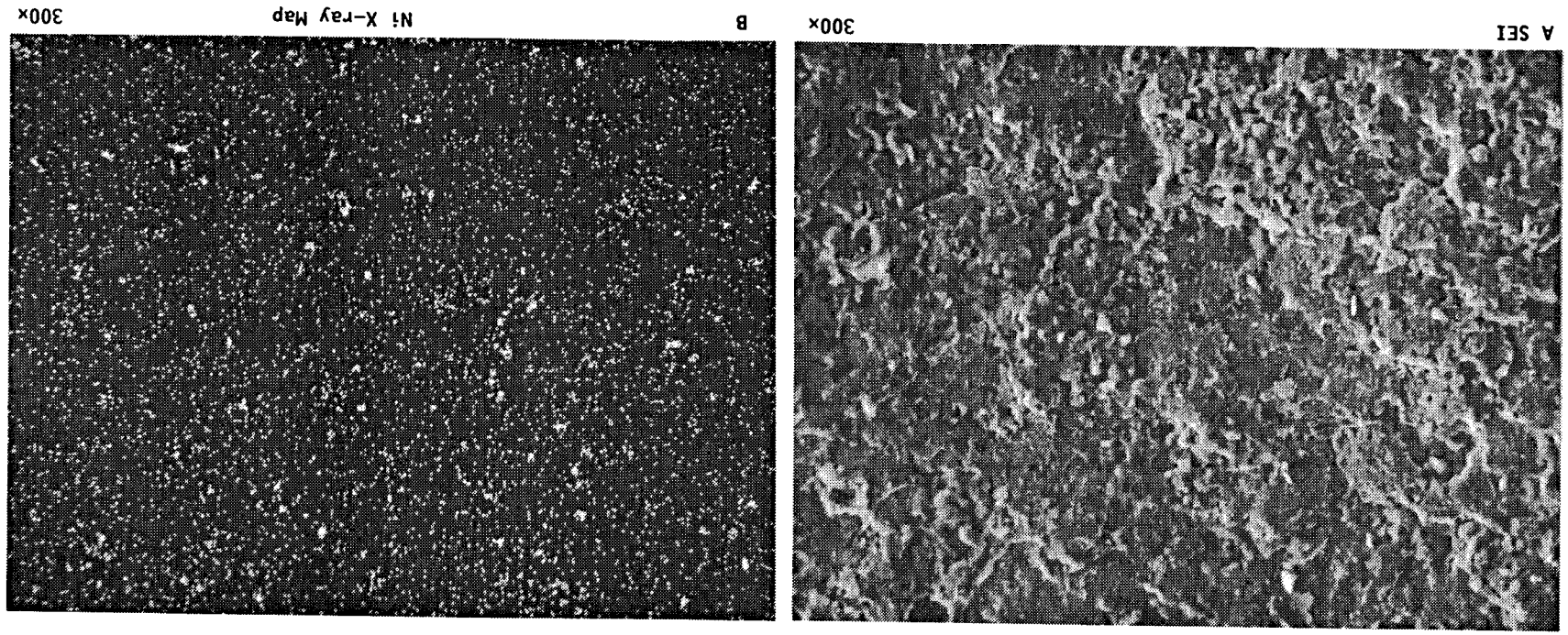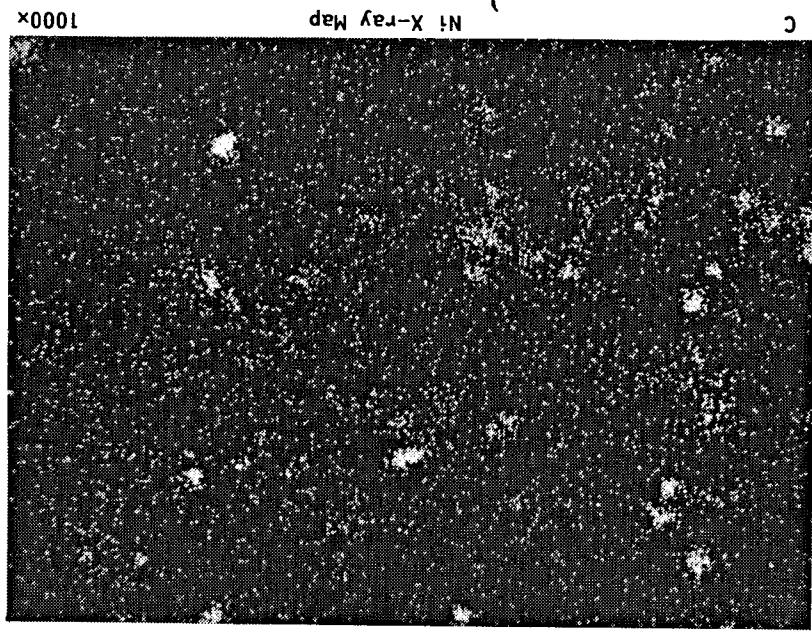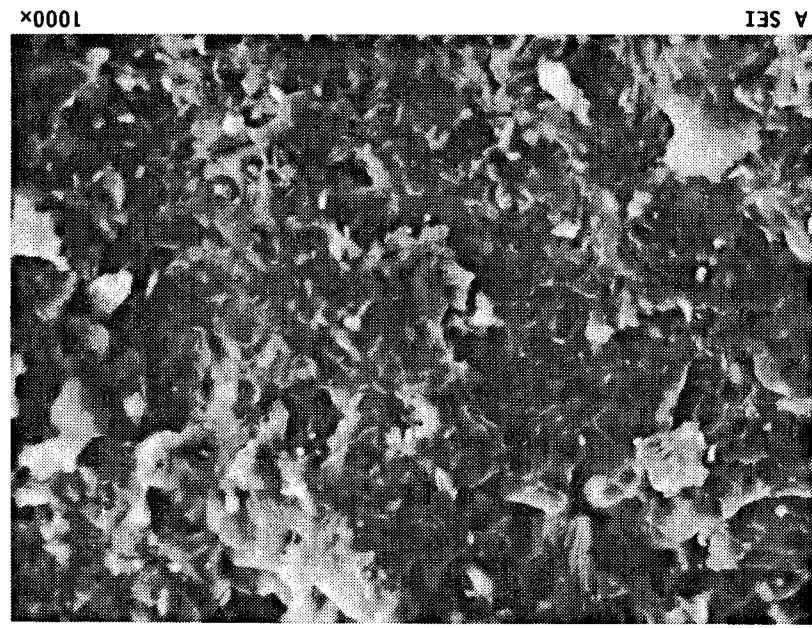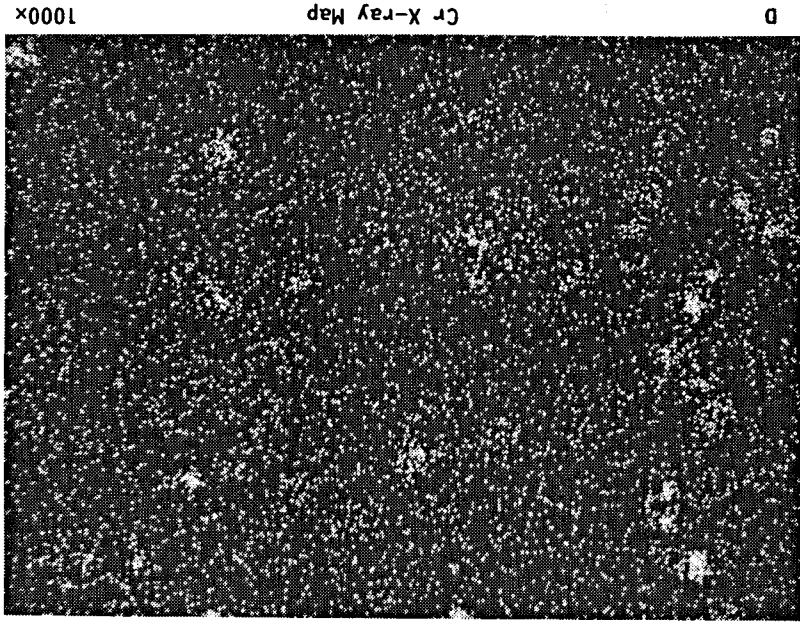
Figure 69.- The ID Surface of a Spalled Ceramic Chip From a 1149C(2100F)
Static Air Furnace Test at a Location of TGO Fracture (1800 Hours).

84
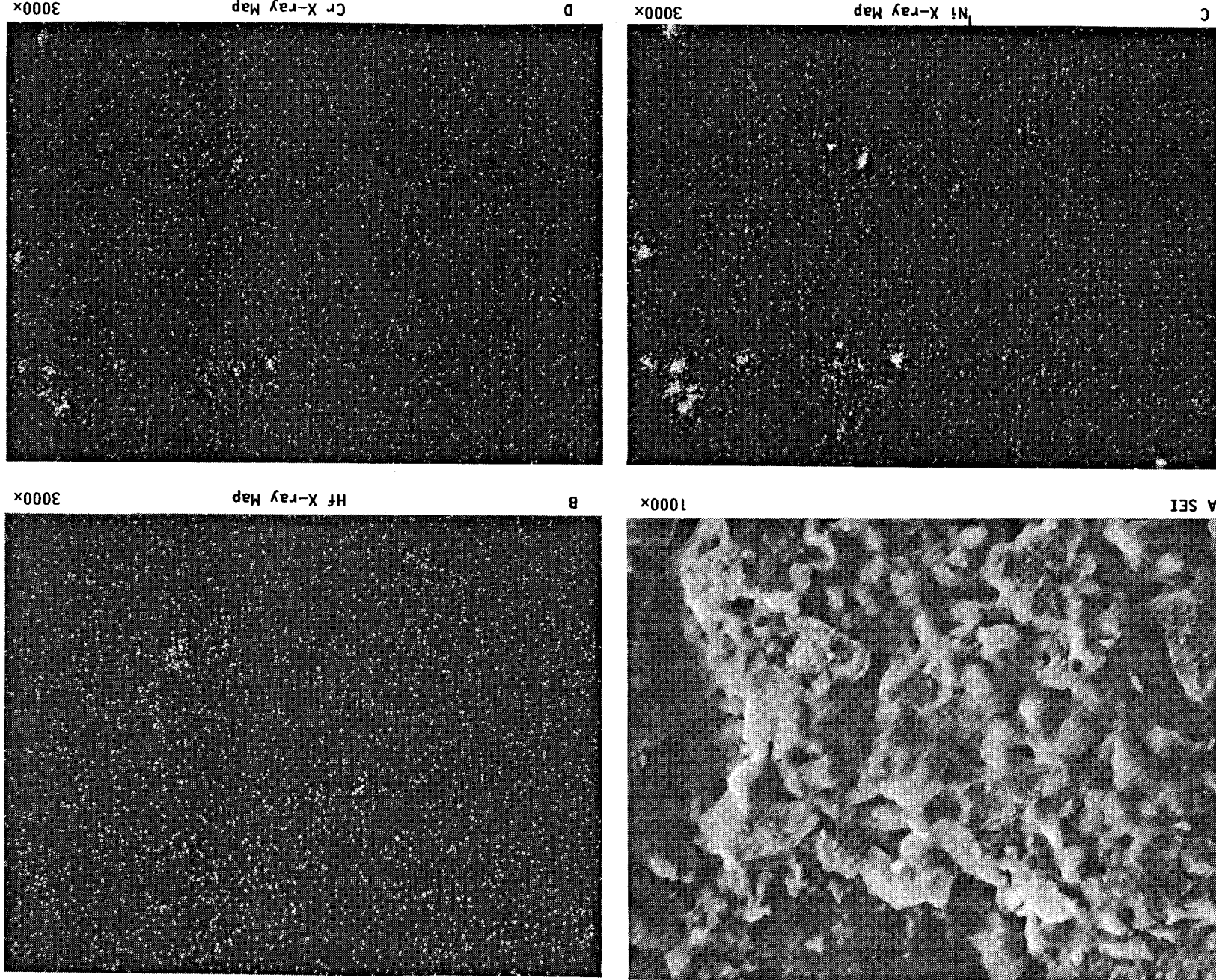
Figure 70.- The ID Surface of a Spalled Ceramic Chip From a 1149C(2100F)
Static Air Furnace Test at a Location Relatively Free of TGO
Fracture (1800 Hours).
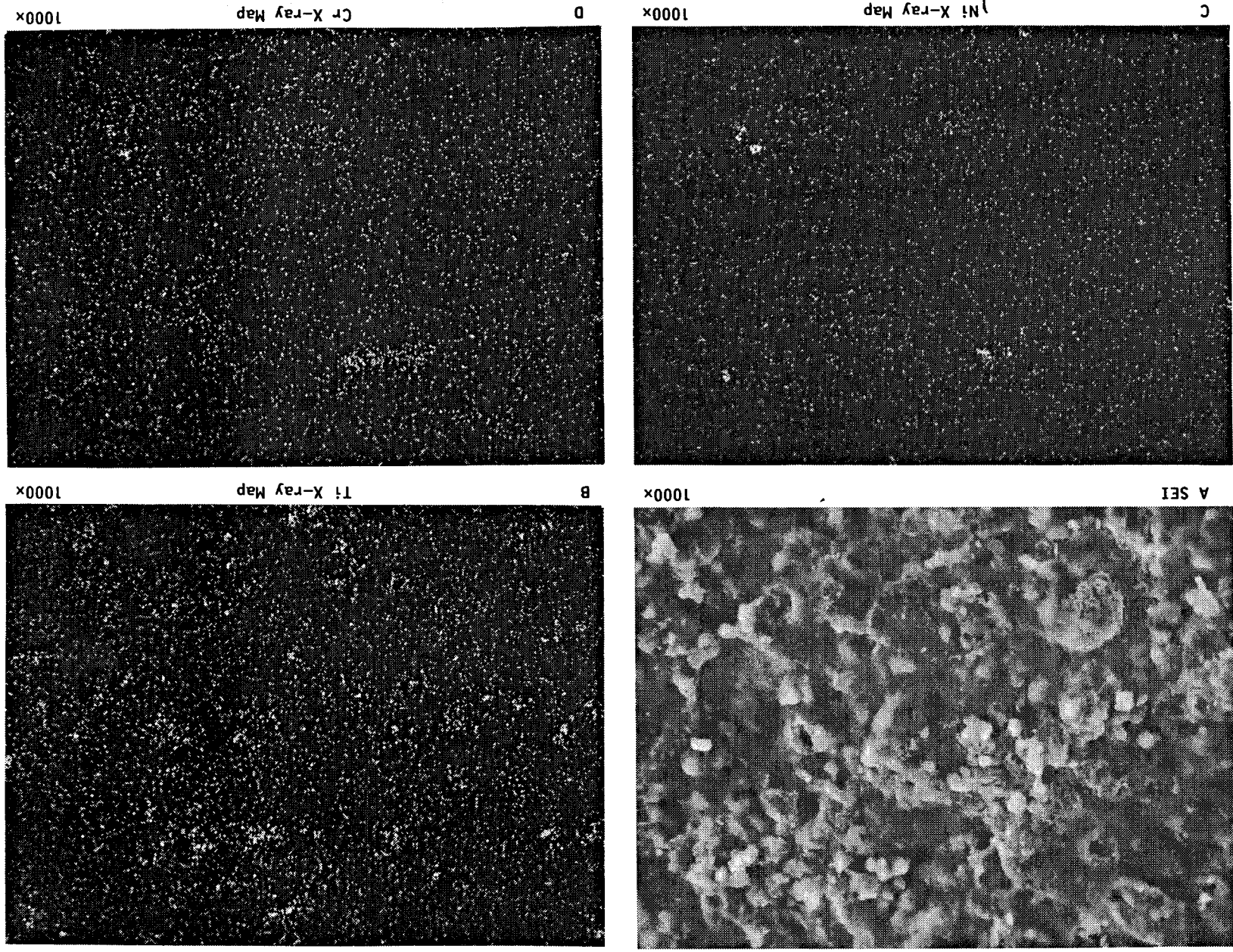
Figure 71.- The ID Surface of a Spalled Ceramic Chip From a Mixed Mode Emphasis 1079C (1975F)/6 Minute Burner Rig Test (1352 Hours to Failure).

A SEI 1000×

B Ti X-ray Map 1000×

C Ni X-ray Map 1000×

D Cr X-ray Map 1000×
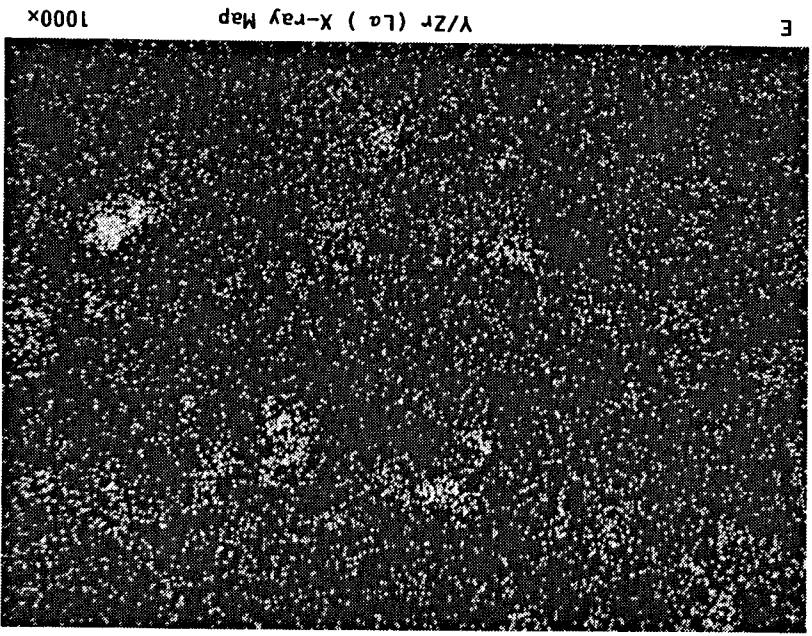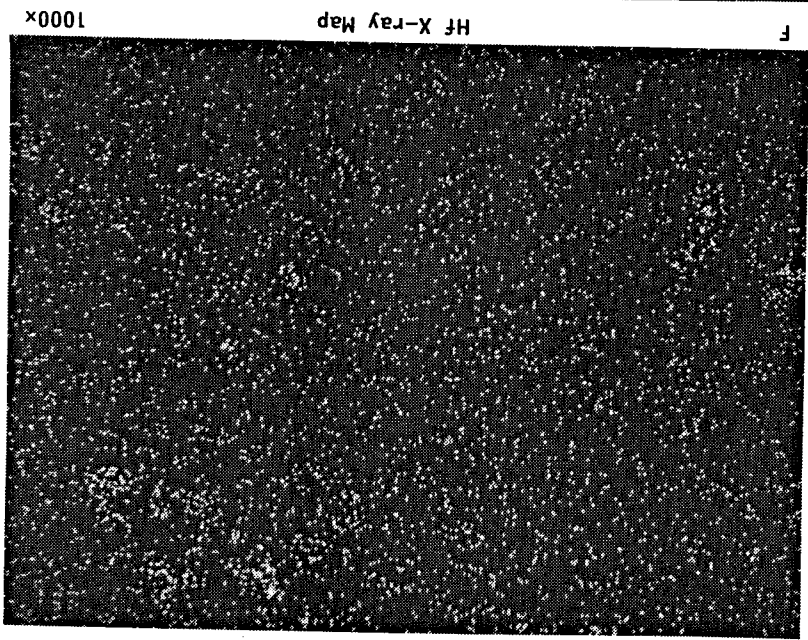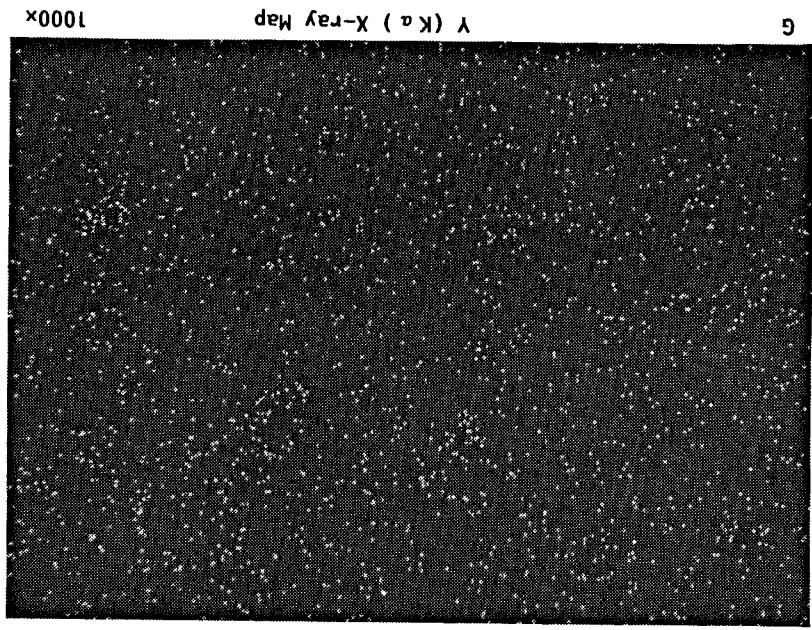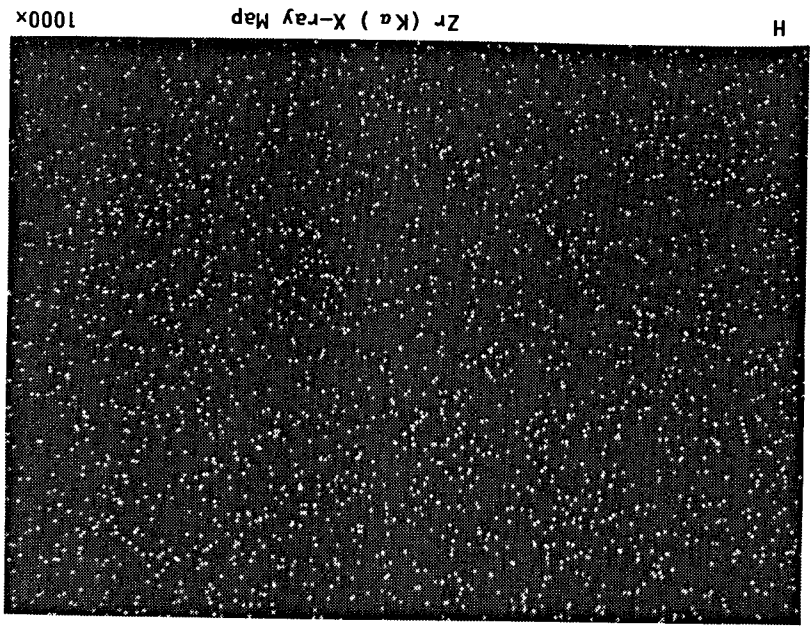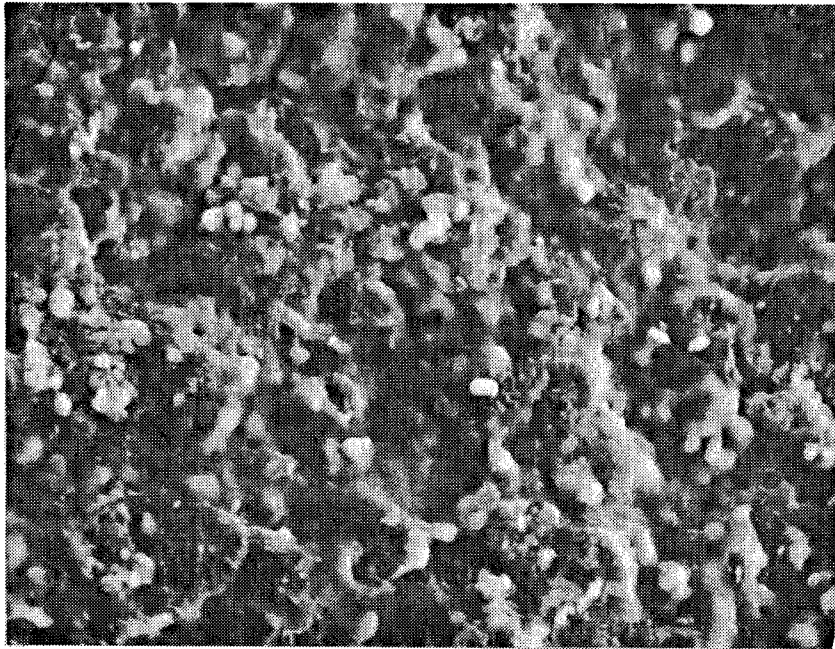
Figure 72.- The ID Surface of a Spalled Ceramic Chip From a Mixed Mode Emphasis 1079C (1975F)/6 Minute Burner Rig Test (1352 Hours to Failure).

A SEI 1000x (3°)

B Detailed SEI 3000x
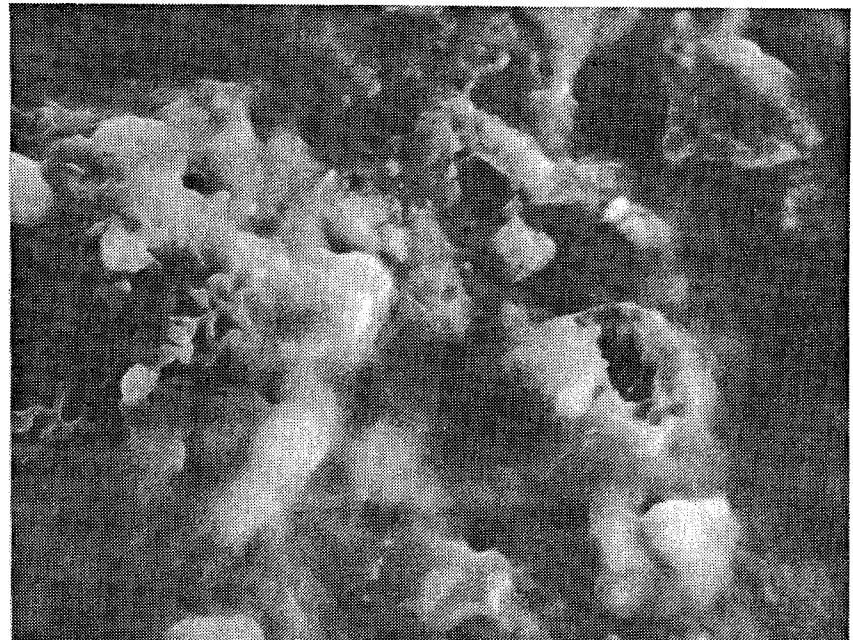
C Detailed SEI 3000x

The continuous alumina scale attached to the zirconia ceramic agrees with observations of metallographic mounts from failed burner rig specimens (Figure 44). Failure occurred within the alumina at the interface between the thermally grown oxide and the metallic undercoat. One exception was strain emphasis test #11 which had patches of the thermally grown oxide missing on the ID surface of the spalled chip so that the EB-PVD zirconia was exposed (see Figure 55a&b and corresponding KEVEX's in Figure 56a through 56c). The strain test had only 14 hours of hot time whereas other tests ranged from 90 to 1800 hours of total hot time exposure. It is hypothesized that as the EB-PVD TBC is exposed to high temperatures, the bond between the thermally grown oxide and the zirconia ceramic improves with time due to sintering and diffusion. Strain test #11 did not acquire enough hot time to improve this bond; hence, in addition to failing at the typical metallic bond coat/thermally grown oxide interface, the alumina also failed in patches along the zirconia interface due to a weak chemical bond. In contrast, the static oxidation test which was exposed for 1800 hours exhibited a continuous alumina scale on the ID surface of the spalled chip (Figures 60a&b and 61a&b) as did the other ceramic chips analyzed (Table XXVI).

The major difference between the failed ceramic chips is the scale surface finish. The TGO morphology ranges from a very regular nodular structure in the strain specimen with only 14 hours to large planar fracture areas for the static furnace 1800 hour specimen. The oxide emphasis specimen with 527 hot hours had a more irregular nodular structure than the strain specimen. The mixed mode specimen, however, had not only a very irregular nodular structure but also a network of a finer secondary structure. The parameters that were considered were hot time/temperature which affects the oxide thickness and the cycle rate which affects the thermal gradients. Longer cycles and longer hot exposure seemed to produce planar fractures which is in agreement with the out-of-plane strength tests (Section 3.2.2.1).

The TGO on four spalled ceramic chips was studied by x-ray mapping for the distribution of elements. These results are summarized in Table XXVI and discussed in the following paragraphs.

The strain emphasis test specimen was tested at 1107C (2150F)/6 minute cycle and failed at 167 hours with only 14 hours hot time. The ID surface appeared off-white with dark blue spots which indicated zirconia with patches of alumina (TGO) still adherent. Due to the short hot time exposure, a good bond did not form between the alumina and the zirconia; hence, a continuous alumina scale was not present. As seen at higher magnification in Figure 64a, the TGO exhibited a very nodular structure, indicating an interfacial failure. Some short range fracture, transgranular fracture, was also present. Hafnium was homogeneously distributed (Figure 65b), yet Ni and Cr were present in a few locally enriched areas (Figure 65c,d). No Ti was detected.

The oxide emphasis specimen was tested at 1107C (2025F)/12 minute cycle and failed at 712 hours with 527 hot hours. The ID surface was uniform light blue-grey indicating a continuous TGO layer. Very few dark blue spots were present. As shown in Figure 65a, the TGO exhibited a more irregular nodular structure. Figures 66a and 67a show the ID of the chip in both a location free of fracture and a location of fractured TGO, respectively. It appears as though the crack growth mode is a mixture of interfacial and transgranular growth present only in localized areas. Corresponding x-ray maps in Figures 65-67 show more evidence of localized Ni, Co, Cr enrichment in fractured areas. Hafnium and titanium were also detected, although not localized. Presence of Y/Zr was also evident.

TABLE XXVI
X-RAY DIFFRACTION AND SEM/KEVEX MICROSTRUCTURAL ANALYSIS OF SPALLED CERAMIC CHIPS

	Strain Emphasis	Oxide Emphasis		Oxidation		Mixed Mode
Test Identification	Task VIIA-Test #11	Task VIIA-Test #1	Task VIIA-Test #3	Task VIA Test	Task VIA Test	Task VIIA Test #13
Test Conditions	1177C(2150F/6 min cycle burner rig	1107C (2025F)/6 min cycle burner rig	1107C/(2025F)/12 min cycle burner rig	1149C(2100F)/10hr cyclic furnace	1149C(2100F) static furnace	1079C(1975F)/6 min cycle burner rig
Time to Failure	167hrs/1728 cycles	243 hrs/3307 cycles	712 hrs/4109 cycles	90 hrs/9 cycles	1800 hrs	1352 hrs/9014 cycles
Corresponding Figs.	55a,55b,56a,56b,56c	57	58	59	60a,60b,61a,61b	62a,62b,63
Scale Continuity	Discontinuity of alumina on ID of chip exposing Zirconia	Pebbly, craze-cracked continuous alumina-based scale adhering to ID of chip	Pebbly, craze-cracked continuous alumina-based scale adhering to ID of chip	Pebbly craze-cracked continuous alumina-based scale adhering to ID of chip	Pebbly craze-cracked continuous alumina-based scale adhering to ID of chip	Pebbly craze-cracked continuous alumina-based scale (spinel also apparent) adhering to ID of chip
ID Scale Surface	Damage, dis-continuous layer	Rough, inhomogeneous nodules	Badly damaged layer: rough, irregular surface with deep craters	Smoothest, most homogeneous surface texture of oxide tests	Badly damaged layer: rough irregular surface	Rough nodules with localized porous regions
ID Scale XRD*	Alpha-hexagonal alumina F.C.C. Zirconia $a_0 = 5.109\mathring{A}$ med.<100> texture		Alpha-hexagonal alumina F.C.C. Zirconia $a_0 = 5.100\mathring{A}$ trace tetragonal zirconia medium <100> texture	Alpha-hexagonal alumina F.C.C Zirconia $a_0 = 5.103\mathring{A}$ trace tetragonal zirconia weak <100> texture	Alpha-hexagonal alumina F.C.C. Zirconia $a_0 = 5.110\mathring{A}$ trace monclinic zirconia trace F.C.C. NiO trace hexagonal $NiCrO_3$	Alpha-hexagonal F.C.C. Zirconia $a_0 = 5.089\mathring{A}$ trace tetragonal zirconia trace monoclinic zirconia Spinel, $NiAl_2O_4$

90

*F.C.C. Zirconia present on ID XRD pattern due to penetration of beam reflections through (<10 m) oxide scale

TABLE XXVI (Continued)

X-RAY DIFFRACTION AND SEM/KEVEX MICROSTRUCTURAL ANALYSIS OF SPALLED CERAMIC CHIPS

	Strain Emphasis	Oxide Emphasis		Oxidation		Mixed Mode
Test Identification	Task VIIA-Test #11	Task VIIA-Test #1	Task VIIA-Test #3	Task VIA Test	Task VIA Test	Task VIIA Test #13
TGO Chemistry	Few locations showing Ni,Co,Cr enrichment, TGO also shows Hf,Y/Zr, but no Ti. (Fig. 64)		more evidence of localized Ni,Co,Cr enrichment. Recognized some micro structural features that show the Ni,Co, Co enrichment. Hf,Ti also detected but not localized, Y/Zr. (Figs. 65,66,67)		Some Ni, Co, Cr enriched area, considerable localized Ti enrichment high but not localized (Figs. 68,69, 70)	Considerable amount of localized Ni,Co,Cr enrichment. Hf,Ti,Y/Zr also present (Figs. 71,72

*F.C.C. Zirconia present on ID XRD pattern due to penetration of beam reflections through (<10 m) oxide scale

The mixed mode emphasis test specimen was tested at 1079C (1975F)/6 minute cycle and failed at 1352 hours with 331 hot hours. The ID surface of the chips were uniform light blue-grey with numerous dark blue spots. The TGO had a very irregular structure as well as a network of a finer, secondary structure (Figure 71a). This fine structure was quite unusual. The detailed structure is shown in Figure 72. X-ray maps in Figure 71 showed some Ni, Co, Cr enriched areas were present; however, a considerable amount of localized Ti enrichment was present. The hafnium level was higher on this sample but not localized.

The static furnace test specimen was tested at 1149C (2100F) in air for 1800 total hours. The ID surface of these chips also exhibited a uniform light blue-grey color, except these chips did not have any well-developed spots. Large areas of planar fracture were present (Figure 68, 69), and some nodular TGO structure was still evident. The predominant crack mode in this case appeared to be transgranular with some interfacial areas. Figure 70 shows a typical area of the chip at a location of TGO fracture. Note the considerable amount of localized Ni, Co, Cr enriched regions. The areas of the chip that were relatively free of TGO fracture have less Ni, Co, Cr enriched regions (Figure 70). Hafnium, Ti, Y/Zr were also present and were homogeneously distributed.

X-ray mapping was also performed on a transverse section through pre-test and post-test samples to determine the chemistry of the thermally grown oxide. The 2.54 cm (1") burner rig sample studied was from oxide emphasis Task VIIA test #3 (see Section 3.4.2.2). Figures 73 through 78 illustrate the system and corresponding elemental x-ray maps. The electron back scatter photomicrograph from the region which the x-ray maps depict, oxygen distribution, aluminum x-ray map, yttrium distribution, hafnium x-ray map, and chromium x-ray map are shown in Figures 74, 75, 76, 77, and 78, respectively. The bond coat is not illustrated in the post-test figures due to failure of the system and its subsequent separation along the thermally grown oxide/metallic bond coat interface. Variations in intensity (the amount of "white dots" representing the presence of that particular element) result from differences in exposure time. Figure 75 shows that the thermally grown oxide is basically an alumina scale, which was in agreement with the KEVEX and x-ray diffraction results. As evidenced in Figures 75a and 75b, the aluminum oxide grows with hot time exposure. Figures 76a and 76a show homogeneous distributions of yttrium and hafnium, respectively. The hafnium is an acceptable ceramic raw material impurity within the EB-PVD ceramic due to the difficulty in physically separating zirconium and hafnium. In comparison, the post-test x-ray maps of yttrium and hafnium (Figures 76b and 77b) illustrate the diffusion of the Y and Hf into random isolated islands within the thermally grown oxide. Chromium is also evident within the thermally grown oxide (see Figure 78) and has the tendency to also diffuse into isolated inhomogeneous islands.

TEM examination was performed on the TGO to further characterize its micro-structure at a much finer scale. A spalled ceramic chip from a 1.27 cm (0.5") burner rig bar that failed at 595 hours in a 1135C (2075F)/6 minute burner rig cycle was studied. In order to prepare the TEM specimen, an electron trans-parent area in the thin, friable TGO layer had to be established. This proved to be a very difficult task, and numerous approaches were attempted to observe the TGO within the plane of oxide as well as to establish a transverse view of the TGO/coating interface. A planar view within the TGO has been prepared successfully as described below.

92
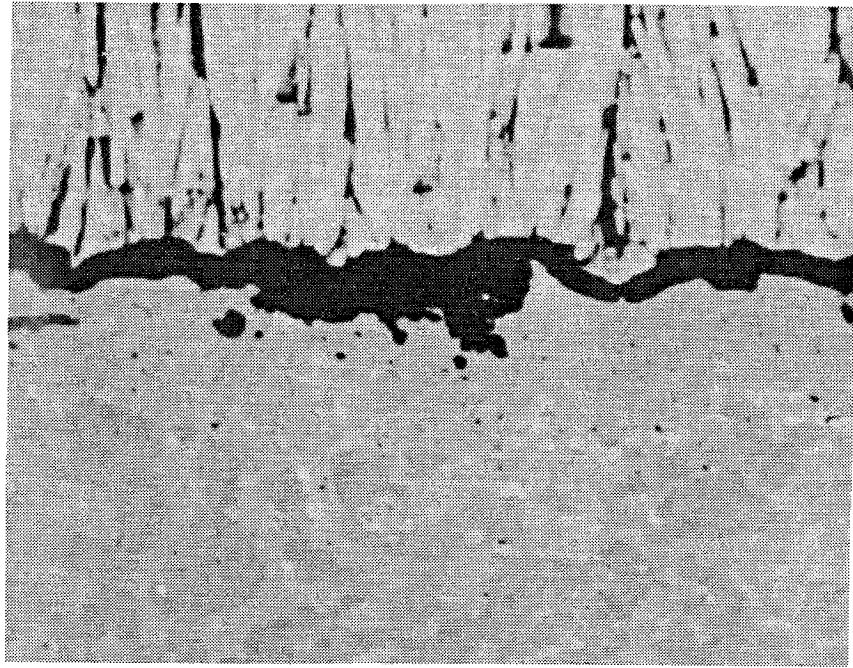
Figure 73a.- Electron Back Scatter Photomicrograph of a Pre-Test 2.54 cm (1")
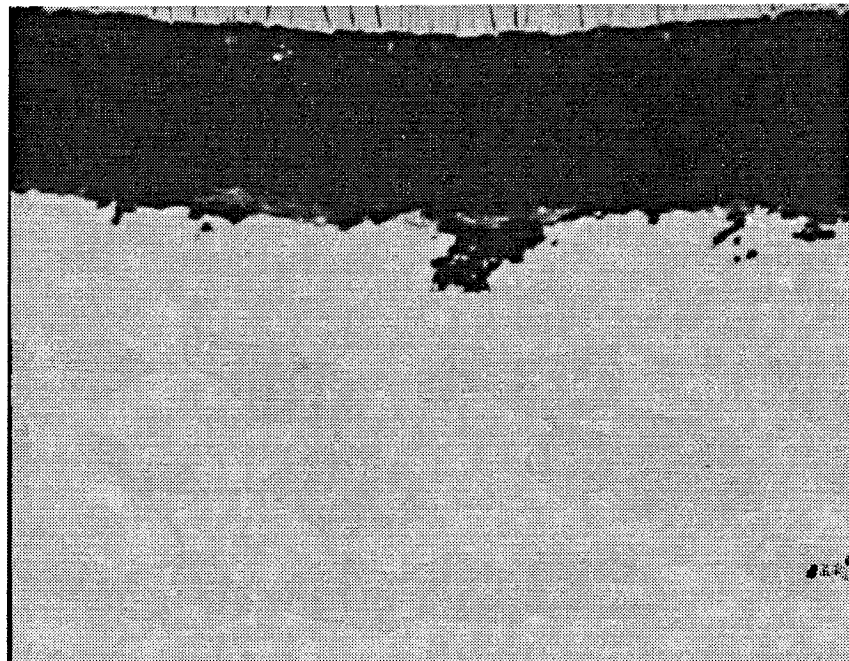Burner Rig Bar Emphasizing the Thermally Grown Oxide. Mag: 2000x
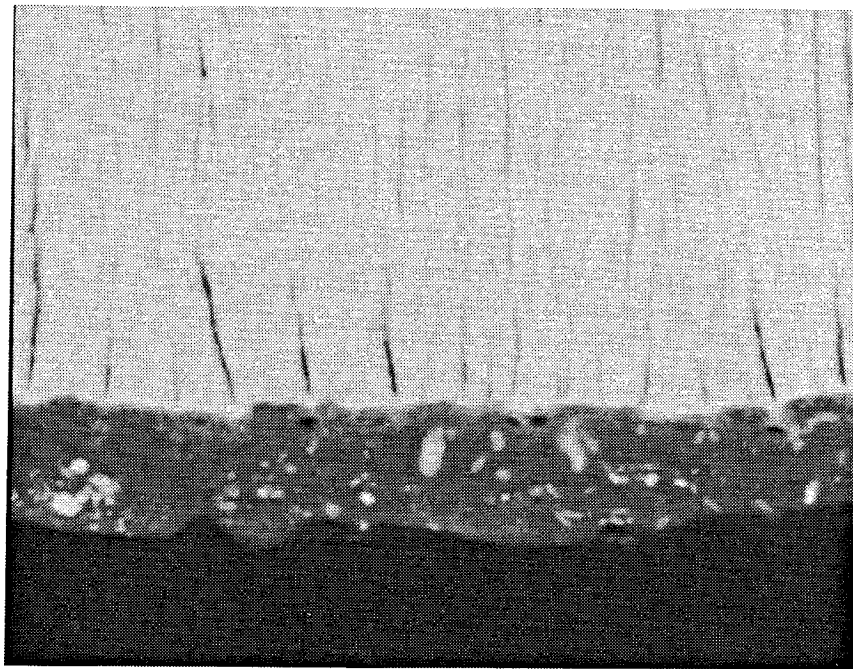
Figure 73b.- Electron Back Scatter Photomicrograph of a Post-Test 2.54 cm
(1") Burner Rig Bar Emphasizing the Thermally Grown Oxide (Oxide
Emphasis TASK VIIA Test #3, 1107C (2025F)/12 Minute Cycle Which
Failed at 712 Hours). Mag: 2000x

93
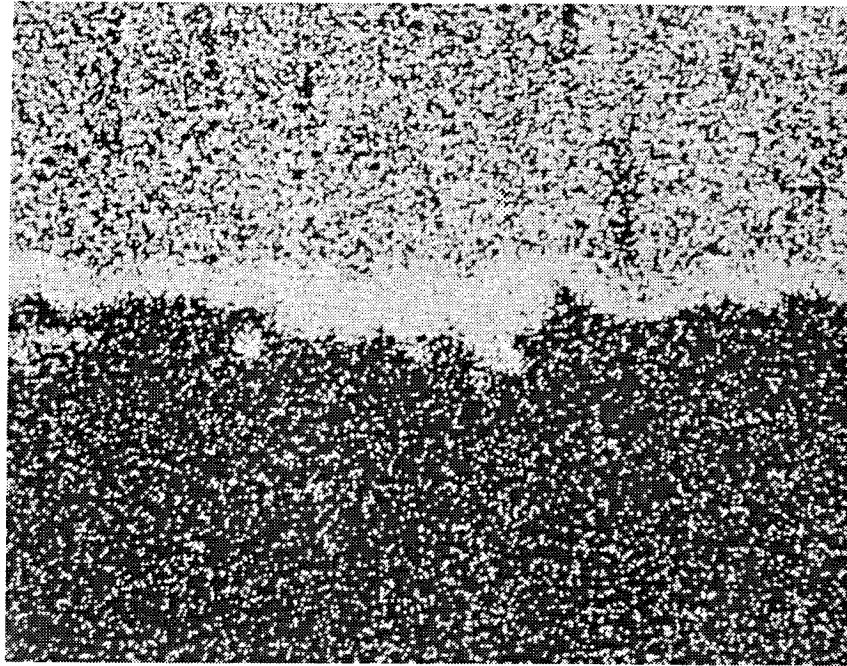
Figure 74a.- X-ray Map of Oxygen Corresponding to Figure 74a of a Pre-Test
2.54 cm (1") Burner Rig Bar Emphasizing the Thermally Grown
Oxide. Mag: 2000x
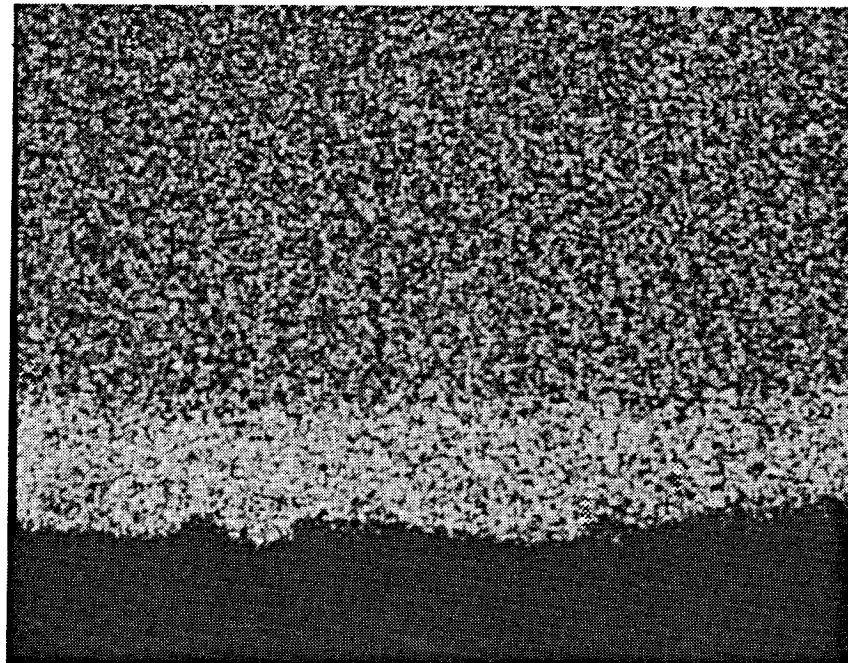
Figure 74b.- X-ray Map of Oxygen Corresponding to Figure 74b of a Post-Test
2.54 cm (1") Burner Rig Bar Emphasizing the Thermally Grown Oxide
(Oxide Emphasis TASK VIIA Test #3, 1107C (2025F)/12 Minute Cycle
Which Failed at 712 Hours). Mag: 2000x
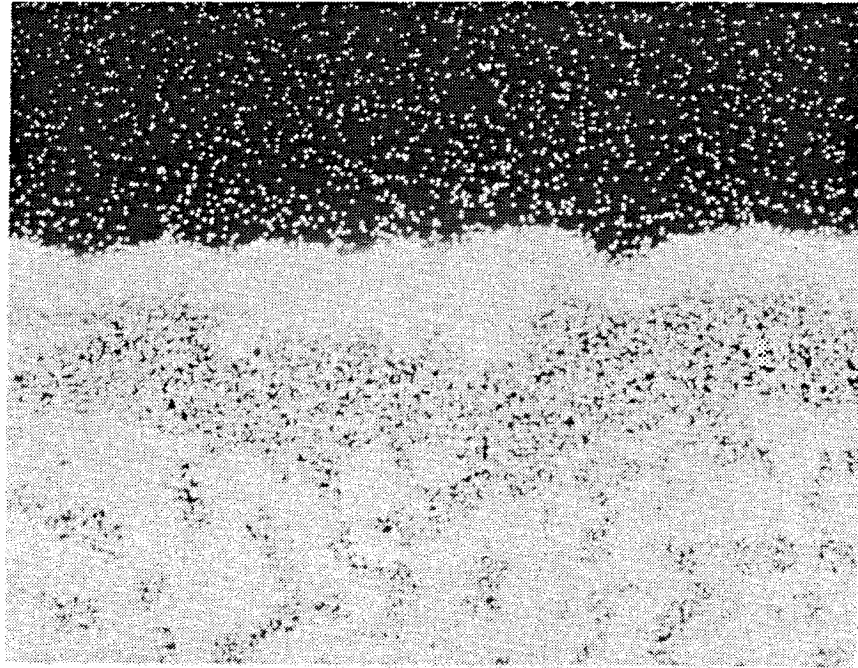
Figure 75a.- X-ray Map of Aluminum Corresponding to Figure 74a of a Pre-Test 2.54 cm (1") Burner Rig Bar Emphasizing the Thermally Grown Oxide. Mag: 2000x
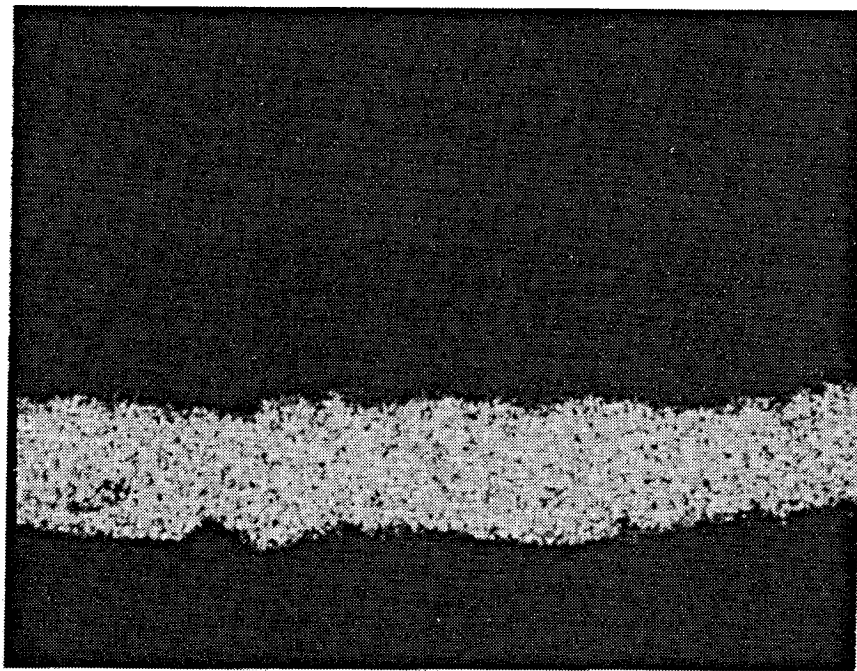
Figure 75b.- X-ray Map of Aluminum Corresponding to Figure 74b of a Post-Test 2.54 cm (1") Burner Rig Bar Emphasizing the Thermally Grown Oxide (Oxide Emphasis TASK VIIA Test #3, 1107C (2025F)/12 Minute Cycle Which Failed at 712 Hours). Mag: 2000x
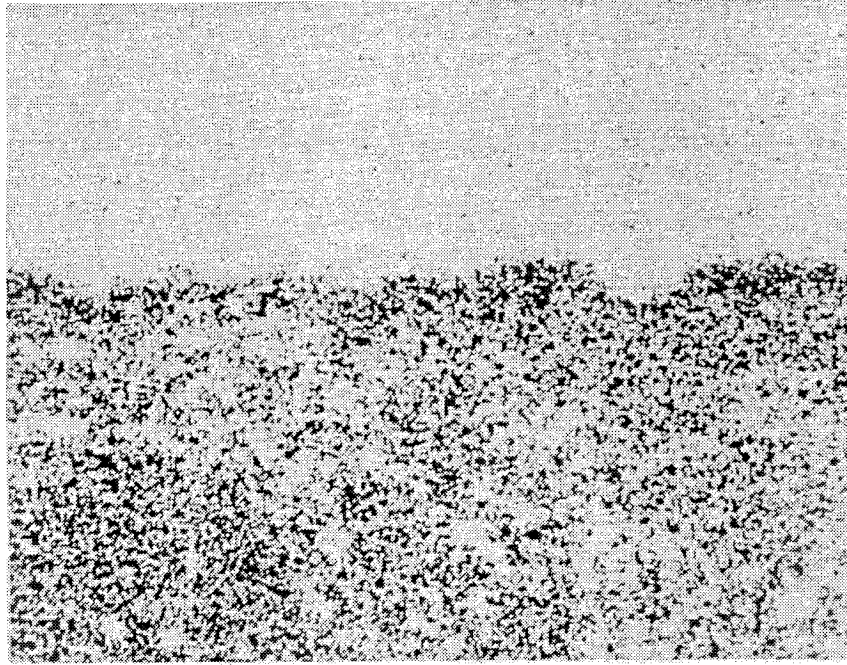
Figure 76a.- X-ray Map of Yttrium Corresponding to Figure 74a of a Pre-Test
2.54 cm (1") Burner Rig Bar Emphasizing the Thermally Grown
Oxide. Mag: 2000x
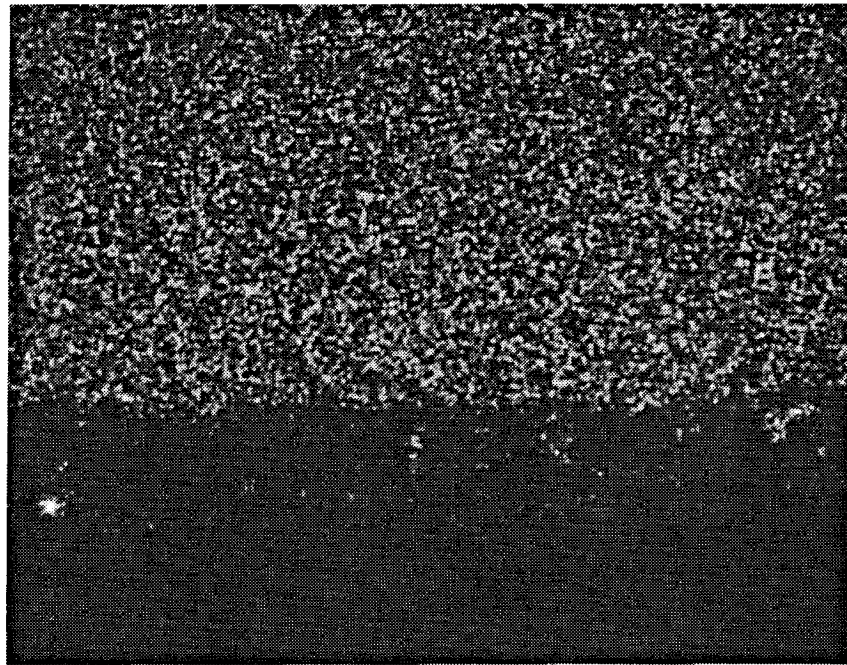
Figure 76b.- X-ray Map of Yttrium Corresponding to Figure 74b of a Post-Test
2.54 cm (1") Burner Rig Bar Emphasizing the Thermally Grown Oxide
(Oxide Emphasis TASK VIIA Test #3, 1107C (2025F)/12 Minute Cycle
Which Failed at 712 Hours). Mag: 2000x
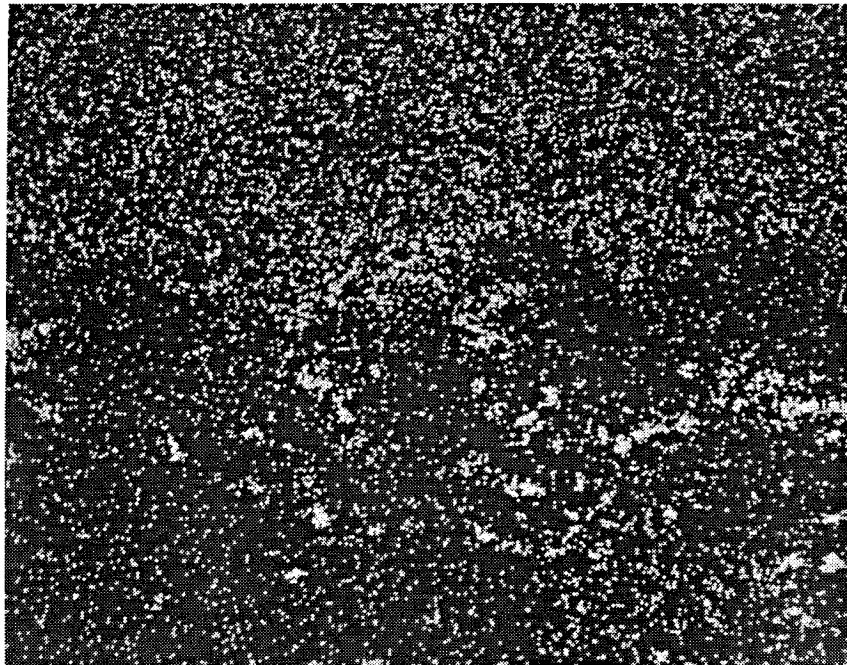
Figure 77a.- X-ray Map of Hafnium Corresponding to Figure 74a of a Pre-Test
2.54 cm (1") Burner Rig Bar Emphasizing the Thermally Grown
Oxide. Mag: 2000x
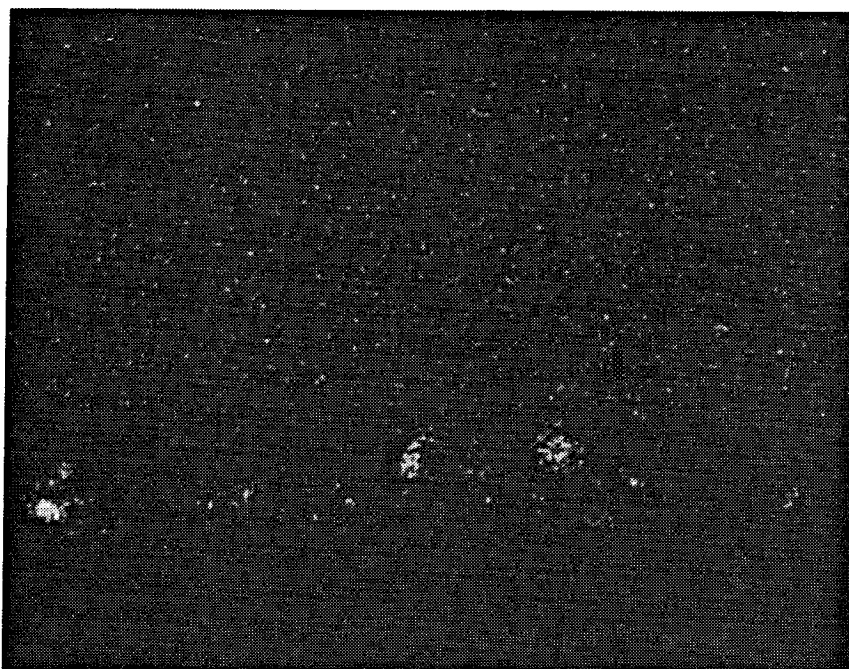
Figure 77b.- X-ray Map of Hafnium Corresponding to Figure 74b of a Post-Test
2.54 cm (1") Burner Rig Bar Emphasizing the Thermally Grown Oxide
(Oxide Emphasis TASK VIIA Test #3, 1107C (2025F)/12 Minute Cycle
Which Failed at 712 Hours). Mag: 2000x
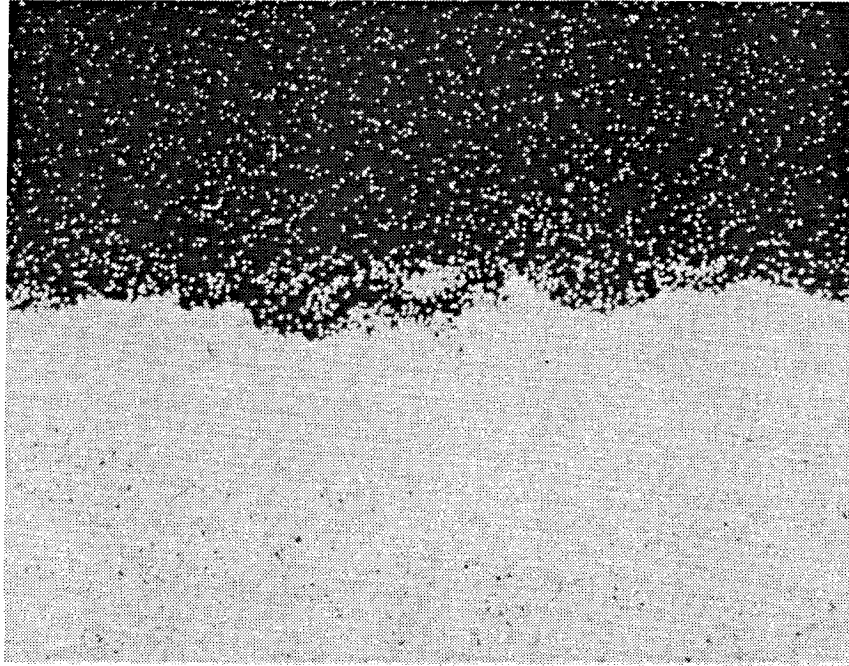
Figure 78a.- X-ray Map of Chromium Corresponding to Figure 74a of a Pre-Test
2.54 cm (1") Burner Rig Bar Emphasizing the Thermally Grown
Oxide. Mag: 2000x

Figure 78b.- X-ray Map of Chromium Corresponding to Figure 74b of a Post-Test
2.54 cm (1") Burner Rig Bar Emphasizing the Thermally Grown Oxide
(Oxide Emphasis TASK VIIA Test #3, 1107C (2025F)/12 Minute Cycle
Which Failed at 712 Hours). Mag: 2000x

A 3 mm (0.118") disc was ultrasonically cut from a spalled coating chip. The most suitable technique for preparing ceramic TEM specimens is ion milling. However, since ion milling is a slow process, another mechanical process was used to take off the initial 7 weight % yttria stabilized zirconia ceramic without harming the TGO. A piece from the same chip was examined in the SEM along with a magnification standard to accurately measure the thickness of the coating. A dimpling machine with a diamond slurry was used to initially grind the ceramic disc to a final thickness of approximately 20 microns (787 microinches). Figure 79 shows a schematic diagram of the sample preparation. The remainder of the zirconia ceramic was removed by ion milling from the 7 weight % yttria stabilized zirconia side of the disc.
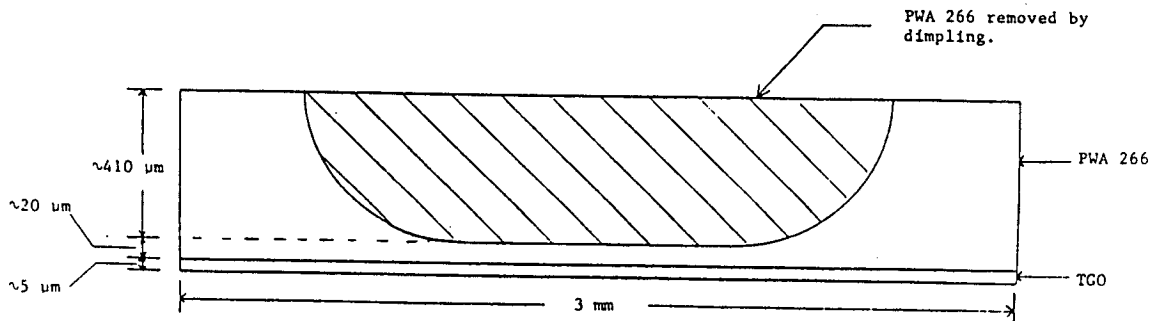
Figure 79.– Schematic of Cross–Section of TEM Specimen. Shaded Area is PWA 266 Removed by a Dimple Grinding Apparatus. The Bottom of the Dimple is Then Ion Milled to Remove the Thin Layer of PWA 266 Remaining Above the TGO and Continued into the TGO to Provide a Sufficiently Thin Area for Examination.

The typical microstructure of the TGO is shown in Figure 80. The TGO matrix consists of clusters of both small (approximately 0.1 microns or 3.94 microinches) and large (0.2 to 0.5 micron or 7.9 to 19.7 microinches) grains. Small precipitates (approximately 30 nanometers or 1.2 microinches) were found within the small grain regions. Large grain regions were devoid of such precipitates.

X–ray energy spectroscopy (XES) and semi–quantitative analysis of the TGO was performed. Typical results for the matrix grains (small and large) and precipitates are provided in Figure 81a and 81b. Aluminum is the primary constituent of both the small and the large grains. A significant amount of Zr as well as small amounts of Y, Mo, Hf, and a trace amount of Cr were also present. The small precipitates located within the small grain regions contained primarily Al, Y, Zr, and Hf with small amounts of Cr and Mo. Due to interference from the surrounding matrix caused by beam spreading, accurate chemical analysis of the precipitates was difficult. This interference may account for variations in chemistry observed for different precipitates. The chemistry that is listed in Figure 81 for a precipitate is derived from a precipitate that had the smallest amount of interference from the matrix. Nevertheless, some interference still occurred and the chemistry only provided relative differences in composition between matrix and precipitates. Higher levels of Y, Hf, and Zr were generally observed in the precipitates as compared to the matrix. These three elements were considered the primary constituents of the precipitates with the Zr originating from the EB–PVD ceramic, the Hf originating mainly from the metallic bond coat, and the Y originating from the EB–PVD ceramic and/or the metallic bond coat. The Al peak is only an interference from the Al–rich matrix.

99

(a)

0.2 μm
100 Kx

(b)

0.2 μm
100 Kx

(c)
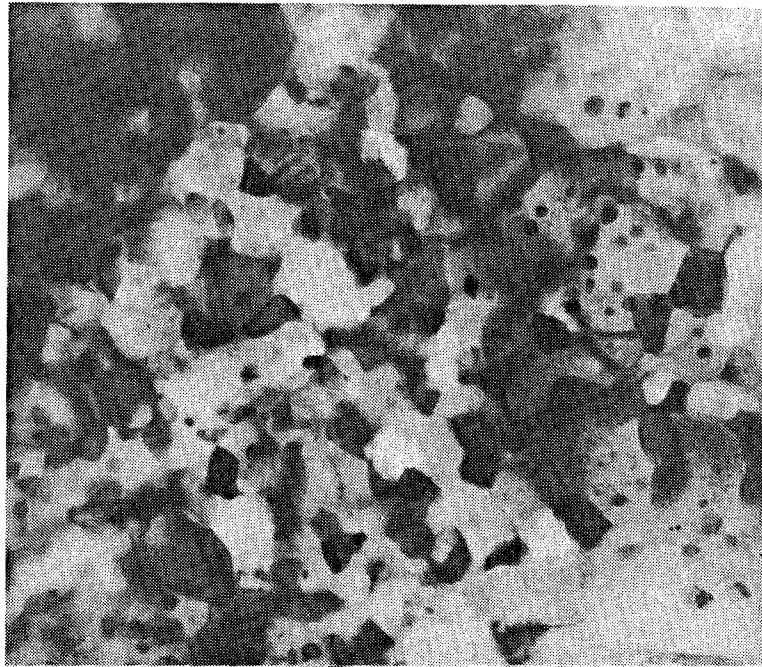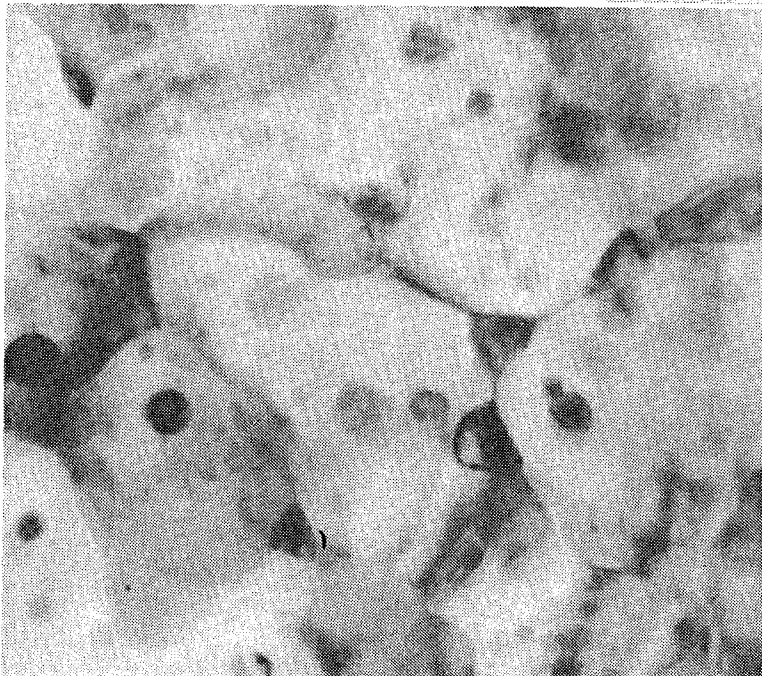
0.1 μm

Figure 80.-
TEM Micrographs of a TGO Layer Adhering to a Spalled
PWA 266 Coating Chip After 595 Hours at 1135C (2075F)
6 Minute Cycle.

a. Small Grain Region Containing Precipitates.
    Grain Size 0.1 microns (3.9 microinches).
b. Large Grain Region Devoid of Precipitates.
    Grain Size 0.2-0.5 microns (7.9-19.7
    microinches).
c. Higher Magnification of Small Grain Region
    Showing Precipitates. Precipitate size 30
    microns (1181.1 microinches).

Vert = 2000 counts

MATRIX CHEMISTRY

Element	Weight Percent	Atomic Percent
Al	80.18	93.29
Cr	0.05	0.03
Y	2.74	0.97
Zr	14.58	5.02
Mo	1.75	0.57
Hf	0.71	0.12

AL
HF

Y
ZR

MO

HF

ZR

Y

ZR
MO

0.000   Range = 20.460 keV   19.580

(A)

266-23
Vert = 5000 counts

PRECIPITATE CHEMISTRY

Element	Weight Percent	Atomic Percent
Al	33.21	67.99
Cr	0.28	0.30
Y	17.04	10.59
Zr	18.36	11.12
Mo	1.44	0.83
Hf	29.67	9.18

AL
HF

Y
ZR

MO

HF

HF

CR   HF

HF

Y   ZR

ZR
Y   MO

0.000   Range = 20.460 keV   20.220

(B)

Figure 81.- XES Chemical Analysis of the TGO.

     a. Large and Small Matrix Grains Consist of Primarily Al.
     b. Precipitates are Richer in Y, Zr, and Hf as Compared to the
        Matrix. Some Interference from the Matrix Is Occurring,
        Therefore, the Numbers Listed Provide Only a Relative
        Difference in Composition Between the Matrix and the
        Precipitates.

Micro-diffraction patterns were also collected. These patterns depicted small and large grains as alpha-alumina (hcp, a_o = 4.75 A, c_o = 12.97 A). The micro-diffraction patterns obtained from the precipitates within the small grain regions are f.c.c. in structure with a lattice parameter of approximately 5.1 A. Based upon this structure and the precipitate chemistry obtained by XES, the precipitates could be in the form of HfO_2, ZrO_2, and $Y_2Hf_2O_7$ since these oxides have lattice parameters close to 5.1 A and are f.c.c. in structure. It is possible that these precipitates play an important role in the strength of the TGO, especially since they would provide transformation toughening.

3.4 TASK VII — EB-PVD CERAMIC LIFE PREDICTION MODEL DEVELOPMENT

The objective of this task was to develop a life prediction model for the EB-PVD ceramic thermal barrier coating. The approach involved generation and correlation of design data, development of a ceramic constitutive model, and employment of a bond coat oxide growth model. Property test data was used to enhance the analytical understanding of the thermal barrier coating behavior.

3.4.1 Mechanical Properties

The objectives of this effort were to obtain EB-PVD zirconia mechanical property data and to create a ceramic constitutive model for use in analysis of EB-PVD ceramic cyclic behavior. Southwest Research Institute (SwRI) and NASA cooperatively defined and SwRI executed a test matrix for establishing tensile and compressive properties of the EB-PVD system (SwRI Project No. 06-1778-001) (Ref. 11). Pratt & Whitney supplied the required property specimens and developed the ceramic constitutive model.

3.4.1.1 Specimen Design and Analysis

Tension and compression testing of the zirconia ceramic was conducted with the uniaxial stress applied parallel to the plane of the coating (perpendicular to the EB-PVD ceramic columns). Since the highly columnar ceramic microstructure did not have enough structural integrity to be machined as compression and tensile specimens in the absence of a substrate, the mechanical properties were measured with the ceramic attached to the substrate. Ceramic properties were calculated by comparative tension and compression testing of thin-walled single crystal superalloy tubes with and without EB-PVD zirconia coating deposited on the external diameter.

The compression specimens were tubular in shape (Figure 82) with 0.056 or 0.114 cm (0.022 or 0.045") substrate wall thicknesses, 1.79 or 1.68 cm (0.705 or 0.660") inside diameters, and 0.216 or 0.190 cm (0.085 or 0.075") coating thicknesses (Figure 83 and Table XXVII). The length of the compression specimens was (0.874"). Monotonic compression tests were conducted over a temperature range from room temperature to 1204C (2200F) (Table XXVII). Sustained load compressive creep tests were conducted at 760C (1400F), 871C (1600F), and 982C (1800F) (Table XXVII).
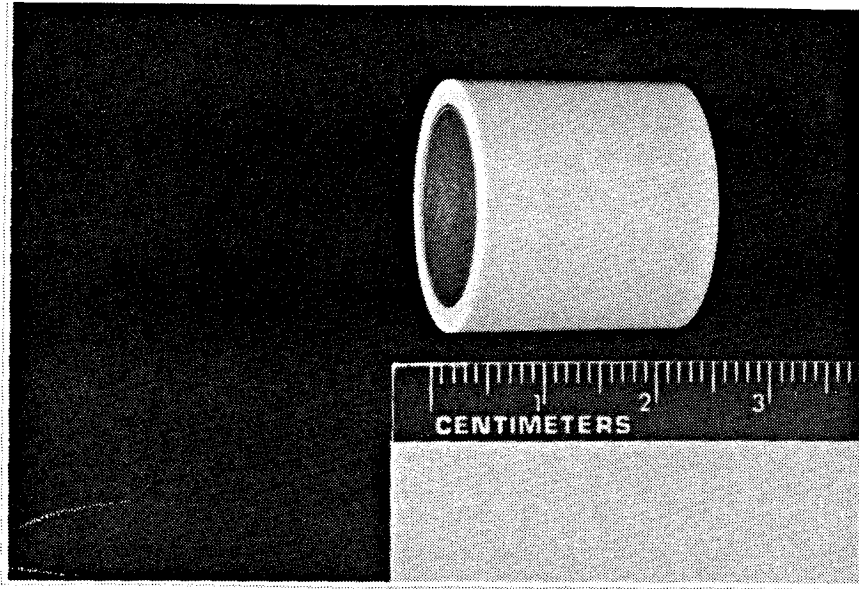
Figure 82.- Fully Processed 0.056 cm (0.22") Thin Wall Compression Specimen.

⊥ | 0.00254 cm (0.001″) | C

∥ | 0.00254 cm (0.001″) | C

2.228 cm (0.877″)
2.217 cm (0.873″)

C

A — SEE TABLE 3

◎ | 0.00254 cm (0.001″) | B

B — SEE TABLE 3
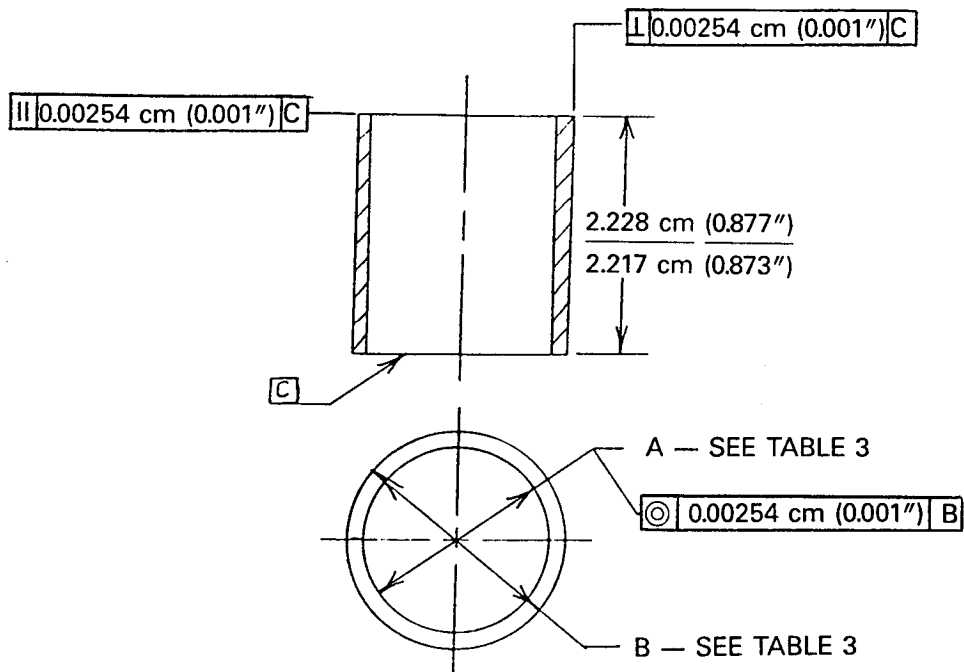
Figure 83.- Compression Specimen Geometry.

TABLE XXVII
COMPRESSION TEST MATRIX

Specimen #	Specimen Type	Test Mode	Temp (C)(F)	Inside Diameter cm(in)	Ceramic Thickness cm(in)	Substrate Wall cm(in)
20	Substrate	Compr	RT	1.7882 (0.7040)	-- --	0.056 (0.022)
18	Coated	Compr	RT	1.7932 (0.7060)	0.216 (0.085)	0.056 (0.022)
33	Substrate	Compr	538 (1000)	1.6739 (0.6590)	-- --	0.114 (0.045)
34	Substrate	Compr	538 (1000)	1.7793 (0.7005)	-- --	0.056 (0.022)
30	Exp-Coated	Compr	538 (1000)	1.7932 (0.7060)	0.196 (0.077)	0.056 (0.022)
17	Substrate	Compr	760 (1400)	1.7897 (0.7046)	-- --	0.056 (0.022)
19	Coated	Compr	760 (1400)	1.7933 (0.7061)	0.216 (0.085)	0.056 (0.022)
32	Substrate	Compr	982 (1800)	1.6761 (0.6599)	-- --	0.114 (0.045)
25	Coated	Compr	982 (1800)	1.6759 (0.6598)	0.208 (0.082)	0.114 (0.045)
26	Coated	Compr	982 (1800)	1.6759 (0.6598)	0.082 (0.082)	0.114 (0.045)
24	Exp-Coated	Compr	982 (1800)	1.6759 (0.6598)	0.175 (0.069)	0.114 (0.045)
31	Substrate	Compr	1204 (2200)	1.6754 (0.6596)	-- --	0.114 (0.045)
28	Exp-Coated	Compr	1204 (2200)	1.6756 (0.6597)	0.193 (0.076)	0.114 (0.045)
21	Coated	Str Relax Creep	760 (1400) 760 (1400) 871 (1600) 982 (1800)	1.7922 (0.7056)	0.216 (0.085)	0.056 (0.022)
		Compr	760 (1400)			
27	Coated	Modulus	204 (400) 427 (800) 537 (1000) 649 (1200) 871 (1600) 1094 (2000)	1.6761 (0.6599)	0.188 (0.074)	0.114 (0.045)

The tensile specimen used is shown in Figure 84. The long, tubular configuration as necessary in order to accommodate the internal mounting of the strain transducer. The gage section (Figure 85) was offset from the center of the specimen in order to provide space for the body of the transducer away from elevated temperatures. The substrate wall thicknesses for the tensile specimens was in the range of 0.0127 to 0.0170 cm (0.0050 to 0.0067") with the EB-PVD ceramic thickness ranging from 0.127 to 0.2667 cm (0.050 to 0.105")(Figure 84 and Table XXVIII). Monotonic tension tests were conducted over a temperature range from room temperature to 1204C (2200F).
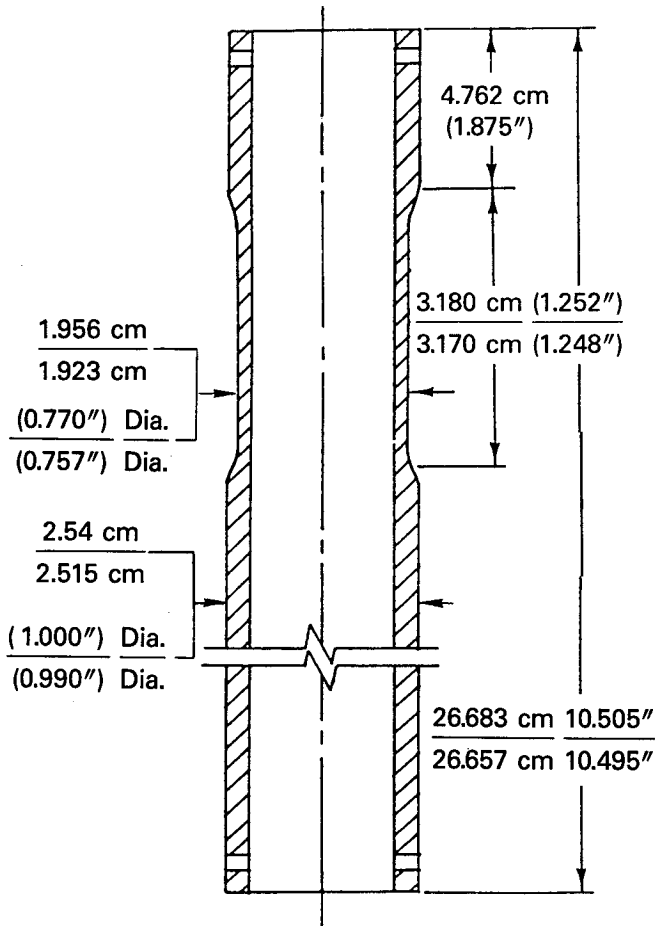
Figure 84.– Tensile Specimen Geometry.
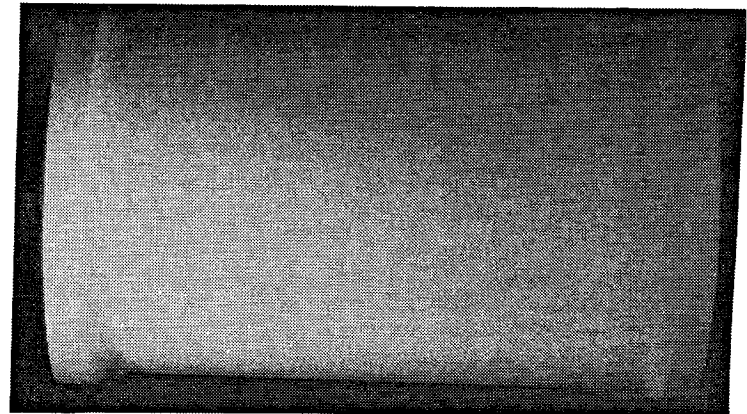
Figure 85.– Gage Section of a Processed Tensile Specimen.

TABLE XXVIII
TENSILE TEST MATRIX

Specimen Number	Specimen Type	Temp C(F)	Specimen Inside Diameter-cm(in)	Interface Diameter cm(in)	Outside Diameter cm(in)
653601	Substrate	RT	1.9065 (0.7506)	N/A N/A	1.9385 (0.7632)
652801	Coated	RT	1.9075 (0.7510)	1.9395 (0.7636)	2.2073 (0.8690)
652805	Coated	RT	1.9063 (0.7505)	1.9398 (0.7637)	2.4435 (0.9620)
653605	Substrate	760 1400	1.9096 (0.7518)	N/A N/A	1.9436 (0.7652)
652902	Coated	760 1400	1.9068 (0.7507)	1.9408 (0.7641)	2.4155 (0.9510)
653602	Coated 1400	760	1.9047 (0.7507)	1.9388 (0.7641)	2.4206 (0.9510)
653502	Coated	760 1400	1.9126 (0.7530)	1.9380 (0.7630)	2.1933 (0.8635)
653704	Coated	871 1600	1.9093 (0.7517)	1.9408 (0.7641)	2.3932 (0.9422)
653701	Substrate	982 1800	1.9088 (0.7515)	NA N/A	1.9428 (0.7649)
653503	Coated	982 1800	1.9055 (0.7502)	1.9380 (0.7630)	2.4219 (0.9535)
652802	Coated	982 1800	1.9113 (0.7525)	1.9454 (0.7659)	2.4770 (0.9752)
653603	Coated	1094 (2000)	1.9118 (0.7527)	1.9444 (0.7655)	2.4181 (0.9520)
653702	Substrate	1204 (2200)	1.9111 (0.7524)	N/A N/A	1.9436 (0.7652)
653504	Coated	1204 (2200)	1.9093 (0.7517)	1.9423 (0.7647)	2.4117 (0.9495)
652803	Coated	1204 (2200)	1.90754 (0.7510)	1.9395 (0.7636)	2.4193 (0.9525)

As illustrated in Figure 86 and 87, the bimaterial ceramic/substrate composite response is generally bilinear in compression and tension. In compression, the onset of bilinear behavior occurs when the substrate becomes plastic, as shown schematically in Figure 86. However, in tension, the bilinear response is attributed to cracking and debonding of the ceramic, after which the load is carried by the substrate (Figure 87). This bimaterial behavior formed the basis for calculation of ceramic properties from the uncoated and ceramic coated specimen responses. When the substrate is perfectly plastic or the ceramic debonds, static equilibrium is sufficient to determine the loads in both components. When both materials are linearly elastic, however, the system is statically indeterminate, and it becomes necessary to apply compatibility conditions to solve for the individual loads in the ceramic and substrate. The ceramic response for the elastic regime was deduced by using the thick walled cylinder solution (Ref. 12 and 13) and applying Hooke's law.
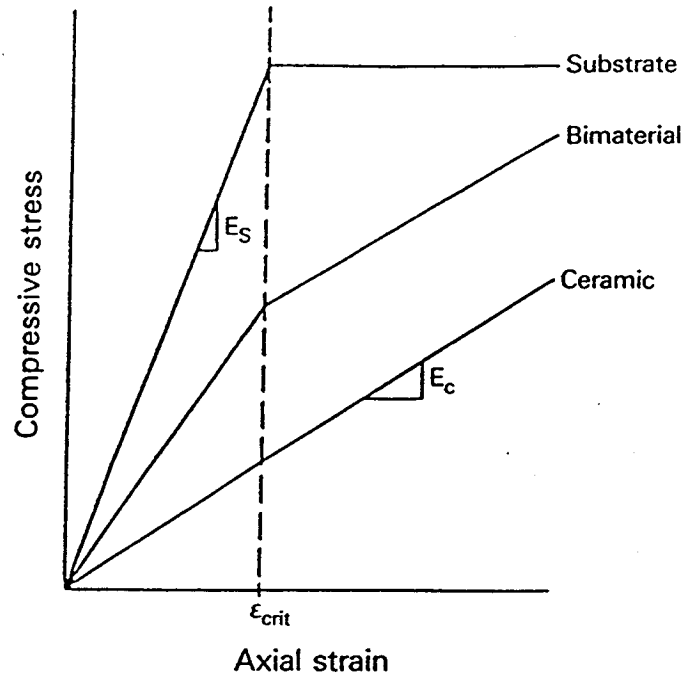
Figure 86.– Schematic Compression Test Response.
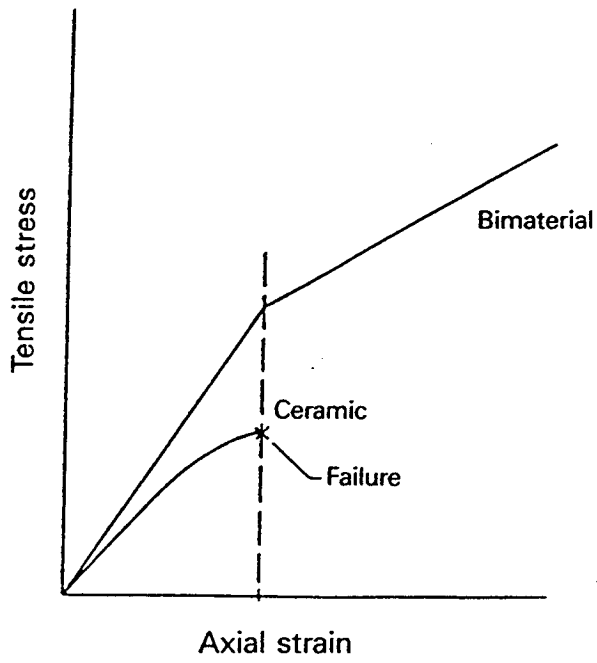
Figure 87.– Schematic Tension Test Response.

3.4.1.2 Compression and Tension Results

Deduced tensile and compressive modulii are shown in Figure 88 and Tables XXIX and XXX. While the compression results seem reasonably consistent, considerably more scatter is seen in the tensile modulus data. Within the limits of this scatter, modulus values appear to be consistent in both tests.

TABLE XXIX
EB-PVD CERAMIC MODULUS IN COMPRESSION VERSUS TEMPERATURE

Specimen ID	Condition	Temperature (C)	(F)	Ceramic Modulus (GPa)	(x 10^6 psi)
18A	Unexposed	24	75	47.99	6.96
27A1	Unexposed	204	400	24.13	3.50
27B1	Unexposed	427	800	19.44	2.82
27C2	Unexposed	538	1000	16.82	2.44
27D2	Unexposed	649	1200	17.37	2.52
21D	Unexposed	760	1400	17.24	2.50
21E	Unexposed	760	1400	37.23	5.40(*)
27E2	Unexposed	871	1600	14.62	2.12
25	Unexposed	982	1800	17.10	2.48
21D	Unexposed	760	1400	17.24	2.50
26	Unexposed	982	1800	2.57	0.373
27F2	Unexposed	1094	2000	3.75	0.544
30	Exposed	538	1000	26.13	3.79
24	Exposed	982	1800	6.60	0.957
28	Exposed	1094	2000	0.	0.(#)

(*) Specimen was a second test of 21D.
(#) Ceramic modulus was very small.

TABLE XXX
EB-PVD CERAMIC MODULUS IN TENSION VERSUS TEMPERATURE

Specimen ID	Temperature (C)	(F)	Ceramic Modulus (GPa)	(x10^6 psi)
652801	22	72	42.40	6.15
652805	22	72	42.20	6.12
653502	760	1400	33.92	4.92
653602	760	1400	5.31	0.770
652902	760	1400	6.03	0.874
653704	871	1600	28.27	4.10
653503	982	1800	29.51	4.28
652802	982	1800	4.18	0.607
652803	1204	2200	14.34	2.08
653504	1204	2200	14.00	2.03
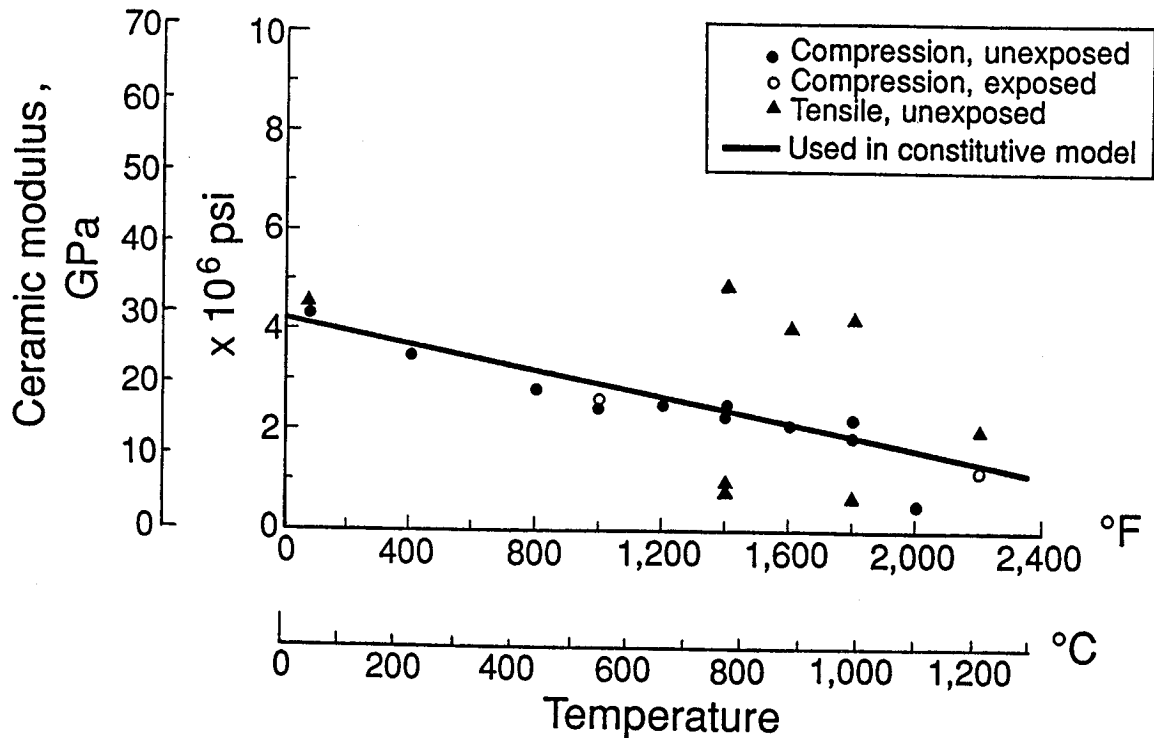
Figure 88.- Influence of Temperature on Ceramic Modulus Calculated From Results of Metallic and Coated Metallic Specimen Tests.

The ceramic response in compression is judged to be linearly elastic up to about 1% strain at room temperature, increasing to about 3% at 982C (1800F). Above this temperature, the linear strain limit drops off to about 2%. Specific results exhibit considerable scatter, and engineering judgment is required to achieve consistent data interpretations. The ceramic remained adherent past yielding of the substrate and up to the point of gross buckling of the substrate. Failed compression specimens are shown in Figures 89-92.

Compression test results of EB-PVD ceramic are compared to plasma sprayed ceramic in Figure 93. As shown, the EB-PVD elastic limit strength is about 310-345 MPa (45-50 ksi) at 538C (1000F). Note that the EB-PVD ceramic exhibits higher strength than the plasma sprayed ceramic at 1/5 the strain rate. On an equal strain rate basis, the plasma sprayed ceramic would be expected to exhibit roughly 10x more inelastic deformation than the EB-PVD ceramic.

Unlike the expectation prior to test, the EB-PVD ceramic does have some apparent in-plane tensile strength (see Figure 94). In general, the specimen tensile behavior was seen to be elastic up to a ceramic fracture strain. At that point the ceramic virtually ceased to have axial (in-plane) load carrying capability but did act to reinforce the substrate, a very striking phenomenon but of little design importance. A room temperature tensile specimen is shown in Figure 95 after testing. During testing, the 0.015 cm(0.006 in) substrate did not fracture, and the ceramic coating did not spall but showed fractures between the columns and localized decohesion in these areas. Good adhesion between the substrate and the ceramic was achieved. After correcting for residual stresses due to fabrication, all EB-PVD ceramic tensile strengths and elastic limits are less than about 6.9 MPa (1.0 ksi).

None
0.045"/
MPC-2-32
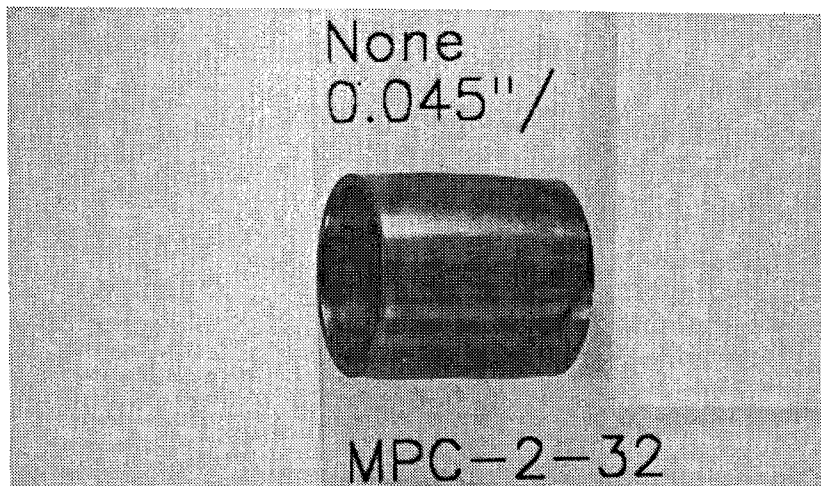
Figure 89.- Uncoated Compression Test Specimen (MPC232) Tested at 982C (1800F).

None
0.045"/0.082"
MPC-2-26
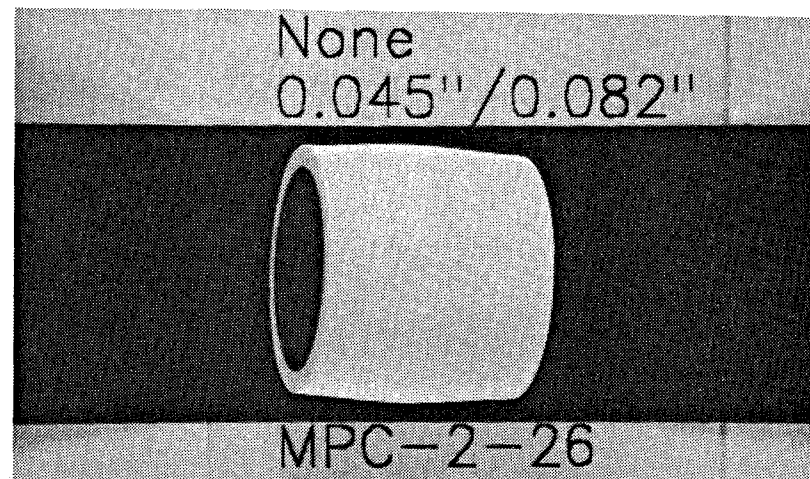
Figure 90.- EB-PVD Ceramic Coated Compression Test Specimen (MPC125) Tested at 982C (1800F).

None
0.045"/0.082"
MPC-2-25
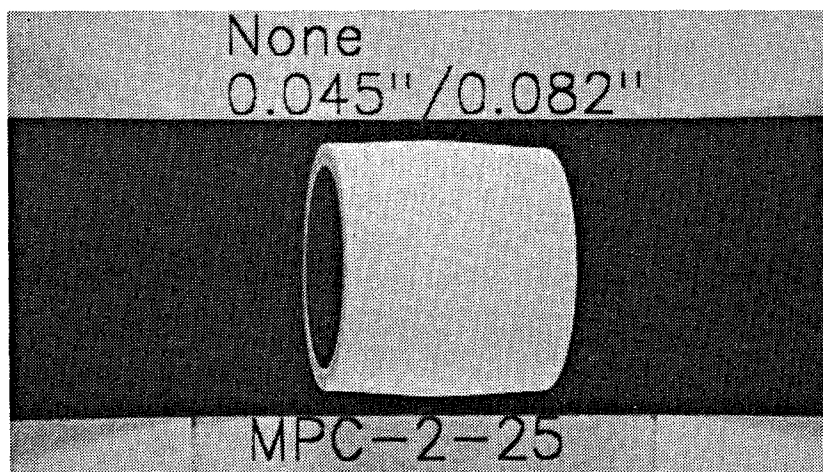
Figure 91.- EB-PVD Ceramic Coated Compression Test Specimen (MPC126) Tested at 982C (1800F).

50 hrs/2100F:Argon
0.045"/0.069"
MPC-2-24
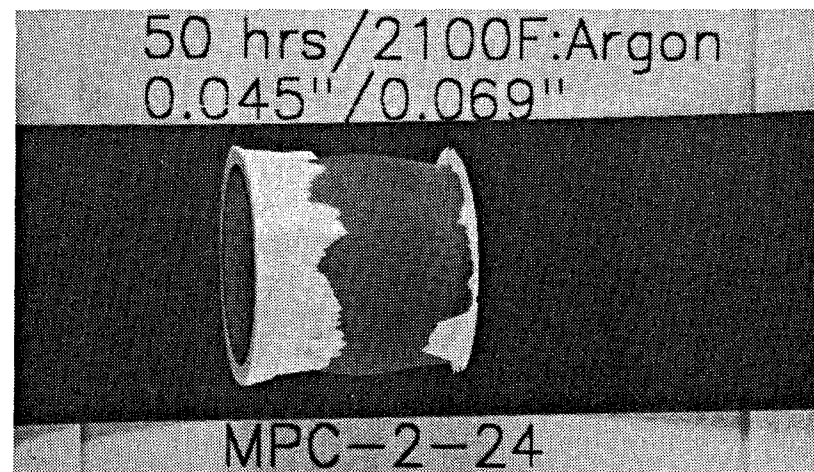
Figure 92.- Thermally Pre-Exposed EB-PVD Ceramic Coated Compression Test Specimen (MPC224) Tested at 982C (1800F).
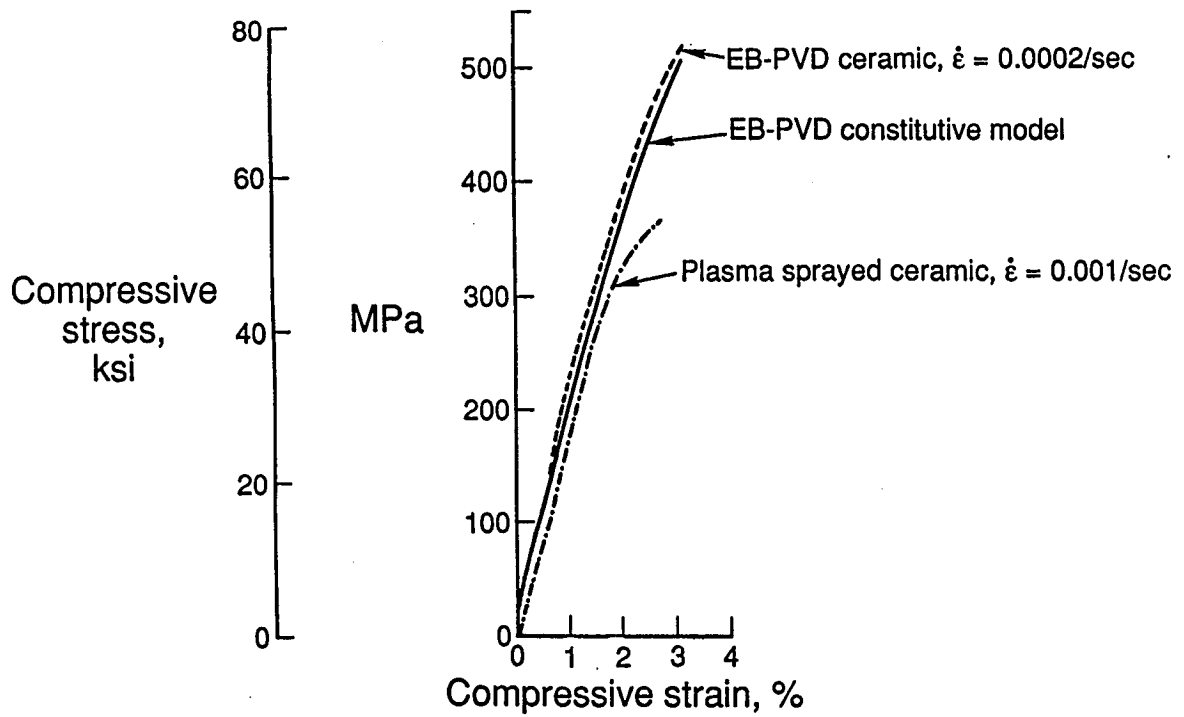
Figure 93.- Comparison of Calculated EB–PVD Compressive Stress-Strain Behavior with Experimentally Measured Results for EB–PVD and Plasma Ceramic at 538C (1000F).
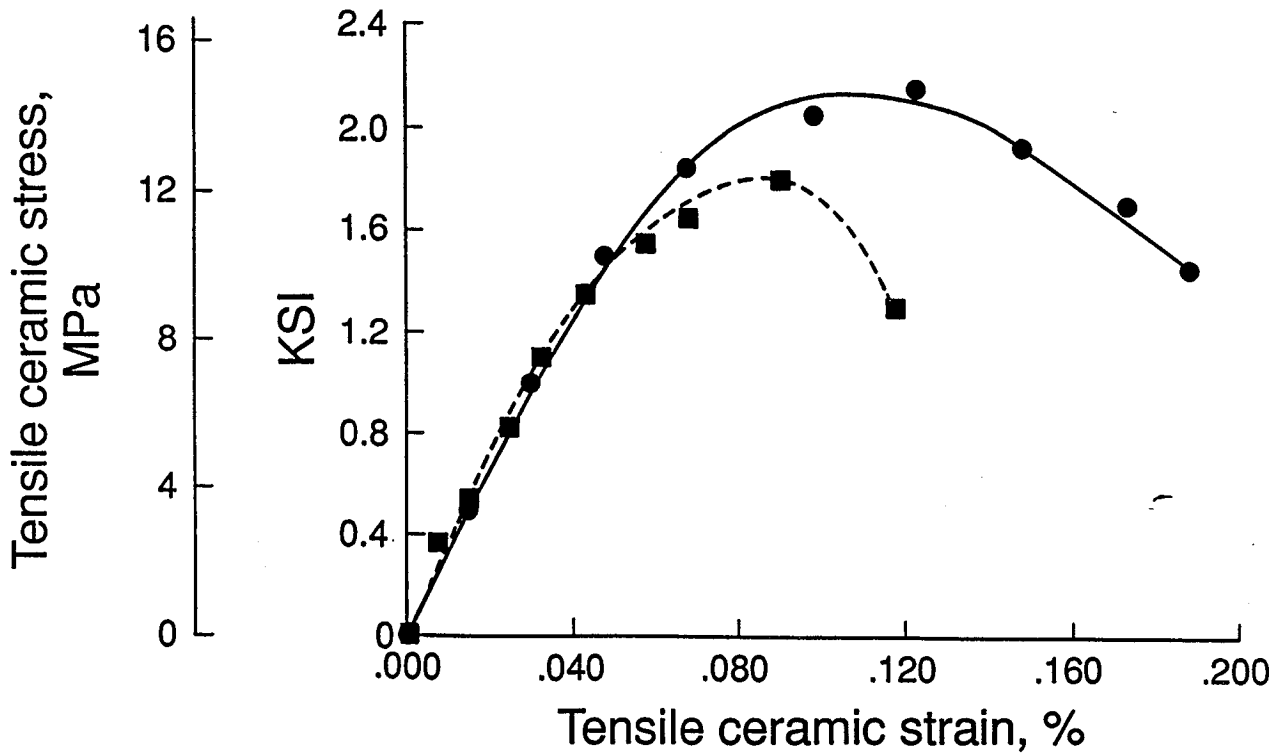
Figure 94.- EB–PVD Ceramic Tensile Stress-Strain Temperature at Room Temperature.

Figure 95.— Room Temperature Post-Test Tensile Specimen.

(a) (1.5x)   (b) (1.5x)   (c) (1.5x)

112
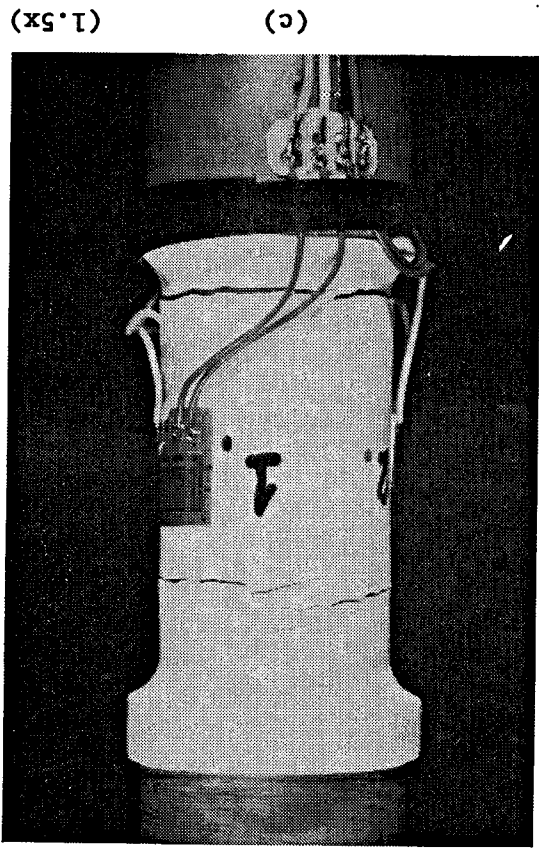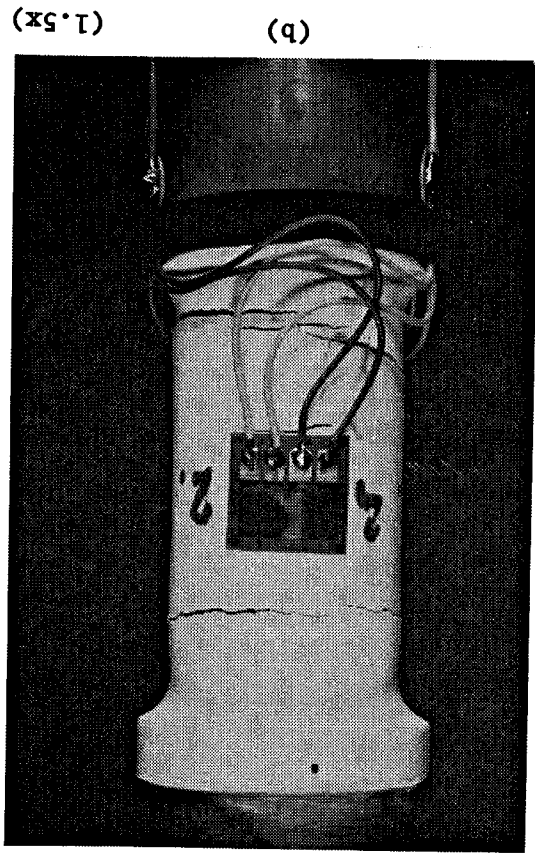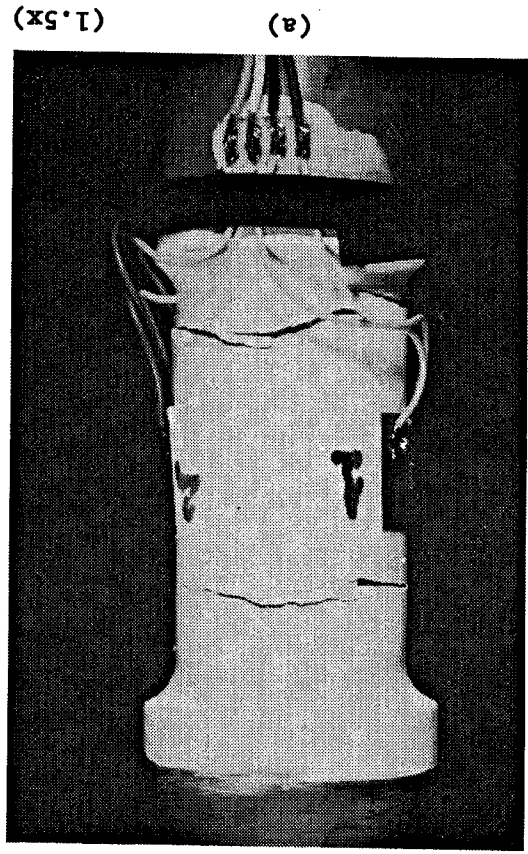
The tensile testing program included planned unloadings at various strain levels to evaluate whether the EB-PVD ceramic fractures would close, causing a re-stiffening of the bimaterial specimen. The conclusion of these tests is affirmative, in that when the strain is reduced to the range of the apparent ceramic fracture strain, the specimens exhibited higher stiffness, consistent with the stiffness prior to ceramic fracture during the first loading. It was thereby concluded that the mechanism of EB-PVD ceramic tensile fracture is consistent with reducing the stiffness to zero above a critical strain level, but requires a bilinear model to account for closure effects as strain is reduced below the critical value.

3.4.1.3 EB-PVD Ceramic Constitutive Model

The EB-PVD ceramic constitutive model development effort concentrated on modeling "first order" ceramic behavior. Elastic modulus was assumed to be a linear function of temperature (Figure 88) and Poisson's ratio was taken to be 0.25. EB-PVD ceramic column separation and accumulated cracking at low tensile stress levels was modeled by assuming that the columns open freely as the ceramic stress transitions into tension. Upon reverse (i.e., compressive-going) loading, the columns close at the same strain level which opened the columns during the tensile-going portion of the cycle. The compressive ceramic behavior was modeled by using Walker's isotropic viscoplastic formulation (Ref. 14). Constitutive model correlation capability is presented in Figure 93. In general, the model duplicates the observed EB-PVD ceramic compressive monotonic behavior quite well. The tensile and compressive EB-PVD constitutive formulations were generalized to 3D and incorporated into computer software. The source code for the EB-PVD ceramic constitutive model is presented in Appendix A. The software is compatible with the MARC general purpose and LAYER (Ref. 15) finite element programs.

3.4.2 Life Prediction Design Data Generation

A series of experiments were conducted to obtain data for correlation of the life prediction model. In these experiments, engine conditions were simulated and a broad range of mechanical and oxidation cyclic conditions were covered. The test method used a burner rig and involved testing of single internally cooled specimens.

3.4.2.1 Experimental Design

TBC life modeling involved correlation of ceramic spallation life measured in an instrumented burner rig with TGO growth characteristics and thermomechanically induced TGO strain levels. It involves exposure of an instrumented, TBC coated superalloy bar in a jet fueled burner rig.

The burner rig test used hollow tube specimens (Figure 96) that were rotated about their own axis in front of the Jet A fueled burner outlet. Combustion took place within the burner, from a combination of fuel and pre-heated air. The specimen temperature was controlled by modulation of the fuel-air ratio. Thermocouple signals were taken from the hot junction located within the wall of the specimen, to recording instrumentation, by use of radio telemetry transmission.
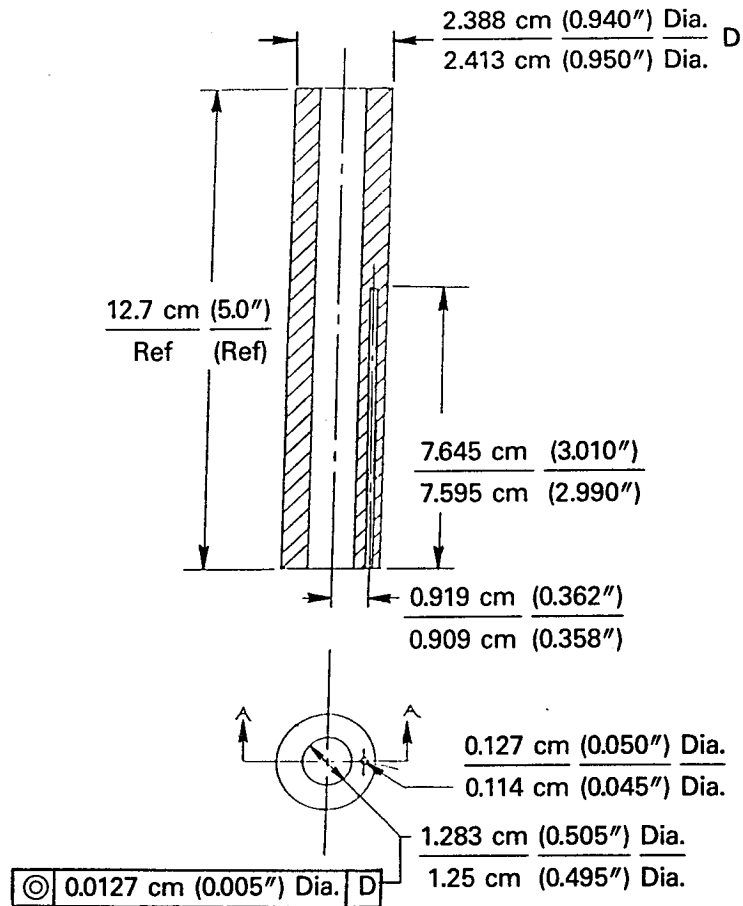
Figure 96.- Burner Rig Specimen Geometry for Design Data Generation Tests.

To simulate engine cycle transients, the specimen was periodically cycled out of the flame into an air cooling jet. The entire specimen drive system moved vertically so as to cycle the specimen from the flame for the hot portion of the cycle to a lowered position for cooling. Cooling was provided by an air jet directed at the specimen in the lowered position. Internal cooling of the hollow specimen was accomplished by flowing air into the bottom of the hollow drive shaft, exiting from the top of the specimen. Thermal stress levels developed in the burner rig specimen were controlled by manipulation of thermal exposure parameters such as temperature, cycle rate, hot and cold cycle times, transient heating rate, and specimen internal cooling air flow rate.

In Phase I, a specimen was instrumented and tested to characterize the variation of temperature with time at various locations in the specimen. This information obtained in Phase I along with the thermal conductivities obtained in Phase II in Section 3.2.1.2 were used to calculate the external and internal heat transfer coefficients and to determine the transient temperature response of the specimen.

Burner rig test parameters were varied to generate design data over a wide range of simulated mission cycles (Table XXXI). These tests were grouped in three generic cycle types: the "strain emphasis" cycle (Tests # 7-12), where many rapid thermal cycles were imposed, the "oxide emphasis" cycle (Tests #1-6), where significant hold time was imposed at the cycle maximum temperature, and the "mixed mode" cycle (Tests # 13-18), which combined elements of the strain and oxide cycles.

114

TABLE XXXI
DESIGN DATA GENERATION EXPERIMENTAL MATRIX

| Test | Emphasis | Interface Temperature | | | | Cycle Time (Min) |
| | | Maximum | | Minimum | | |
		(C)	(F)	(C)	(F)	
1	Oxide	1107	2025	427	800	6
2	Oxide	1107	2025	427	800	6
3	Oxide	1107	2025	427	800	12
4	Oxide	1107	2025	427	800	12
5	Oxide	1107	2025	427	800	24
6	Oxide	1107	2025	427	800	24
7	Strain	1121	2050	21	70	6
8	Strain	1121	2050	21	70	6
9	Strain	1149	2100	21	70	6
10	Strain	1149	2100	21	70	6
11	Strain	1177	2150	21	70	6
12	Strain	1177	2150	21	70	6
13	Mixed Mode	1079	1975	57	135	6
14	Mixed Mode	1079	1975	57	135	6
15	Mixed Mode	1079	1975	57	135	12
16	Mixed Mode	1079	1975	57	135	12
17	Mixed Mode	1107	2025	57	135	6
18	Mixed Mode	1107	2025	57	135	12

3.4.2.2 Design Data Generation Cyclic Thermal Exposure Test Results

The results of the 18 design data generation burner rig tests are presented in
Table XXXII. Due to the variability of the burner rig optical temperature
measurement and control system, the experiments did not run at the exact
temperatures listed in the test matrix. The average maximum and minimum
temperatures recorded from the thermocouple within each specimen is shown in
Table XXXII. These actual temperatures were used in the life modeling effort.

Figures 97, 98, 99 show typical spallation of the EB-PVD ceramic coating on
the 2.54 cm (1") diameter burner rig bar for the three emphasis modes. The
coating fails in a complete band approximately 2.54 cm (1") wide within the
hot zone of the specimen. Such failure prevented oxide thickness measurements
on many specimens due to the lack of realistic oxide thicknesses in the hot
zone. These photos demonstrate that the test/specimen was well designed to
provide an even temperature distribution around the bar. Figure 100 was
included to illustrate a combination cold/hot failure. Actually, the specimen
failed during testing in the burner rig and continued to cycle through
elevated temperatures until the next observation shut down. The bond coat
appears dark due to oxidation at the elevated temperatures. Subsequently,
additional ceramic spalled off at room temperature, leaving a shiny bond coat
surface.

TABLE XXXII
DESIGN DATA GENERATION TEST RESULTS

Test No.	Specimen No.	Test Emphasis	Test Cycle (min.)	Interface Temperature				Actual Cycles	Actual Test Hours	Estimated Hot Hours	Oxide Thickness	
				Maximum		Minimum					(μm)	(microinches)
				(°C)	(°F)	(°C)	(°F)					
1	HSTC2-2A	Oxide	6	1118	2045	552	1025	3307	243	94	5.80	228.35
2	HSTC2-06	Oxide	6	1152	2105	578	1073	1487	126	52	—	—
3	HSTC2-02	Oxide	12	1119	2047	573	1063	4109	712	527	7.91	311.42
4	HSTC2-25	Oxide	12	1133	2072	546	1014	764	132	108	—	—
5	HSTC2-21	Oxide	24	1128	2062	558	1037	1575	641	570	—	—
6	HSTC2-05	Strain	6	1119	2046	44	112	18503	1881	154	4.68	184.25
7	HSTC2-28	Strain	6	1132	2070	46	115	2422	246	20	—	—
8	HSTC2-01	Strain	6	—	—	—	—	8819	808	74	3.75	147.64
9	HSTC2-09	Strain	6	1156	2113	50	123	2658	244	22	—	—
10	HSTC2-29	Strain	6	1153	2107	60	140	2488	253	21	—	—
11	HSTC2-13	Strain	6	1133	2071	43	110	5235	532	44	—	—
12	HSTC2-04	Strain	6	1187	2168	37	98	1728	167	14	4.29	168.90
13	HSTC2-30	Strain	6	1177	2150	68	155	1474	150	12	—	—
14	HSTC2-19	Mixed Mode	6	1092	1998	53	128	9014	1352	331	5.59	220.08
15	HSTC2-07	Mixed Mode	6	1100	2013	48	118	4129	619	151	—	—
16	HSTC2-22	Mixed Mode	12	1107	2025	54	129	2678	625	344	5.50	216.54
17	HSTC2-12	Mixed Mode	12	1105	2021	58	137	2884	663	364	—	—
18	HSTC2-16	Mixed Mode	6	1123	2054	46	114	7546	964	205	—	—
19	HSTC2-18	Mixed Mode	12	1123	2053	51	124	2444	550	314	—	—

)
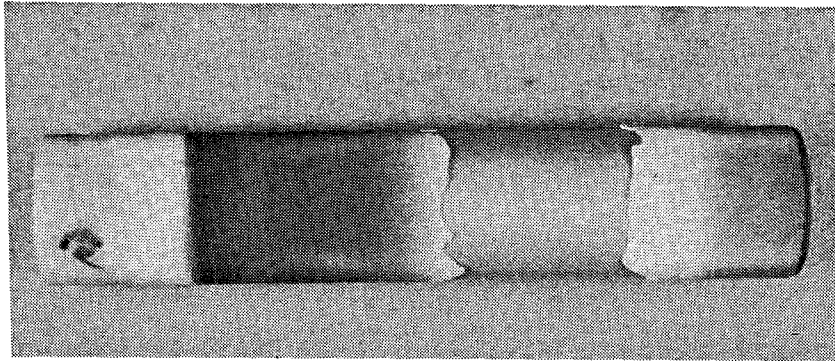
Figure 97.- Failed 2.54 cm (1") Burner Rig Specimen From Oxide Emphasis 1107C (2025F)/24 Minute Cycle Test at 641 Hours.
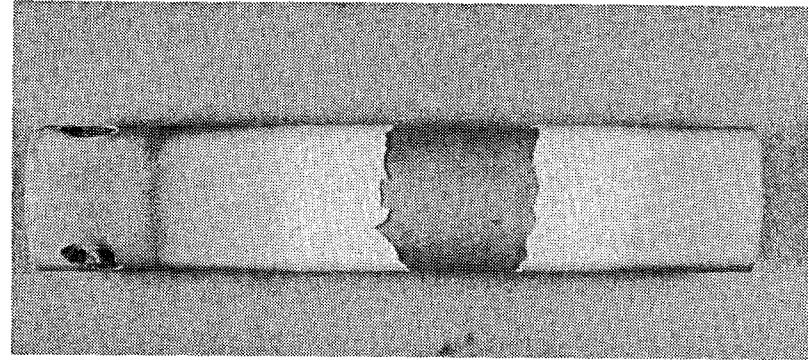
Figure 98.- Failed 2.54 cm (1") Burner Rig Specimen From Strain Emphasis 1149C (2100F)/6 Minute Cycle Test at 253 Hours.
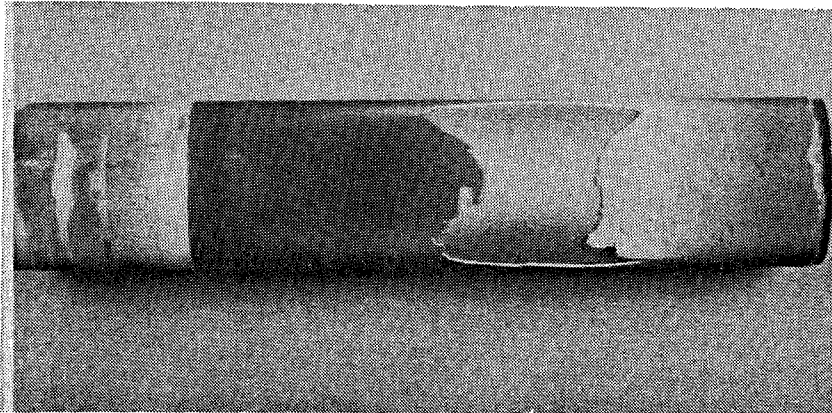
Figure 99.- Failed 2.54 cm (1") Burner Rig Specimen From Mixed Mode Emphasis 1079C (1975F)/6 Minute Cycle Test at 1352 Hours.
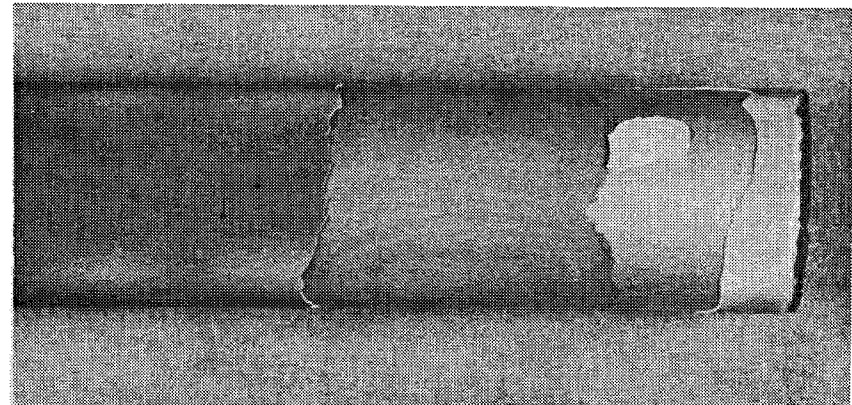
Figure 100.- Failed 2.54 cm (1") Burner Rig Specimen From Strain Emphasis 1177C (2150F)/6 Minute Cycle Test at 167 Hours.

Figures 101-102 show examples of the post-test microstructures of specimens shown above. These figures show that this test faithfully duplicates the engine spallation failure mode: at the interface between the thermally grown oxide and the metallic bond coat.

3.4.3 Life Prediction Model Correlation

Life prediction model parameters were formulated to account for the important life driving forces. This was accomplished through correlation of the design data developed in Task VIIA of this phase. As part of this process, material property data and individual specimen temperature data was used to conduct the required thermal stress analyses. The model correlation was conducted by Dr. Thomas A. Cruse of Vanderbilt University in Nashville, Tennessee.

3.4.3.1 Life Modeling Strategy

Past experience with plasma sprayed TBC (Phase I) indicated that inelastic deformation of the ceramic was a critical life parameter. However, nonlinear analysis of the EB-PVD ceramic behavior during burner rig specimen thermal cycling indicated that the EB-PVD ceramic remains elastic. For that reason and because spallation failure of the EB-PVD TBC system is caused by cracking at the thermally grown oxide/metallic bond coat interface, life modeling efforts have used TGO elastic strains instead of EB-PVD ceramic strains.

The out-of-plane tensile stress predicted for the TGO is quite low [≈ 3.45 MPa (500psi)] compared to the TGO out-of-plane strength [≈ 27.58 MPa (4000 psi)]. Tensile fatigue testing of the plasma sprayed coatings in the first phase of the program showed that tensile fatigue could be incurred, but only for stresses approaching the ultimate strength of the brittle material. The lives increased very rapidly for applied tensile stresses much below the material tensile strength. It therefore seems likely that the damage process involves cyclic microcrack formation in the thermal grown oxide scale, due to the in-plane stress cycle. The out-of-plane stress due to specimen curvature is not likely to be sufficient to contribute to the progressive failure, except in the very last stages of spallation crack growth.

Once the cyclic thermoelastic strain cycles in the oxide layer were modeled for each test condition, life models were defined that included the effect of oxide growth on specimen fatigue life. The resulting damage model was fit to the spallation data generated, and the life correlation between the three generic cycle types was assessed. Finally, the model was confirmed by predicting the verification test results.

3.4.3.2 TBC Fatigue Life Prediction Oxide Scale Growth

The oxide scale growth was discussed in Section 3.3.1.5. Equation 12 is exercised in the life prediction computer program, TBC_LFE2, in the subroutine PREXPO in order to calculate the pre-exposure oxide scale growth.

It was assumed that the quasistatic growth process was governing in order to fit the growth law to cyclic testing with varying temperatures. By assuming this, the temperature affects the increment of oxide growth but not the rate of oxide growth. Therefore, the increment to the inverse power from Equation 11 may be written as

118
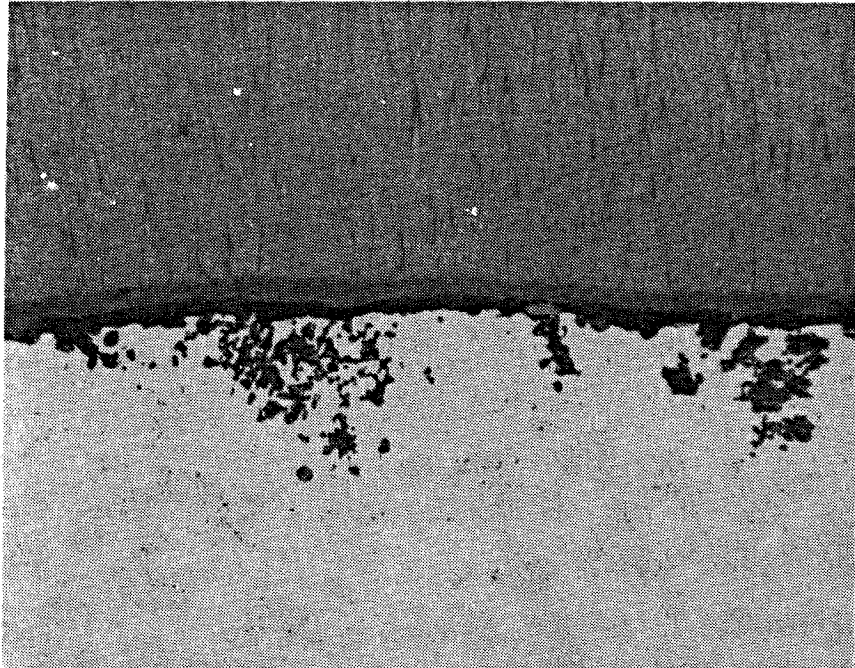
Figure 101.- Transverse Section of a Failed 2.54 cm (1") Burner Rig Specimen From Oxide Emphasis 1107C (2025F)/24 Minute Cycle Test at 641 Hours. Mag: 500x
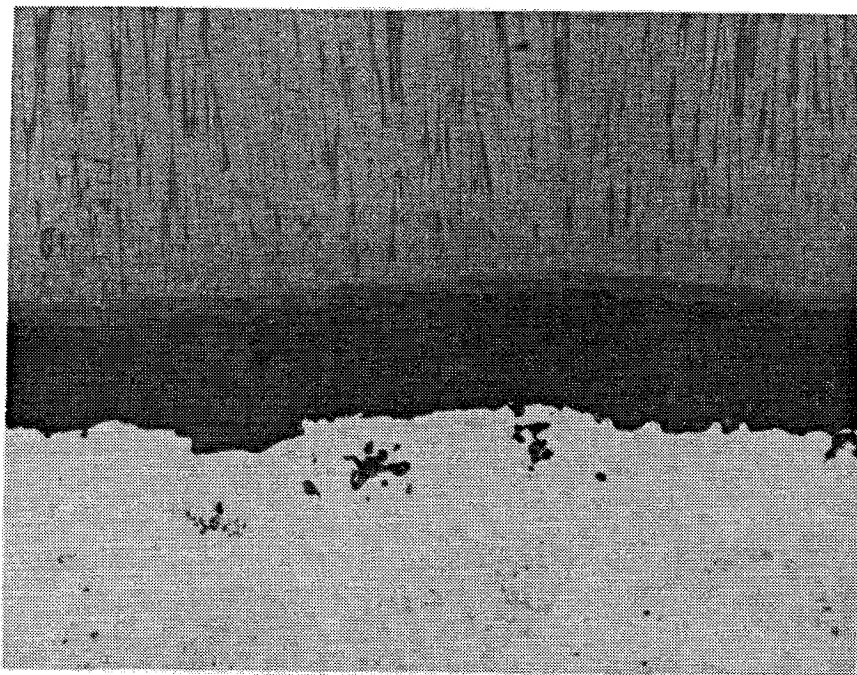
Figure 102.- Transverse Section of a Failed 2.54 cm (1") Burner Rig Specimen From Mixed Mode Emphasis 1079C (1975F)/6 Minute Cycle Test at 1352 Hours. Mag: 500x

$$\delta^{1/n} = \Delta \tau \exp\left[Q\left(\frac{1}{T_o} - \frac{1}{T}\right)\right]$$

<div align="right">Equation 12</div>

The oxide scale growth for a time varying cycle of thermal exposure may then be shown as

$$\delta_F = \left[\sum_{m=1}^{M}\left\{\Delta\tau_m \exp\left[Q\left(\frac{1}{T_o} - \frac{1}{T_m}\right)\right]\right\} + \delta_1^{1/n}\right]^n$$

<div align="right">Equation 13</div>

Equation 13 is used in TBC_LFE2 in subroutine GROWTH. The average temperature is calculated over each input time step.

3.4.3.3 TBC Fatigue Life Prediction Thermomechanical Oxide Strain Cycle

Since spallation failure of the EB-PVD TBC system is caused by cracking at the thermally grown oxide-metallic bond coat interface, a cyclic thermomechanical response model for the oxide scale was selected for the life prediction algorithm. The in-plane TGO mechanical strain was taken to be due to the thermal growth mismatch between the TGO and the substrate, resulting in in-plane TGO elastic strain (or stress). The coefficient of thermal expansion (CTE) for the TGO, not measured in this program, was assumed to be linearly dependent on temperature based on CTE values obtained for aluminum oxide from literature (Ref. 16). The free elongation of the TGO at temperature was taken to be:

$$\delta L/L = \int_{T_{sf}}^{T} \alpha\,(T)dT = \alpha_o(T - T_{sf}) + \frac{1}{2}\alpha_1\left[(T - T_o)^2 - (T_{sf} - T_o)^2\right]$$

<div align="right">Equation 14</div>

where:

T_o = ambient temperature = 21°C (70°F)
T = metal/EB-PVD ceramic interface temperature
T_{sf} = strain (or stress)-free temperature for the oxide(taken to be the maximum metal/EB-PVD ceramic interface temperature + 98C (200F)
$\delta L/L$ = free thermal elongation of the TGO
α_o = 0.65 x 10E-5 mm/mm/C (0.36 x 10^{-5} in/in/F)
α_1 = 1.64 x 10E-9 mm/mm/C (0.91 x 10^{-9} in/in/F)

For the computer program, the difference between Tsf and Tmax is referred to as Tref where Tref is a constant (98C or 200F). The mean stress in the oxide is very sensitive to the stress-free temperature variable, referred to as Tref in the life model. Without the mean stress effect, the life modeling capabilities were inferior.

The in-plane mechanical strain in the TGO was then calculated for a particular cycle by subtracting the results from Equation 14 from the substrate total strain.

$$\epsilon_{(T)} = \epsilon_{ss\,(T)} - \epsilon\left(\delta L(T)/L\right)$$

<div align="right">Equation 15</div>

where: ϵ = mechanical strain in the TGO
ϵ_{ss} = substrate total strain

The substrate total strain was obtained from an elastic 3D analysis for each of the EB-PVD ceramic coated burner rig specimens. The final damage model assumed that only the tensile portion of the in-plane TGO mechanical strain cycle was contributing to the damage. Therefore, the computer code TBC_LFE2 calculated the cyclic in-plane TGO mechanical strain DEL_EPS as equal to the maximum in-plane TGO mechanical strain in the subroutine MECH_STRN. A representative in-plane TGO mechanical strain cyclic history is presented in Figure 103.
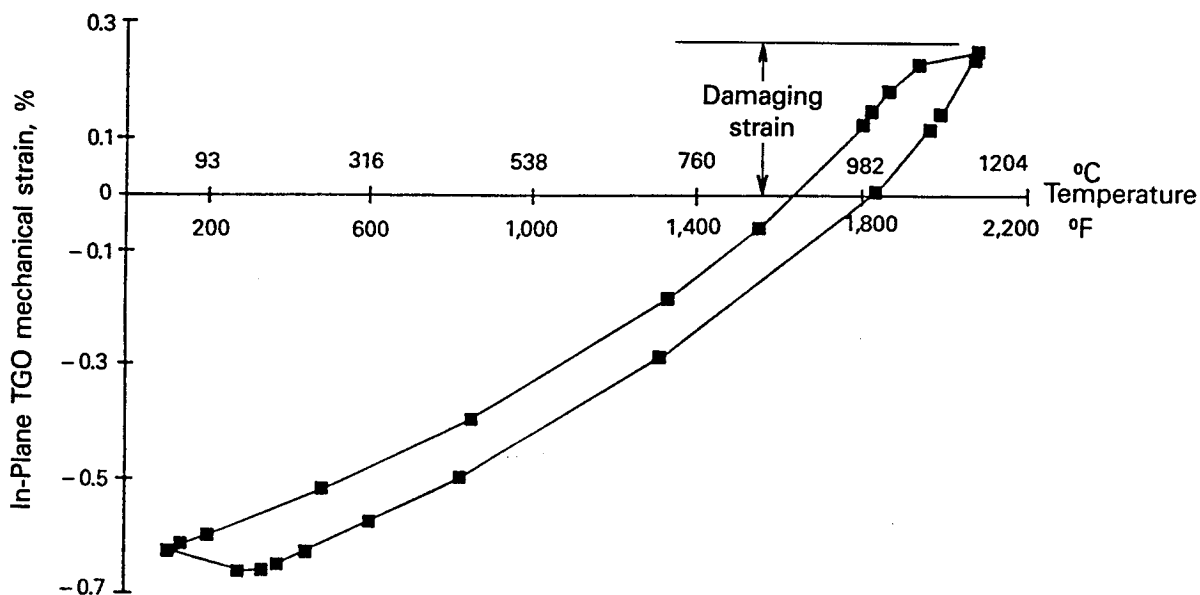
Figure 103.- Representative In-Plane TGO Mechanical Strain History Calculated for the Burner Rig Specimen Geometry and Strain Emphasis Cycle.

Several cyclic damage models for the TGO were evaluated by applying them to the life data from Section 3.4.2.2. Each damage model was taken to be a power law relation, consistent with elementary fatigue models and with the damage model developed for plasma sprayed TBC in Phase I of this program. The general form of the power law life model is

$$N = A\Delta\epsilon^b$$

Equation 16

where N is the cyclic life, A is an empirical normalizing constant, and b is the empirical power law coefficient. The strain range ($\Delta\epsilon$) in Equation 16 was assumed to be the maximum in-plane TGO tensile mechanical strain obtained from Equation 15.

The parameter A was found in the earlier study, Phase I, to depend on the amount of oxide growth, although the specific rationale for the dependence was not determined. The failure site in the plasma sprayed ceramic was within the ceramic adjacent to but not coincident with the irregular thermally grown oxide interface. The EB-PVD failure locations were in the thermally grown oxide layer at the bond coat interface. Therefore, the oxide should be taken into account when considering the cyclic life of the EB-PVD specimens.

The model for the plasma sprayed ceramic also showed that the oxide scale experienced a critical thickness at which the ceramic spalled spontaneously upon removal from the oxidizing test. The concept of a critical oxide thickness was very difficult to justify in the EB-PVD ceramic thermal barrier coating system since the static furnace test failures were not achieved in slow cool

121

tests. Static spallation did occur in some specimens which appear to be the result of large magnitudes of stresses at the end of the ceramic coating and the ability of the bond coat to relax this stress during slow cooling.

Oxide scale growth modification of the parameter A in Equation 16 is required, as will be discussed in the next section. In order to correlate the specimen data, various power law relationships between A and the current value of the oxide thickness were used. The model which performed the best was that reported in Phase I for the plasma system.

The fatigue life model is given as

$$N = [(\Delta\epsilon_{ff}/\Delta\epsilon)(1 - \delta/\delta_c)^c + (\delta/\delta_c)^c]^b \qquad \text{Equation 17}$$

where:

δ_c = critical oxide thickness which causes EB-PVD ceramic spallation without cycling = 0.0140 mm (0.00055 in)

b = 7.64

$\Delta\epsilon_{ff}$ = constant = 0.016 mm/mm (in/in)

c = 1.0

δ = oxide thickness at a particular cycle number

The model in Equation 17 is based upon the possibility that a static spallation will occur in the event of a strain cycle of amount $\Delta\epsilon_{ff}$, the furnace failure strain. Since static furnace failures did not occur, the delta c strain is taken to be an empirical factor. Its suggested value is actually greater than that obtained in any of the furnace tests. Furthermore, the furnace test failure is probably due to edge failure and is not indicative of the proposed failure mode. The failure model is synergistic; some fatigue cycling of the oxide layer is needed to reduce the interface strength. This is consistent with the static test results, where lack of failure was due to the absence of fatigue cycling.

The damage per thermal cycle is obtained by taking the inverse of Equation 17 for each cycle. The value of cyclic damage is computed in TBC_LFE2 in the subroutine DAMAGE. In the subroutine CHECK, the current damage is added to the total previous damage summation. When the total damage sums to one or greater at the end of a cycle, the specimen is considered failed.

The fact that the same life model formulation works for both plasma sprayed and EB-PVD TBC systems suggests that the failure mechanisms are the same for both systems. In earlier studies (Ref. 1, 17) it was not clearly understood why the failure took place in the ceramic directly above the thermally grown oxide, except that the ceramic did develop microcracks and these seemed to be bigger near the oxide layer. While it was known that the TGO would have its own cyclic stress/strain conditions, these were discounted as a failure source due to the ceramic failure. The present study suggests that the maximum in-plane TGO tensile mechanical strain (or stress) is controlling for both types of TBC systems. The increase in life noted for the EB-PVD ceramic systems may be due to the fact that the interface is smooth, resulting in lower stress concentrations in the oxide layer and that the EB-PVD ceramic does not experience microcracking.

The critical oxide thickness defined by the cyclic fatigue correlation has not been achieved in either static or cyclic tests in the EB-PVD system. The cyclic tests performed achieved up to 60%of the critical oxide thickness value before spalling. The fatigue model indicates that cyclic strain is predominant in the cyclic test damage history. The static furnace tests also did not achieve oxide levels on the order of the critical value. Thus, the proposed fatigue model for the EB-PVD TBC system does not conflict with any of the program test results.

3.4.3.4 TBC Fatigue Life Prediction Correlation Results and Discussion

The thermal cycles for each of the burner rig design data generation test specimens were analyzed. Actual and predicted thermal strain cycles are presented in Table XXXIII. The data in this Table is for the case of Tref = 93C (200F) although a Tref of -101C (-150F) was also used to study the sensitivity of the life correlation to this parameter. The resulting interface temperature and substrate strain history (see example in Figure 103 are used to calculate the positive mechanical strain in the oxide. Verification tests (see Section 3.5.1) were included in these analyses.

TABLE XXXIII
SPECIMEN CORRELATION RESULTS FOR Tref = 93C (200F)

Specimen	Test Type	Tmax (C)	Tmax (F)	Tmin (C)	Tmin (F)	Actual Cycles	Predicted Cycles	Ratio
HSTC2-7	Mixed	1100	2013	48	118	4129	5397	1.31
HSTC2-12	Mixed	1105	2021	58	137	2884	3287	1.14
HSTC2-16	Mixed	1123	2054	46	114	7546	3673	0.49
HSTC2-18	Mixed	1123	2053	51	124	2444	1936	0.79
HSTC2-19	Mixed	1092	1998	53	128	9014	7089	0.79
HSTC2-22	Mixed	1107	2025	54	129	2678	2943	1.10
HSTC2-2	Oxide	1119	2047	573	1063	4109	2487	0.61
HSTC2-2A	Oxide	1118	2045	552	1025	3307	4595	1.39
HSTC2-6	Oxide	1152	2105	578	1073	1487	1484	1.00
HSTC2-21	Oxide	1128	2062	558	1037	1575	1224	0.78
HSTC2-25	Oxide	1133	2072	546	1014	764	1707	2.23
HSTC2-1	Strain	1144	2091	35	95	8819	4204	0.48
HSTC2-4	Strain	1187	2168	37	98	1728	821	0.48
HSTC2-5	Strain	1119	2046	44	112	18503	11202	0.61
HSTC2-9	Strain	1156	2113	51	123	2658	2680	1.01
HSTC2-13	Strain	1133	2071	43	110	5235	6017	1.15
HSTC2-28	Strain	1132	2070	46	115	2422	6581	2.72
HSTC2-29	Strain	1153	2107	60	140	2488	2976	1.20
HSTC2-30	Strain	1177	2150	68	155	1474	1196	0.81
HSTC2-8	Verif	1144	2091	42	107	801	1276	1.59
HSTC2-11	Verif	1138	2080	589	1012	840	824	0.98
				35	95			
HSTC2-26	Verif	1156	2112	562	1044	1952	935	0.48

The tensile strain versus actual specimen spallation life is plotted in Figure 104. A correlation line with a slope of 7.5 is drawn through the strain emphasis cycle (SE) life data; the oxide emphasis (OE) and mixed mode cycle (MC) data are parallel but have lower life levels. This observation indicated that the cycles include a damage component in addition to the tensile strain. The oxide emphasis and the mixed mode emphasis data fall on approximately the same line. These two cycles have similar high temperatures and hold times; the plot suggests that the oxide scale growth effect must be included.

The tensile strain versus actual specimen spallation life is plotted in Figure 105 for the case of Tref = -101C(-150F). The slope is about 3.0. Although the tensile strain levels are different, the data trend is the same. However, the separation of the strain emphasis data from the high temperature/high hold time cycles is much larger.

Figure 106 shows the calculated relative final oxide thickness versus strain range for a Tref = 93C (200F). This plot shows that a life trend with oxide scale thickness exists but that it is not the sole damage parameter. Therefore, the life model developed in Phase I was used in the spallation life correlation study. Both values of Tref were used in the correlation to determine the dependence on mean strain (stress).

Figure 107 shows the model correlation using a Tref = -101C(-150F). The parameters for the model were b=3.0, c=1.0, $\Delta\epsilon_{ff}=0.06$, and δc = 0.01 mm(0.0004 inch). The Weibull of the data is illustrated in Figure 108. The data scatter is ±2 of the mean values. The strain emphasis data, however, is not well correlated. The prediction is high for the lower lives and low for the higher lives.

Figure 109 shows the final model correlation. The Tref = 93C(200F) and the correlation slope is approximately 7. The correlation scatter is slightly better for Tref = -101C(-150F), but the correlation within each of the generic cycle types is much better for Tref = 93C(200F). The Weibull in Figure 110 demonstrates this interpretation. The verification data is also within a ±2x scatter band.

Table XXXIII is a summary of the life model correlation results for the EB-PVD specimens. Included in this Table are cycle maximum and minimum temperatures, final computed oxide scale thickness, and cycle predictions.

The issue of test shutdowns was also reviewed. Test shut down actually drives the ceramic into in-plane compression at ambient temperatures, with tensile loading transverse to the oxide due to the specimen curvature. The cycle maximum strain is compressive and does not contribute to fatigue damage, according the the life model. However, if the failure is initiating at the time of the shutdown, the transverse tensile stress may contribute to earlier spallation. The total effect of this premature fracture is probably small, however, due to the high rates of oxide crack growth leading to ceramic spallation.

124
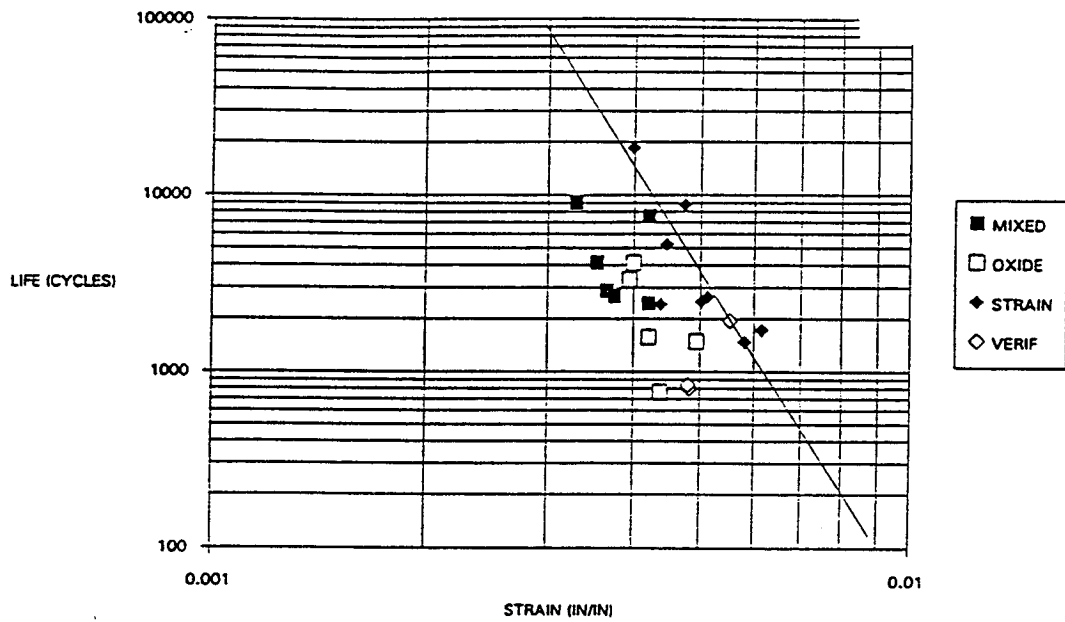
Figure 104.– Tensile Strain Versus Specimen Spallation Cycle Life for
Tref = 93C (200F).
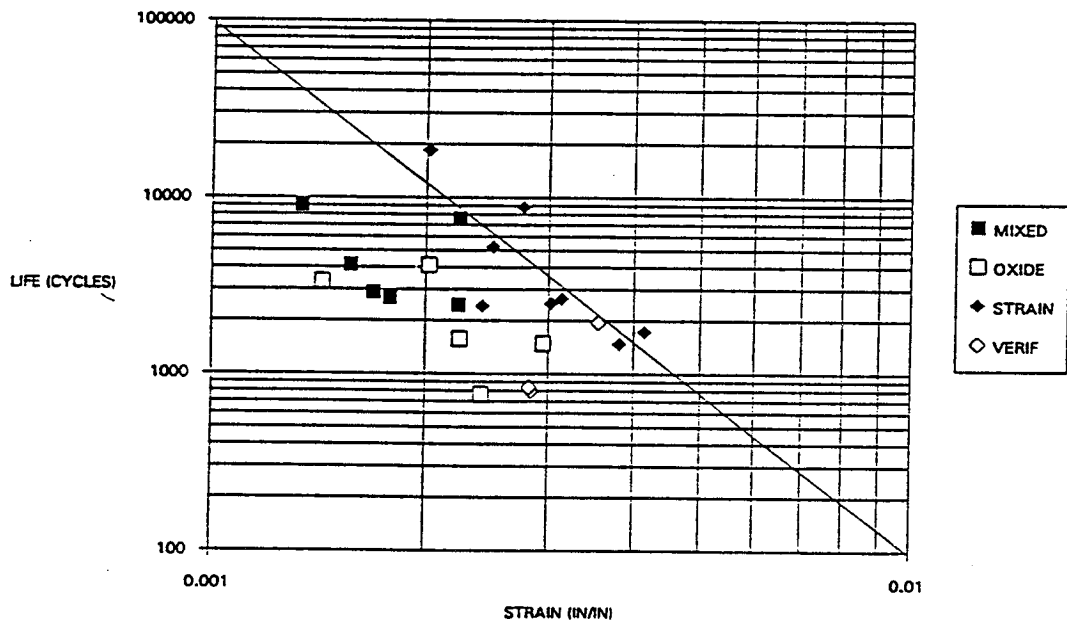
Figure 105.– Tensile Strain Versus Specimen Spallation Cycle Life for
Tref = -101C (-150F).

125
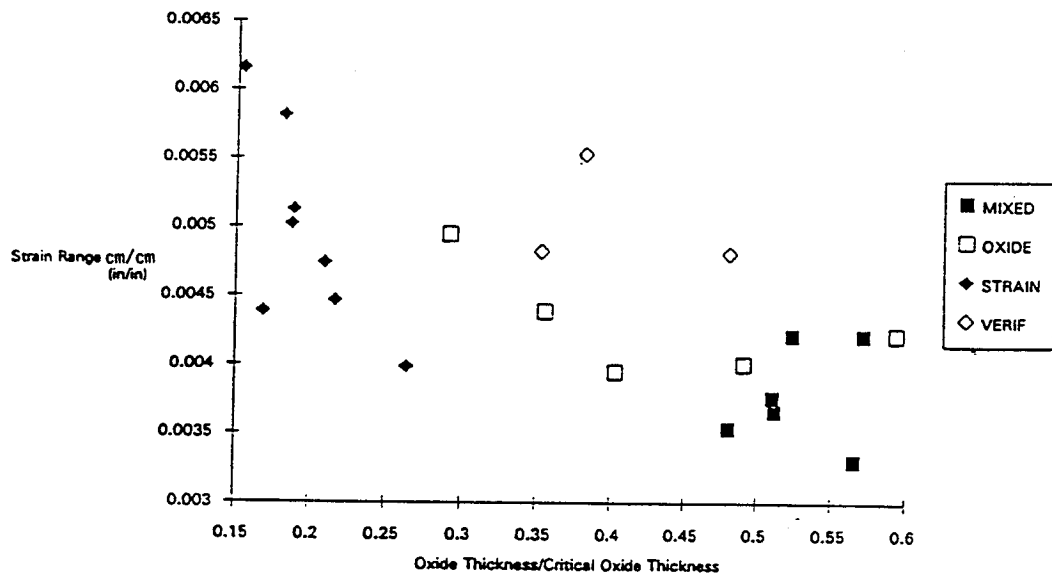
Figure 106.- Oxide Scale Thickness Versus Tensile Strain Range for Tref = 93C (200F).
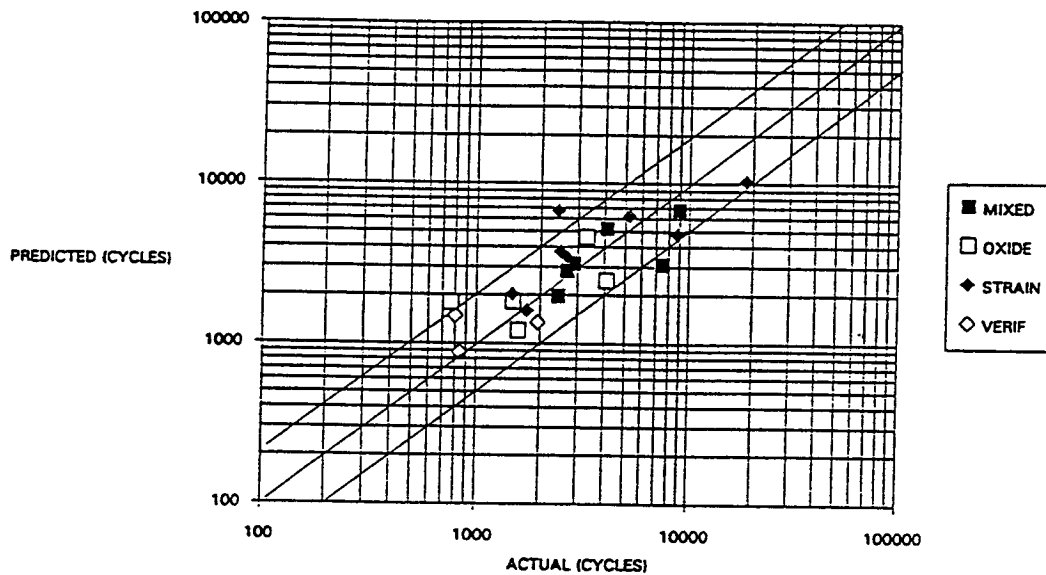
Figure 107.- Spallation Life Correlation Plot for Tref= -101C (-150F).
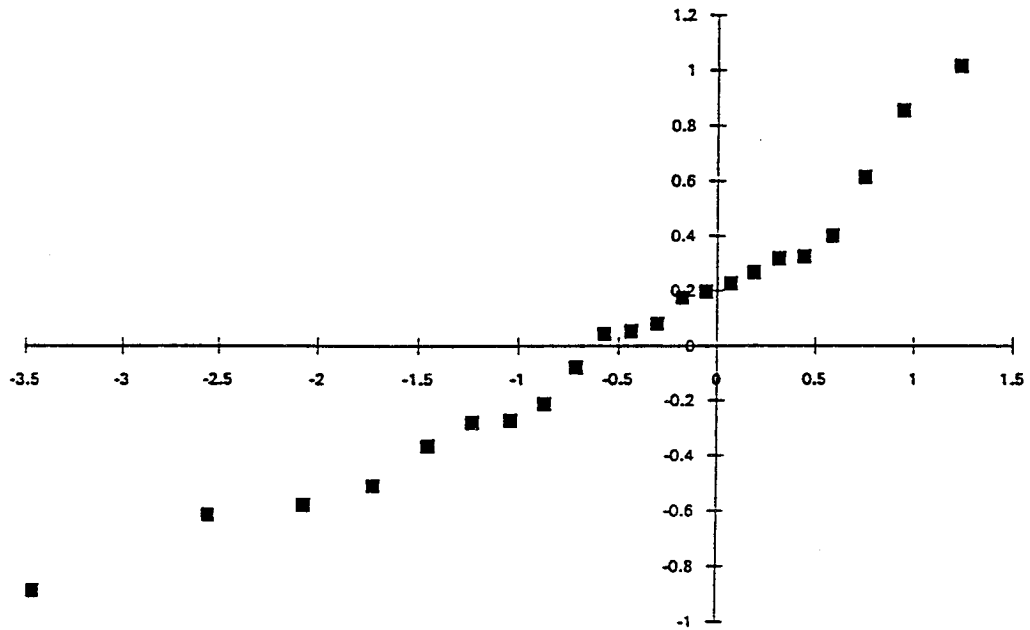
Figure 108.- Weibull Statistical Plot of the Spallation Life Correlation
(P/A) for Tref = -101C (-150F).
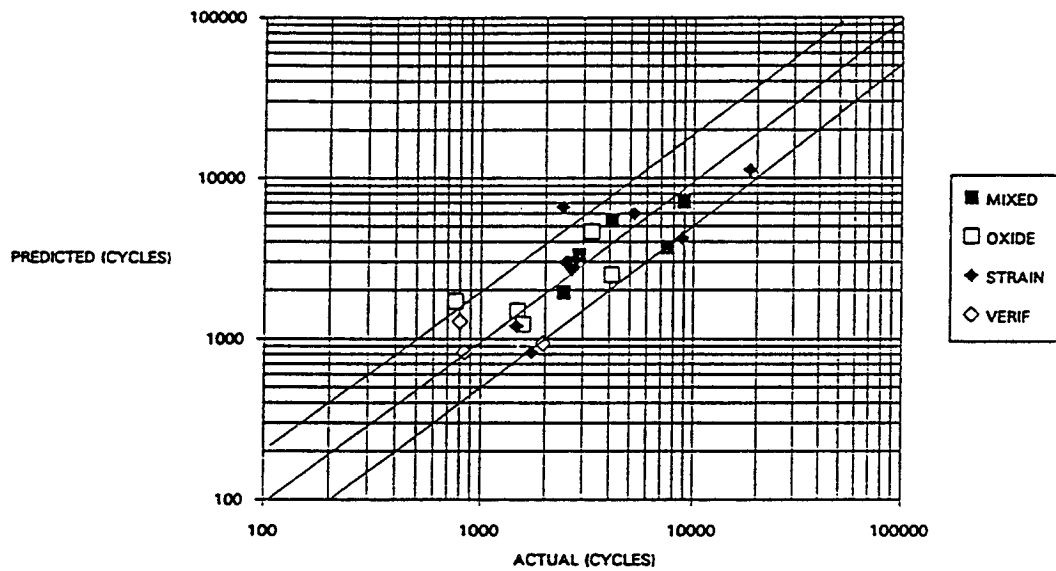
Figure 109.- EB-PVD TBC Life Model Correlation of Specimen Spallation Lives
with Tref = 93C (200F).
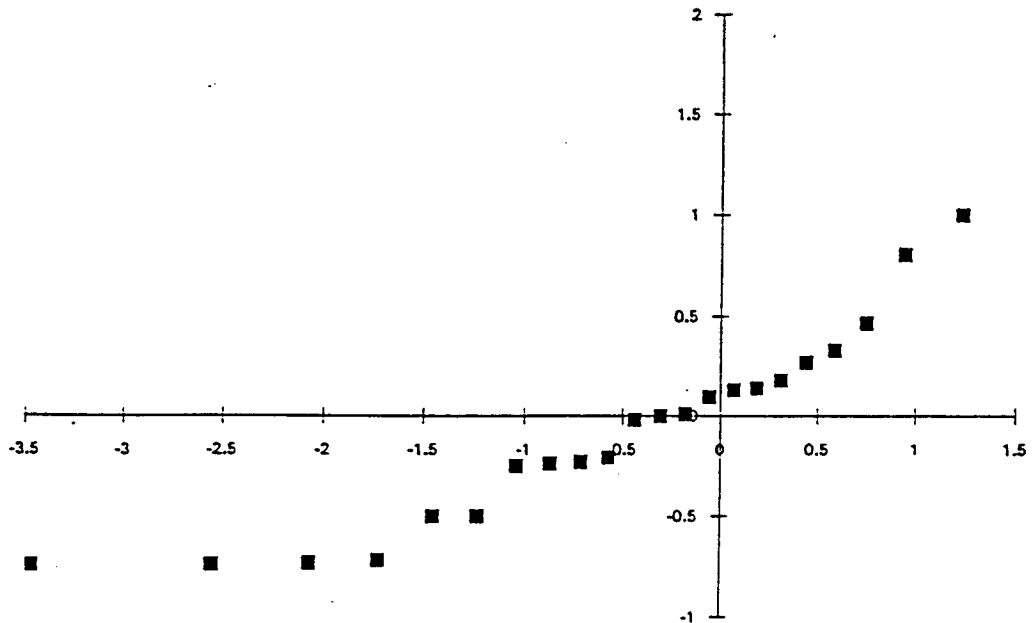
Figure 110.- Weibull Correlation Plot for Tref = 93C (200F).

3.5 TASK VIII - MODEL VERIFICATION

The life prediction model developed for the EB-PVD ceramic coatings was challenged by applying the model to three verification experiments. Results of experiments designed to test the model's validity were reviewed and recommendations made.

3.5.1 Task VIIIA - Verification Experiments

Three specimens were tested at simulated engine conditions. The experiments emphasized the most important life drivers: strain, oxide, and mixed mode, so that the model was truly challenged to account for singular and synergistic degradation modes. Results of the experiments were used to verify the life prediction model.

The model was verified using life data obtained from the 2.54 cm (1") diameter burner rig tests (Section 3.4.2) with modified conditions. The cycles selected to challenge the model and the corresponding lives are listed in Table XXXIV.

3.5.2 Task VIIIB - Analyses/Recommendation

Life prediction analyses were conducted to evaluate the results of the verification experiments conducted in section 3.5.1 Task VIIIA Verification Experiments. The validity of the model was judged according to how closely the model predicted the TBC life for each engine simulation test. Recommendations for further research or refinement required to arrive at a satisfactory engine life prediction methodology for EB-PVD ceramic coatings were made.

128

TABLE XXXIV
VERIFICATION TEST RESULTS

Test #	Test Type	Test Time (hrs)
1	1149C(2100F)/6 min Strain Cycle Small Strain Component (Cooled to 593C or 1000F)	179
2	1149C(2100F)/24 min Oxide Cycle First 100 Cycles Have Large Strain Component (Cooled to 38C or 100F)	285
3	1149C(2100F)/12 min Oxide Cycle Large Strain Component (Cooled to 38C or 100F)	139

The model was tested by predicting the results of three verification tests intended to challenge model predictive capability. The verification test predictions were within a factor of two of the actual lives (see Figure 109 and Table XXXIII). Since the predictive capability of the model fell within a ±2x scatter band, the model was judged to be acceptable.

Recommended future work includes stress computations for all specimens using a finer time step to better define the ends of the strain-temperature cycles. In addition, the model is strongly dependent on the thermally grown oxide thermal expansion coefficient and the thermally grown oxide stress-free temperature. For future life prediction model development, it is suggested that these properties be experimentally obtained. Also, a verification of the initial stress in the composite tube specimens during fabrication is desirable.

3.6 TBC LIFE MODEL COMPUTER CODE

The operation of this computer code, TBC_LFE2.FOR, has been described throughout Section 3.4. The FORTRAN 77 source code TBC_LFE2 is in Appendix B. The following is an updated User Manual for the code TBC_LFE2. The procedure for using TBC_LFE2 is basically the same as for the computer code written in Phase I, TBCLIF. The code is designed to run on PC's or on mainframes, using standard Fortran 77 code. In order to run the code, the user must specify input and output devices if standard devices (FOR005, FOR006) are not used. Running the code on an IBM compatible machine requires adding <input.dat>output.dat to the run line or responding to terminal cues. The input files used for the life modeling are presented in Appendix C.

The input data file consists of two portions. The first portion takes standard parameter data for the cycle definition and for the oxide and damage models. The card images are defined in detail in the MAIN routine of TBC_LFE2. The second card image gives the number of block load histories, the third gives the oxidation parameters. The fourth, fifth, and sixth card images are the critical oxide thickness, the CTE values, and the furnace pre-exposure time and temperatures. The seventh card image contains the life model parameters. An example is given for specimen 11:

129

SPECIMEN 11

2
127 2000
50000.,2220.,0.332
0.00055
0.38e-05,0.91e-09
0,0
0.016,7.64,1.,200.
*BLOCK1
30
0.00,0.01,0.13,2.36,3.04,3.79,5.49,10.19,20.33,33.15,49.16,70.30,80.16,87.00,209.03,839.45,
895.87,928.98,978.65,1083.79,1100.80,1107.76,1111.49,1112.43,1115.51,1122.11,1137.70,1162.86,
1195.72,1224.00
81,81,163,443,485,529,619,847,1249,1595,1871,2064,2100,2107,2106,2105,2105,2105,2105,2105,
2105,2072,1796,1735,1620,1341,892,432,173,81
-0.01468,-0.01473,-0.01465,-0.01346,-0.01315,-0.01282,-0.01213,-0.01036,-0.00692,-0.00353,
-0.00037,0.002439,0.003103,0.00327,0.003269,0.003261,0.00326,0.00326,0.003259,0.003258,0.003258,
0.003301,0.000627,-0.00018,-0.00185,-0.00477,-0.0089,-0.0123,-0.01411,-0.01468
BLOCK2
28
0.00,0.01,0.13,2.36,3.93,4.81,5.21,9.83,20.35,30.25,47.63,59.96,87.00,223.78,518.55,937.17,1009.59,
1046.38,1101.58,1200.93,1201.89,1204.40,1206.48,1206.62,1206.78,1210.67,1217.81,1224.76
966,1004,1049,1202,1217,1237,1280,1433,1673,1870,2043,2114,2121,2119,2119,2119,2119,2119,2119,2119,
2119,2025,1848,1831,1796,1579,1314,966
-0.00836,-0.00831,-0.00825,-0.00736,-0.00719,-0.00701,-0.00661,-0.00515,-0.00264,-0.00033,0.002159,
0.003424,0.003573,0.003573,0.00357,0.003565,0.003564,0.003564,0.003563,0.003562,0.003562,0.003115,
0.001181,0.000967,0.000437,-0.00243,-0.00516,-0.00836

*END

The second portion of data is the block data for each input thermal cycle, including the number of time points, the times for each history point, then the temperatures for each time, and finally the substrate strains for each point. The total number of blocks corresponds to the second card image in the first portion of the input data.

4.0 CONCLUSIONS

This final report covers the work accomplished in Phase II of the program. This phase was directed toward generating a life prediction model for electron beam-physical vapor deposited (EB-PVD) zirconia TBC. Specific results included EB-PVD zirconia mechanical and physical properties, coating adherence strength measurements, interfacial oxide growth characteristics, quantitative cyclic thermal spallation life data, and a spallation life model. These results, summarized below, also included comparison to the Phase I plasma sprayed zirconia TBC system.

o   Spallation of the EB-PVD ceramic TBC occurs by cracking at the thermally grown oxide (TGO) layer-metallic bond coat interface. The plasma sprayed TBC, on the other hand, fails within the plasma sprayed ceramic structure near to but not at the thermally grown oxide.

o   Thermal expansion results show no significant difference between the expansion properties of the plasma and EB-PVD deposited ceramic. Also, no directional or exposure sensitivity was observed in the EB-PVD ceramic.

o   A significant difference (approximately 2X) between the thermal conductivities of the EB-PVD and the plasma sprayed ceramic exists. This is attributed to the anisotropy of the EB-PVD ceramic as compared to the isotropic plasma structure.

o   Monotonic compression and tensile mechanical tests and physical property tests were conducted to obtain the EB-PVD ceramic behavior required for burner rig specimen analysis. The EB-PVD ceramic in-plane tensile strength was low (approximately 6.89 MPa or 1 ksi). The EB-PVD ceramic compression strength was found to be higher than the plasma sprayed ceramic. As part of this effort, a nonlinear constitutive model was developed for the EB-PVD ceramic.

o   Calculated out-of-plane stresses were a small fraction of that required to statically fail the TGO. Thus, EB-PVD TBC spallation was attributed to the interfacial cracking caused by in-plane TGO strains.

o   A bond coat oxidation model was developed as part of the EB-PVD life modeling effort. This oxidation model correlates TGO growth rate, and provides a good fit of the data.

o   A life model based on maximum in-plane TGO tensile mechanical strain and TGO thickness correlated the burner rig specimen EB-PVD ceramic spallation lives within a factor of about ±2X.

o   The life model predictive capability was confirmed by applying the model to three verification tests. Prediction of the verification tests was within the scatter band of the correlated data set.

131

APPENDIX A
EB-PVD CERAMIC CONSTITUTIVE MODEL SOURCE CODE

The following pages provide the FORTRAN 77 source code HYPELA, according to
the technical description in this report.

```
CCCCCCCCCCCCCCCCCCCCCCCCCCCCCCCCCCCCCCCCCCCCCCCCCCCCCCCCCCCCCCCCCCCCC
C
C      SUBROUTINE HYPELA
C
C      CALLED BY: MARC OR LAYER FE PROGRAMS
C
C      PURPOSE: ROUTINE FOR CALCULATING CONSTITUTIVE BEHAVIOR OF
C               PWA 266 EB-PVD CERAMIC COATING.
C
CCCCCCCCCCCCCCCCCCCCCCCCCCCCCCCCCCCCCCCCCCCCCCCCCCCCCCCCCCCCCCCCCCCCCC
C
      SUBROUTINE HYPELA (D,G,E,DE,S,TEMP,DTEMP,NGENS,N,NN,KC,MAT,NDI,
     +                   NSHEAR)
C
      DIMENSION D(NGENS,NGENS),G(NGENS),E(NGENS),DE(NGENS),S(NGENS)
C
C----------------------------------------------------------------------
C
C**** NOTE: THERE ARE 16 STATE VARIABLES USED IN THIS CODE. THIS
C           DIMENSION SHOULD BE SET IN THE MAIN ROUTINE. HERE, THE
C           DIMENSION IS SET TO ONE TO AVOID IMPROPER REDIMENSIONING.
C
C           TEMP(1) = TEMPERATURE
C           TEMP(2) = TIME
C           TEMP(3) = EFFECTIVE INELASTIC STRAIN
C     TEMP(4) TO TEMP(9) = EQUILIBRIM STRESS IN X,Y,Z,XY,YZ,ZX DIRECTIONS
C     TEMP(10) TO TEMP(15) = INELASTIC STRAIN IN X,Y,Z,XY,YZ,ZX DIRECTIONS
C           TEMP(16) = NUMBER OF SUBINCREMENTS (NSPLIT)
C
C----------------------------------------------------------------------
C
      DIMENSION TEMP(1),DTEMP(1)
      DIMENSION DSIG(6),DOMEG(6)
      DIMENSION SIG(6),OMEG(6),C(6)
      DIMENSION DC(6),DET(6),OMEGI(6)
      DIMENSION SUMSIG(6),ET(6),DSI(6),ETI(6)
      DIMENSION DEV(6),OV(6),DAB(6),CI(6),OT(6)
      COMMON/FAR/DUM1,INC
      COMMON/CDC/DUM(18),NCYCLE
C
C**** SECOND INVARIANT FUNCTION
      SINV(X11,X22,X33,X12,X13,X23)=2./3.*(X11*X11+X22*X22+X33*X33+
     +      2.*(X12*X12+X13*X13+X23*X23))
C
C**** THIS SUBROUTINE RETURNS THE ELASTICITY MATRIX D AND INELASTIC
C     STRESS INCREMENT G FOR WALKER'S THEORY (B.N.CASSENTI UTRC)
C     USING THE DIFFERENTIAL FORM OF THE THEORY FOUND IN NASA CR-165533.
C     EQUATIONS ARE INTEGRATED USING A FORWARD DIFFERENCE.
C
C**** UNITS USED IN THIS ROUTINE ARE AS FOLLOWS:
C
C           STRESS = PSI
C           STRAIN = IN/IN
C           TIME   = SEC
C           TEMP.  = F OR R (SEE 'ITEMP' BELOW)
C
C**** USER-DEFINED VARIABLES.
C
C           SFTEMP = TEMPERATURE FOR REFERENCE STIFFNESS MATRIX.
C           MXSPLT = MAXIMUM NUMBER OF SUBINCREMENTS.
```

133

```
C          DRMAX   = MAX. ALLOWABLE EFF. INELASTIC STRAIN INCREMENT
C          NONISO  = TMF INDICATOR; = 0, ISOTHERMAL; = 1, TMF.
C          NELAS   = ELASTIC ANALYSIS INDICATOR; = 1, EL.; = 0, INEL.
C          ITEMP   = TEMPERATURE UNIT INDICATOR; = 0, DEG.F; = 1, DEG.R.
C          NELPR   = ELEMENT NUMBER FOR PRINTOUT.
C          IPR     = PRINTOUT INDICATOR; = 0, NONE; = 1, PRINTOUT.
C          NPRIN   = INTEGRATION POINT FOR PRINTOUT.
C
C-------------------------------------------------------------------------
C
C      SET DUMMY VARIABLES TO ALLOW SUCCESSFUL FORTRAN 77 COMPILATION.
C
       I1=1
       I2=2
       I3=3
       I16=16
C
C-------------------------------------------------------------------------
C**** SET TEMPERATURE FOR REFERENCE STIFFNESS MATRIX.
C      FOR COATINGS, THE STIFFNESS MATRIX SHOULD BE REASSEMBLED
C      FOR EACH MARC INCREMENT FOR ACCURATE SOLUTIONS.
C      THEREFORE, THE REF. TEMP. IS SET TO THE MARC INCREMENT
C      ENDPOINT TEMPERATURE.
C-------------------------------------------------------------------------
C-------------------------------------------------------------------------
C
       SFTEMP=TEMP(I1)+DTEMP(I1)
C
C**** SET MAXIMUM NUMBER OF SUBINCREMENTS.
C
       MXSPLT=200
C
C**** SET MAXIMUM ALLOWABLE EFFECTIVE INELASTIC STRAIN INCREMENT.
C
       DRMAX=.001
C
C**** SET NONISO:
C      NONISO=0 WILL NOT INCLUDE DTEMP/DTIME TERMS
C      NONISO=1 WILL INTERPOLATE TO INCLUDE DTEMP/DTIME TERMS
C
       NONISO=1
C
C**** SET NELAS:
C      FOR INELASTIC ANALYSIS SET NELAS=0
C      FOR ELASTIC ANALYSIS (USEFUL FOR MESH CHECKOUT) SET NELAS=1
C
       NELAS=0
C
C**** SET ITEMP:
C      IF TEMPERATURES PASSED INTO HYPELA ARE IN DEGREES F; ITEMP=0
C      IF TEMPERATURES PASSED INTO HYPELA ARE IN DEGREES R; ITEMP=1
C
       ITEMP=0
C
C**** SET PRINTOUT INDICATORS.
C
       NELPR=1
       IPR=0
       NPRIN=1
C
```

134

```
      DR=0.0
      NQ=0
      NQQ=0
      IF(N.NE.1) GO TO 7
      IF(NN.NE.1) GO TO 7
      IF(NCYCLE.EQ.0) NWALK=0
      NWALK=NWALK+1
      NQ=NWALK-2*NCYCLE
      NQQ=NCYCLE-1
C
C**** INITIALIZE STATE VARIABLES ON FIRST ENTRY TO SUBROUTINE.
C     ON SECOND AND SUBSEQUENT ENTRIES SKIP INITIALIZATION.
C
    7 IF(INC+NCYCLE.NE.0) GO TO 3
      IF (TEMP(I1) .LT. 1.E-9) TEMP(I1)=SFTEMP
      DO 2 J=3,16
      IF (ABS(TEMP(J)).LT.1.E-10) TEMP(J)=1.E-10
    2 CONTINUE
C
C
C**** DETERMINE IF PLANE STRESS,PLANE STRAIN,AXISYMMETRIC,OR 3-D
C     KELTYP=1 FOR PLANE STRAIN AND AXISYMMETRIC PROBLEMS
C     KELTYP=2 FOR PLANE STRESS PROBLEM
C     KELTYP=3 FOR 3-D PROBLEM
C-----------------------------------------------------------------------
C-----------------------------------------------------------------------
C     NOTE: THIS CODE HAS BEEN CHECKED USING THE LAYER PROGRAM
C           (NASA CR-187038). LAYER MIMICS THE MARC FE PROGRAM FOR THE
C           CASE WHICH CORRESPONDS TO KELTYP=3.
C-----------------------------------------------------------------------
C-----------------------------------------------------------------------
C
    3 IF(NDI.EQ.3.AND.NSHEAR.EQ.1) KELTYP=1
      IF(NDI.EQ.2.AND.NSHEAR.EQ.1) KELTYP=2
      IF(NDI.EQ.3.AND.NSHEAR.EQ.3) KELTYP=3
C
C**** SET UP TEMPERATURE AND TIME INCREMENTS.
C
      IF(INC.EQ.0 .AND. ABS(DTEMP(I1)) .LT. 1.E-9) DTEMP(I1)=1.E-12
      IF(INC.EQ.0 .AND. ABS(DTEMP(I2)) .LT. 1.E-9) DTEMP(I2)=1.E-2
      IF(INC.GT.0 .AND. ABS(DTEMP(I2)) .LT. 1.E-9) DTEMP(I2)=1.E-9
C
      DEGM=SFTEMP
C
C**** CALL CON266 TO DETERMINE ELASTIC CONSTANTS FOR REFERENCE
C     STIFFNESS MATRIX.
C
      CALL CON266 (1,NONISO,DEGM,0.,ITEMP,
     = EEM,ANUM,ANM,AK1M,AK2M,AMM,AN1M,AN2M,AN3M,AN4M,AN5M,AN6M,AN7M,
     = OMEGOM,DN1DTM,DN2DTM,DOMDTM,ALAMOM,AMUOM,ALAMM,AMUM,ALAM1M,AMU1M,
     = C1M,C2M,C3M,C4M,C5M)
C
C**** SET ZERO STRAIN INCREMENTS = 1.E-10 TO AVOID DIVISION BY ZERO
C                                      )
      DESINV=SINV(DE(1),DE(2),DE(3),DE(4),DE(5),DE(6))
      IF(DESINV.NE.0.)GO TO 800
      DO 1 J=1,NGENS
      DE(J)=1.E-10
    1 CONTINUE
  800 CONTINUE
```

```
C
C**** PUT STRESSES AND TOTAL STRAINS AT BEGINNING OF MARC INCREMENT
C     INTO SIG AND ET ARRAYS ACCORDING TO ELEMENT TYPE.
C
      GO TO(801,802,803),KELTYP
  801 CONTINUE
      SIG(1)=S(1)
      SIG(2)=S(2)
      SIG(3)=S(3)
      SIG(4)=S(4)
      SIG(5)=0.
      SIG(6)=0.
      ET(1)=E(1)
      ET(2)=E(2)
      ET(3)=E(3)
      ET(4)=0.5*E(4)
      ET(5)=0.
      ET(6)=0.
      GO TO 900
  802 CONTINUE
      SIG(1)=S(1)
      SIG(2)=S(2)
      SIG(3)=0.
      SIG(4)=S(3)
      SIG(5)=0.
      SIG(6)=0.
      ET(1)=E(1)
      ET(2)=E(2)
      ET(3)=-ET(1)-ET(2)
      ET(4)=0.5*E(3)
      ET(5)=0.
      ET(6)=0.
      GO TO 900
  803 DO 804 J=1,6
      SIG(J)=S(J)
      FAC=1.
      IF ( J.GT.3 ) FAC=0.5
      ET(J)=FAC*E(J)
  804 CONTINUE
  900 CONTINUE
C
C**** SET STARTING VALUES OF STATE VARIABLES DURING PRESENT MARC
C     INCREMENT.
C
      DEG=TEMP(11)
      T=TEMP(12)
      R=TEMP(13)
      DO 104 KA=1,6
      J=KA+3
      OMEG(KA)=TEMP(J)
      C(KA)=TEMP(J+6)
      SUMSIG(KA)=0.
  104 CONTINUE
C
C**** DETERMINE NUMBER OF SUBINCREMENTS.
C
      CALL SUB266 (NSPLIT,DE,DTEMP(11),DTEMP(12))
      IF (NELAS.EQ.1) NSPLIT=1
C
      NSPLIT=DR/DRMAX+1.
```

```fortran
      IF (MSPLIT.GT.NSPLIT) NSPLIT=MSPLIT
      IF (NSPLIT.LT.MXSPLT) GO TO 106
      NSPLIT=MXSPLT
      WRITE (6,108) INC,MAT,N,NN
  108 FORMAT (/,5X,'************** MXSPLT WAS EXCEEDED **************',//,
     +        ' INC = ',I4,'/',
     +        ' MAT = ',I10,' * ELEM = ',I4,' * INT PT = ',I2,' *****')
C
C**** SET TEMPERATURE AND TIME SUBINCREMENTS
C
  106 DDEG=DTEMP(11)/NSPLIT
      DT=DTEMP(12)/NSPLIT
C
C**** PUT SUBINCREMENTS OF TOTAL STRAIN INTO ARRAY DET ACCORDING
C     ELEMENT TYPE
C
      GO TO(61,62,63),KELTYP
   61 CONTINUE
      DET(1)=DE(1)/NSPLIT
      DET(2)=DE(2)/NSPLIT
      DET(3)=DE(3)/NSPLIT
      DET(4)=0.5*DE(4)/NSPLIT
      DET(5)=0.
      DET(6)=0.
      GO TO 71
   62 DET(1)=DE(1)/NSPLIT
      DET(2)=DE(2)/NSPLIT
      DET(3)=-DET(1)-DET(2)
      DET(4)=0.5*DE(3)/NSPLIT
      DET(5)=0.
      DET(6)=0.
      GO TO 71
   63 CONTINUE
      DO 64 J=1,6
      FAC=1.
      IF(J.GT.3)FAC=0.5
      DET(J)=FAC*DE(J)/NSPLIT
   64 CONTINUE
   71 CONTINUE
C
C
C-----------------------------------------------------------------------
C**** START OF SUBINCREMENT LOOP.
C
      DO 5 JJ=1,NSPLIT
C
C**** SET STARTING VALUES FOR DEVIATORIC STRESSES
C
      PRESS=(SIG(1)+SIG(2)+SIG(3))/3.
      DO 7777 J=1,6
      ALPHA=1.
      IF(J.GT.3)ALPHA=0.
      DEV(J)=SIG(J)-ALPHA*PRESS
 7777 CONTINUE
C
C**** COMPUTE TEMPERATURE DEPENDENT MATERIAL CONSTANTS
C
      CALL CON266 (2,NONISO,DEG,DDEG,ITEMP,
     = EE,ANU,AN,AK1,AK2,AM,AN1,AN2,AN3,AN4,AN5,AN6,AN7,OMEGO,
     = DN1DT,DN2DT,DOMDT,ALAMO,AMUO,ALAM,AMU,ALAM1,AMU1,
     = C1D,C2D,C3D,C4D,C5D)
```

```
C
C**** FOR ELASTIC ANALYSIS, SET INELASTIC VARIABLES TO 1.E-20
C      AND SKIP TO STRESS SUBINCREMENT COMPUTATION.
C
       IF (NELAS.EQ.0) GO TO 305
       DR=1.E-20
       DO 306  J=1,6
       DC(J)=1.E-20
  306 DOMEG(J)=1.E-20
       GO TO 310
  305 CONTINUE
C
C**** COMPUTE DRAG STRESS
C
       AK=AK1-AK2*EXP(-AN7*R)
C
C**** COMPUTE INELASTIC STRAIN SUBINCREMENTS
C
       DO 67 J=1,6
       OV(J)=1.5*DEV(J)-OMEG(J)
   67 CONTINUE
       ARG1=SINV(OV(1),OV(2),OV(3),OV(4),OV(5),OV(6))
       ARG1=SQRT(ARG1)
       ARG1MN=AK*(1.E-20)**(1/AN)
       IF(ARG1.LE.ARG1MN)ARG1=ARG1MN
       IF(ARG1.GE.AK)      ARG1=AK
       ARG2=(ARG1/AK)**AN
       FAC=(ARG2/ARG1)*DT
       DO 302 J=1,6
       DC(J)=FAC*OV(J)
       IF ( ABS(DC(J)) .LT. 1.E-20) DC(J)=1.E-20
  302 CONTINUE
C
C**** CALCULATE EFFECTIVE INELASTIC STRAIN INCREMENT.
C
       DR=SINV(DC(1),DC(2),DC(3),DC(4),DC(5),DC(6))
       DR=SQRT(DR)
C
C**** CHECK NUMBER OF SUBINCREMENTS BASED ON EFF. INELASTIC STRAIN INC.
C
       SPLIT=NSPLIT
       IF (DR/DRMAX.GT.SPLIT.AND.NSPLIT.LT.MXSPLT) GO TO 800
C
C**** COMPUTE EQUILIBRIUM STRESS SUBINCREMENTS
C      SET INITIAL VALUES OF EQUILIBRIM STRESS OMEGI(J)
C
       CALL OM266 (C,OMEGO,OMEGI)
C
       CALL DO266 (C,DC,OMEGO,DOMDT,DDEG,DAB)
C
       DO 69 J=1,6
       OT(J) = OMEG(J) - OMEGI(J) - AN1 * C(J)
   69 CONTINUE                      )
C
       OM=SINV(OT(1),OT(2),OT(3),OT(4),OT(5),OT(6))
       OM=SQRT(OM)
C
       DG=(AN3+AN4*EXP(-AN5*R))*DR+AN6*DT*OM**(AM-1.)
C
       DO 303 J=1,6
```

```
      DOMEG(J) = (AN1+AN2)*DC(J) - DG*OT(J) + DAB(J)
      IF (NONISO .EQ. 0) GO TO 303
      DOMEG(J) = DOMEG(J) + OT(J)*DN2DT/(AN2+.1)*DDEG + DN1DT*C(J)*DDEG
  303 CONTINUE
C
C**** COMPUTE STRESS SUBINCREMENTS
C
  310 IF(KELTYP.EQ.2)DET(3)=(2.*AMU*DC(3)-ALAM*(DET(1)+DET(2)))/
     =                    (ALAM+2.*AMU)
      DVOL0=0.
      DVOL1=0.
      DO 809 J=1,6
      ET1(J)=ET(J)+DET(J)
      C1(J)=C(J)+DC(J)
      IF (J .GT. 3) GO TO 809
      DVOL0=DVOL0+ET(J)-C(J)
      DVOL1=DVOL1+ET1(J)-C1(J)
  809 CONTINUE
      DO 810 J=1,6
      FAC=1.
      IF (J.GT.3) FAC=0.
      S0=ALAM0*DVOL0*FAC+2.*AMU0*(ET(J)-C(J))
      S1=ALAM1*DVOL1*FAC+2.*AMU1*(ET1(J)-C1(J))
      DSIG(J)=S1-S0
      IF (KELTYP .NE. 2) GO TO 810
      DSIGIN=FAC*2.*AMU*ALAM*DC(3)/(ALAM+2.*AMU)-2.*DC(J)*AMU
      DSIG(J)=DSIGIN+(ALAM+2.*AMU)*FAC*(DVOL1-DVOL0)+2.*AMU*DET(J)
  810 CONTINUE
C******
C For EB-PVD TBC ceramic, SUBROUTINE EBPVD is called to correct the
C calculated in-plane stresses to account for the "finger-like"
C structure of the EB-PVD ceramic.
C******
      CALL EBPVD (NCYCLE,ET1,DET,C1,SIG,DSIG)
C
C**** UPDATE SUBINCREMENT VARIABLES
C
      DEG=DEG+DDEG
      R=R+DR
      T=T+DT
      DO 113 J=1,6
      OMEG(J)=OMEG(J)+DOMEG(J)
      SIG(J)=SIG(J)+DSIG(J)
      C(J)=C1(J)
      ET(J)=ET1(J)
      SUMSIG(J)=SUMSIG(J)+DSIG(J)
  113 CONTINUE
C
C**** END OF SUBINCREMENT LOOP
C
    5 CONTINUE
C
C-----------------------------------------------------------------------
C                                      ï
C
C**** PUT ELASTICITY MATRIX IN D AND INELASTIC STRESS INCREMENT IN G
C
  420 GO TO(814,815,816),KELTYP
  814 CONTINUE
      DO 817 J=1,4
      DO 817 K=1,4
```

```
          D(J,K)=0.
  817 CONTINUE
          DO 818 J=1,3
          DO 818 K=1,3
          ALPHA=0.
          IF(J.EQ.K) ALPHA=1.
          D(J,K)=C5M+ALPHA*C3M
  818 CONTINUE
          D(4,4)=C4M
          GO TO 903
  815 CONTINUE
          D(1,1)=C2M
          D(1,2)=C1M
          D(2,1)=C1M
          D(1,3)=0.
          D(3,1)=0.
          D(2,2)=C2M
          D(2,3)=0.
          D(3,2)=0.
          D(3,3)=C4M
          GO TO 903
  816 CONTINUE
          DO 819 J=1,6
          DO 819 K=1,6
          D(J,K)=0.
  819 CONTINUE
          DO 820 J=1,3
          DO 820 K=1,3
          ALPHA=0.
          IF(J.EQ.K) ALPHA=1.
          D(J,K)=C5M+ALPHA*C3M
  820 CONTINUE
          D(4,4)=C4M
          D(5,5)=C4M
          D(6,6)=C4M
  903 CONTINUE
          DO 821 J=1,NGENS
          G(J)=SUMSIG(J)
          IF (KELTYP .EQ. 2 .AND. J .EQ. 3) G(3)=SUMSIG(4)
          DO 821 K=1,NGENS
  821   G(J)=G(J)-D(J,K)*DE(K)
C
C**** COMPUTE STRESS AT END OF MARC INCREMENT
C
          DO 822 J=1,NGENS
          SUM=0.
          DO 823 K=1,NGENS
          SUM=SUM+D(J,K)*DE(K)
  823 CONTINUE
          DS(J)=SUM+G(J)
  822 CONTINUE
C
C**** PUT STATE VARIABLE INCREMENTS IN TEMP ARRAY FOR NEXT MARC
C       INCREMENT.
C
          DTEMP(I3)=R-TEMP(I3)
          TEMP(I16)=NSPLIT
          DO 923 KA=1,6
          J=KA+3
          DTEMP(J)=OMEG(KA)-TEMP(J)
```

```
      DTEMP(J+6)=C(KA)-TEMP(J+6)
  923 CONTINUE
C
C**** PRINT OUT INTEGRATION POINT INFORMATION, IF REQUESTED.
C
      IF(IPR.EQ.0) GO TO 12
      IF(NELPR.NE.N) GO TO 12
      IF (NN.NE.NPRIN) GO TO 12
C
      WRITE(6,20) INC
   20 FORMAT(11H INCREMENT ,I5)
      IF(NQ.EQ.0) WRITE(6,23) NQQ
      IF(NQ.GT.0) WRITE(6,39) NCYCLE
   23 FORMAT(55H VALUES OF PARAMETERS DURING SOLUTION OF RECYCLE NUMBER,
     1I5)
   39 FORMAT(55H VALUES OF PARAMETERS DURING ASSEMBLY OF RECYCLE NUMBER,
     1I5)
      WRITE(6,29)
   29 FORMAT(18H STRAIN INCREMENTS)
      WRITE(6,30) (DE(J),J=1,NGENS)
   30 FORMAT(6(1X,E12.5))
      WRITE(6,31)
   31 FORMAT(18H STRESS INCREMENTS)
      WRITE(6,30) (DS(J),J=1,NGENS)
C
   12 RETURN
      END
C
CCCCCCCCCCCCCCCCCCCCCCCCCCCCCCCCCCCCCCCCCCCCCCCCCCCCCCCCCCCCCCCCCCCCCC
C
C          SUBROUTINE SUB266
C
C          CALLED BY: HYPELA
C
C          PURPOSE: OBTAIN NUMBER OF SUBINCREMENTS FOR PWA 266 COATING.
C                   FIND MAXIMUM STRAIN INCREMENT AND SET NUMBER OF
C                   SUBINCREMENTS EQUAL TO MAXIMUM VALUE DIVIDED BY
C                   1.E-4. THE MAXIMUM STRAIN INCREMENT IN INTEGRATING
C                   THE CONSTITUTIVE EQUATIONS IN HYPELA WILL THE
C                   NOT EXCEED 1.E-4. IF TIME OR TEMPERATURE
C                   INCREMENTS EXCEED 25 DEG F OR 50 SECS, SET APPROPRIATE
C                   SUBINCREMENT NUMBER.
C
CCCCCCCCCCCCCCCCCCCCCCCCCCCCCCCCCCCCCCCCCCCCCCCCCCCCCCCCCCCCCCCCCCCCCC
C
      SUBROUTINE SUB266 (NSPLIT,DE,DDEG,DT)
C
      DIMENSION DE(6)
C
      DEMAX=ABS(DE(1))
      DO 1 I=2,6
      TEST=ABS(DE(I))
      DEMAX=AMAX1(DEMAX,TEST)
    1 CONTINUE
      ASPLIT=DEMAX/1.E-4
      DTMAX=DT/50.
      DEGMAX=DDEG/25.
      DEGMAX=ABS(DEGMAX)
      ASPLIT=AMAX1(ASPLIT,DTMAX)
      ASPLIT=AMAX1(ASPLIT,DEGMAX)
```

```fortran
      NSPLIT=IFIX(ASPLIT)
      NSPLIT=NSPLIT+1
C
      RETURN
      END
C
CCCCCCCCCCCCCCCCCCCCCCCCCCCCCCCCCCCCCCCCCCCCCCCCCCCCCCCCCCCCCCCCCCCCC
C
C     SUBROUTINE OM266
C
C     CALLED BY: HYPELA
C
C     PURPOSE: CALCULATE VALUES OF EQUILIBRIM STRESS ARRAY OMEGI(J).
C              IF OMEGO IS LESS THAN 0.1, THEN ALL ELEMENTS OF OMEGI(J)
C              ARE SET TO ZERO.
C
CCCCCCCCCCCCCCCCCCCCCCCCCCCCCCCCCCCCCCCCCCCCCCCCCCCCCCCCCCCCCCCCCCCCC
C
      SUBROUTINE OM266 (C,OMEGO,OMEGI)
C
      DIMENSION C(6),AB(6),OMEGI(6)
C
C**** SECOND INVARIANT FUNCTION
      SINV(X11,X22,X33,X12,X13,X23)=2./3.*(X11*X11+X22*X22+X33*X33+
     +                              2.*(X12*X12+X13*X13+X23*X23))
C
      DO 10 J=1,6
   10 OMEGI(J)=0.0
      IF (OMEGO.LT.0.1) RETURN
C
      DENOM=SINV(C(1),C(2),C(3),C(4),C(5),C(6))
      DENOM=DENOM+1.E-30
      AB(1)=-OMEGO+2.*OMEGO*(C(1)*C(1)+C(4)*C(4)+C(6)*C(6)
     =      +1.E-30)/DENOM
      AB(2)=-OMEGO+2.*OMEGO*(C(4)*C(4)+C(2)*C(2)+C(5)*C(5)
     =      +1.E-30)/DENOM
      AB(3)=-OMEGO+2.*OMEGO*(C(6)*C(6)+C(5)*C(5)+C(3)*C(3)
     =      +1.E-30)/DENOM
      AB(4)=2.*OMEGO*(C(1)*C(4)+C(2)*C(4)+C(5)*C(6)+1.E-30)/DENOM
      AB(5)=2.*OMEGO*(C(4)*C(6)+C(2)*C(5)+C(3)*C(5)+1.E-30)/DENOM
      AB(6)=2.*OMEGO*(C(1)*C(6)+C(4)*C(5)+C(3)*C(6)+1.E-30)/DENOM
      ABSUM=AB(1)+AB(2)+AB(3)
      DO 7124 J=1,6
      ALPHA=1.
      IF(J.GT.3)ALPHA=0.
      OMEGI(J)=AB(J)-ALPHA*ABSUM/3.
 7124 CONTINUE
C
      RETURN
      END
C
CCCCCCCCCCCCCCCCCCCCCCCCCCCCCCCCCCCCCCCCCCCCCCCCCCCCCCCCCCCCCCCCCCCCC
C                            )
C     SUBROUTINE DO266
C
C     CALLED BY: HYPELA
C
C     PURPOSE: CALCULATE SUBINCREMENT OF EQUILIBRIM STRESS OMEGI(J)
C              DUE TO A TEMPERATURE CHANGE AND STORE IN ARRAY DAB(J).
C              IF OMEGO IS LESS THAN 0.1, THEN ALL ELEMENTS OF DAB(J)
```

142

```
C
C                ARE SET TO ZERO.
C
CCCCCCCCCCCCCCCCCCCCCCCCCCCCCCCCCCCCCCCCCCCCCCCCCCCCCCCCCCCCCCCCCCCCCCCCC
C
      SUBROUTINE DO266 (C,DC,OMEGO,DOMDT,DDEG,DAB)
C
      DIMENSION C(6),DC(6),DAB(6)
C
C**** SECOND INVARIANT FUNCTION
      SINV(X11,X22,X33,X12,X13,X23)=2./3.*(X11*X11+X22*X22+X33*X33+
     +                             2.*(X12*X12+X13*X13+X23*X23))
C
      DO 10 J=1,6
   10 DAB(J)=0.0
      IF (OMEGO.LT.0.1) RETURN
C
      DDENOM=(C(1)*DC(1)+C(2)*DC(2)+C(3)*DC(3)+
     =       2.*(C(4)*DC(4)+C(5)*DC(5)+C(6)*DC(6)))
      DOM=DOMDT*DDEG
      DOM1=DOM-2.*OMEGO*DDENOM
      DENOM=SINV(C(1),C(2),C(3),C(4),C(5),C(6))
      DENOM=DENOM+1.E-30
      DAB(1)=-DOM+2.*DOM1*(C(1)*C(1)+C(4)*C(4)+C(6)*C(6)+1.E-30)/DENOM
      DAB(2)=-DOM+2.*DOM1*(C(4)*C(4)+C(2)*C(2)+C(5)*C(5)+1.E-30)/DENOM
      DAB(3)=-DOM+2.*DOM1*(C(6)*C(6)+C(5)*C(5)+C(3)*C(3)+1.E-30)/DENOM
      DAB(4)=2.*DOM1*(C(1)*C(4)+C(2)*C(4)+C(5)*C(6)+1.E-30)/DENOM
      DAB(5)=2.*DOM1*(C(4)*C(6)+C(2)*C(5)+C(3)*C(5)+1.E-30)/DENOM
      DAB(6)=2.*DOM1*(C(1)*C(6)+C(4)*C(5)+C(3)*C(6)+1.E-30)/DENOM
      DAB(1)=DAB(1)+2.*OMEGO*(DC(1)*C(1)+DC(4)*C(4)+DC(6)*C(6)+1.E-30)/
     =       DENOM
      DAB(2)=DAB(2)+2.*OMEGO*(DC(4)*C(4)+DC(2)*C(2)+DC(5)*C(5)+1.E-30)/
     =       DENOM
      DAB(3)=DAB(3)+2.*OMEGO*(DC(6)*C(6)+DC(5)*C(5)+DC(3)*C(3)+1.E-30)/
     =       DENOM
      DAB(4)=DAB(4)+2.*OMEGO*(DC(1)*C(4)+DC(2)*C(4)+DC(5)*C(6)+1.E-30)/
     =       DENOM
      DAB(5)=DAB(5)+2.*OMEGO*(DC(4)*C(6)+DC(2)*C(5)+DC(3)*C(5)+1.E-30)/
     =       DENOM
      DAB(6)=DAB(6)+2.*OMEGO*(DC(1)*C(6)+DC(4)*C(5)+DC(3)*C(6)+1.E-30)/
     =       DENOM
      DAB(1)=DAB(1)+2.*OMEGO*(C(1)*DC(1)+C(4)*DC(4)+C(6)*DC(6)+1.E-30)/
     =       DENOM
      DAB(2)=DAB(2)+2.*OMEGO*(C(4)*DC(4)+C(2)*DC(2)+C(5)*DC(5)+1.E-30)/
     =       DENOM
      DAB(3)=DAB(3)+2.*OMEGO*(C(6)*DC(6)+C(5)*DC(5)+C(3)*DC(3)+1.E-30)/
     =       DENOM
      DAB(4)=DAB(4)+2.*OMEGO*(C(1)*DC(4)+C(2)*DC(4)+C(5)*DC(6)+1.E-30)/
     =       DENOM
      DAB(5)=DAB(5)+2.*OMEGO*(C(4)*DC(6)+C(2)*DC(5)+C(3)*DC(5)+1.E-30)/
     =       DENOM
      DAB(6)=DAB(6)+2.*OMEGO*(C(1)*DC(6)+C(4)*DC(5)+C(3)*DC(6)+1.E-30)/
     =       DENOM
C
      RETURN
      END                          )
C
CCCCCCCCCCCCCCCCCCCCCCCCCCCCCCCCCCCCCCCCCCCCCCCCCCCCCCCCCCCCCCCCCCCCCCCCC
C
C      SUBROUTINE EBPVD
C
```

```
C        CALLED BY: HYPELA
C
C        PURPOSE: Correct the calculated in-plane stresses of EB-PVD
C                 TBC ceramic coating to account for the observed
C                 "zero" tensile load carrying capability.
C
CCCCCCCCCCCCCCCCCCCCCCCCCCCCCCCCCCCCCCCCCCCCCCCCCCCCCCCCCCCCCCCCCCCCCCCCC
C
         SUBROUTINE EBPVD (NCYCLE,ET1,DET,C1,SIG,DSIG)
C
         DIMENSION ET1(6),DET(6),C1(6),SIG(6),DSIG(6)
C******
C For each recycle, recalculate the in-plane stresses (i.e., in the
C X and Y directions) to account for "zero" in-plane tensile load
C carrying capability. The in-plane quantities are assumed to lie in
C storage locations 1 and 2 of the arrays.
C******
         IF (NCYCLE .GT. 0) THEN
            DO 1820 J=1,2
C******
C Establish the elastic strain sign by normalizing the elastic
C strain and store the result in the variable SWITCH.
C******
            ELAS = ET1(J)-C1(J)
            SWITCH = ELAS / ABS(ELAS+1.E-10)
C******
C If SWITCH is greater than or equal to zero, a positive (tensile)
C strain sign is indicated and:
C   1) If the current stress is less than zero:
C        a) If the endpoint stress is greater than zero the zero stress
C           axis was crossed and the stress increment is reset so that
C           the endpoint stress will be zero.
C   2) If the current stress is greater than or equal to zero the zero
C      stress axis was already crossed and all further tensile straining
C      is assumed to be accommodated without stress. The stress
C      increment is set to zero.
C******
            IF (SWITCH .GE. 0.) THEN
               IF (SIG(J) .LT. 0.) THEN
                  IF (SIG(J)+DSIG(J) .GT. 0.) THEN
                     DSIG(J) = -SIG(J)
                  ENDIF
               ELSE
                  DSIG(J) = 0.
               ENDIF
            ELSE
C******
C If SWITCH is less than zero, a negative (compression) strain sign
C is indicated and:
C   1) If the current stress is greater than or equal to zero:
C        a) If the stress increment is less than zero, the stress axis
C           was crossed and the stress increment is recalculated based
C           on the portion of the elastic strain which contributes to
C           a compressive stress (i.e., the ceramic starts to pick up
C           compressive load).
C        b) If the stress increment is greater than or equal to zero and
C           the endpoint stress is greater than zero, positive stress
C           relaxation has occurred and the zero stress axis was crossed.
C           The stress increment is reset so that the endpoint stress is
C           zero.
```

144

```
C   2) If the current stress is less than zero,
C       a) and the endpoint stress is greater than zero,
C           positive stress relaxation has occurred and the zero stress
C           axis was crossed. The stress increment is reset so that the
C           endpoint stress is zero.
C       b) and the endpoint stress is less than or equal to zero,
C           the ceramic is in compression and no change to the stress
C           increment is required.
C******
              IF (SIG(J) .GE. 0.) THEN
                  IF (DSIG(J) .LT. 0.) THEN
                      DSIG(J) = DSIG(J) * ABS(ELAS/(DET(J)+1.E-10))
                  ELSE IF (SIG(J)+DSIG(J) .GT. 0.) THEN
                      DSIG(J) = -SIG(J)-DSIG(J)
                  ENDIF
              ELSE
                  IF (SIG(J)+DSIG(J) .GT. 0.) THEN
                      DSIG(J) = -SIG(J)
                  ENDIF
              ENDIF
          ENDIF
 1820     CONTINUE
      ENDIF
C
      RETURN
      END
C
CCCCCCCCCCCCCCCCCCCCCCCCCCCCCCCCCCCCCCCCCCCCCCCCCCCCCCCCCCCCCCCCCCCCC
C
C       SUBROUTINE CON266
C
C       CALLED BY: HYPELA
C
C       PURPOSE: THIS SUBROUTINE CALCULATES ALL OF THE TEMPERATURE
C               DEPENDENT MATERIAL CONSTANTS FOR PWA 266 CERAMIC
C               COATING FOR WALKER'S TIME DEPENDENT FORMULATION OF
C               NASA CR-165533.
C
C       NOTE: ALL CONSTANTS ARE DETERMINED AT THE BULK OR MEAN
C             TEMPERATURE OF THE INCREMENT. ENDPOINT TEMPERATURES ARE
C             USED TO DETERMINE ENDPOINT LAME ELASTIC CONSTANTS AND
C             TEMPERATURE RATE TERMS.
C
CCCCCCCCCCCCCCCCCCCCCCCCCCCCCCCCCCCCCCCCCCCCCCCCCCCCCCCCCCCCCCCCCCCCC
C
      SUBROUTINE CON266 (ISF,NONISO,DEG,DDEG,ITEMP,
     + EE,ANU,AN,AK1,AK2,AM,AN1,AN2,AN3,AN4,AN5,AN6,AN7,OMEGO,
     + DN1DT,DN2DT,DOMDT,ALAMO,AMUO,ALAM,AMU,ALAM1,AMU1,C1,C2,C3,C4,C5)
C
      DIMENSION TABT(10),EET(10),ANUT(10),AK1T(10),AK2T(10),AMT(10),
     + AN1T(10),AN2T(10),AN3T(10),AN4T(10),AN5T(10),AN6T(10),AN7T(10),
     + OMEGOT(10),ANT(10)
      DIMENSION AN12(2),AN22(2),OMO2(2),EE2(2),ANU2(2)
C                                            )
C**** DEFINE THE TABLE OF TEMPERATURES, TABT. THERE ARE A SET OF
C     MATERIAL CONSTANTS AT EACH TEMPERATURE VALUE OF TABT.
C
      DATA TABT /  70., 600.,1000.,1200.,1400.,
     +            1600.,1800.,2000.,2200.,2400./
C
```

```
C**** ELASTIC MODULUS, PSI
C
      DATA EET /.415E7,.346E7,.294E7,.268E7,.243E7,
     +          .217E7,.191E7,.165E7,.139E7,.113E7/
C
C**** NO POISSON RATIOS (ANUT) AVAILABLE FOR PWA 266.
C     ANUT CONSTANTS ARE FOR ALUMINA (AL2O3)
C
      DATA ANUT /.25,.25,.25,.25,.25,
     +           .25,.25,.25,.25,.25/
C
C**** SATURATED DRAG STRESS TERM, K1, PSI
C
      DATA AK1T /1.E5,1.E5,1.E5,1.E5,1.E5,
     +           1.E5,1.E5,1.E5,1.E5,1.E5/
C
C**** DRAG STRESS TERM, K2, PSI
C     INITIAL DRAG STRESS   = K1 - K2
C
      DATA AK2T /0.,0.,0.,0.,0.,
     +           0.,0.,0.,0.,0./
C
C**** BACK STRESS THERMAL RECOVERY TERM EXPONENT, M. M IS ARBITRARILY
C     SET TO 2.0 SO THAT DIVISION BY ZERO IS AVOIDED IN SUBROUTINE
C     HYPELA. ZERO BACK STRESS THERMAL RECOVERY IS ATTAINED BY SETTING
C     AN6T = 0.0 FOR ALL TEMPERATURES (SEE BELOW).
C
      DATA AMT /2.,2.,2.,2.,2.,
     +          2.,2.,2.,2.,2./
C
C**** BACK STRESS GROWTH TERM, N1, PSI
C
      DATA AN1T /0.,0.,0.,0.,0.,
     +           0.,0.,0.,0.,0./
C
C**** BACK STRESS LINEAR HARDENING TERM, N2, PSI
C
      DATA AN2T /.8500E7,.8000E7,.7420E7,.4950E7,.3360E7,
     +           .2365E7,.1720E7,.1285E7,.0975E7,.0800E7/
C
C**** BACK STRESS LINEAR DYNAMIC RECOVERY TERM, N3, PSI
C
      DATA AN3T /100.,100.,100.,100.,100.,
     +           100.,100.,100.,100.,100./
C
C**** BACK STRESS EXPONENTIAL DYNAMIC RECOVERY TERM, N4, PSI
C
      DATA AN4T /0.,0.,0.,0.,0.,
     +           0.,0.,0.,0.,0./
C
C**** BACK STRESS EXPONENTIAL DYNAMIC RECOVERY TERM, N5
C
      DATA AN5T /0.,0.,0.,0.,0.,
     +           0.,0.,0.,0.,0./
C
C**** BACK STRESS THERMAL RECOVERY TERM, N6, (1/PSI)**M
C
      DATA AN6T /0.,0.,0.,0.,0.,
     +           0.,0.,0.,0.,0./
C
```

```
C**** DRAG STRESS EXPONENTIAL GROWTH TERM, N7
C
      DATA AN7T /0.,0.,0.,0.,0.,
     +           0.,0.,0.,0.,0./
C
C**** INITIAL BACK STRESS, OMEGO
C
      DATA OMEGOT /0.,0.,0.,0.,0.,
     +             0.,0.,0.,0.,0./
C
C**** INVERSE OF THE INELASTIC FLOW EQUATION EXPONENT, 1/N
C
      DATA ANT /.0165,.0545,.0820,.0946,.1072,
     +          .1185,.1295,.1400,.1505,.1608/
C
C**** SET VARIABLE TO INDICATE THE NUMBER OF MATERIAL CONSTANT DATA
C     SETS.
C
      NTP=10
C
C**** CALCULATE THE TEMPERATURES ASSOCIATED WITH THE BEGINNING (0),
C     BULK OR MEAN (M), AND END (1) OF THE INCREMENT.
C
      DEG0=DEG
      DEG1=DEG+DDEG
      DEGM=(DEG0+DEG1)/2
      IF (ITEMP.EQ.0) GO TO 1
      DEGM=DEGM-460.
      DEG0=DEG0-460.
      DEG1=DEG1-460.
C
C**** CALCULATE THE INTERPOLATION FACTOR, FAC, BASED ON THE MEAN
C     TEMPERATURE FOR MATERIAL CONSTANT DETERMINATION.
C         IF DEGM < TABT(1)  ; USE TABT(1) MATERIAL CONSTANTS
C         IF DEGM > TABT(NTP); USE TABT(NTP) MATERIAL CONSTANTS
C
    1 CONTINUE
      I = 1
    5 IF (DEGM .LE. TABT(I)) THEN
          IF (I .EQ. 1) THEN
              FAC = 0.
              I   = 2
          ELSE
              FAC = (DEGM - TABT(I-1)) / (TABT(I) - TABT(I-1))
          ENDIF
      ELSE
          IF (I. EQ. NTP) THEN
              FAC = 0.
              I   = NTP + 1
          ELSE
              I = I + 1
              GO TO 5
          ENDIF
      ENDIF
C
C**** CALCULATE ELASTIC MODULUS AND POISSON'S RATIO.
C
      EE  = FAC * (EET(I) - EET(I-1)) + EET(I-1)
      ANU = FAC * (ANUT(I)-ANUT(I-1)) + ANUT(I-1)
C
```

```
C****   FOR FIRST CALL OF 'CON266': DETERMINE CONSTANTS C1 THROUGH C5
C       TO ESTABLISH REFERENCE STIFFNESS MATRIX.
C
        IF ( ISF .NE. 1 ) GO TO 25
C
        ALAM = EE*ANU / ((1.-2.*ANU) * (1.+ANU))
        AMU  = (1. - 2.*ANU) * ALAM / (2.*ANU)
        C1   = 2.*AMU*ALAM / (ALAM + 2.*AMU)
        C2   = 4.*AMU*(ALAM + AMU) / (ALAM + 2.*AMU)
        C3   = 2.*AMU
        C4   = AMU
        C5   = ALAM
        GO TO 9999
C
C**** CALCULATE THE BALANCE OF THE MATERIAL CONSTANTS.
C
   25 AK1  = FAC * (AK1T(I) - AK1T(I-1)) + AK1T(I-1)
      AK2  = FAC * (AK2T(I) - AK2T(I-1)) + AK2T(I-1)
      AM   = FAC * (AMT(I) - AMT(I-1)) + AMT(I-1)
      AN1  = FAC * (AN1T(I) - AN1T(I-1)) + AN1T(I-1)
      AN2  = FAC * (AN2T(I) - AN2T(I-1)) + AN2T(I-1)
      AN3  = FAC * (AN3T(I) - AN3T(I-1)) + AN3T(I-1)
      AN4  = FAC * (AN4T(I) - AN4T(I-1)) + AN4T(I-1)
      AN5  = FAC * (AN5T(I) - AN5T(I-1)) + AN5T(I-1)
      AN6  = FAC * (AN6T(I) - AN6T(I-1)) + AN6T(I-1)
      AN7  = FAC * (AN7T(I) - AN7T(I-1)) + AN7T(I-1)
      OMEGO= FAC * (OMEGOT(I) - OMEGOT(I-1)) + OMEGOT(I-1)
      AN   = FAC * (ANT(I) - ANT(I-1)) + ANT(I-1)
      DN1DT=0.
      DN2DT=0.
      DOMDT=0.
C
C**** DETERMINE TEMPERATURE RATE TERMS AND ENDPOINT EE AND ANU.
C**** DETERMINE THE APPROPRIATE TABT TEMPERATURES TO USE AND CALCULATE
C       THE ENDPOINT MATERIAL CONSTANTS.
C
      DO 60  J=1,2
      DEG2 = DEGO
      IF ( J .EQ. 2 ) DEG2 = DEG1
      I = 1
   70 IF (DEG2 .LE. TABT(I)) THEN
          IF (I .EQ. 1) THEN
              FAC = 0.
              I   = 2
          ELSE
              FAC = (DEG2 - TABT(I-1)) / (TABT(I) - TABT(I-1))
          ENDIF
      ELSE
          IF (I. EQ. NTP) THEN
              FAC = 0.
              I   = NTP + 1
          ELSE
              I = I + 1
              GO TO 70
          ENDIF
      ENDIF
C
      AN12(J) = FAC * (AN1T(I) - AN1T(I-1)) + AN1T(I-1)
      AN22(J) = FAC * (AN2T(I) - AN2T(I-1)) + AN2T(I-1)
      OM02(J) = FAC * (OMEGOT(I) - OMEGOT(I-1)) + OMEGOT(I-1)
```

148

```
      EE2(J)  = FAC * (EET(I) - EET(I-1)) + EET(I-1)
      ANU2(J) = FAC * (ANUT(I) - ANUT(I-1)) + ANUT(I-1)
C
   60 CONTINUE
C
C**** CALCULATE THE TEMPERATURE RATE TERMS
C
      IF (NONISO .EQ. 1) THEN
          DN1DT = (AN12(2) - AN12(1)) / (DDEG + 1.E-6)
          DN2DT = (AN22(2) - AN22(1)) / (DDEG + 1.E-6)
          DOMDT = (OM02(2) - OM02(1)) / (DDEG + 1.E-6)
      ELSE
      ENDIF
C
C**** END OF CONSTANT DETERMINATION
C
   40 CONTINUE
C
C****  CALCULATE ACTUAL CONSTANT VALUES AS REQUIRED
C      THE INELASTIC FLOW EQUATION EXPONENT WAS INPUT AS THE INVERSE
C      TO PROVIDE THE GOOD INTERPOLATION CAPABILITY.
C
      AN     = 1. / AN
C
C****  DETERMINE LAME CONSTANTS AT THE BEGINNING, MEAN, AND END
C      TEMPERATURES.
C
      ALAM0 = EE2(1)*ANU2(1) / ((1. - 2.*ANU2(1)) * (1. + ANU2(1)))
      AMU0  = (1. - 2.*ANU2(1)) * ALAM0 / (2. * ANU2(1))
      ALAM  = EE*ANU / ((1. - 2.*ANU) * (1. + ANU))
      AMU   = (1. - 2.*ANU) * ALAM / (2. * ANU)
      ALAM1 = EE2(2)*ANU2(2) / ((1. - 2.*ANU2(2)) * (1. + ANU2(2)))
      AMU1  = (1. - 2.*ANU2(2)) * ALAM1 / (2. * ANU2(2))
C
 9999 RETURN
      END
```

)

APPENDIX B
FORTRAN SOURCE CODE

The following pages provide the FORTRAN 77 source code TBC_LFE2, according to the technical description in this report. An ASCII file and an IBM PC executable file were delivered to NASA Lewis Research Center via a floppy disk. To execute the code, type: TBC_LFE2 <DATA.FIL >DATA.OUT, or >LPT1. The delivered floppy disk also contains the input data files for each specimen.

```
C ********************************************************************
C
C PURPOSE:
C
C      This program predicts the spallation life (in cycles) of thermal barrier
C      coating (TBC) systems applied over metallic substrates.  Damage
C      caused by cyclic thermomechanical strains in the growing
C      oxide layer during the life of the TBC-metallic system is predicted.
C      Life is considered to consist of blocks of cycles,
C      with the cycles within a block being identical.
C
C      Damage accumulated during each block of thermal cycles is
C      accumulated using Miners Rule.
C
C INPUT DATA:
C
C      There are two portions of input data.  The first portion
C      contains the general information for the program.  The second
C      portion has sets of repetitive data arranged in data blocks.
C      Each block data set begins with a comment card, *BLOCKn.  An
C      *END card is used to terminate the execution of the program and
C      designates the end of the input data.
C
C    Portion I.
C
C      Card #    Items     Data Type    Remarks
C      ------    -----     ---------    -------
C        1      HEADNG     character    general problem description card
C                          string       ( up to 80 characters )
C
C        2      NUMBLK     integer*4    total number of blocks
C                                        ( up to 20 )
C
C        3      CYCBLK(I)  integer*4    number of thermal cycles in each block
C               (I=1,NUMBLK)                ( could be more than one card )
C
C        4      Q,T0,EN    real*8       Oxide growth model parameters
C
C        5      THKCRT     real*8       critical oxide thickness
C
C        6      AL0, AL1   real*8       Linear and quadratic thermal expansion
C               TREF       real*8       Reference temperature for stress-free oxide
coeff
C
C        7      TIMFUR,    real*8       pre-exposure time in the furnace (sec),
C               TMPFUR                        and temperature (deg F)
C                                       (Farenheit)
C
C        8      EPS_EFF    real*8       Asymptotically critical strain constant
C               B,C        real*8       Life equation parameters
depostn

C                                       temperature
C
C    Portion II.
C
C        9     '*BLOCKn'   character   comment card
C                          string      ( n is the block number. )
C
```

151

```
C       10      NTIME         integer*4   total number of time steps into which
C                                         a typical thermal cycle is divided
C                                         (up to 50, for integration of
C                                         oxide growth equation )
C
C       11      CYTIME(L)     real*8      vector of time points into which a
C               (L=1,NTIME)               thermal cycle of block is divided
C                                         (seconds, in order of increasing
C                                         time, time = 0 at the beginning of
C                                         the thermal cycle )
C
C       12      TMPINF(L)     real*8      vector of temperatures at interface
C               (L=1,NTIME)               between bond and ceramic  (deg F)
C                                         temperatures are those associated
C                                         with times in vector CYTIME )
C
C       13      EPS_SS(L)     real*8      vector of substrate strains at each
C               (L=1,NTIME)               time point.
C
C       14      '*END'                    last card of input deck
C
C    NOTE:
C         Cards 9, 10, 11, 12, 13 and 14 could be more than one card.
C         Repeat cards 7 to 14  NUMBLK times.
C
C
C
C  Variables:
C
C     CYCBLK(I) —  number of cycles in each block of input (integer)
C     DAMCYC    —  damage for one cycle
C     DAMISN    —  mission damage
C     DEL_EPS   —  cyclic thermomechanical strain in the oxide
C     DEL_L     —  instantaneous free thermal expansion of the oxide
C     EPS_MECH(I)-  oxide free thermal strain less the substrate strain
C     EPS_MAX   —  max mechanical strain in oxide in given cycle
C     EPS_MAX   —  min mechanical strain in oxide in given cycle
C     FLAG      —  0: normal input reading
C                  1: *END card is encountered
C     ICYCLE    —  cycle counter for the mission
C     INCR      —  the increment at which intermediate results (within a
C                  block of cycles) are printed
C     NIN       —  input unit number
C     NOUT      —  output unit number
C     NUM       —  number of printout per thermal cycle  ( set to 25 )
C     NSTATU    —  status file unit number
C                  (The status file contains the status report of the
C                  execution of the program.)
C     NUMBLK    —  total number of blocks of input  ( up to 20 )
C     REMAIN    —  the increment at which the last result
C                  for a block of cycles are printed
C     STOP      —  a logical flag, indicating if the damage has
C                  reached 1.0
C                  .false.;  damage < 1.0
C                  .true. ;  damage >= 1.0
C
C     TRANK     —  conversion from deg F to deg R
C     TREF      —  stress-free temperature above the oxide deposition
C
```

```
C     THKCRT   -  critical oxide thickness (in)
C     THKFUR   -  the scale growth of furnace pre-exposure (in)
C     THKNES   -  the oxide thickness gain (in)
C     TIMFUR   -  pre-exposure time in the furnace (sec.)
C     TMPFUR   -  pre-exposure furnace temperature (F)
C     TMAX,MIN -  max and min values of interface temperature in given cycle
C
C
C ********************************************************************
C
C
      IMPLICIT REAL*8 (A-H,O-Z)
      INTEGER*4 CYCBLK(20),FLAG,NUMCYC,FREQ,REMAIN
      LOGICAL*1 STOP
      COMMON / IO_UNITS / NIN,NOUT,NSTATU
      COMMON / OXIDE    / Q,T0,EN,THKCRT
      COMMON / PRE_EXP  / TIMFUR,TMPFUR
      COMMON / PARAMS   / AL0,AL1,TRANK,B,C,TREF,EPS_FF
      COMMON / CYCLE    / NTIME,CYTIME(50),TMPINF(50),EPS_SS(50)
      COMMON / PRINTING / NUM, NUMCYC(20), FREQ(20), IFREQ
C
C input/output units defined
C
      NIN    = 5
      NOUT   = 6
      NSTATU = 8
      NUM = 25
      IFREQ  = 100
      TRANK  = 459.67D0
C
C   open the three disk files for execution
C

      OPEN (UNIT=NSTATU, FILE='NSTATUS.TXT')
C     OPEN (UNIT=NIN, FILE='TBC.DAT')
C     OPEN (UNIT=NOUT,FILE='TBC.OUT')
C
C initalize the oxide growth flag
C
      ITEST = 0
C
C read and write the basioc parameters and execution data
C
      CALL INPUT (NUMBLK, CYCBLK)
C
C compute the oxide growth due to thermal exposure prior to cycling
C
      THKNES = 0.D0
      THKFUR = 0.D0
      IF (TIMFUR.GT.0.) CALL PREXPO (THKFUR)
      THKNES = THKFUR
C
C
C initialize the mission damage DAMISN, the flag variable FLAG,
C    the cycle counter ICYCLE and the thickness gain THKNES
C
      DAMISN = 0.D0
      FLAG = 0
      ICYCLE = 0
```

153

```
C
      WRITE (NOUT,1008) THKFUR
C
C  repeat the following calculation for all the blocks
C
      DO 100 NBLK = 1, NUMBLK
C
C  read the block data
C
      CALL BLKDAT (NBLK, FLAG)
      IF (FLAG .EQ. 1) CALL MESAGE (1,NBLK)
      IF (FLAG .EQ. 1) GO TO 999
C
C  set up printing and solution counting parameters
C                                .
      CALL INCREM (CYCBLK(NBLK), NUM, INCR, REMAIN)
      CALL MECH_STR (DEL_EPS)
      NL = NUM
C
C  write out block labels
C      .
      WRITE (NOUT, 1010) NBLK
      WRITE (NOUT, 1020)
      IF (INCR.EQ.1.AND.REMAIN.EQ.0) NL=CYCBLK(NBLK)
C
C
      DO 50 J=1,NL
C
      DO 40 K=1,INCR
C
C  compute the oxide thickness after one thermal cycle of block.
C     following line of code needed to fool the optimizing compiler
C
      IF (K.GT.56983) GO TO 100
      CALL GROWTH (ICYCLE, THKNES, ITEST)
C
C  compute damage for this cycle
C
      CALL DAMAGE (DAMCYC, THKNES, DEL_EPS, AD1, AD2)
C
C  check the mission damage
C
      CALL CHECK (DAMCYC, DAMISN, STOP)
C
      IF(STOP) PRINT*,'TRUE'
C ·
C
   75 IF(STOP) GO TO 990
C
   40 CONTINUE
      THK = THKNES/THKCRT
      CALL PRINT (NBLK,CYCBLK,ICYCLE,THK,AD1,AD2,DAMISN)
   50 CONTINUE
C
C  compute damage for remaining cycles in block
C
      IF (REMAIN.EQ.0) GO TO 100
      DO 80 J = 1, REMAIN
      CALL GROWTH (ICYCLE, THKNES, ITEST)
```

154

```
          CALL DAMAGE (DAMCYC, THKNES, DEL_EPS, AD1, AD2)
          CALL CHECK (DAMCYC, DAMISN, STOP)
          IF(STOP) PRINT*,'TRUE'
          IF(STOP) GO TO 990
   80 CONTINUE
C
      CALL PRINT (NBLK,CYCBLK,ICYCLE,THK,AD1,AD2,DAMISN)
C
  100 CONTINUE
      GO TO 999
C
  990 CONTINUE
      WRITE (NOUT, 1040)
      CALL PRINT (NBLK,CYCBLK,ICYCLE,THK,AD1,AD2,DAMISN)
C
C
  999 CONTINUE
      WRITE (NOUT,1050)
      STOP
C
C
C     format statements
C
 1008 FORMAT (5X,'FURNACE PRE-EXPOSURE THICKNESS (in) ...... (THKFUR) =',
     $1X,E10.4,/)
 1010 FORMAT (1H1,' R E S U L T S   F O R   B L O C K   N O .',I5,///)
 1020 FORMAT (19X,'NUMBER OF',5X,'CURRENT VALUE',21X,'     ',
     $     7X,'CURRENT',/,
     $     10X,'TOTAL    CYCLES IN    OF OXIDE RATIO    DAMFAC AD1',
     $     2X,'DAMFAC AD2       VALUE OF',/,
     $     10X,'CYCLES   THIS BLOCK    THK/THKCRT',7X,'R*(1-THK)^C',
     $     6X,'(T/Tc)^C       DAMAGE',/,
     $     10X,6('-'),3X,10('-'),4X,14('-'),3X,10('-'),3X,14('-'),
     $     3X,8('-') )
 1040 FORMAT (' > >  < <   CURRENT DAMAGE IS GREATER THAN OR EQUAL TO 1.0.',
     $       '    — PROGRAM TERMINATED.')
 1050 FORMAT (' *** E N D   O F   P R O G R A M ***')
C
      END
```

```
      SUBROUTINE INPUT (NUMBLK, CYCBLK)
C
C
C  Purpose:  reading of the general data and printing the echo of the
C            input
C
C  Variables:
C
C     B        -  exponent in the life equation
C     C        -  exponent in the life equation
C     CYCBLK(I) -  number of cycles in each block of input (integer)
C     EPS_FF   -  asymptotic strain parameter
C     EN       -  oxide growth equation coefficient
C     HEADNG   -  problem description
C     NIN      -  input unit number
C     NOUT     -  output unit number
C     NSTATU   -  status file unit number
C     NUMBLK   -  total number of blocks of input  ( up to 20 )
C     THKCRT   -  critical oxide thickness
C     TIMFUR   -  pre-exposure time in the furnace (sec)
C     TMPFUR   -  pre-exposure furnace temperature (deg F)
C
C  ********************************************************************
C
C
      IMPLICIT REAL*8 (A-H,O-Z)
      DIMENSION HEADNG(10)
      INTEGER*4 CYCBLK(20)
      COMMON / IO_UNITS / NIN,NOUT,NSTATU
      COMMON / OXIDE    / Q,T0,EN,THKCRT
      COMMON / PRE_EXP  / TIMFUR,TMPFUR
      COMMON / PARAMS   / AL0,AL1,TRANK,B,C,TREF,EPS_FF
      COMMON / CYCLE    / NTIME,CYTIME(50),TMPINF(50),EPS_SS(50)
      COMMON / PRINTING / NUM, NUMCYC(20), NFREQ(20), IFREQ
C
C  read the block data, one block at a time
C
      READ  (NIN,1010) HEADNG
      WRITE (NOUT,1020) HEADNG
C
      READ  (NIN,*) NUMBLK
      READ  (NIN,*) (CYCBLK(I),I=1,NUMBLK)
      DO 5 I = 1, NUMBLK
      NFREQ(I) = CYCBLK(I) / IFREQ
    5 NUMCYC(I) = CYCBLK(I)
C
C  preselect the printing frequency data
C
      WRITE (NOUT,1030) NUMBLK
      WRITE (NOUT,1040) CYCBLK
C
      READ (NIN,*) Q, T0, EN
      READ (NIN,*) THKCRT
      READ (NIN,*) AL0, AL1
      WRITE (NOUT,1070) Q
      WRITE (NOUT,1080) T0
      WRITE (NOUT,1090) EN
      WRITE (NOUT,1100) THKCRT
      WRITE (NOUT,1140) AL0, AL1
```

156

```
C
      READ(NIN,*) TIMFUR, TMPFUR
      WRITE (NOUT,1110) TIMFUR
      WRITE (NOUT,1120) TMPFUR
C
      READ (NIN,*) EPS_FF, B, C, TREF

      WRITE (NOUT,1130) EPS_FF, B, C, TREF
C
      RETURN
C
C     format statements
C
 1010 FORMAT (10A8)
 1020 FORMAT (20X,10A8,///)
 1030 FORMAT (5X,'TOTAL NUMBER OF BLOCKS ................... (NUMBLK) =',
     $      I5,/)
 1040 FORMAT (5X,'NUMBER OF THERMAL CYCLES IN EACH BLOCK ... (CYCBLK) =',
     $2X,10I5,/,60X,10I5,/)
 1045 FORMAT (60X,10I5)
 1070 FORMAT (5X,'OXIDIDATION RATE PARAMET (deg R).......... (  Q  ) =',
     $      1X,E10.4,/)
 1080 FORMAT (5X,'RATE EFFECTIVE TEMPERATURE FOR OXIDE.(R).. (  To ) =',
     $      1X,E10.4,/)
 1090 FORMAT (5X,'EXPONENT FOR OXIDE GROWTH RATE............ (  EN ) =',
     $      1X,E10.4,/)
 1100 FORMAT (5X,'CRITICAL OXIDE THICKNESS (in) ............ (THKCRT) =',
     $      1X,E10.4,/)
 1110 FORMAT (5X,'PRE-EXPOSURE TIME IN THE FURNACE (sec) ... (TIMFUR) =',
     $      1X,E10.4,/)
 1120 FORMAT (5X,'FURNACE TEMPERATURE (deg F) .............. (TMPFUR) =',
     $      1X,E10.4,/)
 1130 FORMAT (5X,'CRITICAL STRAIN =', F8.5, ' IN/IN', 3X, 'B =',
     $F8.3, 3X,'C =',F6.1,3X,'T_Ambient for oxide =', F10.2, ' Deg F',/)
 1140 FORMAT (5X,'ALPHA_0 =', E12.3, ' IN/IN/Deg F', 3X, 'ALPHA_1 =',
     $      E12.3,' IN/IN/Deg F',/)
      END
```

```fortran
      SUBROUTINE PREXPO (THKFUR)
C
C
C  Purpose:  computation of the scale growth of furnace pre-exposure
C            (assuming that furnace is used to pre-expose specimens)
C
C  Variables:
C
C     TEMP     -  temperature in degrees Rankine
C     THKFUR   -  the scale growth during furnace pre-exposure (in)
C     TIMFUR   -  pre-exposure time in the furnace (sec)
C     TMPFUR   -  pre-exposure furnace temperature (Rankine)
C
C ***********************************************************************
C
C
      IMPLICIT REAL*8 (A-H,O-Z)
      COMMON / OXIDE   / Q,T0,EN,THKCRT
      COMMON / PRE_EXP / TIMFUR,TMPFUR
      COMMON / PARAMS  / AL0,AL1,TRANK,B,C,TREF,EPS_FF
C
      T1 = TMPFUR + TRANK
      THKFUR = (TIMFUR*EXP(Q*(1./T0 - 1./T1)))**EN
      THKFUR = THKFUR/1.E06
C
      RETURN
      END
```

```
      SUBROUTINE BLKDAT (NBLOCK, FLAG)
C
C
C  Purpose:  reading of the block data
C
C  Variables:
C
C     CMMENT   -- a comment card, *BLOCKn; where n is the block number
C     CYTIME(I) --  time points into which a typical thermal cycle of
C                block is divided;  where I = 1, NTIME
C     FLAG     -- 0: normal input reading
C                1: *END card is encountered
C     NBLOCK   -- the current block number
C     NIN      -- input unit number
C     NOUT     -- output unit number
C     NSTATU   -- status file unit number
C     NTIME    -- total number of time steps in each cycle  (up to 150)
C     TMPINF(I) -- vector of temperatures at interface between bond and
C                ceramic;  where I = 1, NTIME
C
C  *********************************************************************
C
C
      IMPLICIT REAL*8 (A-H,O-Z)
      INTEGER*4 FLAG
      DIMENSION CMMENT(10)
      COMMON / IO_UNITS / NIN,NOUT,NSTATU
      COMMON / OXIDE    / Q,T0,EN,THKCRT
      COMMON / PRE_EXP  / TIMFUR,TMPFUR
      COMMON / PARAMS   / AL0,AL1,TRANK,B,C,TREF,EPS_FF
      COMMON / CYCLE    / NTIME,CYTIME(50),TMPINF(50),EPS_SS(50)
C
C
      READ(NIN,1010) CMMENT
      IF (CMMENT(1) .EQ. '*END    ') FLAG = 1
      IF (CMMENT(1) .EQ. '*END    ') GO TO 99
C
      WRITE (NOUT,1015) NBLOCK
      WRITE (NOUT,1100) CMMENT
C
      READ (NIN,*) NTIME
      READ (NIN,*) (CYTIME(I),I=1,NTIME)
      READ (NIN,*) (TMPINF(I),I=1,NTIME)
      READ (NIN,*) (EPS_SS(I),I=1,NTIME)
C
      WRITE (NOUT,1040)
      DO 50 I=1,NTIME
      WRITE(NOUT,1050) I,CYTIME(I),TMPINF(I),EPS_SS(I)
   50 CONTINUE
C
   99 CONTINUE
      RETURN
C
C    format statements
C
 1010 FORMAT (10A8)
 1015 FORMAT (1H1,10X,' D A T A   F O R   B L O C K   N U M B E R ',I5,
     S ///)
 1040 FORMAT (10X,'TIME STEP',4X,'CYCLE TIME',2X,'INTERFACE TEMP',
```

```
      $      2X,'SUBSTRATE STRAIN',/,26X,'(sec)',8X,'(deg F)',8X,
      $      'IN/IN',/,10X,'———',4X,10('-'),2X,14('-'),
      $      2X,14('-'),/)
 1050 FORMAT(11X,I5,5X,2X,E10.4,4X,E10.4,4X,E10.4)
 1100 FORMAT (5X, 10A8)
C
      END
```

```
      SUBROUTINE INCREM (NCYC,NUM,INCR,REMAIN)
C
C
C   Purpose:  establishing increment at which intermediate results are
C             printed
C
C   Variables:
C
C   INCR   —  the increment at which intermediate results are
C             printed
C   NUM    —  number of printouts per thermal cycle
C   NCYC   —  number of cycles in the current block
C   REMAIN —  the increment at which the last result for a block
C             of cycles are printed
C
C****************************************************************************
C
C
      INTEGER*4 REMAIN
C
C
      INCR = NCYC/NUM
      REMAIN = MOD(NCYC,NUM)
C
      IF(NCYC.LE.NUM) INCR = 1
      IF(NCYC.LE.NUM) REMAIN = 0
C
      RETURN
      END
```

```
      SUBROUTINE MECH_STR (DEL_EPS)
C
C
C  Purpose:  computation of DEL_EPS; the mechanical strain range due to
C            thermal mismatch for one cycle of thermal loading
C
C  Variables:
C
C     DEL_L  change in free length due to temperature rise above T_FREE
C     TMAX, TMIN  max and min temperatures in the cycle
C     EPS_MAX, EPS_MIN max and min mechanical strains in the cycle
C
C     The mechanical strain is the free thermal strain minus the strain
C         of the substrate at that temperature/time - EPS_SS
C **********************************************************************
C
C
      IMPLICIT REAL*8 (A-H,O-Z)
      COMMON / PARAMS   / AL0,AL1,TRANK,B,C,TREF,EPS_FF
      COMMON / CYCLE    / NTIME,CYTIME(50),TMPINF(50),EPS_SS(50)
      COMMON / IO_UNITS / NIN,NOUT,NSTATU
      DIMENSION EPS_MECH(50)
C
C  find min-max temperature points
C
      DEL_L = 0.0D0
      TMAX = 0.0D0
      TMIN = 3000.D0
      DO 10 I=1,NTIME
      TEST = TMPINF(I)
C
C  find temperature range and stress-free temperature; Stress-free
C     temperature is given as the maximum temperature at which the
C     oxide is assumed to be deposited + TREF, a user-supplied param
C
      IF (TEST.GT.TMAX) TMAX = TEST
      IF (TEST.LT.TMIN) TMIN = TEST
      TSF = TMAX + TREF
   10 CONTINUE
C
C  compute free length and resulting mechanical strain at each temperature
C     The oxide is assumed to be deposited (stress-free) at TMAX
      DO 15 I=1,NTIME
      DEL_L = AL0*(TMPINF(I) - TSF) + 0.5*AL1*((TMPINF(I) -70.)**2
      X                              - (TSF-70.)**2)
      EPS_MECH(I) = - DEL_L + EPS_SS(I)
   15 CONTINUE
C
C  Find max strain range for the cycle
C
      EPS_MAX = -0.1D0
      EPS_MIN = 0.1D0
      DO 20 I=1,NTIME
      TEST = EPS_MECH(I)
      IF (TEST.GT.EPS_MAX) EPS_MAX = TEST
   20 IF (TEST.LT.EPS_MIN) EPS_MIN = TEST
      DEL_EPS = EPS_MAX
C
      WRITE (NOUT, 100)
```

162

```
      WRITE (NOUT, 110) TMAX, TMIN, EPS_MAX, EPS_MIN, DEL_EPS
      RETURN
100 FORMAT (//, 10X, '  TMAX  ', 5X, '   TMIN   ', 5X, ' EPS_MAX ',
    $       5X, ' EPS_MIN ', 5X, ' DEL_EPS ',/)
110 FORMAT (10X, F6.0, 8X, F6.0, 8X, F8.6, 6X, F8.6, 6X, F8.6,/)
      END
```

```fortran
      SUBROUTINE GROWTH (ICYCLE, THKNES, ITEST)
C
C
C  Purpose: computation of the thickness gain for one cycle
C
C  Variables:
C
C     EN        -  oxide growth equation coefficient EN=0.332
C     Q         -  Rate constant for scale growth Q=50000 deg R
C     T0        -  Temperature normalizing constant T0=2220 deg R
C     CYTIME(I) -  time points into which a typical thermal cycle of
C                  block is divided;  where I = 1, NTIME
C     ICYCLE    -  cycle counter for the mission
C     NTIME     -  total number of time steps in each cycle  (up to 150)
C     TEMP      -  temperature in degrees Rankine
C     THK1      -  scale growth for temperature at time i (in)
C     THK2      -  scale growth for temperature at time i+1 (in)
C     THKNES    -  the oxide thickness gain (in)
C     TMPINF(I) -  vector of temperatures at interface between bond and
C                  ceramic;  where I = 1, NTIME
C
C **********************************************************************
C
C
      IMPLICIT REAL*8 (A-H,O-Z)
      COMMON / IO_UNITS / NIN,NOUT,NSTATU
      COMMON / OXIDE    / Q,T0,EN,THKCRT
      COMMON / PRE_EXP  / TIMFUR,TMPFUR
      COMMON / PARAMS   / AL0,AL1,TRANK,B,C,TREF,EPS_FF
      COMMON / CYCLE    / NTIME,CYTIME(50),TMPINF(50),EPS_SS(50)
C
      NT = NTIME - 1
C
C  Initialize the oxide thickness from pre-exposure
C
      ITEST = ITEST + 1
C
C  Initialize the current thickness for incremental growth calculation;
C     thickness is measured in micrinches in this relationship.
C     Formulation same as Dave Nissley in order to obtain same results
C
      THKNES = THKNES*1.D06
      THK1 = THKNES
C
      DO 30 I=1,NT
      J = I+1
C
C  Compute the average temperature in the time step in deg R
C
      TBAR = 0.5*(TMPINF(J) + TMPINF(I)) + TRANK
      IF (TBAR.LE.T0) GO TO 30
      THK2 = (EXP(Q*(1.D0/T0 - 1.D0/TBAR))*(CYTIME(J) - CYTIME(I))
     X       + THK1**(1.D0/EN))**EN
      THK1 = THK2
   30 CONTINUE
      ICYCLE = ICYCLE + 1
C
C
      THKNES = THK2/1.D06
```

```
RETURN
END
```

```
      SUBROUTINE DAMAGE (DAMCYC, THKNES, DEL_EPS, AD1, AD2)
C
C
C Purpose: computation of damage for the current cycle
C
C Variables:
C
C    B     —  strain exponent in the life equation
C    C     —  exponent in the thickness effectiveness term
C    DAMCYC —  damage for one cycle
C    N     —  life of TBC in cycles
C    THKCRT —  critical oxide thickness (in)
C    THKNES —  the oxide thickness gain (in)
C    EPS_F  —  the current fracture strain
C    EPS_FF —  the reference fracture strain
C
C ***********************************************************************
C
C
      IMPLICIT REAL*8 (A-H,O-Z)
      REAL*8 N
      COMMON / IO_UNITS / NIN,NOUT,NSTATU
      COMMON / PARAMS   / AL0,AL1,TRANK,B,C,TREF,EPS_FF
      COMMON / OXIDE    / Q,T0,EN,THKCRT
      COMMON / CYCLE    / NTIME,CYTIME(50),TMPINF(50),EPS_SS(50)
C
C
      RATIO = EPS_FF/DEL_EPS
      THK = THKNES/THKCRT
C
      IF (THK.GT.1.) THK = 1.
      AD1 = RATIO*(1.-THK)**C
      AD2= THK**C
      N = (RATIO * (1.-THK)**C + THK**C) ** B
C
C
      DAMCYC = 1/N
C
C
      RETURN
      END
```

```
      SUBROUTINE CHECK (DAMCYC, DAMISN, STOP)
C
C
C   Purpose: summing current cycle's damage to mission damage and
C            checking if the damage has reached 1.0
C
C   Variables:
C
C      DAMCYC -  damage for one cycle
C      DAMISN -  mission damage
C      NIN    -  input unit number
C      NOUT   -  output unit number
C      NSTATU -  status file unit number
C      STOP   -  a logical flag, indicating if the damage has
C                 reached 1.0
C
C  ************************************************************************
C
C
      IMPLICIT DOUBLE PRECISION (A-H,O-Z)
      LOGICAL*1 STOP
      COMMON /IOUN/ NIN,NOUT,NSTATU
C
C
      STOP = .FALSE.
      DAMISN = DAMISN + DAMCYC
      IF(DAMISN .LT. 1.0D0) GO TO 99
      STOP = .TRUE.
C
   99 CONTINUE
      RETURN
C
      END
```

```fortran
      SUBROUTINE PRINT (NBLK, CYCBLK, ICYCLE, THK, AD1
     *            ,AD2, DAMISN)
C
C
C  Purpose:  printing the intermediate results
C
C  Variables:
C
C     CURCYC    -  number of cycles in the current block
C     CYCBLK(I)  -  number of cycles in each block
C     DAMISN    -  mission damage
C     DELEPP    -  the plastic strain per cycle given by the total of
C                  all cyclic plastic strain effects
C     ICYCLE    -  cycle counter for the mission
C     NBLK      -  the current block number
C     NIN       -  input unit number
C     NOUT      -  output unit number
C     NSTATU    -  status file unit number
C     THK       -  ratio of the oxide thickness gain (in)
C                  to the critical oxide thickness THKCRT
C     AD1,AD2   -  separate damage entities
C
C  **********************************************************************
C
C
      IMPLICIT DOUBLE PRECISION (A-H,O-Z)
      INTEGER*4 CURCYC,CYCBLK(20)
      COMMON / IO_UNITS / NIN,NOUT,NSTATU
C
C
      CURCYC = ICYCLE
      IF(NBLK.EQ.1) GO TO 20
C
      NB = NBLK-1
      DO 10 I=1,NB
      CURCYC = CURCYC - CYCBLK(I)
   10 CONTINUE
C
   20 CONTINUE
C
      WRITE(NOUT,1010) ICYCLE,CURCYC,THK,AD1,AD2,DAMISN
C
C
      RETURN
C
C     format statement
C
 1010 FORMAT (4X,2I12,7X,D12.6,1X,D12.4,3X,D12.4,F10.5)
C
      END
```

168

```
      SUBROUTINE MESAGE (ICODE, NUM)
C
C
C  Purpose: reporting the status of the execution of the program to
C          the status file, NSTATU
C
C  Variable:
C
C     ICODE  —  error code number
C     NIN    —  input unit number
C     NOUT   —  output unit number
C     NSTATU —  status file unit number
C     NUM    —  an integer number to be output to the status file
C
C  ***********************************************************************
C
C
      COMMON /IOUN/ NIN,NOUT,NSTATU
C
C
      IF (ICODE .EQ. 1) WRITE(NSTATU,1010) NUM
1010 FORMAT(5X,' NO INPUT DATA FOR THE BLOCK NUMBER ',I2,'.  —',
     $           ' program terminated.')
C
      END
```

APPENDIX C
CYCLE DATA FOR TBC_LFE2

The listing in this Appendix is of the file TBC_LIFE.DAT. This file contains
the time, temperature, and strain input data for each test cycle.

```
SPECIMEN DATA BLOCK FOR CORRELATION
1
20000
50000.,2220.,0.332
0.00055
0.38e-05,0.91e-09,200.
0,0
0.016,7.64,1.
SPECIMEN 01
25
0.00,1.32,1.73,2.30,3.66,6.85,11.73,26.50,56.90,72.35,79.03,91.10,
96.02,98.72,100.25,101.36,102.61,110.36,118.12,141.50,172.94,230.5
6,
282.62,348.76,366.00
93,272,332,370,442,602,823,1322,1845,1973,1999,2086,2099,1966,1873
,1852,1811,
1563,1341,849,475,191,140,95,93
-0.01467,-0.01433,-0.01406,-0.01382,-0.01329,-0.01208,-0.01035,-0.
00591,-0.00028,
0.001516,0.001896,0.003353,0.003596,0.002665,0.001584,0.001302,0.0
00668,-0.00243,
-0.00481,-0.00924,-0.01209,-0.01405,-0.01438,-0.01467,-0.01467
SPECIMEN 02
26
0.00,0.01,0.09,2.38,4.05,5.00,5.21,9.79,19.74,29.20,47.53,59.63,86
.44,145.35,
475.59,486.28,509.65,562.24,601.59,601.16,604.37,606.58,606.94,610
.76,617.96,
624.00
1020,1065,1100,1246,1261,1283,1305,1442,1647,1825,2002,2066,2073,2
071,2069,
2069,2068,2068,2068,2068,1980,1802,1758,1562,1316,1020
-0.00793,-0.00781,-0.00777,-0.00692,-0.00675,-0.00655,-0.00634,-0.
00502,-0.00288,
-0.00084,0.001588,0.002677,0.002815,0.002807,0.002773,0.002772,0.0
02769,0.002764,
0.002758,0.002758,0.002339,0.000482,-0.00017,-0.00266,-0.00518,-0.
00793
SPECIMEN 2A
24
0.00,0.01,0.15,2.26,3.95,4.83,5.16,9.63,19.75,29.67,46.60,58.33,92
.11,119.10,221.72,
233.14,232.60,236.98,240.04,240.25,240.37,246.10,255.42,264.05
981,1017,1063,1200,1201,1220,1255,1394,1619,1815,1984,2059,2066,20
66,
2066,2066,2066,1983,1797,1782,1755,1532,1298,981
-0.00824,-0.0082,-0.00814,-0.00734,-0.00729,-0.00713,-0.0068,-0.00
548,-0.00319,
-0.00097,0.001302,0.002514,0.002698,0.002699,0.002701,0.002701,0.0
02701,0.002344,
0.000436,0.000248,-0.00014,-0.00296,-0.00533,-0.00824
SPECIMEN 04
```

25
0.00,1.36,1.85,2.71,4.27,7.48,13.45,30.46,63.71,80.95,88.65,106.82
,108.02,110.58,
111.75,112.76,113.33,120.65,127.70,148.26,178.18,226.77,274.05,328
.11,348.00
96,295,339,392,467,615,867,1386,1908,2041,2089,2173,2174,2019,1954
,1908,1888,
1624,1395,889,483,205,135,105,96
-0.01468,-0.01425,-0.01405,-0.01371,-0.01316,-0.01204,-0.01004,-0.
00534,0.000511,
0.002546,0.003344,0.004922,0.004999,0.003706,0.002878,0.002195,0.0
01848,-0.00172,
-0.00427,-0.00891,-0.01204,-0.01396,-0.01443,-0.01462,-0.01468
SPECIMEN 05
25
0.00,1.32,1.73,2.30,3.66,6.85,11.73,26.50,56.90,72.35,79.03,91.10,
96.02,98.72,
100.25,101.36,102.61,110.36,118.12,141.50,172.94,230.56,282.62,348
.76,366.00
110,303,340,378,447,601,818,1299,1805,1930,1973,2037,2053,1917,184
6,1804,1768,
1533,1323,847,485,210,144,116,110
-0.01457,-0.01415,-0.01397,-0.01374,-0.01323,-0.01207,-0.01037,-0.
00612,-0.00077,
0.000898,0.001534,0.002537,0.002849,0.001902,0.001134,0.00059,0.00
0049,-0.00276,
-0.00499,-0.00926,-0.01202,-0.01393,-0.01435,-0.01455,-0.01457
SPECIMEN 06
24
0.00,0.01,0.15,2.26,3.95,4.83,5.16,9.63,19.75,29.67,46.60,58.33,
92.64,126.32,254.42,268.59,267.94,273.24,276.96,277.21,277.35,284.
30,
295.60,306.06
1028,1065,1112,1250,1251,1270,1306,1447,1674,1873,2043,2119,2126,2
126,2126,2126,
2126,2042,1854,1839,1812,1586,1349,1028
-0.00785,-0.0078,-0.00774,-0.00692,-0.00687,-0.0067,-0.00636,-0.00
5,-0.00262,
-0.00029,0.002174,0.003499,0.003697,0.003698,0.0037,0.0037,0.0037,
0.00332,0.00124,
0.001038,0.000613,-0.00238,-0.00484,-0.00785
SPECIMEN 07
32
0.00,0.01,0.12,2.28,2.87,3.87,5.61,10.18,20.02,33.08,50.51,70.76,
79.46,85.50,112.87,283.02,289.76,299.65,308.55,321.89,378.38,387.8
2,
399.15,404.45,408.77,410.11,413.25,421.13,438.48,468.93,507.87,540
.00
105,107,184,448,483,540,627,838,1212,1549,1831,2000,2031,2040,2038
,2037,2037,
2037,2036,2036,2036,2036,2036,2004,1740,1676,1580,1310,894,438,190
,105

-0.01455,-0.01457,-0.01451,-0.01339,-0.01313,-0.01271,-0.01203,-0.
01039,-0.00722,
-0.00396,-0.00082,0.001509,0.002031,0.002197,0.002195,0.002182,0.0
02181,0.002181,
0.00218,0.002179,0.002174,0.002174,0.002173,0.002199,-0.00016,-0.0
01,-0.00231,
-0.0051,-0.00889,-0.01227,-0.01401,-0.01455
SPECIMEN 08
30
0.00,0.01,0.18,2.34,3.02,3.80,5.51,10.13,19.92,32.92,51.01,69.17,7
8.17,115.30,209.25,
352.19,361.82,378.91,394.30,417.38,503.93,507.77,511.57,512.84,515
.60,522.18,537.39,
562.96,592.58,624.00
94,81,171,438,481,527,619,843,1236,1592,1901,2066,2104,2114,2115,2
116,2116,2116,2116,
2117,2117,2085,1804,1733,1628,1350,910,442,196,94
-0.0146,-0.01471,-0.01461,-0.01347,-0.01316,-0.01282,-0.01213,-0.0
1039,-0.00704,-0.00356,
0.000003,0.002458,0.003153,0.003406,0.003419,0.003438,0.003439,0.0
03441,0.003444,0.003447,
0.003459,0.00349,0.000736,-0.00029,-0.00176,-0.00469,-0.00875,-0.0
1221,-0.01395,-0.0146,
SPECIMEN 09
26
0.00,1.33,1.57,2.33,3.29,6.23,11.29,25.28,54.35,69.15,72.58,87.13,
89.93,89.99,92.31,93.89,
94.95,95.48,102.77,110.39,130.38,160.83,208.96,253.45,309.97,330.0
0
121,319,343,398,452,608,854,1349,1871,2000,2025,2110,2121,2121,198
8,1904,1858,1840,1586,
1348,879,486,225,160,129,121
-0.0145,-0.01406,-0.01395,-0.01361,-0.01321,-0.01204,-0.01009,-0.0
0566,0.000058,0.001907,
0.002298,0.00374,0.003972,0.003977,0.003017,0.002024,0.001379,0.00
109,-0.00218,-0.00475,
-0.00899,-0.01201,-0.01382,-0.01425,-0.01446,-0.0145
SPECIMEN 11A
30
0.00,0.01,0.13,2.36,3.04,3.79,5.49,10.19,20.33,33.15,49.16,70.30,8
0.16,87.00,209.03,839.45,
895.87,928.98,978.65,1083.79,1100.80,1107.76,1111.49,1112.43,1115.
51,1122.11,1137.70,1162.86,
1195.72,1224.00
81,81,163,443,485,529,619,847,1249,1595,1871,2064,2100,2107,2106,2
105,2105,2105,2105,2105,
2105,2072,1796,1735,1620,1341,892,432,173,81
-0.01468,-0.01473,-0.01465,-0.01346,-0.01315,-0.01282,-0.01213,-0.
01036,-0.00692,-0.00353,
-0.00037,0.002439,0.003103,0.00327,0.003269,0.003261,0.00326,0.003
26,0.003259,0.003258,0.003258,
0.003301,0.000627,-0.00018,-0.00185,-0.00477,-0.0089,-0.0123,-0.01

```
411,-0.01468
SPECIMEN 11B
28
0.00,0.01,0.13,2.36,3.93,4.81,5.21,9.83,20.35,30.25,47.63,59.96,87
.00,223.78,518.55,937.17,1009.59,
1046.38,1101.58,1200.93,1201.89,1204.40,1206.48,1206.62,1206.78,12
10.67,1217.81,1224.76
966,1004,1049,1202,1217,1237,1280,1433,1673,1870,2043,2114,2121,21
19,2119,2119,2119,2119,2119,2119,
2119,2025,1848,1831,1796,1579,1314,966
-0.00836,-0.00831,-0.00825,-0.00736,-0.00719,-0.00701,-0.00661,-0.
00515,-0.00264,-0.00033,0.002159,
0.003424,0.003573,0.003573,0.00357,0.003565,0.003564,0.003564,0.00
3563,0.003562,0.003562,0.003115,
0.001181,0.000967,0.000437,-0.00243,-0.00516,-0.00836
SPECIMEN 12
30
0.00,0.01,0.18,2.34,3.02,3.80,5.51,10.13,19.92,32.92,51.01,69.17,7
8.17,127.77,268.01,481.39,495.76,
521.27,544.24,578.70,707.89,711.77,715.57,716.84,719.60,726.18,741
.39,766.96,796.58,828.00
124,113,198,452,492,536,623,836,1209,1547,1840,1997,2034,2043,2044
,2045,2045,2045,2045,2045,2046,
2015,1749,1681,1581,1318,899,455,221,124
-0.01442,-0.01453,-0.01443,-0.01334,-0.01304,-0.01272,-0.01205,-0.
0104,-0.00724,-0.00398,-0.00071,
0.00145,0.002053,0.002274,0.002286,0.002302,0.002304,0.002305,0.00
2308,0.00231,0.002321,0.002346,
-6.5E-05,-0.00097,-0.00231,-0.00503,-0.00885,-0.01214,-0.0138,-0.0
1442
SPECIMEN 13
26
0.00,1.14,1.75,2.33,3.70,6.91,11.83,26.70,57.68,73.84,77.58,93.47,
95.91,95.99,98.77,100.35,101.51,
102.15,110.33,118.35,141.77,173.40,232.38,286.22,354.62,366.00
108,283,342,380,450,607,828,1317,1833,1962,1987,2070,2079,2079,193
7,1864,1821,1802,1553,1333,852,
486,207,142,112,108
-0.01472,-0.0144,-0.01413,-0.01389,-0.01337,-0.01218,-0.01042,-0.0
0604,-0.00044,0.001377,0.001751,
0.003147,0.00332,0.003325,0.002324,0.001477,0.000888,0.000588,-0.0
0256,-0.00494,-0.0093,-0.01212,
-0.01407,-0.01449,-0.0147,-0.01472
SPECIMEN 16
31
0.00,0.01,0.15,2.51,2.83,4.02,5.70,10.16,20.16,33.03,49.20,69.66,7
8.89,85.81,113.00,257.55,259.71,
269.96,277.25,288.18,304.57,319.65,324.36,328.89,330.01,333.04,341
.31,358.04,389.23,423.79,460.00,
101,96,180,458,477,546,632,843,1233,1575,1849,2035,2071,2081,2079,
2080,2080,2080,2080,2080,2080,
2080,2048,1767,1712,1617,1326,914,436,199,101
```

-0.01456,-0.01463,-0.01454,-0.01332,-0.01318,-0.01267,-0.01201,-0.
01037,-0.00705,-0.00372,-0.00063,
0.001993,0.002632,0.002835,0.002841,0.002851,0.002851,0.002852,0.0
02853,0.002854,0.002855,0.002856,
0.002884,0.000223,-0.00052,-0.00188,-0.00493,-0.00872,-0.01227,-0.
01394,-0.01456
SPECIMEN 18
30
0.00,0.01,0.15,2.15,2.83,4.01,5.69,9.80,20.24,32.18,49.94,71.20,82
.24,103.92,237.59,445.69,485.25,
509.90,546.88,685.53,688.88,693.64,697.63,698.60,701.20,708.00,723
.07,747.96,780.84,810.00
111,124,214,462,504,571,656,850,1253,1570,1868,2048,2082,2079,2078
,2078,2078,2077,2077,2077,2077,
2047,1763,1710,1615,1337,909,464,203,111
-0.01451,-0.01447,-0.01438,-0.01332,-0.01301,-0.0125,-0.01184,-0.0
1033,-0.00687,-0.00377,-0.00039,
0.002223,0.002841,0.002841,0.002836,0.002828,0.002826,0.002825,0.0
02823,0.002818,0.002818,0.00287,
0.000177,-0.00056,-0.00191,-0.00483,-0.00877,-0.01208,-0.01393,-0.
01451
SPECIMEN 19
26
0.00,0.01,0.11,2.41,2.72,3.88,5.52,9.88,20.52,32.51,50.15,68.28,82
.02,92.33,155.74,250.85,397.35,
404.33,408.73,410.26,413.48,421.17,438.95,468.39,508.98,540.00
115,128,205,473,491,555,637,835,1231,1536,1819,1976,2024,2021,2020
,2019,2018,1990,1729,1659,1561,
1299,884,448,196,115
-0.01449,-0.01445,-0.01439,-0.01321,-0.01308,-0.01259,-0.01196,-0.
01042,-0.00703,-0.00409,-0.00095,
0.001164,0.001946,0.001943,0.001935,0.001922,0.001902,0.001976,-0.
00031,-0.00124,-0.00253,-0.00521,
-0.00898,-0.0122,-0.01398,-0.01449
SPECIMEN 21
26
0.00,0.01,0.16,2.54,3.97,4.87,5.07,9.61,19.81,29.53,48.10,61.00,10
1.21,398.86,893.91,969.29,1138.88,
1351.21,1441.75,1444.37,1446.55,1446.69,1446.84,1450.88,1457.99,14
64.34
993,1028,1073,1221,1224,1245,1265,1413,1640,1831,2015,2083,2080,20
80,2081,2081,2081,2081,2081,1998,
1817,1802,1771,1556,1306,993
-0.00814,-0.0081,-0.00804,-0.00715,-0.00709,-0.0069,-0.00671,-0.00
531,-0.00297,-0.00078,0.001767,
0.002922,0.00293,0.002935,0.002942,0.002943,0.002946,0.002949,0.00
2951,0.002597,0.000704,0.000512,
0.000047,-0.00271,-0.00526,-0.00814
SPECIMEN 22
30
0.00,0.01,0.11,2.25,2.90,3.72,5.34,9.92,20.41,32.39,50.24,71.25,81
.91,98.07,233.59,521.88,576.51,

663.37,680.85,693.28,718.75,723.72,727.58,728.58,731.18,737.79,752
.95,778.01,809.79,840.00
116,129,203,469,508,554,637,849,1246,1556,1848,2022,2055,2051,2051
,2050,2050,2049,2049,2049,2049,
2019,1744,1689,1597,1331,904,463,209,116
-0.01448,-0.01444,-0.01437,-0.01325,-0.01297,-0.01262,-0.01198,-0.
01032,-0.00692,-0.0039,-0.00062,
0.001833,0.002408,0.002407,0.002401,0.002388,0.002385,0.002381,0.0
0238,0.00238,0.002379,0.002415,
-0.00008,-0.00083,-0.00212,-0.00489,-0.00882,-0.01209,-0.01389,-0.
01448
SPECIMEN 25
28
0.00,0.01,0.13,2.36,3.93,4.81,5.21,9.83,20.35,30.25,47.63,59.96,87
.00,151.47,286.90,479.24,512.51,
529.42,554.78,600.93,601.89,604.40,606.48,606.62,606.78,610.67,617
.81,624.76
969,1006,1050,1200,1213,1233,1276,1424,1658,1851,2019,2089,2095,20
94,2094,2093,2093,2093,2093,2093,
2093,2002,1829,1812,1778,1567,1308,969
-0.00834,-0.00829,-0.00823,-0.00736,-0.0072,-0.00703,-0.00663,-0.0
0521,-0.00278,-0.00056,0.001814,
0.003014,0.003155,0.003155,0.003152,0.003148,0.003147,0.003147,0.0
03146,0.003145,0.003145,0.002718,
0.000886,0.000681,0.000176,-0.00257,-0.00522,-0.00834
SPECIMEN 26
25
0.00,0.0028,0.72,1.39,3.04,3.62,6.56,11.32,24.84,54.71,68.69,73.06
,86.72,106.82,
192.85,289.96,291.62,294.02,295.15,298.53,304.88,313.35,322.38,326
.79,330.00
986,987,1086,1124,1188,1207,1294,1416,1688,1999,2082,2100,2113,211
2,2112,2112,
2032,1916,1871,1770,1572,1345,1134,1044,986
-0.00811,-0.00811,-0.0079,-0.00769,-0.00719,-0.00702,-0.0062,-0.00
502,-0.00216,
0.001899,0.003277,0.003597,0.003942,0.003943,0.003943,0.003943,0.0
03926,0.002148,
0.00153,0.000006,-0.00237,-0.00481,-0.00679,-0.00759,-0.00811
SPECIMEN 28
25
0.00,1.32,1.73,2.31,3.67,6.86,11.76,26.56,57.02,72.51,75.49,91.31,
95.99,98.69,100.22,101.34,102.59,
110.35,118.12,141.22,175.65,230.38,282.50,342.09,366.00
113,310,347,385,455,611,830,1317,1828,1954,1974,2062,2078,1940,186
9,1826,1789,1553,1340,862,473,215,
150,122,113
-0.01457,-0.01412,-0.01394,-0.0137,-0.01319,-0.01201,-0.01028,-0.0
0596,-0.0005,0.001239,0.001533,
0.002943,0.003245,0.002276,0.001472,0.000907,0.000347,-0.00255,-0.
00483,-0.00913,-0.01211,-0.0139,
-0.01433,-0.01451,-0.01457

SPECIMEN 29
25
0.00,1.23,1.68,2.44,3.57,6.96,12.05,26.36,56.65,71.81,78.83,94.62,
95.99,98.61,100.17,101.26,102.62,
110.17,118.66,142.37,174.74,228.65,279.32,337.25,366.00
138,323,366,416,475,641,869,1342,1858,1984,2031,2110,2115,1982,190
7,1865,1824,1592,1359,875,507,
244,178,148,138
-0.01441,-0.01402,-0.01382,-0.0135,-0.01307,-0.0118,-0.00998,-0.00
573,-0.00012,0.001674,0.002399,
0.003773,0.003873,0.002912,0.002051,0.001463,0.000822,-0.00212,-0.
00465,-0.00904,-0.01187,-0.01371,
-0.01416,-0.01435,-0.01441
SPECIMEN 30
25
0.00,1.32,1.73,2.30,3.66,6.85,11.73,26.50,56.90,72.35,79.03,91.10,
96.02,98.72,100.25,101.36,102.61,
110.36,118.12,141.50,172.94,230.56,282.62,348.76,366.00
153,352,391,429,501,660,883,1379,1901,2030,2075,2140,2157,2017,194
4,1900,1863,1621,1404,913,540,
256,190,160,153
-0.01432,-0.01387,-0.01369,-0.01344,-0.01291,-0.01169,-0.0099,-0.0
0539,0.000433,0.002374,0.00312,
0.004298,0.00466,0.003554,0.00265,0.002013,0.001384,-0.00179,-0.00
419,-0.00873,-0.01163,-0.01364,
-0.01408,-0.01428,-0.01432
*END

C-3

REFERENCES

1. DeMasi, J.T., Ortiz, M., and Sheffler, K.D., "Thermal Barrier Coating Life Prediction Model Development," Phase I Final Report, Contract NAS3-23944, NSAA CR-182230, 1989.

2. Miller, R.A., and Lowell, C.E., "Failure Mechanisms of Thermal Barrier Coatings Exposed to Elevated Temperature," Thin Solid Films, 99 (1982), p.265.

3. Sheffler, K.D., and Gupta, D.K., "Current Status and Future Trends in Turbine Application of Thermal Barrier Coatings," ASME Paper 88-GT-286 (June 1988).

4. Strangman, T.E., U.S. Patent No. 4,321,311, "Columnar Grain Ceramic Thermal Barrier Coatings," March, 1982.

5. Duvall, D.S., "Processing Technology for Advanced Metallic and Ceramic Turbine Airfoil Coatings," Proc. Second Conf. on Advanced Materials for Fuel Capable Heat Engines (Palo Alto, CA: Electric Power Research Institute, 1977), pp. 6-102.

6. Sumner, I.E., and Ruckle, D.L., "Development of Improved Durability Plasma Sprayed Ceramic Coatings for Gas Turbine Engines," AIAA Paper No. 80-1193, June 1980.

7. Grot, A.S., and Martyn, J.K., "Behavior of Plasma-Sprayed Ceramic Thermal Barrier Coating for Gas Turbine Applications," ACerS Bull., 60, 8, August 1981, p.807.

8. Grisaffe, S.J., and Levine, S.R., "Proc. First DOE/EPRI Conf. on Advanced Materials for Alternative Fuel Capable Directly Fired Heat Engines (Palo Alto, CA: Electric Power Research Institute, 1979), p.680.

9. Ruckle, D.L., "Evaluation of Plasma Sprayed Ceramic Coatings for Turbine Engine Components," Thin Solid Films, 64, 1979, p. 680.

10. Meier, S.M., Sheffler, K.D., and Nissley, D.M., "Status of Ceramic Thermal Barrier Coatings--Gas Turbine Applications and Life Prediction Methods, Proceedings of the 1990 Coatings for Advanced Heat Engine Workshop, Conf. 9008151, Castine, Maine, August 6-9, 1990.

11. Cruse, T.A., Nagy, A., and Popelar, C.F., "Mechanical Testing of Advanced Coatings System: Volume I," Final Report, SwRI Project No. 06-1778-001, Cooperative Agreement No. NCC 3-89, Southwest Research Institute, San Antonio, Texas, June 1990.

12. Timoshenko, S.P., and Goodier, J.N., Theory of Elasticity, 3rd ed., McGraw-Hill Book Co., New York, 1970, pp. 69-71.

13. Boresi, A.P., and Sidebottom, O.M., Advanced Mechanics of Materials, 4th ed., John Wiley and Sons, New York, pp.492-500.

14. Walker, K.P., "Research and Development Program for Nonlinear structural Modeling With Advanced Time-Temperature Dependent Constitutive Relationships," NASA CR-165533, November 1981.

15. Nissley, D.M., "Layer User and Programmer Manual," NASA CR-187038, November 1990.

16. ASM International Editorial Staff, ASM Engineered Materials Reference Book, ASM International, Metals Park, Ohio, 1989, pp 151-164.

17. Cruse, T.A., Stewart, S.E., and Ortiz, M., "Thermal Barrier Coating Life Prediction Model Development", Journal of Engineering for Gas Turbines and Power, 110, 1988, p. 610-616.

1.REPORT NO. NASA CR 189111	2. GOVERNMENT ACCESSION NO.	3.RECIPIENT'S CATALOG NO.
4.TITLE AND SUBTITLE Thermal Barrier Coating Life Prediction Model Development (HOST) Phase II – Design Life Capable Models		5. REPORT DATE July 1991
		6.
7.AUTHOR(S) Susan Manning Meier Keith D. Sheffler		8. PERFORMING ORG. REPT. NO.
9.PERFORMING ORGANIZATION NAME AND ADDRESS UNITED TECHNOLOGIES CORPORATION Pratt & Whitney Development Operations and Materials Engineering		10. WORK UNIT NO.
		11. CONTRACT OR GRANT NO. NAS3-23944
12. SPONSORING AGENCY NAME AND ADDRESS National Aeronautics and Space Administration Lewis Research Center 21000 Brookpark Road, Cleveland, Ohio 44135		13.TYPE REPT / PERIOD COVERED Final Report
		14. SPONSORING AGENCY CODE

15. SUPPLEMENTARY NOTES
Project Manager: Dr. Robert A. Miller
NASA Lewis Research Center, Cleveland, Ohio 44135

16. ABSTRACT
The objective of this program was to generate a life prediction model for electron-beam-physical vapor deposited (EB-PVD) zirconia thermal barrier coating (TBC) on gas turbine engine components. Specific activities involved in development of the EB-PVD life prediction model included measurement of EB-PVD ceramic physical and mechanical properties and adherence strength, measurement of the thermally grown oxide (TGO) growth kinetics, generation of quantitative cyclic thermal spallation life data, and development of a spallation life prediction model.

Life data useful for model development was obtained by exposing instrumented, EB-PVD ceramic coated cylindrical specimens in a jet fueled burner rig. Monotonic compression and tensile mechanical tests and physical property tests were conducted to obtain the EB-PVD ceramic behavior required for burner rig specimen analysis. As part of that effort, a nonlinear constitutive model was developed for the EB-PVD ceramic. Spallation failure of the EB-PVD TBC system consistently occurred at the TGO-metal interface. Calculated out-of-plane stresses were a small fraction of that required to statically fail the TGO. Thus, EB-PVD spallation was attributed to the interfacial cracking caused by in-plane TGO strains. Since TGO mechanical properties were not measured in this program, calculation of the burner rig specimen TGO in-plane strains was performed by using alumina properties. A life model based on maximum in-plane TGO tensile mechanical strain and TGO thickness correlated the burner rig specimen EB-PVD ceramic spallation lives within a factor of about $\pm 2X$.

17. KEY WORDS (SUGGESTED BY AUTHOR(S)) Thermal Barrier Coating Electron Beam-Physical Vapor Deposited Ceramic Life Prediction	18. DISTRIBUTION STATEMENT

19. SECURITY CLASS THIS (REPT) Unclassified	20. SECURITY CLASS THIS (PAGE) Unclassified	21. NO. PGS	22. PRICE *